STUDIES ON INTERACTION BETWEEN QUINOLONE DERIVATIVES (ANTIBIOTICS) AND TRANSITION METALS

A

DISSERTATION SUBMITTED TO THE UNIVERSITY OF DHAKA IN PARTIAL FULFILMENT OF THE REQUIREMENTS OF THE DEGREE OF DOCTOR OF PHILOSOPHY IN CHEMISTRY

SUBMITTED BY

HOSSAIN MOHAMMAD NASEEM AKHTAR

REGISTRATION NO. 189

SESSION-2009-2010

JULY, 2014

PHYSICAL CHEMISTRY RESEARCH LABORATORY

DEPARTMENT OF CHEMISTRY

UNIVERSITY OF DHAKA

DEDICATED

TO

My affectionate little mother (my daughter)

Syeda Sirajum Monira (Odree)

ACKNOWLEDGEMENT

First of all I am grateful to **Almighty Allah** for enabling me to successfully complete my Ph.D thesis.

A journey is easier and titillate when you travel together. Interdependence is certainly more valuable than independence. It is a pleasure moment that I have now the opportunities to express my deep sense of gratitude for all those who are instrumental in accomplishing this work successfully.

It is my great pleasure that I ingenuously express my deepest sense of gratitude and sincere appreciation to my reverend supervisor, **Dr. Md. Qamrul Ehsan**, M.Sc.(Dhaka), D.Sc.(Tohoku), Professor, Department of Chemistry, University of Dhaka for his constant supervision, valuable suggestions and discussions on different aspects of this research. Without his invaluable, scholastic, constructive and inspiring guidance to the completion of this research, the achievement would not have been materialized.

I am also thankful to **Dr. Tasmery S. A. Islam** and **Dr. Etmina Ahmed**, Professors and former Chairpersons, Department of Chemistry, University of Dhaka for their kind advises during my studies.

I am thankful to **Dr. Pradip Kumar Bakshi**, for his important suggestions, **Dr. Tanvir Muslim**, for his technical support in computer operations, to **Dr. Abdul Jabbar**, for his cordial help in discussing different electrochemical techniques and to **Mr. Ershad Halim** for supplying elemental analysis of the compounds.

I wish to express my sincere appreciation and thanks to **Dr. S. M. Mizanur Rahman**, Professor, Department of Chemistry, University of Dhaka for his kind advises, encouragement and constant help from the very beginning of my overall studies.

I gratefully acknowledge my indebtness to **Dr. Mahmuda Yasmin**, Chairman, Department of Microbiology, University of Dhaka for her co-operation in the Antibacterial testing.

I extend my profound gratitude and indebtness to our Chairperson **Dr. Nilufar Nahar**, Professor, Department of Chemistry, University of Dhaka, for making facilities of the laboratory available which enable d to work in a congenial and comfortable atmosphere.

I express my deepest sense of gratitude to my beloved **father, Late Syed Mohammad Akhtar Hossain**, who left this wonderful world on 29th November 2004, for his inspiration and support throughout my life.

I feel a deep sense of gratitude to my **mother, Late Shamsi Ara Ummey Akhtar**, who breathed her last on 11th March 2010, who formed the part of my vision and taught me the good things that really matter in life. Her well nourished advice and conception still provides a persistent inspiration for my journey in this life.

Sincere thanks and appreciations are acknowledged to **Mr. A. B. Imtiaj Ahmed**, former General Manager, Quality Operations, Square Pharmaceuticals, Dhaka Unit, for his technical support in running FTIR, NIR and DSC. Thanks are also to **Mr. Faiz Ahmed**, for his assistance in drawing of some curves.

I cannot find adequate words for expressing my gratitude to the researchers, laboratory technicians and well-wishers, who cheerfully volunteered their services at different stages during the progress of work.

I expressed my gratitude to my **wife, Mrs. Sabiha Sultana** for her moral support and companion ship during my work.

Last but not the least it is a great pleasure for me to express my love and gratitude to my **daughter**, **Syeda Sirajum Monira (Odree)** for presenting me with her aweet smile every morning during the difficult stage of preparation of the thesis which inspired me beyond description.

Hossain Mohammad Naseem Akhtar
Department of Chemistry
University of Dhaka

CHAPTER 1 INTRODUCTION

PART-I

ELECTROCHEMICAL STUDIES OF THE METAL-CIPROFLOXACIN INTERACTION IN SOLUTION

CHAPTER 2 EXPERIMENTAL

CHAPTER 3 RESULTS AND DISCUSSION

CHAPTER 6 RESULTS AND DISCUSSION

UNIVERSITY OF DHAKA
DEPARTMENT OF CHEMISTRY
Dhaka-1000, Bangladesh

Dr. M. Q. Ehsan
Professor

Tel: 9661900-59/4884
FAX: (880-2)-8615583
E-mail: mqehsan@yahoo.com

Certificate

This is to certify that the thesis entitled "*STUDIES ON INTERACTION BETWEEN QUINOLONE DERIVATIVES (ANTIBIOTICS) AND TRANSITION METALS*" is the record of the research work done by Mr. Hossain Mohammad Naseem Akhtar, research scholar, Depertment of Chemistry, Dhaka University, under my guidance for the award of Doctor of Philosophy in Physical Chemistry and that this thesis has not previously formed the basis for the award of any degree, diploma or other similar title to the candidate.

This is also to certify that the thesis represents the independent work of the candidate.

Dr. M. Q. Ehsan

ABSTRACT

The redox behavior of few first row transition metal ions, Cr(III), Mn(II), Ni(II), Cu(II) and Zn(II) in presence and absence of the ligand ciprofloxacin were studied in the aqueous medium using Cyclic Voltammetry. Chronoamperomety and chronocoulometry were also performed to know some other electrochemical aspects.

It was found that the redox systems involved in Cu(II), Mn(II) as well as Cu(II)-Ciprofloxacin and Mn(II)-Ciprofloxacin interactions in solutions are quasi-reversible. But the Zn(II) and Cr(III) systems are near to reversible and the Zn(II)-Ciprofloxacin and Cr(II)-Ciprofloxacin interactions are quasi-reversible and irreversible respectively.

The findings from the Chronoamperometric study in solution is that after interaction the spike height is decreased, indicating towards a decrease in the rate of electrolysis. And from the Chronocoulometric study, it is observed that the charge at τ are decreased in all the cases. Both of these facts combinedly indicate occurance of interaction between the metal and ligand. The observations from the plots Q vs $t^{1/2}$ and $-Q_r$ vs θ gives conclusion that adsorption of reactant or products occur on the electrode after compound formation.

The solid product obtained from the interaction between metal ions and Ciprofloxacin were characterized by different physoci chemical methods. Cr(III), Mn(II) and Ni(II) form compounds with Ciprofloxacin in a ratio of 1:2 and on the other hand Cu(II) and Zn(II) form 1:1 compounds. All the compounds are stable in air and light. The compounds are insoluble in non-polar solvents but soluble in polar solvents. Almost all of the compounds have higher melting points which implies that the compounds have ionic character to some extent.

The compounds were further characterized by IR spectra, electronic absorption spectra as well as NIR spectra. The observations of the spectral analysis do not show any significant changes with that of the ligand. Therefore it may be said that the products obtained after interaction are adduct type of compounds. DSC study signifies their endothermic and exothermic natures.

The redox properties of the products obtained were studied at Glassy Carbon working electrode. But in case of Cr(III) compound Platinum working electrode was used.

The findings from the cyclic voltammetric study of all metal-Ciprofloxacin compounds implies that the electrochemical process involved are quasi-reversible. It was also found that almost all the systems are diffusion controlled as well as adsorptive controlled. The concentration effects of all the compounds show a gradual increase of peak current with the increase in concentrations giving indication towards diffusion controlled situations.

The findings from the Chronoamperometric study is that after compound formation the spike height is decreased, indicating towards a decrease in the rate of electrolysis. And from the Chronocoulometric study, it is observed that the charge at τ are decreased in all the cases. Both of these facts combinedly indicate that new compound formation occurs after interaction. And the observations from the plots Q vs $t^{1/2}$ and $-Q_r$ vs θ gives conclusion that adsorption of reactant or products occur on the electrode also after compound formation.

The concentration effect on Chronoamperometric as well as chronocoulometric study of of all the Metal-Ciprofloxacin compounds show a linear relationship of concentration and spike height.

The findings from the antibacterial activity of the Metal-Ciprofloxacin compounds show that Mn(II)-Ciprofloxacin and Ni(II)-Ciprofloxacin compound are more active against *Salmonella sp*. compared to Ciprofloxacin. Similar is the case for *E.coli*. Mn(II)-Ciprofloxacin compound is more active than Ciprofloxacin in case of *Bacillus sp.* and *S. aureus*. As a result, it may be concluded that compared to Ciprofloxacin, Mn(II)-Ciprofloxacin compound shows the best activity against bacteria among the five Metal-Ciprofloxacin compounds used in the present study.

1 INTRODUCTION

1.1 Background of the Research

The human body is an amazing machine. It is a miracle creation. The body consists of close to 100 trillion cells, the basic unit of life. These cells are organized biologically to eventually form the whole body. Any condition that impairs normal function, is termed as disease. Then medicine is a must to get rid of this. Medicine is the science and art of healing. It encompasses a variety of health care practices evolved to maintain and restore health by the prevention and treatment of illness in human beings.

The word *medicine* is derived from the Latin *ars medicina*, meaning *the art of healing*. It is the science as well as art of healing and encompasses a variety of health care practices evolved to maintain and restore health by the prevention and treatment of illness in human beings. Contemporary medicine applies health science, biomedical research, and medical technology to diagnose and treat injury and disease, typically through medication or surgery, but also through therapies as diverse as psychotherapy, external splints & traction, prostheses, biologics, ionizing radiation and others.

Different types of medicines are used in the modern world for the treatment of different type of diseases and disorders. Among those antibiotics are a broad class of medicine, which inhibits bacterial growth or kills bacteria. There are different classes of antibiotics. These are classified on the basis of their mechanism of action, chemical structure or on the spectrum of activity. Quinolones are one of the most used and valuable class of antibiotics. They prevent bacterial DNA from unwinding and duplicating. Quinolones are divided into different generations based on their antibacterial action. The earlier-generation agents are, in general, more narrow-spectrum than the later ones. Some examples of different generations are as follows. At present, the first generation is rarely used. Flumequine is a member of first generation, which is now used for veterinary use. The most widely used second generation quinolone is ciprofloxacin. Now-a-days ciprofloxacin has become the most

popular, which has multiple uses. Levofloxacin is the most well-known of the third generation. It also has extensive use. Gatifloxacin is the member of the forth generation. There are also some some quinolones, which are dedicated for veterinary use. Enrofloxacin is such an extensively used quinolone.

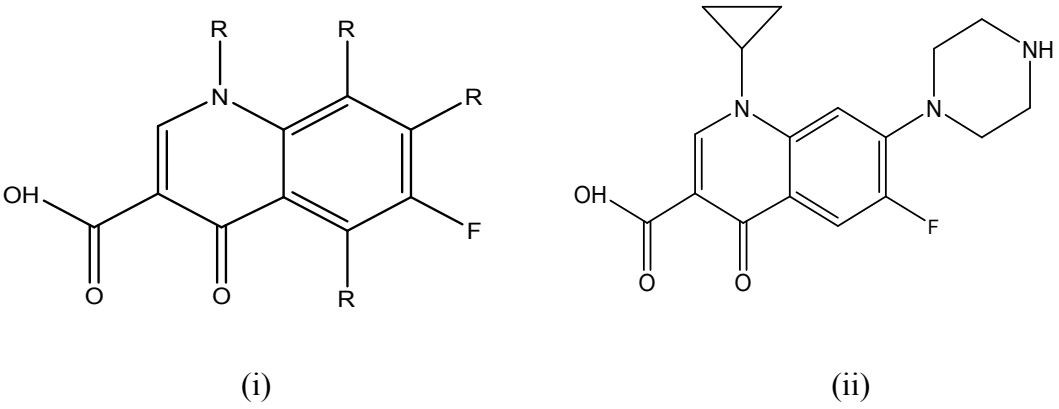

(i) (ii)

Fig 1.1 Structure of (i) Quinolones and (ii) Ciprofloxacin

Ciprofloxacin is a synthetic antibiotic. It kills bacteria by interfering with the enzymes that cause DNA to rewind after being copied, which stops synthesis of DNA and of protein. Ciprofloxacin is used to treat a number of infections including: infections of bones and joints, endocarditis, gastroenteritis, malignant otitis externa, respiratory tract infections, cellulitis, urinary tract infections, prostatitis, anthrax, chancroid, among others. In the present study Ciprofloxacin was taken into consideration because of these extreme importance in the treatment of various disorders.

The word “transition metal” has different possible meanings in chemistry. The IUPAC definition defines a transition metal as "an element whose atom has an incomplete *d* sub-shell, or which can give rise to cations with an incomplete *d* sub-shell". Most scientists describe a "transition metal" as any element in the d-block of the periodic table (all are metals), which includes groups 3 to 12 on the periodic table. In actual practice, the f-block lanthanide and actinide series are also considered transition metals and are called "inner transition metals".

There are a number of properties shared by the transition elements that are not found in other elements. These are resulting from the partially filled *d* shell. These include the formation of compounds whose colour is due to $d - d$ electronic transitions and

the formation of compounds in many oxidation states, due to the relatively low reactivity of unpaired *d* electrons[1]. Another remarkable property is the formation of many paramagnetic compounds due to the presence of unpaired *d* electrons.

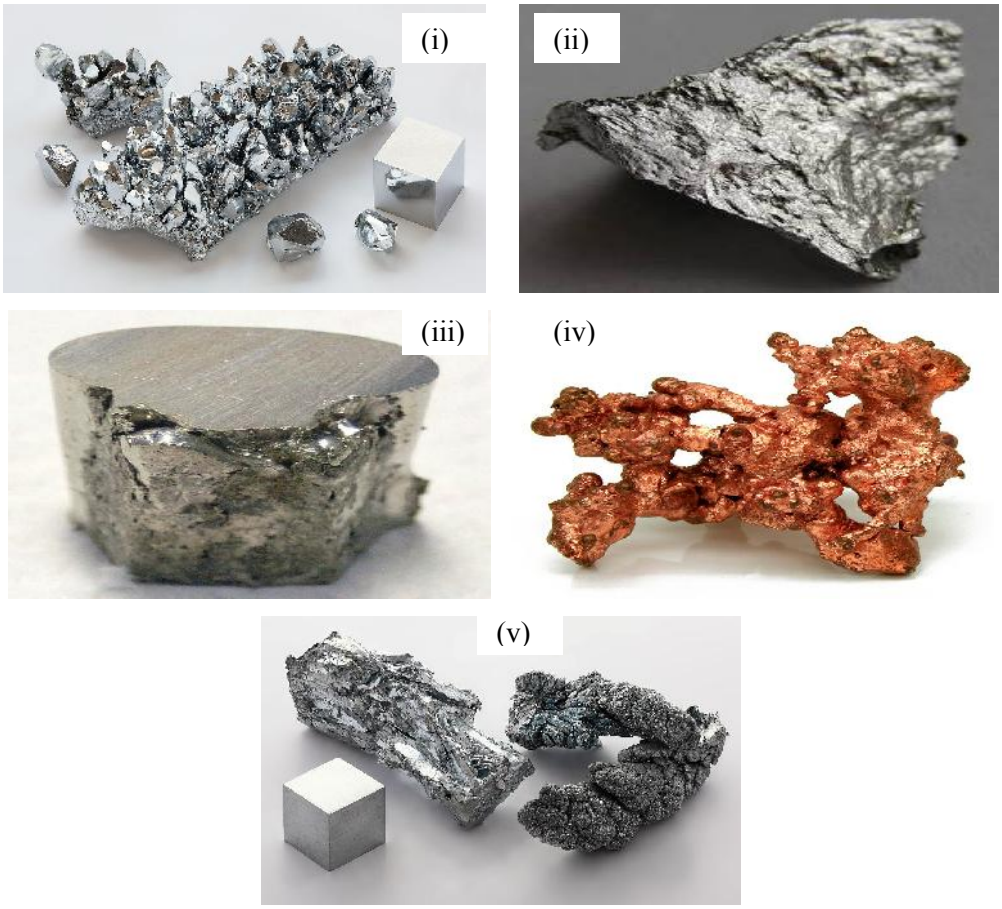

Fig 1.2 Images of metallic (i) Chromium, (ii) Manganese, (iii) Nickel, (iv) Copper and (v) Zinc.

Chromium is one of the transition metals. It is positioned in group VI B of the periodic table. Its function includes the glucose tolerance factor which stimulates insulin activity and controls the uptake of glucose by the muscles and organs. Chromium stimulates glucose metabolism and controls blood cholesterol levels. It reduces atherosclerosis as well as stimulates the synthesis of proteins. Moreover, it increases resistance to infection and suppresses hunger pains. Manganese is another transition metal found in group VII B in the periodic table and is an antioxidant. It is necessary for the functioning of the brain. Manganese is required for the metabolism of energy and is involved in the metabolism of calcium. It is also required to produce melanin and to synthesize fatty acids as well as helpful in producing urea. Manganese is necessary for building proteins and nucleic acid and for normal bone structure.

Moreover it is involved in the formation of thyroxin in the thyroid gland. Nickel is the group VIII element. It is involved in different enzymatic activities in various microorganisms and plants. Copper is placed at group IB in the periodic table and is a natural anti plaque and anti bacterial agent. It is an essential nutrient required by the body in daily dietary amounts of 1-2 mg for adults. Conclusive studies show that copper keeps water clean by keeping down microbial growth. In oriental cultures, benefits of copper have been recognized for thousands of years and people store drinking water overnight in copper utensils. Copper is also needed for certain critical enzymes to function in the body. Zinc is another transition element with its position in group IIB in the periodic table. It is distributed mostly in the brain, muscle, bones, kidney, and liver of human body, with the highest concentrations in the prostate and parts of the eye. It is also a key factor in prostate gland function and reproductive organ growth.

Recent studies have demonstrated that the bioavailability of a trace metal (e.g. Cr, Mn, Ni, Cu Zn) to cause biotoxicity depends on the forms of the metal species. And it was also studied that the metal ion, M^{n+}, being relatively small in size can be more harmful to biota than its complexes form ML_n (complexation). For example methyl cyanocobalamin complex being so large, cannot penetrate through the cell membrane to cause biotoxicity. Now the key question is, how to access the molecular information has become one of the most challenging issues of analytical chemistry during the past decade, because of its very significant impact on different aspects of human life and the environment, including energy related industries.

For the above reason, it is very much important to know about the redox behavior of those metals, coordinating nature as well as their complexation features with the ligand (Ciprofloxacin). That is why the present study is fully accomplished to observe the complexation nature of the metals with the ligand (Ciprofloxacin) and also the redox behavior of the metals in the absence (uncoordinated) and presence (coordinated) of the ligand (Ciprofloxacin).

The study of metal ligand complexes is important in analytical separation procedures like ion exchange chromatography and solvent extraction, in industrial catalytic phenomena, in metallurgy, in power generating units like fuel cells. This information

is also important in electrochemistry, particularly in electroplating of an anticorrosion liquids, in pollution chemistry and photochemistry[2].

The process of departure of a third or fourth electron from a doubly or trebly charged ion takes place at the enormously high temperatures in the center of a star. But it is at first a little surprising to find it happening so readily at room temperature[3].

The primary event in most cyclic voltammetric experiments is the oxidation or reduction of a dissolved chemical species at an electrode. The most striking feature of this process is the ease with which a doubly or trebly charged ion gives up a third or fourth electron[3]. It is therefore a very effective method in studying the redox behavior of electroactive species. Understanding the redox nature of coordination compounds, using different metals, their biological importance can be found.

Chronoamperometry and chronocoulometry are very closely related to each other. The later is the integrated form of the former. Along with other informations, chronocoulometry gives very significant ideas about the adsorption of electroactive species. These methods are also adopted in the present study to investigate about the adsorption of the metals (Cr, Mn, Ni, Cu Zn) in the absence and presence of the ligand (ciprofloxacin).

1.2 Antibiotics

The term “antibiotic” is often used synonymously with the term antibacterial. It is actually a compound or substance that kills or slows down the growth of bacteria. The term *antibiotic* was coined by Selman Waksman in 1942 to describe any substance produced by a microorganism that is antagonistic to the growth of other microorganisms in high dilution. This definition excluded substances that kill bacteria, but are not produced by microorganisms (such as gastric juices and hydrogen peroxide). It also excluded synthetic antibacterial compounds such as the sulfonamides. Many antibacterial compounds are relatively small molecules with a molecular weight of less than 2000 atomic mass units.

1.2.1 History of antibiotics

Before the early 20th century, treatments for infections were based primarily on medicinal folklore. Mixtures with antimicrobial properties that were used in treatments of infections were described over 2000 years ago[4]. Many ancient cultures, including the ancient Egyptians and ancient Greeks, used specially selected mold and plant materials and extracts to treat infections[5, 6]. More recent observations made in the laboratory of antibiosis between micro-organisms led to the discovery of natural antibacterials produced by microorganisms. Louis Pasteur observed, "if we could intervene in the antagonism observed between some bacteria, it would offer perhaps the greatest hopes for therapeutics"[7].

The term *antibiosis*, meaning "against life," was introduced by the French bacteriologist Vuillemin as a descriptive name of the phenomenon exhibited by these early antibacterial drugs[8]. Antibiosis was first described in 1877 in bacteria when Louis Pasteur and Robert Koch observed that an airborne bacillus could inhibit the growth of *Bacillus anthracis*. These drugs were later renamed antibiotics by Selman Waksman, an American microbiologist, in 1942.

In 1928 Alexander Fleming observed antibiosis against bacteria by a fungus of the genus *Penicillium*. Fleming postulated that the effect was mediated by an antibacterial compound named penicillin, and that its antibacterial properties could be exploited for chemotherapy. He initially characterized some of its biological properties, but he did not pursue its further developmen.

In 1939 the first pioneering efforts were given by Florey and Chain. Since then the importance of antibiotics, including antibacterials, to medicine has led to intense research into producing antibacterials at large scales. Following screening of antibacterials against a wide range of bacteria, production of the active compounds is carried out using fermentation, usually in strongly aerobic conditions.

1.2.2 Classification of antibiotics

The classification of antibiotics are commonly based on their mechanism of action, chemical structure, or spectrum of activity. Most of them target bacterial functions or growth processes[8]. Penicillins and ephalosporins target the bacterial cell wall,

polymixins the cell membrane, quinolones and sulfonamides interfere with essential bacterial enzymes and have bactericidal activities. Those that target protein synthesis (aminoglycosides, macrolides, and tetracyclines) are usually bacteriostatic[9].

Categorization is further based on their target specificity. "Narrow-spectrum" antibacterial antibiotics target specific types of bacteria, such as Gram-negative or Gram-positive bacteria, whereas broad-spectrum antibiotics affect a wide range of bacteria. Following a 40-year hiatus in discovering new classes of antibacterial compounds, three new classes of antibacterial antibiotics have been brought into clinical use: cyclic lipopeptides (such as daptomycin), glycylcyclines (such as tigecycline), and oxazolidinones (such as linezolid)[9].

1.2.3 Side-effects of antibiotics

Antibacterials are screened for any negative effects on humans or other mammals before approval for clinical use. However, some antibacterials have been associated with a range of adverse effect. Side-effects range from mild to very serious depending on the antibiotics used, the microbial organisms targeted, and the individual patient. Adverse effects range from fever and nausea to major allergic reactions, including photodermatitis and anaphylaxis. Common side-effects include diarrhea, resulting from disruption of the species composition in the intestinal flora, resulting, for example, in overgrowth of pathogenic bacteria, such as *Clostridium difficile*. These can also affect the vaginal flora, and may lead to overgrowth of yeast species of the genus *Candida* in the vulvo-vaginal area[10]. In addition to this side-effects can result from interaction with other drugs, such as elevated risk of tendon damage from administration of a quinolone antibiotic with a systemic corticosteroid.

1.3 Quinolones

Quinolones are a family of synthetic broad-spectrum antibacterial drugs[11]. In comparison to other antibiotic classes, these have among the highest risk of causing colonization with MRSA and *Clostridium difficile*[11]. Most of the quinolones in clinical use belong to the subset fluoroquinolones, which have a fluorine atom attached to the central ring system, typically at the C-6 position or C-7 position. The

first generation of the quinolones begins with the introduction of nalidixic acid in 1962 for treatment of urinary tract infections in humans.

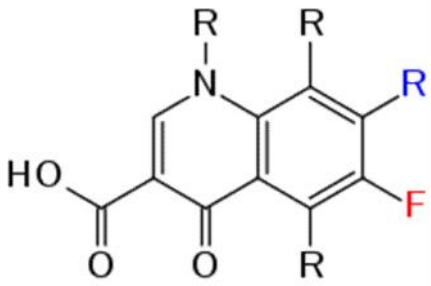

Fig 1.3 General structure of Quinolones.

1.3.1 History of quinolones

The history of quinolones is based on nalidixic acid to a large extent. Nalidixic acid is considered to be the predecessor of all members of the quinolone family, including the second, third and fourth generations commonly known as fluoroquinolones. This first generation also included other quinolone drugs, such as pipemidic acid, oxolinic acid, and cinoxacin. Though it is generally accepted nalidixic acid is to be considered the first quinolone drug, this has been disputed over the years by a few researchers who believe chloroquine, from which nalidixic acid is derived, is to be considered the first quinolone drug, rather than nalidixic acid.

1.3.2 Medical uses of quinolones

Fluoroquinolones are broad-spectrum antibiotics. These play an important role in treatment of serious bacterial infections, especially hospital-acquired infections and others in which resistance to older antibacterial classes is suspected.

Fluoroquinolone use for pneumonia is increasing, and with it so is bacterial resistance to fluoroquinolones. For severe forms of community-acquired pneumonia, the fluoroquinolones are associated with reduced hospitalization rates, but with no differences found in mortality between other antibiotic classes.

In some cases of bronchitis antibiotics including fluoroquinolones can be effective. However, only about 5-10% of bronchitis cases are caused by a bacterial infection; most cases of bronchitis are caused by a viral infection and are self-limiting and resolve themselves in a few weeks. It has been recommended that antibiotics are limited in most cases to those whose symptoms fail to resolve on their own.

Fluoroquinolones are often used for genitourinary infections. They are widely used in the treatment of hospital-acquired infections associated with urinary catheters. In community-acquired infections, they are recommended only when risk factors for multidrug resistance are present or after other antibiotic regimens have failed. However, for serious acute cases of pyelonephritis or bacterial prostatitis where the patient may need to be hospitalised, fluoroquinolones are recommended as first-line therapy.

1.3.3 Adverse effects of quinolones

i) Fluoroquinolones are in general well tolerated, with most side effects being mild to moderate. On occasion, serious adverse effects occur. Some of the serious adverse effects that occur more commonly with fluoroquinolones than with other antibiotic drug classes include central nervous system (CNS) and tendon toxicity.

ii) Certain quinolones are more strongly associated with increased toxicity to certain organs. For example, moxifloxacin carries a higher risk of QTc prolongation[12], and gatifloxacin has been most frequently linked to disturbed blood sugar levels, although all quinolones carry these risks[13, 14]. Sparfloxacin is associated with phototoxicity and QTc prolongation; thrombocytopenia and nephritis are seen with tosufloxacin; and hepatotoxicity with trovafloxacin[15]. Simultaneous use of corticosteroids is present in almost one-third of quinolone-associated tendon rupture[16]. The risk of adverse events is further increased if the dosage is not properly adjusted, for example if there is renal insufficiency[13].

iii) Fluoroquinolones are considered high-risk antibiotics for the development of *Clostridium difficile* and MRSA infections. A previously rare strain of *C. difficile* that

produces a more severe disease with increased levels of toxins is becoming epidemic, and may be connected to the use of fluoroquinolones.

1.3.4 Pharmacology of quinolones

The basic pharmacophore, or active structure, of the fluoroquinolone class is based upon the quinoline ring system[17]. The addition of the fluorine atom at C6 distinguishes the successive-generation fluoroquinolones from the first-generation quinolones.

Development of numerous fluoroquinolone drugs is the result of various substitutions made to the quinoline ring. Each substitution is associated with a number of specific adverse reactions, as well as increased activity against bacterial infections, whereas the quinoline ring, in and of itself, has been associated with severe and even fatal adverse reactions.

1.3.5 Mechanism of action of quinolones

Quinolones inhibit the topoisomerase II ligase domain, leaving the two nuclease domains intact. This modification, coupled with the constant action of the topoisomerase II in the bacterial cell, leads to DNA fragmentation via the nucleasic activity of the intact enzyme domains. Recent evidence has shown eukaryotic topoisomerase II is also a target for a variety of quinolone-based drugs. Thus far, most of the compounds that show high activity against the eukaryotic type II enzyme contain aromatic substituents at their C-7 positions.

Quinolones can enter cells easily via porins and, therefore, are often used to treat intracellular pathogens such as *Legionella pneumophila* and *Mycoplasma pneumoniae*. For many Gram-negative bacteria, DNA gyrase is the target, whereas

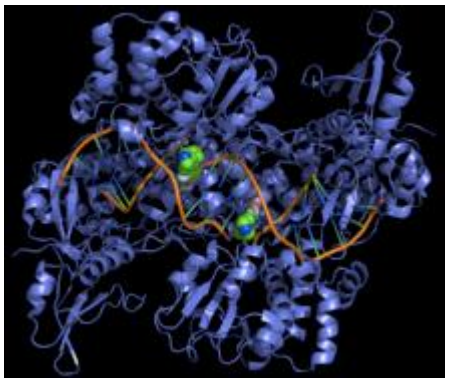

Fig 1.4 Structure of bacterial DNA gyrase complexed with DNA and two ciprofloxacin molecules (green).

topoisomerase IV is the target for many Gram-positive bacteria. Some compounds in this class have been shown to inhibit the synthesis of mitochondrial DNA[18-21].

1.3.6 Interactions of quinolones

Some drugs such as Theophylline, nonsteroidal anti-inflammatory drugs and corticosteroids enhance the toxicity of fluoroquinolones[21]. Some products containing multivalent cations, such as aluminium- or magnesium-containing antacids and products containing calcium, iron, or zinc, invariably result in marked reduction of oral absorption of fluoroquinolones. Other drugs that interact with fluoroquinolones include antacids, sucralfate, probenecid, cimetidine, warfarin, antiviral agents, phenytoin, cyclosporine, rifampin, pyrazinamide, and cycloserine[21].

Many fluoroquinolones, especially ciprofloxacin, inhibit the cytochrome P450 isoform CYP1A2. This inhibition causes an increased level of drugs that are metabolized by this enzyme. This includes antidepressants such as amitriptyline and imipramine, clozapine (an atypical antipsychotic), caffeine, olanzapine (an atypical antipsychotic), ropivacaine (a local anaesthetic), theophylline (a xanthine), and zolmitriptan (a serotonin receptor agonist)[22].

1.3.7 Generations of quinolones

Quinolones are classified into different category in various ways. Such as

i) some researchers group these drugs by patent dates.
ii) some by a specific decade (i.e., '60s, '70s, '80s, etc.)
iii) others by the various structural changes.

Researchers divide the quinolones into generations on the basis of their antibacterial spectrum. The earlier-generation agents are more narrow-spectrum than the later ones. No standard is employed to determine which drug belongs to which generation. The only universal standard applied is the grouping of the nonfluorinated drugs within the 'first-generation' heading.

The first generation is rarely used today. A number of the second-, third-, and fourth-generation drugs have been removed from clinical practice due to severe toxicity issues or discontinued by their manufacturers.

a) First-generation

- cinoxacin
- flumequine (carcinogen)(veterinary use)
- nalidixic acid (genotoxic carcinogen)
- oxolinic acid
- piromidic acid
- pipemidic acid
- rosoxacin

b) Second-generation

The second-generation class is sometimes subdivided into "Class 1" and "Class 2".

- ciprofloxacin
- norfloxacin (restricted use)
- enoxacin
- ofloxacin
- fleroxacin
- pefloxacin
- lomefloxacin
- rufloxacin
- nadifloxacin

c) Third-generation

Unlike the first- and second-generations, the third-generation is active against streptococci.

- balofloxacin
- sparfloxacin
- grepafloxacin
- temafloxacin
- levofloxacin
- tosufloxacin
- pazufloxacin

d) Fourth-generation

Fourth generation fluoroquinolones act at DNA gyrase and topoisomerase IV. This dual action slows development of resistance.

- clinafloxacin
- sitafloxacin
- gatifloxacin
- trovafloxacin
- gemifloxacin
- prulifloxacin
- moxifloxacin (restricted use)

e) In development

- garenoxacin(application withdrawn due to toxicity)
- delafloxacin An anionic fluoroquinoline in clinical trials
- JNJ-Q2 Completed Phase II for MRSA

f) Veterinary use

The quinolones have been widely used in agriculture, and several agents having veterinary but not human, use exist.

- danofloxacin
- marbofloxacin
- difloxacin
- orbifloxacin
- enrofloxacin
- sarafloxacin
- ibafloxacin

Among all the Quinolone derivatives Ciprofloxacin was selected for the present study because of its widely use and importance in the medicinal field.

1.4 Ciprofloxacin

Ciprofloxacin is a synthetic antibiotic of the fluoroquinolone drug class. It is a second-generation fluoroquinolone antibacterial. It kills bacteria by interfering with the enzymes that cause DNA to rewind after being copied, which stops synthesis of DNA and of protein. It interacts with other drugs, herbal and natural supplements, a characteristic it shares with other widely used antibacterial drugs such as amoxicillin, trimethoprim, azithromycin, cephalexin, and doxycycline.

1.4.1 Chemistry of ciprofloxacin

Ciprofloxacin is 1-cyclopropyl-6-fluoro-1,4-dihydro-4-oxo-7-(1-piperazinyl)-3-quinolinecarboxylic acid. Its empirical formula is $C_{17}H_{18}FN_3O_3$ and its molecular weight is 331.4 g/mol. It is a faintly yellowish to light yellow crystalline substance. Ciprofloxacin hydrochloride (USP) is the monohydrochloride monohydrate salt of ciprofloxacin. It is a faintly yellowish to light yellow crystalline substance with a molecular weight of 385.8 g/mol. Its empirical formula is $C_{17}H_{18}FN_3O_3HCl•H_2O$.

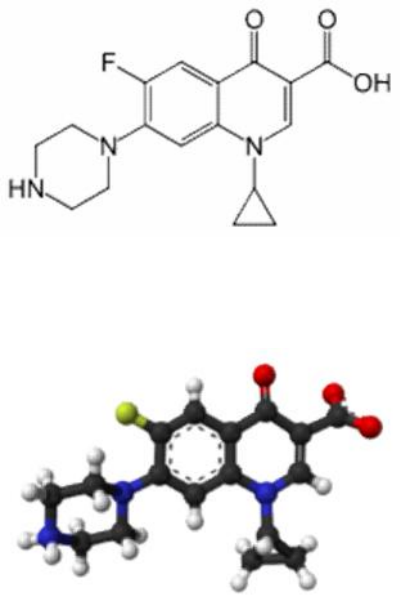

Fig 1.5 Structure of Ciprofloxacin.

1.4.2 History of ciprofloxacin

The patent history for ciprofloxacin makes reference to a 1982 European Patent (patent number 0049355), as well a German patent dated 21 January 1986. Bayer

introduced ciprofloxacin in 1987 and it was later approved by the U.S. FDA on 22 October 1987 for use in the United States to treat specific bacterial infections. In 1991, the intravenous formulation was introduced. The current United States patent appears to be held by Bayer, being the assignee. The United States patent was applied for in January 1987, but was not approved until 1996 according to the patent history.

1.4.3 Pharmacokinetics of ciprofloxacin

The effects of 200–400 mg of ciprofloxacin given intravenously are linear. Drug accumulation does not occur when administered at 12 hour intervals. Bioavailability is approximately 70-80%, with no significant first pass effect. IV administration produces a similar serum levels as those achieved with administration of 500 mg administered orally. IV administration over 60 minutes given every 8 hours produces similar serum levels of the drug as 750 mg administered orally every 12 hours. Biotransformation is hepatic. The elimination half life is 4 hours.

1.4.4 Mechanism of action of ciprofloxacin

Ciprofloxacin is a broad-spectrum antibiotic active against both Gram-positive and Gram-negative bacteria. It functions by inhibiting DNA gyrase, a type II topoisomerase, and topoisomerase IV[23], enzymes necessary to separate bacterial DNA, thereby inhibiting cell division.

This mechanism can also affect mammalian cell replication. In particular, some congeners of this drug family (for example those that contain the C-8 fluorine) display high activity not only against bacterial topoisomerases but also against eukaryotic topoisomerases and are toxic to cultured mammalian cells and *in vivo* tumor models. Although quinolones are highly toxic to mammalian cells in culture, its mechanism of cytotoxic action is not known. Quinolone-induced DNA damage was first reported in 1986 (Hussy and others.).

Recent studies have demonstrated a correlation between mammalian cell cytotoxicity of the quinolones and the induction of micronuclei. As such, some fluoroquinolones may cause injury to the chromosome of eukaryotic cells[24].

There continues to be debate as to whether or not this DNA damage is to be considered one of the mechanisms of action concerning the severe adverse reactions experienced by some patients following fluoroquinolone therapy.

1.4.5 Medical uses of ciprofloxacin

i) Ciprofloxacin is used to treat a number of infections including: infections of bones and joints, endocarditis, gastroenteritis, malignant otitis externa, respiratory tract infections, cellulitis, urinary tract infections, prostatitis, anthrax, chancroid, among others.

ii) Some other uses are for acute uncomplicated cystitis in females, Acute sinusitis, skin and skin structure infections, infectious diarrhea, Typhoid fever (enteric fever) caused by *Salmonella typhi* and uncomplicated cervical and urethra gonorrhea (due to *N. gonorrhoeae*)

iii) Ciprofloxacin is also used in combination with other specific drugs: a) Complicated intra-abdominal infections (in combination with metronidazole), b) Empirical therapy for febrile neutropenic patients (in combination with piperacillin).

iv) Ciprofloxacin is not recommended to treat community acquired pneumonia (CAP) as a stand-alone first-line agent.

1.4.6 Contraindications of ciprofloxacin

Ciprofloxacin is also considered to be contraindicated for the treatment of certain sexually transmitted diseases by some experts due to bacterial resistance. There are only four contraindications found within the 2009 package insert:

- "Coadministration of ciprofloxacin with other drugs primarily metabolized by CYP1A2 results in increased plasma concentrations of these drugs and could lead to clinically significant adverse events of the coadministered drug."

- "Concomitant administration with tizanidine is contraindicated."

- "Ciprofloxacin is contraindicated in persons with a history of hypersensitivity to ciprofloxacin, any member of the quinolone class of antimicrobial agents, or any of the product components."

- "Local I.V. site reactions are more frequent if the infusion time is 30 minutes or less. These may appear as local skin reactions that resolve rapidly upon completion of the infusion. Subsequent intravenous administration is not contraindicated unless the reactions recur or worsen."

Ciprofloxacin is also considered to be contraindicated within the pediatric population (except for the indications outlined under licensed use above), pregnancy, nursing mothers, and in patients with epilepsy or other seizure disorders.

Pregnancy: The fluoroquinolones rapidly cross the blood-placenta and blood-milk barriers, and are extensively distributed into the fetal tissues. For this reason, the fluoroquinolones are contraindicated during pregnancy due to the risk of spontaneous abortions and birth defects. The fluoroquinolones have also been reported as being present in the mother's milk and are passed on to the nursing child, which may increases the risk of the child suffering from this syndrome as well, even though the child had never been prescribed or taken any of the drugs found within this class.

Pediatric population: Fluoroquinolones are not licensed by the U.S. FDA for use in children due to the risk of fatalities as well as permanent injury to the musculoskeletal system, with two exceptions. Ciprofloxacin is being licensed for the treatment of complicated urinary tract infections and pyelonephritis due to *Escherichia coli*, and inhalational anthrax (postexposure), and levofloxacin was recently licensed for the treatment of inhalational anthrax (postexposure). However, the fluoroquinolones are licensed to treat lower respiratory infections in children with cystic fibrosis in the UK.

1.4.7 Special precautions for ciprofloxacin

The status of the patient's renal function and hepatic function must also be taken into consideration to avoid an accumulation that may lead to an overdose and the development of toxicity. Ciprofloxacin is eliminated primarily by renal excretion. However, the drug is also metabolized and partially cleared through the liver and the intestines. Modification of the dosage is *recommended* using the table found within the package insert for those with impaired liver or kidney function. However, since the drug is known to be substantially excreted by the kidneys, the risk of toxic reactions to this drug may be greater in patients with impaired renal function. The duration of treatment depends upon the severity of infection and is usually 7 to 14 days.

1.4.8 Adverse effects of ciprofloxacin

i) The serious adverse effects that may occur as a result of ciprofloxacin therapy include irreversible peripheral neuropathy, spontaneous tendon rupture and tendonitis, acute liver failure or serious liver injury (hepatitis), QTc prolongation/torsades de pointes, toxic epidermal necrolysis (TEN), and Stevens–Johnson syndrome, severe central nervous system disorders (CNS) and Clostridium difficile associated disease (CDAD: pseudomembranous colitis), as well as photosensitivity/phototoxicity reactions.

ii) Psychotic reactions and confusional states, acute pancreatitis, bone marrow depression, interstitial nephritis and hemolytic anemia may also occur during ciprofloxacin therapy.

iii) Additional serious adverse reactions include temporary, as well as permanent, loss of vision, irreversible double vision, drug induced psychosis and chorea (involuntary muscle movements), impaired color vision, exanthema, abdominal pain, malaise, drug fever, dysaesthesia and eosinophilia. Pseudotumor cerebri, commonly known as idiopathic intracranial hypertension (IIH), (also referred to as increased intracranial pressure), has been reported to occur as a serious adverse reaction to ciprofloxacin.

iv) Children and the elderly are at a much greater risk of experiencing such adverse reactions. Tendonitis and other forms of tendon damage may manifest during fluoroquinolone therapy, and long after it had been discontinued.

v) Serious visual complications have also been reported to occur with ophthalmic fluoroquinolone therapy, which may also occur with ciprofloxacin eye drops, especially corneal perforation, but also evisceration and enucleation. This increased incidents of corneal perforation may be due to fluoroquinolones causing alterations in stromal collagen, leading to a reduction in tectonic strength. As noted previously permanent double vision (diplopia) has also been reported. An unusual case of seizures has also been reported with ciprofloxacin ear drops in an elderly patient.

1.4.9 Interactions of ciprofloxacin with drugs

The toxicity of drugs that are metabolised by the cytochrome P450 system is enhanced by concomitant use of some quinolones. Coadministration may dangerously increase coumarin (warfarin) activity; INR should be monitored closely. They may also interact with the GABA A receptor and cause neurological symptoms; this effect is augmented by certain nonsteroidal anti-inflammatory drugs. Quercetin, a flavonol, occasionally used as a dietary supplement, may interact with fluoroquinolones, as quercetin competitively binds to bacterial DNA gyrase. Some foods, such as garlic and apples, contain high levels of quercetin; whether this inhibits or enhances the effect of fluoroquinolones is not entirely clear. Ciprofloxacin can reduce phenytoin plasma levels, which may, in some cases, result in seizures. Ciprofloxacin may interfere with the levels of thyroid medications resulting in hypothyroidism.

"Coadministration of ciprofloxacin with other drugs primarily metabolized by CYP1A2 results in increased plasma concentrations of these drugs and could lead to clinically significant adverse events of the coadministered drug".

Concurrent administration of ciprofloxacin with magnesium or aluminum antacids, sucralfate or products containing calcium, iron, or zinc (including multivitamins or other dietary supplements) may substantially decrease the absorption of ciprofloxacin, resulting in serum and urine levels considerably lower than desired.

1.4.10 Effect of overdose of ciprofloxacin

Overdose of ciprofloxacin is very serious. It may result in reversible renal toxicity. Treatment of overdose includes emptying of the stomach via induced vomiting or by gastric lavage. Careful monitoring and supportive treatment, monitoring of renal function and maintaining adequate hydration is recommended by the manufacturer. Administration of magnesium, aluminum, or calcium containing antacids can reduce the absorption of ciprofloxacin. Hemodialysis or peritoneal dialysis removes only less than 10 percent of ciprofloxacin. Ciprofloxacin may be quantitated in plasma or serum to monitor for drug accumulation in patients with hepatic dysfunction or to confirm a diagnosis of poisoning in acute overdose victims.

1.4.11 Bacterial resistance of ciprofloxacin

Ciprofloxacin has different types of uses. It is commonly used for urinary tract and intestinal infections (traveler's diarrhea) and was once considered a powerful antibiotic of last resort, used to treat especially tenacious infections. Not all physicians agreed with this assessment, as evidenced by its widespread use to treat minor infections as well as non-approved uses. As a result in recent years many bacteria have developed resistance to this drug, leaving it significantly less effective than it would have been otherwise.

Resistance to ciprofloxacin and other fluoroquinolones may evolve rapidly, even during a course of treatment. Numerous pathogens, including *Staphylococcus aureus*, enterococci, and *Streptococcus pyogenes* now exhibit resistance worldwide. Widespread veterinary usage of the fluoroquinolones, particularly in Europe, has been implicated.

1.5 Coordination

Coordination is the donation of electron pair or one-sided sharing of electrons. Coordination compounds are also known as complex compounds. These are the chemical substances formed by the combination of components which are capable of independent stable existence[25]. In complex compounds, the neutral molecules or ions which are attached with the central ion, are called ligands.

According to Lewis concept, in most of the coordination compounds the ligands act as Lewis bases and the central ion acts as Lewis acid, i.e. in most of the complex compounds the ligands donate one or more electron pair to the central metal ion. In some complex compounds the ligands also acts both as donor and acceptor.

$$M^{n+} \quad + \quad xL \quad \rightarrow \quad [MLx]^{n+}$$

(Central metal ion) (Ligand) (Complex compound)

The atom in a ligand which actually donate the electron pair to the central metal ion is called donor atom. The ligands are attached with the central metal ion through their donor atom (or atoms).

Conventionally complex compounds are formulated as consisting of a central atom or ion surrounded by ligands (a set of other atoms, ions or small molecules). When the above resulting conglomeration is charged, it is called complex ion.

The stability of a complex ion or species is governed by some metal factors as well as some ligand factors. Metal factors are: **i)** charge and size, **ii)** variation in d-orbitals, **iii)** number of electrons in the d-orbitals, **iv)** electronegativity of the metal. Ligand factors are: **i)** electron donating capacity of the donor atom in the ligand, **ii)** basicity of the ligand, **iii)** chelate effect, **iv)** ring size, **v)** steric effect of the large ligands, **vi)** entropy effect, **vii)** π-bonding effect of ligand.

1.6 Biological Role of Metals and its Complexes

One of the most serious problems, facing the world today is the contamination of the environment by toxic metals. One area of particular interest is the detection of heavy metals and metalloids in environmental matrices, complexation with chelating agents to reduce the degree of toxicity, characterization and the elucidation of their pathways through various environmental compartments. Focalizing on their degree of toxicity[26] metal and metalloid ions can be divided into three groups. The metal or metalloids of the first group are toxic at all the concentrations and have no known biological functions; this group includes lead, cadmium and mercury. The ions of the second group includes arsenic, bismuth, indium, antimony and thallium; they also

have no known biological functions, but are less toxic. However, they are still toxic if present in more than trace concentration (ppm level). The final groups includes essential trace metals or metalloids such as Zinc, Copper, Nickel, Cobalt, Manganese, Iron, Selenium which are required for various biochemical and physiological processes are toxic above certain concentrations.

1.6.1 Chromium

In foods and waters, trivalent chromium (Cr(III) or Cr^{3+}) occurs in trace amounts and appears to be benign[17]. In contrast, hexavalent chromium (Cr(VI) or Cr^{6+}) is very toxic and mutagenic when inhaled. Cr(VI) has not been established as a carcinogen when in solution, although it may cause allergic contact dermatitis (ACD).

Deficiency of chromium, involving a lack of Cr(III) in the body, or perhaps some complex of it, such as glucose tolerance factor is controversial, or is at least extremely rare.

The LD50 for chromium(VI) ranges between 50 and 150 mg/kg[27]. In the body, chromium(VI) is reduced by several mechanisms to chromium(III) already in the blood before it enters the cells. The chromium(III) is excreted from the body, whereas the chromate ion is transferred into the cell by a transport mechanism, by which also sulfate and phosphate ions enter the cell. The acute toxicity of chromium(VI) is due to its strong oxidational properties. After it reaches the blood stream, it damages the kidneys, the liver and blood cells through oxidation reactions. Hemolysis, renal and liver failure are the results of these damages. Aggressive dialysis can improve the situation[28].

Chromium salts (chromates) are also the cause of allergic reactions in some people. Chromates are often used to manufacture, amongst other things, leather products, paints, cement, mortar and anti-corrosives. Contact with products containing chromates can lead to allergic contact dermatitis and irritant dermatitis, resulting in ulceration of the skin, sometimes referred to as "chrome ulcers". This condition is often found in workers that have been exposed to strong chromate solutions in electroplating, tanning and chrome-producing manufacturers.

1.6.2 Manganese

Manganese has very important roles in the biological systems. It is an essential trace nutrient in all forms of life. The classes of enzymes that have manganese cofactors are very broad, and include oxidoreductases, transferases, hydrolases, lyases, isomerases, ligases, lectins, and integrins. The reverse transcriptases of many retroviruses (though not lentiviruses such as HIV) contain manganese. The best-known manganese-containing polypeptides may be arginase, the diphtheria toxin, and Mn-containing superoxide dismutase (Mn-SOD).

Human body contains about 12 mg of manganese, which is stored mainly in the bones; in the tissue, it is mostly concentrated in the liver and kidneys. In the human brain, the manganese is bound to manganese metalloproteins, most notably glutamine synthetase in astrocytes.

This metal is also important in photosynthetic oxygen evolution in chloroplasts in plants. The oxygen-evolving complex (OEC) is a part of photosystem II contained in the thylakoid membranes of chloroplasts; it is responsible for the terminal photooxidation of water during the light reactions of photosynthesis, and has a metalloenzyme core containing four atoms of manganese. For this reason, most broad-spectrum plant fertilizers contain manganese.

1.6.3 Nickel

Nickel plays important roles in the biology of microorganisms and plants. In fact,

urease (an enzyme that assists in the hydrolysis of urea) contains nickel. The NiFe-hydrogenases contain nickel in addition to iron-sulfur clusters. Such [NiFe]-hydrogenases characteristically oxidise H_2. A nickel-tetrapyrrole coenzyme, Cofactor F430, is present in the methyl coenzyme M reductase, which powers methanogenic archaea. One of the carbon monoxide dehydrogenase enzymes consists of an Fe-Ni-S cluster[138]. Other nickel-containing enzymes include a rare bacterial class of superoxide dismutase and glyoxalase I enzymes in bacteria and several parasitic

eukaryotic trypanosomal parasites (this enzyme in higher organisms, including yeast and mammals, uses divalent zinc, Zn^{2+}).

Nickel sulfide fume and dust are believed carcinogenic, and various other nickel compounds may be as well. Nickel carbonyl, $[Ni(CO)_4]$, is an extremely toxic gas. The toxicity of metal carbonyls is a function of both the toxicity of the metal as well as the carbonyl's ability to give off highly toxic carbon monoxide gas, and this one is no exception; nickel carbonyl is also explosive in air. Sensitized individuals may show an allergy to nickel, affecting their skin, also known as dermatitis. Sensitivity to nickel may also be present in patients with pompholyx. Nickel is an important cause of contact allergy, partly due to its use in jewellery intended for pierced ears. Nickel allergies affecting pierced ears are often marked by itchy, red skin. Many earrings are now made nickel-free due to this problem.

1.6.4 Copper

Rich sources of copper include oysters, beef and lamb liver, Brazil nuts, blackstrap molasses, cocoa, and black pepper. Good sources include lobster, nuts and sunflower seeds, green olives, avocados, and wheat bran. Copper proteins have diverse roles in biological electron transport and oxygen transportation, processes that exploit the easy interconversion of Cu(I) and Cu(II).

Copper is also a component of other proteins associated with the processing of oxygen. In cytochrome c oxidase, which is required for aerobic respiration, copper and iron cooperate in the reduction of oxygen. Copper is also found in many superoxide dismutases, proteins that catalyze the decomposition of superoxides, by converting it (by disproportionation) to oxygen and hydrogen peroxide:

$$2\ HO_2 \rightarrow H_2O_2 + O_2$$

Copperiedus refers to the consequences of an excess of copper in the body. Copperiedus can occur from eating acid foods cooked in uncoated copper cookware, or from exposure to excess copper in drinking water or other environmental sources.

Copper in the blood exist in two forms: bound to ceruloplasmin (85–95%) and the rest "free" loosely bound to albumin and small molecules. Free copper causes toxicity, as it generates reactive oxygen species such as superoxide, hydrogen peroxide, and the hydroxyl radical. These damage proteins, lipids and DNA.

Chronic (long-term) effects of copper exposure can damage the liver and kidneys. Mammals have efficient mechanisms to regulate copper stores such that they are generally protected from excess dietary copper levels.

1.6.5 Zinc

Zinc is an essential trace element, necessary for plants, animals, and microorganisms. Zinc is found in nearly 100 specific enzymes (other sources say 300), serves as structural ions in transcription factors and is stored and transferred in metallothioneins.

There are 2-4 grams of zinc distributed throughout the human body. Most zinc is in the brain, muscle, bones, kidney, and liver, with the highest concentrations in the prostate and parts of the eye. Semen is particularly rich in zinc, which is a key factor in prostate gland function and reproductive organ growth.

In humans, zinc plays "ubiquitous biological roles"[29]. It interacts with "a wide range of organic ligands",[29] and has roles in the metabolism of RNA and DNA, signal transduction, and gene expression. It also regulates apoptosis.

Although zinc is an essential requirement for good health, excess zinc can be harmful. Excessive absorption of zinc suppresses copper and iron absorption. The free zinc ion in solution is highly toxic to plants, invertebrates, and even vertebrate fish. The Free Ion Activity Model is well-established in the literature, and shows that just micromolar amounts of the free ion kills some organisms. A recent example showed 6

micromolar killing 93% of all *Daphnia* in water[30].

1.7 Cyclic Voltammetric Study

Voltammetry comprises a group of electroanalytical methods in which information about the analyte is derived from the measurement of current as a function of applied potential during an electrolysis that is carried out under conditions that encourage polarization of the indicator, or working electrode.

In other words, voltammetry is essentially an electrolysis on a microscale, using a micro working electrode. As the name implies, it is a current-voltage technique. The potential of the micro working electrode is veried (scanned slowly) and the resulting current is recorded as a function of applied potential. The recording is called a voltammogram .

Cyclic voltammetry is the most widely used technique for acquiring qualitative information about electrochemical reactions. The power of cyclic voltammetry results from its ability to rapidly provide considerable information on the thermodynamics of redox processes, on the kinetics of heterogeneous electron-transfer reactions, and on coupled chemical reactions or adsorption processes. Cyclic voltammetry is often the first experiment performed in an electroanalytical study. In particular, it offers a rapid location of redox potentials of the electroactive species and convenient evaluation of the effect of media upon the redox process.

1.7.1 Theory of cyclic voltammetry

The important parameters in a cyclic voltammogram are the peak potentials (E_{pc}, E_{pa}) and peak currents (i_{pc}, i_{pa}) of the cathodic and anodic peaks respectively as well as the half-peak potential ($E_{p/2}$). The number of electrons (n) transferred in the electrode reaction for a reversible couple can be determined from the separation between the peak potentials:

$$\Delta E_p = E_{pa} - E_{pc} = 0.057/n \quad (1)$$

which is valid when the switching potential is at least 100/n mV past the cathodic peak potential. The former potential for a reversible couple is centered between the peak potentials.

$$E^{\circ} = (E_{pc} + E_{pa})/2 \quad (2)$$

For quasi-reversible systems, the reduction potential is given by

$$E^{\circ} \approx (E_{pc} - E_{pa})/2 \quad (3)$$

The peak current (in amperes) for the oxidant (assuming the initial scan is cathodic) is

$$i_p = n^{3/2} F^{3/2} (\pi \nu D_{ox}/RT)^{1/2} A C_{ox} \chi(\sigma t) \quad (4)$$

where $\chi(\sigma t)$ is a tabulated function whose value is 0.446 for a simple, diffusion-controlled electron transfer reaction, R is in $JK^{-1}mol^{-1}$, T is in Kelvin. At 25°C equation (4) reduces to

$$i_p = (2.69*10^5) n^{3/2} A D^{1/2}_{ox} \nu^{1/2} C_{ox} \quad (5)$$

where A is the area of the electrode in cm^2, D is diffusion co-efficient of the species in mol/cm^3, ν is the scan rate in V/sec. this equation is known as the Randle-Seveik equation. To measure accurately peak currents, it is essential to establish the correct baseline. But for more complicated systems, it is difficult. Because the peak may be somewhat broad, so that the peak potential may be difficult to determine, it is sometimes more convenient to report the potential at half the peak height $(E_{p/2})_c$.

For a reversible wave, E_p is independent of the scan rate, and i_p, as well as any other point on the wave, is proportional to $\nu^{1/2}$. A convenient normalized current function is $i_p/\nu^{1/2}C$, which depends on $n^{3/2}$ and $D^{1/2}$. For a simple diffusion-controlled reaction, this current function is a constant independent of the scan rate.

On the reverse scan, the position of the peak depends on the switching potential. Reversibility can also be ascertained by plotting i_{pc} or i_{pa} versus the square root of the scan velocity. The plots should be linear with intercepts at the origin. Since equation (5) is valid for both cathodic and anodic peaks, the ratio of peak currents is unity or a reversible system:

$$i_{pa}/i_{pc} = 1 \quad (6)$$

1.7.2 Application of cyclic voltammetry

The cyclic voltammetry technique has a wide range of applications. It provides information about :

i)reaction reversibilities a very rapid means of analysis of suitable systems,

ii)investigation of stepwise reactions,

iii)qualitative diagnosis of chemical reactions that precede or succeed the redox process,

iv)direct investigation of reactive intermediates,

v)determination of charge transfer rate constants and

vi)evaluation of the interfacial behavior of electroactive compounds.

1.8 Chronoamperometry and Chronocoulometry

The electrochemical excitation in both the chronoamperometric and chronocoulometric experiments is a potential step applied suddenly to an electrode. The response of the ensuring electrode reaction is a current decay with time; in chronoamperometry this current-time curve is the measured response. In chronocoulometry one measures the integral of the current time response, as a charge-time curve. Because of the basic similarity of the two methods, they are considered together.

1.8.1 Theory

In chronoamperometric method current-time dependence is monitored. As mass transport under these conditions is solely by diffusion, the current-time curve reflects the change in the concentration gradient in the vicinity of the surface. This involves a gradual expansion of the diffusion layer associated with the depletion of the reactant, and hence decreased slope of the concentration profile as time progresses. Accordingly, the current (at a planar electrode) decays with time as given by the *Cottrell equation:*

$$\mathbf{i = nFACD^{1/2}\pi^{-1/2}t^{-1/2}}$$

where, n = number of electrons transferred/molecules

F = Faraday's constant (96,500 C mol^{-1})

A = Electrode area (cm^2)

D = Diffusion co-efficient (cm^2s^{-1})

C = Concentration (mol $cm^{-3)}$

Such an $it^{1/2}$ constancy is often termed "Cottrell behavior". Deviations from such behavior occur at long times (usually over 100s) as a result of natural convection effects, or when using microelectrodes with high perimeter-to-area ratios.

Since charge is the integral of current with respect to time, response for the chronocoulometric experiment can be obtained simply by integrating the current response for the chronoamperometric experiment, and is shown in Fig 3.2.1(b). Similarly the equation for Q vs. t curve (the Anson equation) is obtained by integrating the Cottrell equation.

$$\mathbf{Q = 2nFACD^{1/2}\pi^{-1/2}t^{1/2}}$$

Therefore, under these conditions, there is a linear relationship between the charge and the square root of time. A plot of Q vs. $t^{1/2}$ is often reffered to as the Anson plot[31].

1.8.2 Charged Response signal

The charge response signal for a double potential step chronocoulometry is charge due to electrolysis of 'Ox' or 'Red' as in equation (1).

$$\mathbf{Ox+ne=Red} \qquad \mathbf{(1)}$$

It involves application of a positive potential step, causing reduction of 'Ox' at the condition $C_{Red(0,t)}=0$ followed at time τ by negative potential step causing reoxidation of the product Red (generated during $t<\tau$) at the condition $C_{Red(0,t)}=0$. Consider applying to a working electrode a potential step sufficiently negative that the concentration of the reactive species Ox is forced immediately to an essential zero value.

$$\mathbf{C_{Ox(0,t)}=0} \qquad \mathbf{(2)}$$

For an experiment controlled by Ox diffusion, the used initial condition is that of a homogeneous solution at t=0,

$$\mathbf{C_{Ox(x,0)}=C^{b}_{Ox}} \qquad \mathbf{(3)}$$

The boundary condition semi-infinite diffusion is

$$\mathbf{C_{Ox(\infty,t)}=0} \qquad \mathbf{(4)}$$

Applying equation (2) and boundary conditions (3) and (4) to Fick's law for Ox, yields and expression for the concentration of Ox as a function of time and distance from the electrode surface is obtained

$$\mathbf{C_{Ox(x,t)}=C^{b}_{Ox}}\mathit{erf}\mathbf{[}\mathit{x/(2D^{1/2}_{ox}t^{1/2})}\mathbf{]} \qquad \mathbf{(5)}$$

Where erf denotes error function. Diffusion layer thickness is crudely approximated by the term $(Dt)^{1/2}$ cm. The current flow is proportional through Fick's First Law, to instantaneous concentration gradient of Ox at the electrode surface. Accordingly,

$$i=nFD_{Ox}(\partial C_{Ox(0,t)}/\partial x) \quad (6)$$

which when applied to the differentiated equation (5) gives the *Cottrel* equation

$$i=nFC^{b}_{Ox}(D_{Ox}/\pi t)^{1/2} \quad (7)$$

The Cottrel equation shows that diffusion controlled electrolysis of reactant 'Ox' at a planar, stationary electrode gives a current as a $t^{-1/2}$ function which is proportional at any given time to the bulk concentration of electrode reactant. A current vs $t^{-1/2}$ plot is called a Cottrel plot and its linearity (with zero intercept) constitutes a criterion for simple diffusion control of the electrolysis rate. For reversible charge electrolysis rate. For reversible charge transfer simultaneous solution of Fick's law for 'Ox' and 'Red' and use of equation (2) and other appropriate boundary conditions give

$$i=nFC_{Ox}^{b}(D_{Ox}/\pi t)^{1/2}\{1+(D_{Ox}/D_{Red})^{1/2}\exp[nF(E-E^{\circ})/RT]\}^{-1} \quad (8)$$

The chronocoulometric or response of the potential step experiment is elicited from (6) and (8) simply by integrating the current-time equation. For the case of sufficiently negative E_{final} this gives

$$Q=2nFC^{b}_{Ox}(D_{Ox}t/\pi)^{1/2} \quad (9)$$

At times $t<\tau$ the current and charge time curves are described by (5) and (9). Equation (9) shows that the diffusion component to the charge is zero at t=0, yet a plot of the total charge, Q vs. $t^{1/2}$ generally does not pass through the origin, because additional components arise from the double layer charging and from the electroreduction of any Ox molecules that be adsorbed at E_i.

At times $t>\tau$ the oxidation of 'Red' occurs from the diffusion layer of 'Red' created during the negative potential step. The diffusion profile of 'Red' at time τ is thus in effect the initial condition of reverse potential step. The 'Red' diffusion profile is connected to that of 'Ox' by the expression stating that the flux of 'Red' leaving the electrode surface equals that of 'Ox' arriving

$$D_{Ox}(\partial C_{Ox(0,t)}/\partial t)=-D_{Red}(\partial C_{Ox(0,t)}/\partial x) \quad (10)$$

Applying these conditions to a Fick's law solution one can obtain the diffusion profile of 'Red' for $t<\tau$

$$C_{Red(x,t)}=C^{b}_{Ox}(D_{Ox}/D_{Red})^{1/2}erfc[x/(2D^{1/2}_{Ox}t^{1/2})] \quad (11)$$

Where erfc is the complementary error function.

On the basis of equation (11) Christie obtained an expression (12) for i_a when $t<\tau$ for reverse potential step. Consequently,

$$i_a=nFD^{1/2}_{Ox}C^{b}_{Ox}[1/(t-\tau)^{1/2}-1/t^{1/2}]/\pi^{1/2} \quad (12)$$

Consequently,

$$Q_a=2nFD^{1/2}_{Ox}C^{b}_{Ox}[t^{1/2}-(t-\tau)^{1/2}]/\pi^{1/2} \quad (13)$$

Where i_a and Q_a represent the anodic current and charges respectively at time $t>\tau$.

Consider the case in which at t=0, 'Ox' is in equilibrium between its absorbed and solution forms.

Both Ox_{ads} and Ox_{soln} are presumed to be electroactive. Application of a potential step sufficiently negative to produce $C_{Ox\ (soln)\ (0,t)} = C_{Ox\ (ads)\ (0,t)} = 0$ yield the normal diffusional current-time response for electrolysis of Ox_{soln}, but the adsorbed species Ox_{ads} does not require mass transport step prior to reduction and present in a limited amount determined by the surface excess of Ox_{ads} (Γ_o at t=0). To record chronocoulometric (Q-t) response the charge attributable of the Ox_{ads} is considered to be

$$Q_{ads}=nF\Gamma_o \quad (14)$$

The expression for the chronocoulometric response in the presence of reactant absorption is then

$$Q=2nFC^{b}_{Ox}(D_{Ox}t/\pi)^{1/2}+Q_{ads}+Q_{dl} \quad (15)$$

Where C^{b}_{Ox} is the bulk concentration of Ox_{soln} and Q_{dl} is the difference in the charge on the electrode double layer between $E_{initial}$ and E_{final} of the potential step and Q_{ads} represent $F\Gamma_o$ at $E_{initial}$.

The correction for Q_{dl} is obtained from a potential step from $E_{initial}$ to E_{final} in supporting electrolyte solution alone. The chronocoulometric method of adsorption

measurement was used by Christie and co-workers[32].

$$Q=2nFC^{b}_{Ox}(D_{Ox}t/\pi)^{1/2}+nFA\Gamma_{o}+Q_{dl} \quad (16)$$

Double potential step experiment, introduced by Anson[33] and theoretically characterized by Christie and associates[34], eliminates much of the experimental error incurred in the Q_{dl} corrected by acquiring Q_{dl} + Q_{ads} and Q_{dl} data in a single experiment. In a double potential step chronocoulometric experiment with reactant adsorption at $t \leq \tau$ is given by equation (15) and $t > \tau$ [34] is given equation (16)

$$Q_{a}=2nFC^{b}_{Ox}(D_{Ox}t/\pi)^{1/2}[\tau^{1/2}+(t-\tau)^{1/2}]+Q_{ads}(2/\pi\sin^{-1}(\tau/t)^{1/2}) \quad (17)$$

This expression described charge for oxidation of 'Red', differs from the diffusion only equation (11) only by the last term, which accounts for the extra quantity of 'Red' arising from previous reduction of Ox_{ads}. This term is small and well approximated by a simple expression; making such an approximation and now measuring charge as a difference between Q_a and the cathodic charge at τ gives

$$Q_{r}-Q_{a}=2nFC^{b}_{Ox}(D_{Ox}t/\pi)^{1/2}[1+a_{1}\Gamma_{o}\pi^{1/2}/(2C^{b}_{Ox}D^{1/2}_{Ox}\tau^{1/2})][\tau^{1/2}+(t-\tau)^{1/2}-$$
$$t^{1/2}]+a_{o}Q_{ads}+Q_{dl} \quad (18)$$

The term a_o and a_1 are constants and typical values are a_o = -0.0688 and a_1 = 0.970.

These theory assumes, in expressing the Q_{dl} for E_{init} at $t > \tau$, instantaneous reestablishment of the Ox_{ads} layer after the reverse potential step.

A plot of Q ($t > \tau$) vs. $t^{1/2}-(t-\tau)^{1/2}$ must pass through origin if neither reactant "Ox" nor product "Red" in equation (1) are specifically adsorbed on the electrode surface. If we consider the following equation derived by Kambara[34, 35].

$$Q_{r}=2nFC^{b}_{Ox}(D_{Ox}t/\pi)^{1/2}[\tau^{1/2}+(t-\tau)^{1/2}-t^{1/2}]+Q_{dl} \quad (19)$$

Where

$$Q_{r}=Q_{r}-Q(t>\tau) \quad (20)$$

and

$$Q_{r}=2nFC^{b}_{Ox}(D_{Ox}t/\pi)^{1/2}+Q_{dl} \quad (21)$$

Now if Q value obtained from the time less than τ is plotted versus $t^{1/2}$ and on the same graph $-Q_r$ is plotted versus $[\tau^{1/2}+(t-\tau)^{1/2}-t^{1/2}] = \theta$, there will be two straight lines

which intersects each other at Q = 0 axis with equal slope, if there is no adsorption of reactant or product[36]. Any deviation from such condition means adsorption.

1.8.3 Applications

Chronoamperometry has different applications. Some of these are as follows:

i)measuring the diffusion co-efficient of electroactive species or the surface area of the working electrode.

ii) to record the charge versus time dependence

iii) study of mechanisms of electrode processes and

iv) measuring the quantity of adsorbed reactants.

Chronocoulometry also has some important applications. It is useful for measuring electrode surface areas, diffusion co-efficients, the time window of an electrochemical cell, adsorption of electroactive species and the mechanisms and rate constants for chemical reactions coupled to electron transfer reactions.

1.9 Literature Survey

The placement of the subject of electrode processes in its proper content needs the brief review of the structure of the field of electrochemistry. These observations complementarily laid the foundation of concepts regarding the electrical nature of matter and the nature of electrical phenomena, the study of which occupied much of the activities of chemists and physicists.

M. Q. Ehsan and co-workers[37] have studied the redox behavior of Fe in iron-pyridoxin (vitamin B_6) complex. In this study, iron-vitamin B_6 complex has been prepared and its redox behavior were investigated using cyclic voltammetric method at different pH values using HEPES buffer at carbon paste electrode. They have found the Fe(II)/Fe(II) system with respect to this complex to be irreversible, which has been concluded on the basis of the peak current ratios and the peak separation potentials.

Another cyclic voltammetric study on the Fe(II)/Fe(II) system in iron-saccharin and iron-saccharin-phenanthroline complex have been done by the same group[38]. In this work, the redox behavior of iron (in the complexed form) has been studied firstly in the presence of only primary ligand (saccharin) as well as in the presence of a secondary ligand (phenanthroline). In the aqueous medium, Fe(II)/Fe(II) redox

process in iron-saccharin complex has been found to be a diffusion controlled and quasi-reversible. But in iron-saccahrin-phenanthroline complex it has shown much similarity with ideal reversible system. In the presence of secondary ligand, the peak separation has also been decreased. In both the cases, peak separation have decreased with increasing pH values. The system is quasi-reversible in this case.

An interesting work on the redox behavior of As(II) and As(V) in the presence of cysteine and methionine has been done[39]. Here in the aqueous medium As(III) has shown two cathodic and two anodic peaks. And As(V) has given one pair of anodic and cathodic peak. Their interactions with the ligands mentioned above have also been accomplished. As the amounts of both type of As increased in the presence of the two ligands, the current has been increased. This means that with the increase in the amount of the electroactive species, the amount of current is increased.

The interaction of copper with glutamic acid has been investigated using cyclic voltammetric technique[40]. Glassy carbon electrode was used as working electrode and 0.1 M KCl has been used as supporting electrolyte. The redox behavior of copper in absence and presence of glutamic acid are described. Interaction of copper with glutamic acid at different environment of counter ions (Cl^-, NO_3^-, SO_4^{2-}) are described. Similar investigations were done in the aqueous medium in absence of supporting electrolyte.

Works on the interaction of Fe(II) and Fe(II) with ranitidine have also been accomplished at different working electrode using sulphuric acid and nitric acid as the medium adopting the cyclic voltammetric technique[41]. The redox process in the case of Fe(II) at GCE has been found to be adsorptive controlled. Again the interaction of Fe(II) with ranitidine has been noticed by a decrease in peak current. This decrease in peak currents has given successively lower values with the increase in the mole fraction of the ligand. The same findings has been shown at different pH values. At Au and Pt electrodes, also have given the same results. In case of the interaction between Fe(III) and ranitidine, similar observations have been found.

The electrochemical redox behavior of Mn(II)/Mn(IV) system at different environment have been investigated using cyclic voltammetry[42]. In the CV two pairs of well defined cathodic and anodic peaks appear for transfer of two electrons in two

separate steps. The peak position and peak currents are different for uncoordinated and coordinated manganese. The electrode processes are diffusion controlled. The effect of pH on the redox behavior of Mn(II)/Mn(IV) system has been studied using acetate buffer. Extent of interaction between Mn(II) and aspartic acid has also been

studied.

Another work has been done on the interactions of Fe(II) and Fe(II) with 2,6 diacetyl pyridine using cyclic voltammetric method[43]. This also have shown that that after interactions the peak currents have been decreased to a greater extent, indicating towards successful interaction.

An interesting research work done by R. J. Mannan and co-workers[44] has reflected the interaction between cystein and Fe(III). Here the redox behavior of cystein has been changed in the presence of Fe(II) at Pt electrode. The reduction wave have been shifted to more cathodic value with increased peak height, while on the anodic cycle, two peaks of reduced heights are found, which has concluded that the extent of complexation of Fe(III) with cystein is relatively insignificant. At GC electrode no complexation between Fe(III) and cystein has been observed.

Cyclic voltammetric characteristics at a GC electrode coated with a N_f (nafion) membrane incorporating RP (denoted as GC/N_f[RP]) soaked in a pH 1.5 HCl-KCl aqueous solution has been compared with neat RP (denoted as GC/RP), where RP means iron(III) ruthenocyanide, Ruthenium purple. In both the systems a redox couple of Fe(III)/(II) in RP has been observed at the same position[45]. But the peak separation between the oxidation and reduction peaks has been found to be larger for the GC/N_f[RP], showing a slower kinetics of the electrode reaction than for the neat RP.

Voltammetric studies for determining complexation ratio has also been done. It has been found that in case of copper, the formation of 1:5 (Cu-glycine) species is about 80%, and of 1:3 (metal:glycine) species is more than 80% for zinc and more than 60% for cadmium[46]. An initial study of the possibilities of cyclic voltammetric techniques in the simultaneous determination of mixtures of oxidizable amino acids was done by J. Saurina and others. CVs of the mixtures of these amino acids can be used as multivariate data for the determination of such amino acids. Hence these oxidizable

amino acids can be quantified in complex mixtures from a simple recording of the voltammogram[47].

R. J. Mannan *et al* studied voltammetric behavior of cysteine with Fe(II), Cu(II), and Zn(II) ions at Pt and glassy carbon electrodeand determined charge transfer rate constant, R_f values which show an order of Fe(II)-cysteine<Cu(II)-Cysteine<Zn(II)-Cysteine[48].

M. Q. Ehsan and his coworkers studied the electrochemical behavior of copper-aspartic acid complex at glassy carbon electrode in aqueous acetate buffer medium and found the irreversible redox behavior of the dissolve complex[49].

A. H. Khan *et al* reported the electrochemical behavior of copper-glutathione interactions at thin mercury film electrode in artificial sea water based on differential pulse anodic stripping voltammetry (DPASV)[50]. from the analysis of the pseudo-voltammograms, it was observed that the electrode processes for Cu^{2+} ion and CuGSH complexes in ASV are reversible. The DeFord and Hume formation, $F_j([X])$, for reversible reactions, confirmed the formation of the complexes CuGSH, $Cu(GSH)_2$, $Cu(GSH)_3$ and $Cu(GSH)_4$ and the overall formation constants, log β_j , in the range 7.95 to 29.5.

From the potentiometric studies on ternary complexes formation between Zn(II) and sulphur containing ligands such as L-Cysteine, D-penicillamine, L-cysteic acid and imidazole histamine and L-histidine by F. Nair *et al* in aq. Perchlorate medium. The mixed ligand complex species $ZnABH_2$, ZnABH, ZnAB or $ZnAB_2$ were detected in addition to various binary species due to ligands A and B. proton is affected with the primary ligand (H) and the other with the secondary ligand, the primaryligands binds the metal in a bidentate manner and the secondary ligands bind the metal, in a uni, bi and tetradentate manner[51].

Formation constants of ternary complexes MLA, where M=Cu(II) or Ni(II), L=2,2′,2″-terpyridine and A=alanine, phenylalanine, tyrosine, tryptophan, threonine, methionine or histidine were determined by Yogi *et al* pH metrically in aq. Solution at 35.0˚C and 0.2 M (KNO_3). It was assured in terms of the parameter log K with respect to the metal ion, Cu(II) ternary complexes are substantially unstable relative to the corresponding Ni(II) complexes[52].

Gockel *et al* determined the compositions and stabilities of different complexes of Zinc with cysteine, histidine and their derivatives by potentiometric technique. The stabilities of Zn complexes of cysteine and histidine were detd. Together with those three derivatives. Of equal in which one of their three donor functions (carboxyl, amino and mercapto and imidazole respectively) was blocked. By using potentiometric titration of aq. Solutions, the 1;1 and 1:2 complexes of all four cystein and all four histidine derived ligands were observed. All cysteine derived complexes are more stable than the corresponding histidine derived complexes by 1-2 orders of magnitude for the 1:2 compound. For the cysteine series, the sequence of stabilities is cysteine > cysteine Et ester >> N(alpha) amylcysteine >> S-methylcysteine. For the histidine series, the corresponding sequence is histidine > histidine Me ester > N,N-imidazole-dimethylhistidine > N(alpha) acetyl histidine. The order of stabilities can be explained by the relative strength of the Zn-S and Zn-N coordination, by charge effects and by chelate ring sizes[53].

Electrophoretic studies on determination of stability constants of Zn(II) and Cd(II) mixed complexes (M = methionine-cysteine system) were carried out by B. B. Tiwari and his coworkers. The stability constants of different complex species of some metal ions viz. Zn^{2+} and Cd^{2+} with methionine were determined electrophoretically at ionic strength 0.1 M perchloric acid and 85˚C. The stability constants of the complexes M(II)-methionine-cysteine 7.30 and 7.62 (log K values) for Zn and Cd(II) complexes[54].

The formation of 1:1:1 mixed ligand metal (M) complexes by Cu(II), Ni(II), Zn(II) and Cd(II) with cis-1,2,3,4-cyclopentanetetracarboxylic acid as primary ligand and L-histidine and L-cysteine as secondary ligands was studied by Gupta and his research groups potentiometrically by employing the modified Irving and Rossotti method. The stability constant and free energy of coordination were determined. At (25 ± 1˚C) in aq. Solution at ionic strength 0.2 M ($NaClO_4$)[55].

The influence of properties and concentration of acetate and alkylsulphate as buffer and ion-pair agents as well as pH value on the complex formation of copper amino acidsqand their UV absorption spectra have been studied by Da, Shilu and Wang. Amino acids show stronger UV absorption with molar absorptivity bove 10^3 at 230-254 nm due to formation of the complex ions of copper-amino acid and their ion pairs

with hexyl sulfonate[56]. Ternary complexes of divalent ions of Co, Ni, Zn, Cd, Mg and Ca with adenosine-5-triphosphate as the primary ligand and glycine, alanine, valine, norvaline, leucine, serine, methionine, threonine, aspartic acid, uracil and thymine as secondary ligands were studied potentiometrically by Koteswar and his coworkers and the formation constants were reported at 35˚C and ionic strength 0.2 M (KNO_3). The difference between the stability constant of the ternary complexes and the corresponding binary complexes are expended quant. In terms of the parameter Δlog K. Ternary complexes of all metal ions containing phenylalanine, tryptophan, uracil or thymine have Δlog K values for ternary complexes of all metal ions with all metal ions with the other ligands are more negative than expected. This trend is more noticeable in ternary complexes containing aspartic acid[57].

Complex formation between Co(II), Ni(II) and Cu(II) and the amino acids (cysteine, cystine and methionine) in the solid state were studied by elemental analysis, IR and electronic spectra and magnetic susceptibilities. The structures of the complexes were established by Omayama *et al*[58].

The formation of complexes of Cu with methionine(I) was studied by Lopez *et. al* in a buffered medium (phthalate + HCl + NaOH) by using voltammetric and polarographic techniques. The concentration of Cu was held constant and that of I, as well as pH, was varied. In a strongly acidic medium, 3 waves approved. At a very low pH, the main process is the absorption of Cl^- on the surface of the Hg electrode. The complex of Cu with I begins to form at pH 5; at this moment, an intermediate wave potential variation of -50 to -100 mV arises. The Cu complex with I in a buffered medium behaves as a labile type complex. Polarographic and voltammetric techniques were studied by Lopez and Gomaloo to study the complex of Cu with methionine(I) in 0.5 M $LiClO_4$ at several pH values and I concentrations. The Cu complex with I is not formed in very acidic medium, i.e. when the amino acid is in the LH_2^+ state; but it begins to form at pH 4. At pH 4, only some of the Cu complexed, with the appearance of 2 waves. The first wave ($E_{1/2}$ = -10mV) is possiblydue to the reduction of Cu(II), and the 2nd ($E_{1/2}$ = -230mV) is due to the Cu-methionine complex[59].

M. Q. Ehsan and Quyser[60] prepared a complex of β-N-oxalyl-α, β-diamino propionic acid (ODAP) with Cu(II) in aqueous medium and suggested the empirical formula [$Cu(C_5H_6N_2O_5).2H_2O$] by comparing the C, H, N data. It was characterized by IR,

UV spectral analysis and the d-values from the powder diffraction photograph. The redox behavior of the compound was examined by cyclic voltammetric analysis. The molecular model suggests distorted octahedral geometry around the central metal atom.

Mixed ligand complexes of saccharin and 4,4′-bipyridyl with Co(II), Ni(II), Cu(II) and Zn(II) were synthesized by in the aqueous medium[61]. Elemental analysis, IR and UV-visible spectral analysis were used to characterize the compounds. From powder photographs d-values are reported. Molecular modeling of the compounds were done to get idea about the structure. Bonding patterns of all the compounds are slightly distorted octahedral.

Farook *et al*[62] determined the composition and stabilities of (1:1) complexes of Cr(II) with number of amino acids including L-proline potentiometrically. A few mixed ligand complexes of chromium with triene and amino acids including L-proline have been reported to be synthesized and characterized by UV, IR and chemical analysis[63].

Isothiocyanato complexes of first row transition metals with quadridentate tripodal ligand, tris(2-aminoethyl)amine, (tren) were prepared and characterized[64]. Empirical formula of the compounds was determined on the basis of elemental analysis. All except Co compounds have the general formula [M(tern0NCS]SCN (M = Mn(II), Ni(II), Cu(II) and Zn(II)). In the case of Co compound, chloride ion remains counter ion. The compounds were examined by IR, UV-vis spectral analysis and X-ray powder pattern. M. Q. Ehsan *et al* also prepared the trivalent metals, Cr(III) and Fe(II) complexes of the same ligand and characterized by C, H, N analyisis and IR, UV-visible spectral analysis[65].

M. Q. Ehsan and his co-workers reported that DL-aspartic acid reacts with Mn(II), Co(II), Ni(II) and Pd(II) to give stable complexes[66]. It forms 1:1 complexes with Co(II) and Ni(II), where both the carboxylic acid groups remain deprotonated, 2:1 complexes with Mn(II) and Pd(II), where at least one carboxylic acid group is protonated. He also prepared and characterized mixed ligand complexes, M(ASP)(L).H_2O, M=Hg(II) and Pb(II), ASP=DL-aspartic acid, L=2,2′bipyridyl and 1,10-phenanthroline. DL-aspartic acid reacts witn Zr(IV), Ru(III), Pt(IV) and U(VI) in

the aqueous medium and produces complex compounds of stoichiometry $ZrO(C_4H_6NO_4)Cl.2H_2O$, $Ru(C_4H_5NO_4)$ $1.2H_2O$, $Pt(C_4H_6NO_4)2Cl_3.3H_2O$ and $UO_2(C_4H_5NO_4).2H_2O$[67]. The composition of the complexes were confirmed by elemental analysis and characterized by spectral and thermal analysis.

M. Q. Ehsan *et al* synthesized metal complexes of L-glitamic acid of general formula $M(C_5H_7NO_4).2H_2O$ [M= Co(II), Ni(II), Cu(II) and Zn(II)] in aqueous medium[68]. The compounds are characterized by elemental analysis, IR and electronic spectral analysis, thermal analysis etc. bonding pattern of all the compounds are same, both the carboxylic acid groups are in the deprotonated state and participate in the bond formation with the metal ion. The d-values of the compounds have also been reported.

M. Q. Ehan reported the signals of protons and nitrogens in the ENDOR spectra of the trigonal bipyramidal copper complexes, $[Cu(trenNH_3](ClO_4)_2$ and [Cu(tren)NCS]SCN and separate them by taking the ESR spectra of the same sample at two different micro wave frequencies, and taking ENDOR spectra at the same positions of ESR spectra. The NH_2 protons in the complexes were identified by process of deuteration[69].

DL-aspartic acid reacts with Zn(II), Mo(II), Hg(II) and Pb(II) in aqueous medium to give complexes of stoichiometry $Zn(C_4H_5NO_4).3H_2O$, $(MoO_3)_2NH_4(C_4H_6NO_4)$, $Hg(C_4H_5NO_4).H_2O$ and $Pb(C_4H_6NO_4)NO_3.2H_2O$[70]. These complexes have been characterized by elemental analysis and their IR, NMR, UV, thermal and electrolytic properties studied.

Although the copper salt of leucine was first prepared in 1854 by Gossmann[71], it has been reported that Zn salts (e.g. $ZnCl_2$ / $ZnAc_2$ / $ZnSO_4$) form two complexes such as $Zn(Met)Cl_2$ and $Zn(Met)_2,2H_2O$ in aqueous system which has been characterized by chemical analysis, IR and X-ray diffraction.

When glycine in hot aqueous solution was treated with excess of copper carbonate, the filtrate assumed to be a deep blue color; on condensation of the solution followed by treatment with ethanol, crystals of a compound of copper with glycine in the ratio of 1:2 could be separated as the formulation (Fig 1.6).

N-Phenyl glycine also form similar complex of green color. The glycine-copper complex, however, is non-ionic, and the corresponding bracketed representation possesses no ionic charge. Nevertheless, it seems probable that the carboxylate group may retain its ionic character[72]. The glycine anion forms two covalent bonds with the cupric ion resulting in a five-membered ring, and, in as much as the coordination number of copper is 4.

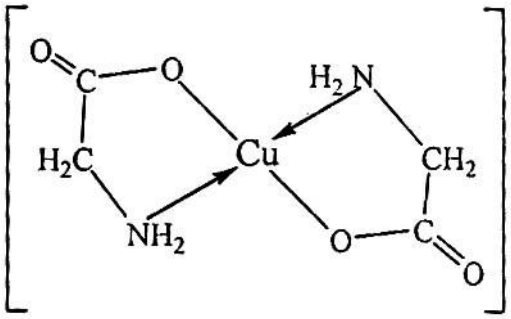

Fig.1.6. The structure of Cu(II)-glycinate

Tschugaeff and Serbin were able to form the triglycine complex with the poorly coordinating chromium atom but were unable to prepare the corresponding tri-β-alanine complex (as well as the tri-γ-aminobutyric acid complex)[73]. Formula (Fig 1.7) of this indicates that Cr^{3+} has a coordination number of 6.

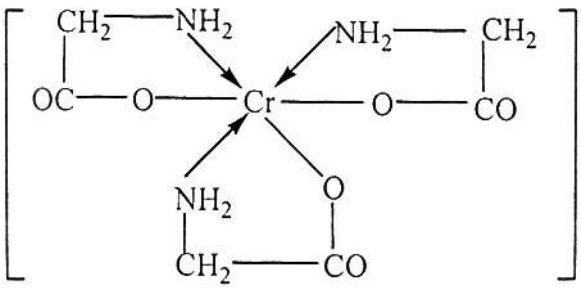

Fig 1.7 The structure of glycine complex of Cr(III).

The empirical formula of the copper complex of aspartic acid, prepared by the interaction of 1 mole of L-aspartic acid and 1 mole of cupric salt is $C_4H_5O_4NCu.nH_2O$, the water of crystallization being rather variable[74].Actually the compound consists of a double molecule whose constitution is $[Cu(C_4H_5O_4N)_2]Cu.nH_2O$, in which copper is both bound and ionic. With the addition of sodium hydroxide to this complex, copper hydroxide precipitates and the ionic copper is replaced by two Na^+ ions to form a new complex, the interior of the brackets remaining the same. This new complex can also be obtained without precipitation of copper hydroxide by treating with disodium aspartate[75]. The metal complexes of the aldehyde derivatives of the α-amino acid esters are extremely interesting representatives of this class of compounds. They are prepared by treating the copper (or nickel) complex of salicyl-aldehyde with the hydrochloric acid salts of the α-amino amino acid esters in the presence of sodium acetate. After being heated briefly in ethanol solution and cooling, olive green crystals of the copper complex with glycine ester or light green rystals of the nickel complex with glycine ester separated.

Another unusual reaction, also by analogy of some biological interest, was involved in the reaction of salicylaldehyde-Cu with leucine ethyl ester-HCl and sodium acetate. A green solution in ethanol resulted, from which no crystals appeared on cooling. After prolonged standing green coloured crystals began to separate, which on analysis indicated the presence of the imino compound. When air was removed from the reaction mixture and the process was carried out anaerobically, the imino complex was not obtained and it would appear that an oxidative degradation, analogous to what occurs in the biological oxidation of α-amino acids had taken place. With diamino acids aand diamino acid esters, still other complexes were obtained[76]. Thus, with L-lysine ethyl ester.HCl, salicylaldehyde-Cu and sodium acetate the complex (Fig 1.8) was obtained.

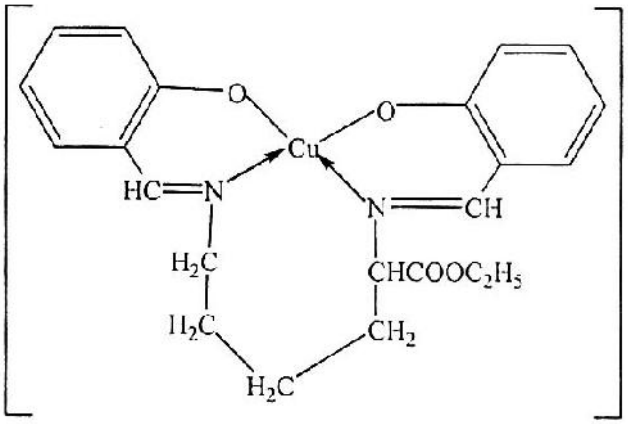

Fig 1.8 The structure of Cu-salicylaldehyde complex with L-lysine ethyl ester.HCl.

With free lysine-HCl under the same conditions the double complex was obtained, which after crystallization from pyridine, contained two molecules of pyridine of crystallization. Copper complexes of amino acid amides were prepared by Rising and Yang as part of their series of studies on the biuret reaction[77]. These complexes were non-conducting in aqueous solution and processes the empirical formula Cu(amino acid amide)$_2$. They were prepared in the absence of alkali and yielded red coloured compounds. The amides so employed were derived from glycine, leucine, alanine and aspartic acid. Proof of its structure was was furnished by Pfeiffer and Saure, who treated diglycyl-o-phenylenediamine with copper acetate and sodium hydroxide to yield blue-violet crystals of copper complex.

In 1887, Schulze and Steiger[78] prepared arginine-cupric sulfate and arginine-cupric nitrate complex. The later complex being used subsequently by Sorensen, Hoyrup and Andersen[79] for the isolation of arginine from protein hydrolysates. The ornithine-cupric nitrate[80], orthinine-cupric sulfate[81] and lysine-cupric chloride[82] were also prepared. Histidine dissolves basic cupric carbonate to form a dark blue solution, thus indicating the formation of a complex, but the later has not been isolated in view of its high solubility. The reaction of lysine monohydrochloride with freshly prepared basic cupric carbonate, $Cu(OH)_2.CuCO_3$, is conducted at a pH too low to convert the ε-amino group to the uncharged form; this group thus possesses a positive charge[83]. The preparation of a number of copper and nickel complexes of the L-amino acids

[(L-amino acid)2M], particularly those of L-alanine, L-isoleucine, L-phenylalanine and L-tyrosine, were described by Pfeiffer and Christeleit[84]; these were generally obtained by heating the amino acid with an excess of copper or nickel carbonate in water, followed by condensation of the filtrate and precipitation with ethanol. Zinc complexes with the amino acids and with glycylglycine were also found to exist in the 1:2 ratio. A measure of the association of various metals with glycine was first undertaken in the classic work of Ley whereby the relative stability of the complexes followed in the order Cu > Ni > Zn ~ Co > Cd > Mn and the procedure employed was that of conductivity. For copper and nickel complexes of formula MA2, the relative stability was glycine > α-alanine > β-alanine[85, 86].

The order of stability of complex formation among the metals is Cu > Ni > Zn > Co > Cd > Fe ~ > Mn > Mg[87], in substantial agreement with that found by Flood and Loras[88] for glycine, namely Hg > Cu > Ni > Zn > Co > Cd, and that found by Maley and Mellor[89] for glycine, alanine and valine, namely Cu > Zn > Co > Mn. Zn is another metal which forms quite stable complexes with histamine and histidine.

The complex electrochemical redox behavior of Mn(II)/Mn(IV) system at different environment have been investigated using cyclic voltammetry[90]. In the CV two pairs of well defined cathodic and anodic peaks appear for transfer of two electrons in two separate steps. The peak position and peak currents are different for uncoordinated and coordinated manganese. The electrode processes are diffusion controlled. The effect of pH on the redox behavior of Mn(II)/Mn(IV) system has been studied using acetate buffer. Extent of interaction between Mn(II) and aspartic acid has also been studied.

The detailed redox behavior of copper-saccharin (Cu-sac) complex was examined using the cyclic voltammetriv technique. It was found that the adsorption process suppresses the Faradaic process of the Cu-sac complex. The effect of the introduction of secondary ligands such as 1,10-phenanthroline(phen), pyridine(py) and bypyridine(bp) on the redox behavior of the Cu-sac complex in aqueous solution was studied where these ligands contribute on the charge transfer kinetics of the complex. The heterogeneous charge transfer rate constants are found to follow the order $Cu(NO_3)_2$ > Cu-sac-bp > Cu-sac > Cu-sac-phen > Cu-sac-py[91].

Cobalto-bis and tris-cysteine are each coordinated via the amino and sulphydryl groups; in the bis compound two molecules of water are involved in coordination with the cobalt. Coordination in the green-tris-cysteinate was apparently through the sulphydryl and amino groups, whereas in the isomeric red tris-cysteinate coordination with cobalt was through sulphydryl and carboxyl group[92, 93] (Fig 1.9).

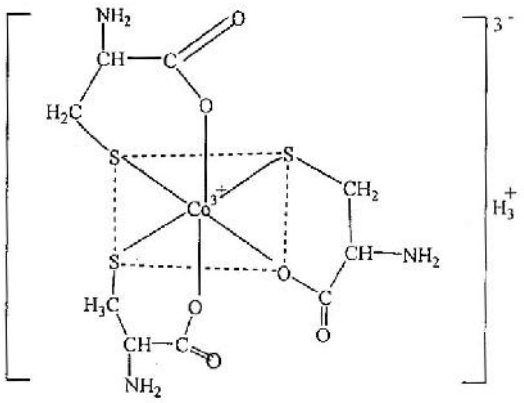

Fig 1.9 The structure of Co(III) tris-cycteine.

1.10 Aim of the Work

In this competitive world of globalization, industrial problem oriented academic research has a great importance. Continuous up gradation in every sphere of life has proved the necessity of the research in every discipline of the society. From this perception I would like to plan my Doctoral research related with pharmaceutical industrial demand. In the past few decades, there has been a hiatus in the momentum of research and discovery of 'Novel' medicinal compounds. In the early nineteenth century, the people has extracted pure substances from plant materials. These substances were of consistence quality but only a few of the compounds isolated proved to be satisfactory as therapeutic agents and even for commercial demand. A change in attitude towards drug safety in the early nineteenth century coupled with the toxicity of compounds derived from natural sources has drastically reduced their use in recent years while the searching of new synthetic patent drugs are increasing rapidly due to more facilitated in commercial use. One of the major factors leading to more rational approach to new drugs has provided knowledge of biological mechanisms. In the past three decades the biological sources have undergone a major

redirection towards molecular understanding of biological systems. It is important to understand the broad implications of this trend in research in the modern pharmaceutical industry. The determination of the structure of a biologically active molecule provides a two-fold benefit to pharmacy and medicine. It makes possible research leading to synthesis and modification of the structure. Total synthesis is made possible by the knowledge of chemical structure and in some instance, it is economically important in reducing the cost of the drug. Recently combination drug has brought a dramatic attention and great demand from the clinical and biopharmacological viewpoints due to their efficacy, less toxicity and side effects in the treatment of different diseases. It might be expected complexation of drug with metals may lead to improved bioavailability by increasing solubility of the drug in the gastrointestinal fluid, may lower toxicity or may give a sustained release product when this is required as a medication. Sometimes complexation may increase the solubility of drug which is a very important pharmaceutical aspect during storage.

Again metals have essential catalytic physiological function, in the ionic form, to perform in living systems, including human. Specific organs in human system can be damaged by excess metal ions. Free metal ions are more toxic than metal chelates. Therefore the chelating agents are used in medicine for the formation of soluble easily excreatable metal chelates by sequestering metal ions in the circulation of blood.

Various electrochemical techniques are useful for studying the redox behavior, obtaining information about the mechanism of reaction, knowledge about adsorbed species, reaction intermediates and products. From this large kingdom of electrochemical techniques, cyclic voltammetry has been chosen for this present study because of its effectiveness in investigating the redox behavior of electroactive species. Another technique named chronoamperometry and its integrated form, which is known as chronocoulometry has also been employed in the present study to observe the adsorption phenomena of the electroactive species.

The principal aim of the present work was to synthesize new biologically important molecules using Quinolone derivatives (Ciprofloxacin) and metal ions (Cr^{3+}, Mn^{2+}, Ni^{2+}, Cu^{2+} and Zn^{2+}), characterization and their electrochemical studies.

i) to synthesis new molecules which are the combination of nutritional suppliments and have a biological importance.

ii) to characterize the new species by physicochemical, chemical and spectral analysis.

iii) the development of analytical methodologies to ensure the quality of the new pharmaceutics.

iv) to investigate actual biological process occurring in human system by the in vitro study of the complexes.

v) to study the redox behavior of the metals by electrochemical studies.

vi) the studies of the toxic metals complexes will provide new informations about the alteration of the degree of toxicity for chelation and even about the activities of this element in the biological system.

To achieve the above objectives the following steps were carried out in the present study

1. Preparation of some metal compounds of Ciprofloxacin with metals like Cr(III), Mn(II), Ni(II), Cu(II) and Zn(II).
2. Characterization of the compounds by means of
   a) Elemental analysis for the determination of molecular composition.
   b) Estimation of metal content by titrimetric methods.
   c) Spectral analysis by UV-visible, FTIR and NIR spectrophotometer.
3. Investigation of some physical properties such as solubility and melting temperature determination.
4. Conductance study of the compounds.
5. DSC (Differential scanning calorimetry) analysis of the compounds.
6. Electrochemical studies
   a) Study of the redox behavior by Cyclic voltammetric technique of
      i) free ligands
      ii) free metals
      iii) metal-ligand interactions in solution and
      iv) metal-ligand compounds and their concentration effect.
   b) Investigation of the adsorption criterion by Chronoamperometric as well as chronocoulometric technique of

i) free ligands

ii) free metals

iii) metal-ligand compounds and their concentration effect and

iv) metal-ligand interactions in solution.

7. Antibacterial activity test of Metal-Ciprofloxacin compounds.

2 EXPERIMENTAL

Materials, Methods and Equipments

The redox behavior of Ciprofloxacin, a quinolone derivative and few biologically important metal ions as well as Ciprofloxacin-metal interactions were studied using different electrochemical chemical methods. The sources of different chemicals, the instruments and brief description of the methods are given below.

2.1 Chemicals

The supporting electrolyte was prepared employing potassium chloride (MERCK, Germany). Solutions were prepared using ciprofloxacin hydrochloride (Dr. Reddy's Laboratory, India) and the chloride salts of chromium, manganese, nickel, copper and zinc (all of MERCK, Germany). Cleaning of the electrodes and all the solutions were prepared using de-ionized water. 99.997% Nitrogen was used for purging purpose.

2.2 Electrochemical Methods

2.2.1 Cyclic voltammetry

The voltammetric cell: A voltammetric cell consists of the micro working electrode, the auxiliary electrode and a reference electrode. The three electrodes are immersed in the sample solution. With a three electrode system, the recorded potential is that between the working electrode and the reference electrode, with essentially no flow of current and no distorting iR drop. The working electrode is the electrode at which the reaction of the interest occurs. The reference electrodes provides a stable and reproducible potential (independent of the sample composition), against which the potential of the working electrode is compared. An inert conducting material such as platinum wire or graphite rod is usually used as the current carrying auxiliary electrode.

Solvents and supporting electrolytes: Electrochemical measurements are commonly carried out in a medium that consists of solvent containing a supporting electrolyte. The choice of the solvent is dedicated primarily by the solubility of the analyte and its

redox activity, and by solvent properties such as the electrical conductivity, electrochemical activity and chemical reactivity. Water has been used as a solvent more than any other media, nonaqueous solvents [e.g. acetonitrile, propylene carbonate, dimethyl formamide (DMF), dimethyl sulfoxide (DMSO), or methanol] have also frequently been used. Mixed solvents may also be considered for certain applications.

Supporting electrolytes are required in controlled potential experiments to decrease the resistance of the solution, to eliminate electromigration effects and to maintain a constant ionic strength (i.e. "swamping out" the effect of variable amounts of naturally occurring electrolytes). The inert supporting electrolyte may be an inorganic salt (e.g. potassium chloride or nitrate, ammonium chloride), a mineral acid, or a buffer. Buffer systems (such as acetate, phosphate or citrate) are used when a pH control is essential.

The working potential range: The potential range over which voltammetric techniques can be used will depend on the electrode material, the solvent, the supporting electrolyte and the acidity of the solution. If a platinum electrode is used in aqueous solution, the limiting positive potential would be oxidation of water ($H_2O \rightarrow 1/2O_2 + 2H^+ + 2e^-$), unless the supporting electrolyte contains a more easily oxidizable ion (e.g. Cl^-). The negative limiting potential will be from reaction of hydrogen ions.

Carbon electrodes are frequently used for voltammetry. Their positive potential limit will be essentially the same as with platinum electrode, but more negative potential can be reached because hydrogen has a rather high overvoltage on carbon.

Cyclic voltammetric wave form: Cyclic voltammetry consists of cycling the potential of a stationary electrode immersed in a quiescent solution and measuring the resulting current. The excitation signal is a linear potential scan with a triangular waveform (Fig 2.1) and this triangular potential excitation signal sweeps the potential of the working electrode back and forth between two designated values called the switching potentials. At the same speed, the triangle returns and permits the display of a complete voltammogram with cathodic (reduction) and anodic (oxidation) wave forms one above the other.

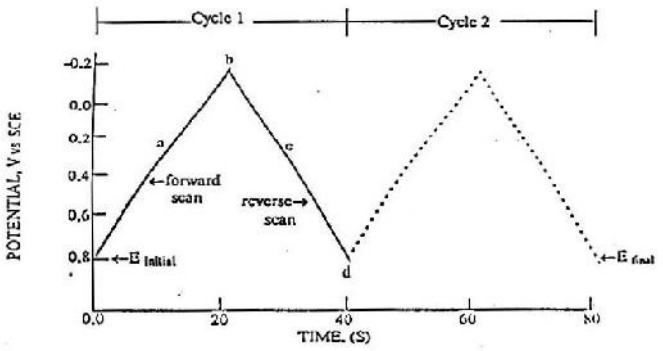

Fig 2.1 A typical excitation signal for cyclic voltammetry.

Mechanism of peak formation in cyclic voltammetry: The current at the stationary working electrode is measured under diffusion-controlled, mass transfer conditions. In the Fig 2.2, when the experiment is initiated, the initial potential applied at point a is chosen to avoid any electrolysis of electroactive species. The potential is then scanned in the negative direction, which becomes sufficiently negative to cause a reduction of an electroactive species at the electrode surface. Then the cathodic current begins to flow at b and increases rapidly until the surface concentration of oxidant at the electrode surface approaches zero, as signaled by the current, now diffusion controlled, peaking at point c. the final rise at point d is caused by the discharge of the supporting electrolyte. The potential is switched to scan in the positive direction at the switching potential. Finally, the electrode potential becomes sufficiently positive to bring about oxidation of the reductant that had been accumulating adjacent to the electrode surface. At this point an anodic current begins to flow and to counteract the cathodic current. The anodic current increases rapidly until the surface concentration of the accumulated reductant approaches zero, at point f, the anodic current peaks. The anodic current then decays as the solution surrounding the electrode is depleted of reductant formed during the forward scan.

2.2.2 Chronoamperometry and chronocoulometry

The metal systems were also studied with chronoamperometric and chronocoulometric techniques which are double potential step processes. The chronoamperometric (CA) experiment gives a current versus time curve, which is known as current response or chronoamperogram. It shows a current spike followed

by a gradual decay in current. The spike is due to initial electrolysis of species at the electrode surface and decay is due to diffusion of molecules to the electrode surface[31].

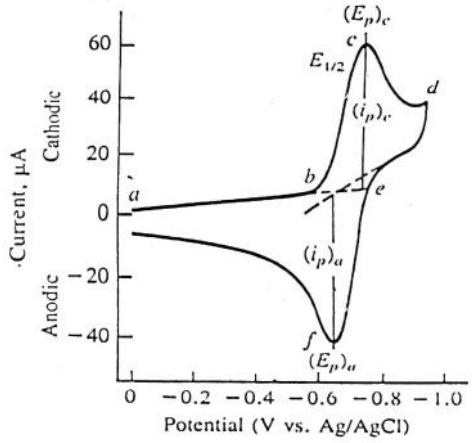

Fig 2.2 A typical schematic cyclic voltammogram.

The forward step, that is, the transition from initial potential (E_1) to first step potential (E_2) at t=0, is that the electrode must instantly reduce the metal from higher oxidation state to lower one,

$$M^{n+} + e \rightarrow M^{(n-1)+}$$

For a period τ, it causes a build up of the reduction product in the region near the electrode.

However, in the second phase of the experiment, after t=τ, the potential returns to E_1, where only the oxidized form is stable at the electrode. The ionic radical produced by reduction cannot coexist there; hence a large anodic current follows as it begins to reoxidize, then the current declines in magnitude[94].

Chrocoulometry (CC) is the integrated form of the chronoamperometry. So that in CC the monitored response is charge. It is also known as chronocoulogram. In the double potential step CC, the potential is stepped from an initial value to a second value and then back to the initial value. The step from initial to the second is termed as forward potential step whereas the step from the second to the initial value is termed as reverse step[94].

Now if Q value obtained from time less than τ is plotted versus $t^{1/2}$ and on the same graph $-Q_r$ is plotted versus $\theta=[\tau^{1/2} + (t - \tau)^{1/2} - t^{1/2}]$, there will be two straight lines which intersects each other at Q=0 axis with equal slope, if there is no adsorption of reactant or product[95]. Any deviation from such condition means adsorption.

Excitations and responses: In a chronoamperometric experiment, a potential step is applied to the working electrode (Fig 2.3(a)) and the resulting current-time response (Fig 2.3(b)) is measured. In the simplest case, the initial working electrode potential (E_{init}) is sufficiently positive that reaction

Ox + ne Red (1)

does not proceed, and the potential attained by the step E_{final} is sufficiently negative to drive the surface concentration of the reactant Ox immediately to zero. The initially large cathodic current rapidly decays as the solution near the electrode surface becomes depleted of Ox. The current-time (i-t) response, or chronoamperogram, is interesting with respect to its shape and magnitude of current at any given time and to its dependency on the value of E_{final}.

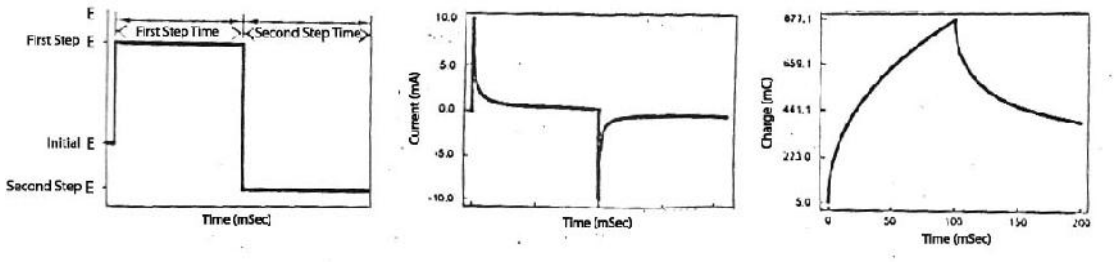

(a) (b) (c)

Fig 2.3 (a) Potential wave form of the double potential step technique, (b) the current response and (c) the charge response.

The chrocoulometric experiment is operationally identical to chronoamperometry except that one integrates the current attributable to reaction (1) and records charge versus time (Fig 2.3 (a) and (b)). While the charge-time measurement is in principle no more informative than the current-time measurement, in practice Q-t data are sometimes more easily interpreted. As in chronoamperometry, parameters of interest in the q-t curve, or chronocoulogram, are shape, amplitude, and dependency on E_{final}. Useful variants of these experiments exist, notably once in which a reverse step excitation follows the initial "forward" one. In such cases reaction (1) is driver in the oxidation direction following application of the reverse step. For chronoamperometry

and chronocoulometry, the reverse E-t curve and transition time (τ), reverse i-t curve shape and amplitude, and reverse Q-t curve shape and amplitude, respectively, are determined by (a) the quantity of species Red generated during the forward electrolysis time and (b) any factors tending to change the recordable part of this amount of Red, such as diffusion of Red away from the electrode surface; any chemical instability of Red; and any adsorption of Red on the electrode surface. A primary use of the reverse step experiments is studying chemical decay pathways of Red.

Mechanisms: There is a current spike followed by a gradual decay in current in the chroamperometric technique. This response can be rationalized by noting that current is a measure of the rate of electrolysis. Since the current is directly proportional to the rate of electrolysis, the current response is a potential step is a current "spike" (due to initial electrolysis of species at the electrode surface) followed by the time dependent decay (due to diffusion of molecules to the electrode surface).

The forward step, that is, the transition from initial potential (E_i) to first step potential (E_2) at t=0, is as follows. First the electrode must instantly reduce the metal nearly to the stable ionic radical, which may be

$$An + e \rightarrow An^-$$

This act requires a very large current but subsequently current is required only because the reduction has created a concentration gradient that produces, in turn, a net flux of metal to the electrode surface[35]. Since this element cannot exist with the electrode at E_2, it must be eliminated by reduction. For a period τ, it causes a build up of the reduction product in the region near the electrode.

However, in the second phase of the experiment, after, t=τ, the potential returns to E_1, where only the oxidized form is stable at the electrode. The ionic radical produced by reduction cannot coexist there; hence a large anodic current follows as it begins to reoxidize, then the current declines in magnitude as the depletion effect sets in[35].

Chronocoulometry is a method in which the current is integrated so that the monitored response is charge, Q[33, 96, 97] . Thus it involves measurement of charge versus time response to an applied potential waveform. Double potential step chronocoulometry is performed by applying a potential step to the working electrode[35, 97, 98]. The potential

is stepped from an initial value to a second value and back to the initial value. The step from initial to the second is termed as forward potential step whereas the step from the second to the initial value is termed as reverse step[35].

2.3 Apparatus

This study was carried out using an Epsilon Electroanalyzer developed by BIOANALYTICAL SYSTEMS, INC. U.S.A. and in a pyrex glass microcell with teflon cap. The Glassy carbon electrode was used as working electrode, Ag/AgCl electrode and Pt wire were used as reference and counter electrodes respectively in the cell. All the electrodes were prepared by BIOANALYTICAL SYSTEMS, INC. U.S.A. An AGE (VELP SCIENTIFICA) magnetic stirrer with a teflon coated magnetic bar was employed for stirring the solutions. A METTLER TOLEDO pH meter was used to measure the pH of the solutions. Preparation of the solutions were done using volumetric flasks (10 mL, 25 mL, 50 mL, 100 ml and 250 mL) and graduated as well as volumetric pipets (5 mL and 10 mL). All glasswares were made of pyrex glass. Cleaning of the working electrode was accomplished using polishing cloth prepared by ADVANCED ANALYTICS, U.S.A.

2.4 Experimental Setup

2.4.1 Computer controlled potentiostat

In this study the current-voltage measurement system was an Epsilon potentiostat developed by BIOANALYTICAL SYSTEMS, INC. U.S.A. A potentiostat system sets the control parameters of the experiment. Its purpose is to impose on the working electrode a cyclic linear potential sweep and to output the resulting current-potential curve. This sweep is described in general by its initial (E_i), switching (E_s) and final (E_f) potentials and scan rates (mV/s).[3]

2.4.2 Electrochemical cell

A three-electrode electrochemical cell was used in this study. The voltammetric cell also contains a teflon cap. The electrochemical reaction of interest takes place at the working electrode and the electrical current at this electrode due to electron transfer is termed as faradaic current. The counter electrode is driven by the potentiostatic circuit

to balance the faradaic process at the working electrode with an electron transfer of opposite direction[3].

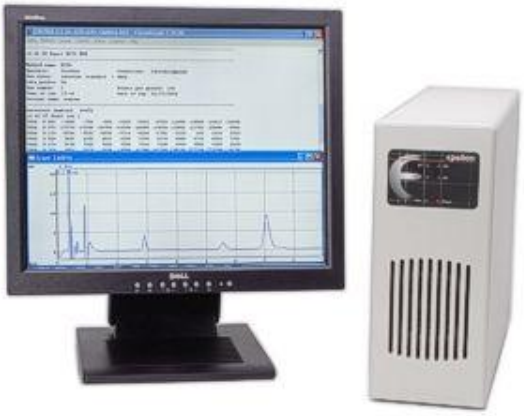

Fig 2.4 Computer controlled potentiostat from BIOANALYTICAL SYSTEMS, INC. U.S.A.

2.4.3 Electrodes

The electrodes used in this study are,

i) Glassy carbon and Platinum solid disk electrode, as the working electrode,
ii) Ag/AgCl (Saturated KCl) electrode as reference electrode,
iii) Pt wire as counter electrode.

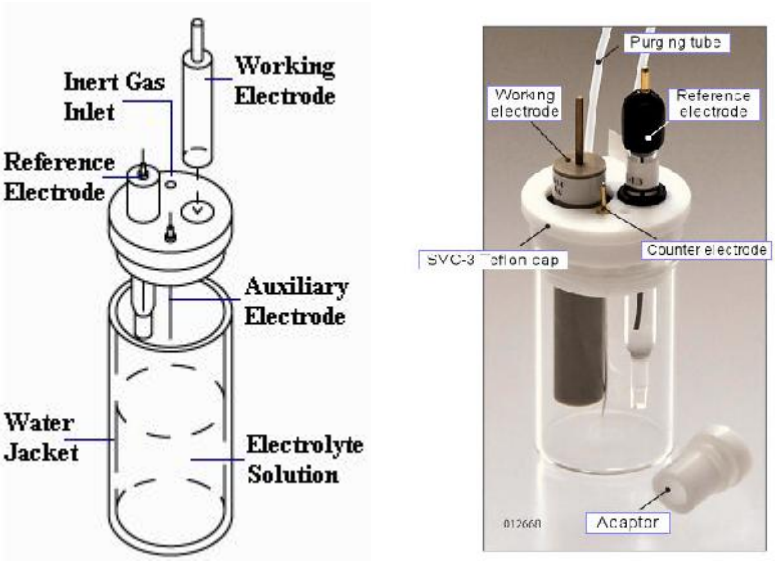

Fig 2.5 Schematic diagram and typical image of an electrochemical cell.

Fig 2.6 Cell stand and arrangement of the electrochemical set up.

Fig 2.7 Glassy Carbon and Platinum working electrodes.

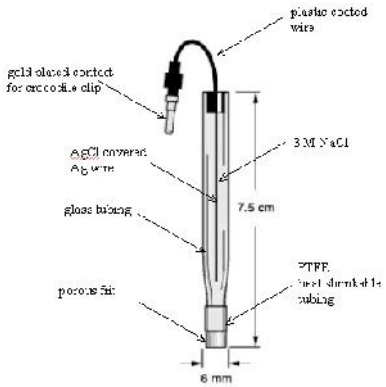

Fig 2.8 An Schematic diagram of Ag/AgCl reference electrode.

Fig 2.9 Platinum wire used as counter electrode.

2.4.4 Nitrogen purging

Before the experiment, it is necessary to remove dissolved oxygen, which has a cathodic signal that can interfere with observed current response. This was done by purging the solution with an inert gas such as N_2 (99.997 %).

2.4.5 Preparation of electrodes

Preparation of the glassy-carbon electrode involves its polishing and washing. It was polished with fine alumina powder on a polishing cloth wet with de-ionized water for about five minutes. After polishing, the electrode was rinsed with a plenty of de-ionized water and was wiped-off with a clean tissue paper. The reference and the counter electrodes were also rinsed with a plenty of de-ionized water before use.

2.5 Preparation of Supporting Electrolyte Solution

0.1 M and sturated Potassium Chloride (KCl) solution was prepared to use as supporting electrolytic solution.

2.6 Preparation of Various Stock Solutions

2.6.1 Stock solution of ciprofloxacin (in KCl)

Stock solutions of ciprofloxacin were prepared in 0.1 M and saturated potassium chloride (KCl) solution.

2.6.2 Stock solution of parent metal salts (in KCl)

Stock solutions of the chloride salts of manganese, nickel, copper and zinc were prepared in 0.1 M potassium chloride (KCl) solution and of chromium was prepared in saturated potassium chloride.

2.6.3 Stock solution of metal-ciprofloxacin compounds (in KCl)

Stock solutions of the ciprofloxacin compounds of manganese, nickel, copper and zinc were prepared in 0.1 M potassium chloride (KCl) solution and of chromium in saturated potassium chloride.

2.7 Precautions

The precautions that must be taken to perform any electrochemical experiments under potentiostatic condition are stated below:

i) the electrode connection should be perfect.

ii) a cell should never be disconnected while the experiment is in progress.

iii) the computer should never be turned off during an experiment.

iv) if the main power turns off, the system should be shut down and all electrode should be disconnected quickly.

3 RESULTS AND DISCUSSION

3.1 Electrochemical Studies of the Metal, Ligand and Metal-Ligand Interactions

Cyclic voltammetry : In the field of electrochemistry, cyclic voltammetry is the most widely used technique for acquiring qualitative information about electrochemical reactions. Cyclic voltammetry is often the first experiment performed in an electroanalytical study. In particular, it offers a rapid location of redox potentials of the electroactive species and convenient evaluation of the effect of media upon the redox process.

In the present study, at first the redox behavior of Ciprofloxacin, Cu(II), Mn(II) and Zn(II) was analyzed using 0.1 N potassium chloride (KCl) as supporting electrolyte. This set of experiment was done using Glassy carbon electrode (GCE) as working electrode. Then another set of analysis was done for Ciprofloxacin and Cr(III) using saturated potassium chloride (KCl) as supporting electrolyte. This was accomplished using Platinum (Pt) electrode as supporting electrolyte. In all the cases Ag/AgCl (Saturated KCl) electrode was used as reference electrode and a Pt wire was used as counter electrode.

After the completion of cyclic voltammetric characterization of Ciprofloxacin and the individual metals, Ciprofloxacin-Metal interactions were also studied. The interactions of Ciprofloxacin with Cu(II), Mn(II) and Zn(II) were done using Glassy carbon working electrode (GCE) in 0.1 M potassium chloride solution. While Ciprofloxacin-Cr(III) interaction was done in saturated potassium chloride solution using Platinum (Pt) working electrode. The ratios for the interactions of Ciprofloxacin with Cu(II), Mn(II) and Zn(II) was 1:1, 1:2 and 1:1 respectively. Again the ratio for Cr(III)-Ciprofloxacin interaction was 1:2.

The studies were done using different potential windows, as potential range depends on the electrode material, the solvent, the supporting electrolyte and the acidity of the solution.

Potential window for Ciprofloxacin was from -2.300 V to 2.000 V in 0.1 M potassium chloride at Glassy carbon electrode (GCE). But it was from -0.900 V to 1.400 V in saturated potassium chloride at Platinum working electrode.

The potential windows were from -0.850 V to 1.180 V for Cu(II), -0.900 V to 1.500 V for Mn(II) and -1.700 V to -0.400 V for Zn(II) in 0.1 M potassium chloride at Glassy carbon electrode (GCE). In addition to this the potential window was found to be from 0.250 V to 1.700 V for Cr(III) in saturated potassium chloride at Platinum electrode.

Finally the potential windows are also found different for different interaction studies. It was found from -1.800 V to 2.000 V for Cu(II)-Ciprofloxacin interaction. For Mn(II)-Ciprofloxacin interaction it was from -1.400 V to 2.000 V. Again for Zn(II)-Ciprofloxacin interaction it is from -1.700 V to -0.400 V. All of these interactions were studied at Glassy carbon electrode (GCE) in 0.1 M potassium chloride (KCl). In addition to these the potential window for Cr(III)-Ciprofloxacin interaction was from -1.000 V to 1.7000 V, for which the working electrode was a Platinum (Pt) electrode and saturated potassium chloride was used as supporting electrolyte.

The above mentioned all the observations were found at room temperature. Scan rate variation for all the systems were also examined. Each system was analyzed at six different scan rates, which were 0.050 Vs^{-1}, 0.100 Vs^{-1}, 0.150 Vs^{-1}, 0.200 Vs^{-1}, 0.250 Vs^{-1} and 0.300 Vs^{-1}.

Chronoamperometry and chronocoulometry : In the field of electrochemistry, chronoamperometry as well as chronocoulometry has achieved their importance in characterizing the rate of electrolysis and adsorption criteria of a system. These experiments are a potential step applied suddenly to an electrode. The response of the ensuring electrode reaction is a current decay with time; in chronoamperometry this current-time curve is the measured response. In chronocoulometry one measures the

integral of the current time response, as a charge-time curve. Because of the basic similarity of the two methods, they are considered together.

In the present study, at first the redox behavior of Ciprofloxacin, Cu(II), Mn(II) and

Zn(II) as well as the interactions of Ciprofloxacin with above metals were analyzed using 0.1 N potassium chloride (KCl) as supporting electrolyte by cyclic voltammetric technique. This set of experiment was done using Glassy carbon electrode (GCE) as working electrode. Then another set of analysis was done for Ciprofloxacin and Cr(III) as well as the interaction between them, using saturated potassium chloride (KCl) as supporting electrolyte. This was accomplished using Platinum (Pt) electrode as supporting electrolyte. In all the cases Ag/AgCl (Saturated KCl) electrode was used as reference electrode and a Pt wire was used as counter electrode. Then with reference to the pair of peaks found, chronoamperometric study was accomplished and the corresponding integrated form, that is the chrococoulometric response is also obtained from it.

For Cu(II) and Mn(II) two sets of chronoamperometric experiments were done as both of them shows two pair of peaks in their cyclic voltammetric study. And for Zn(II) and Cr(III) there are one set of experiment reffering to the only pair of peaks in their CV study. After interactions with ciprofloxacin there were two pair of peak for Cu(II) and so for Cu(II)-Ciprofloxacin interaction there are two sets of chronoamperometric responses. But for the rest other metals there is only set of experiments as in those cases the CV responses are only of one pair.

3.1.1 Cyclic voltammetric study of Cu(II), Ciprofloxacin and Cu(II)-Ciprofloxacin interaction at Glassy Carbon Electrode (GCE).

Redox behavior of Cu(II)

The redox behaviour of Cu(II) (in solution of $CuCl_2$) in 0.1M potassium chloride and at varying scan rate was studied using cyclic voltammetric technique within the potential window from -0.850 V to 1.180 V at room temperature at glassy carbon electrode (GCE). A CV of the above system at scan rate 0.100 Vs^{-1} is given in Fig 3.1.1.

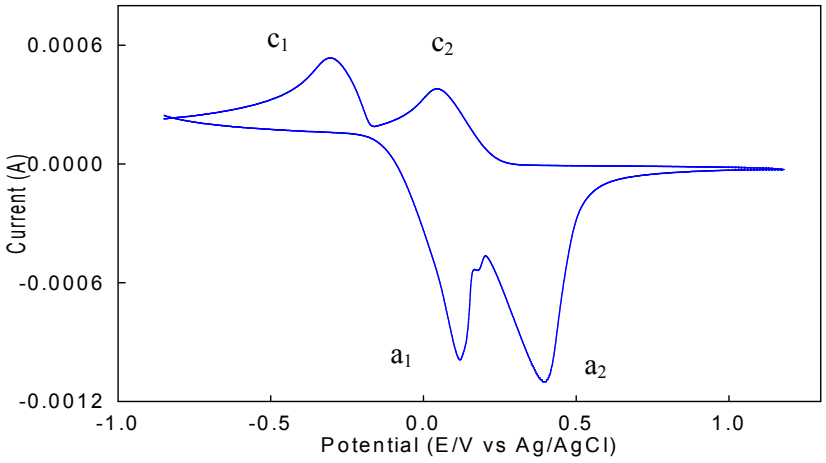

Fig 3.1.1 Cyclic voltammogram of Cu(II) in 0.1 M KCl at scan rate 0.100 Vs^{-1}.

The CV shows two cathodic peaks (c_1 and c_2) at the potentials of -0.297 V and 0.177 V due to reduction of Cu(II) to Cu(I) and Cu(I) to Cu(0) respectively and the same number of peaks in anodic region (a_1 and a_2) at 0.196 V and 0.402 V due to oxidation of Cu(0) to Cu(I) and Cu(I) to Cu(II) respectively. The electrode reaction may be presented by the following equations:

Cathodic reaction: $Cu^{2+} + e \longrightarrow Cu^{+}$

$Cu^{+} + e \longrightarrow Cu^{0}$

Anodic reaction: $Cu^{0} - e \longrightarrow Cu^{+}$

$$Cu^{+} - e \longrightarrow Cu^{2+}$$

The overall reaction is:

$$Cu^{2+} \underset{-e}{\overset{+e}{\rightleftharpoons}} Cu^{+} \underset{-e}{\overset{+e}{\rightleftharpoons}} Cu^{0}$$

The system was also studied at different scan rates. Scan rate may be defined as the fraction of the potential window analyzed per unit time. The size of the diffusion layer above the electrode surface becomes different depending upon the voltage scan rates used. In a slow voltage scan the diffusion layer grows much further from the electrode in comparison to a fast scan. Therefore, the necessity of scan rate variation is beyond description. It is found that with the increase in scan rate, almost all the peaks become broader. Such behavior has been ascribed to slower charge propagation, probably due to difference in salvation and or permeability.

Fig 3.1.2 shows the voltammograms of Cu(II) at different scan rates. With the increase in scan rate both the cathodic peaks shifts towards more negative (or less positive) potential. On the other hand, both the peaks in the anodic region shifts towards more positive potentials. Table 3.1.1 gives the current-potential data for the above system. It is seen that with increasing scan rate (Table 3.1.1), the peak separation potential for both the pair of peaks (ΔE_{p1} and ΔE_{p2}) increases because both the cathodic peak shifts towards negative and those of anodic towards positive. Here the cause responsible is the effect of iR drop. Current passage through either a Galvanic or an electrolytic cell requires a driving force or a potential to overcome the resistance of the ions to move towards the anode or the cathode. Just as in metallic conduction, this force follows Ohm's law and is equal to the product of the current in amperes and the resistance of the cell in Ohms. The force is generally referred to as the Ohmic potential, or the IR drop. This fact occurs because for positive (cathodic) current, the actual working electrode potential is less negative than the applied (measured) potential, while for negative (anodic) current, the

shift is in the positive direction[3]. In short it may be said that it indicates the limitation due to charge transfer kinetics. Plots of ΔE_{p1} and ΔE_{p2} vs ν are shown in Fig 3.1.3.

The peak currents (both in the cathodic and anodic region) increases with increasing scan rate. This can be rationalized by considering the size of the diffusion layer and the time taken to record the scan. The voltammogram takes longer to record as the scan rate is decreased. Therefore, the size of the diffusion layer above the electrode surface becomes

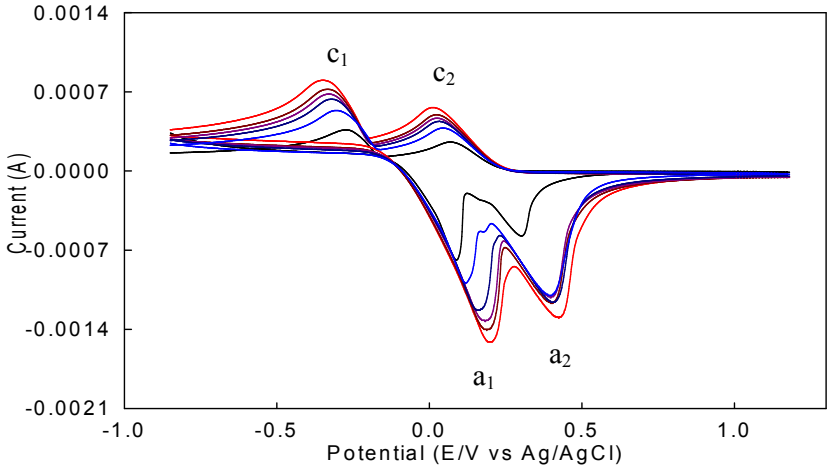

Fig 3.1.2 Cyclic voltammogram of Cu(II) in 0.1 M KCl at different scan rates.

Table 3.1.1 Current-potential data for Cu(II) in 0.1 M KCl at different scan rates.

Scan rate ν (Vs^{-1})	SQRT of scan rate	Cathodic peak potential E_{pc1} (V) [-]	Anodic peak potential E_{pa1} (V)	Cathodic peak current i_{pc1} (μA)	Anodic peak current i_{pa1} (μA) [-]	Peak potential separation $\Delta E_{p1}= E_{pa1}- E_{pc1}$	Peak current ratio i_{pa1}/ i_{pc1}
0.050	0.2236	0.251	0.105	123.23	380.51	0.356	3.09
0.100	0.3162	0.297	0.196	237.61	392.51	0.493	1.65
0.150	0.3872	0.312	0.207	253.14	399.18	0.519	1.58
0.200	0.4472	0.327	0.218	277.82	402.92	0.545	1.45
0.250	0.5000	0.339	0.229	292.58	420.64	0.568	1.44
0.300	0.5477	0.352	0.238	340.13	440.26	0.590	1.29
ν (Vs^{-1})		E_{pc2} (V)	E_{pa2} (V)	i_{pc2} (μA)	i_{pa2} (μA) [-]	$\Delta E_{p2}= E_{pa2}- E_{pc2}$ (V)	i_{pa2}/ i_{pc2}
0.050	0.2236	0.233	0.351	98.65	250.33	0.118	2.54

0.100	0.3162	0.177	0.402	120.55	290.18	0.225	2.41
0.150	0.3872	0.151	0.415	139.05	296.11	0.264	2.13
0.200	0.4472	0.128	0.423	170.74	302.45	0.295	1.77
0.250	0.5000	0.087	0.429	203.19	315.08	0.342	1.55
0.300	0.5477	0.049	0.437	240.58	326.41	0.388	1.36

different depending upon the voltage scan rate used. In a slow voltage scan the diffusion layer grows much further from the electrode in comparison to a fast scan. Consequently, the flux to the electrode surface is considerably smaller at slow scan rates than it is at faster rates. As the current is proportional to the flux towards the electrode the magnitude of the current becomes lower at slow scan rates and higher at high scan rates. Again the CV wave shape becomes more irreversible with higher scan rates. This happens because increasing the scan rate is equivalent to increasing the rate of diffusion to the reduced material from the electrode. As a consequence, the diffusion process competes with the back electron transfer[3]. The general conclusion for this fact is the combination of diffusion and surface control behaviour of the redox system [35, 99].

Again the forward scan peak currents (i_{pc1} and i_{pc2}) are proportional to the square root of the scan rate, which means the system to be diffusion controlled. Diffusion occurs only when a concentration gradient is set up. If the gradient arises from a constant rate of removal of the species across one face of the volume, then this constant flux makes the concentration of the diffusing species vary with distance and time[100]. Moreover with increasing $\nu^{1/2}$, the peak currents (Randle-Sevseik plot) for both cathodic and anodic peaks increases linearly (Fig 3.1.4), giving the conclusion that the processes are adsorptive controlled [35, 99].

The peak current ratio for the first pair of peaks are more than unity and decreases with increasing scan rate (Fig 3.1.5). Similar is the case for the second pair. These facts implies that system shows different character from the reversible behavior[101, 102].

Fig 3.1.6 show that peak current function ($i_p/\nu^{1/2}$) for the first cathodic peak gives a lower value at scan rate 0.050 Vs^{-1} then a sudden increase at 0.100 Vs^{-1}. After that there is a gradual decrease upto scan rate 0.250 Vs^{-1} and again a sudden increase at scan rate

$0.300Vs^{-1}$. For the second cathodic peak, the value decreases gradually upto scan rate $0.150\ Vs^{-1}$ and then increases with increasing scan rate. Both of these facts indicate that the electrochemical process under the investigation do not followed by any chemical process, i.e. it does not follow EC mechanism[101, 102].

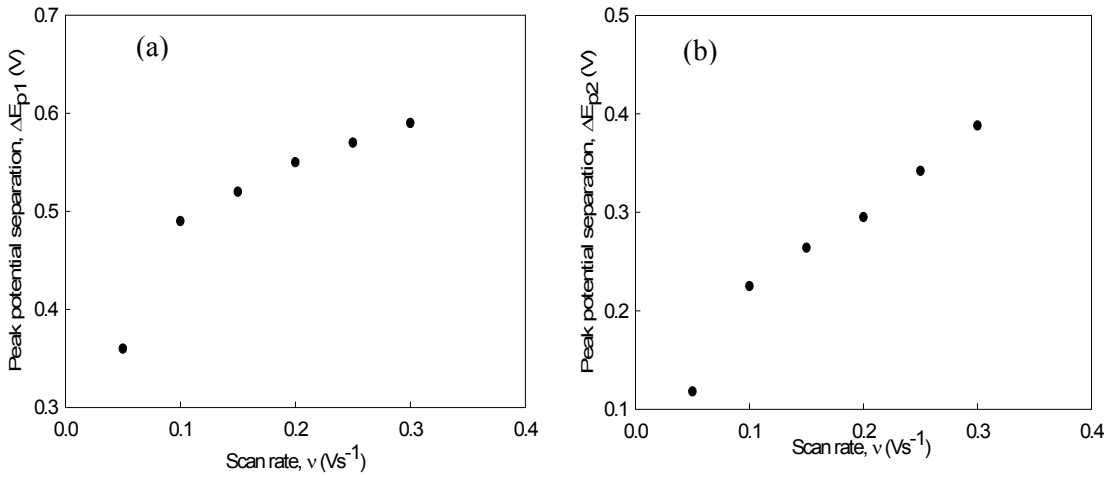

Fig 3.1.3 Variation of peak potential separation with scan rate for Cu(II) in 0.1M KCl solution (a) first pair (b) second pair of peaks.

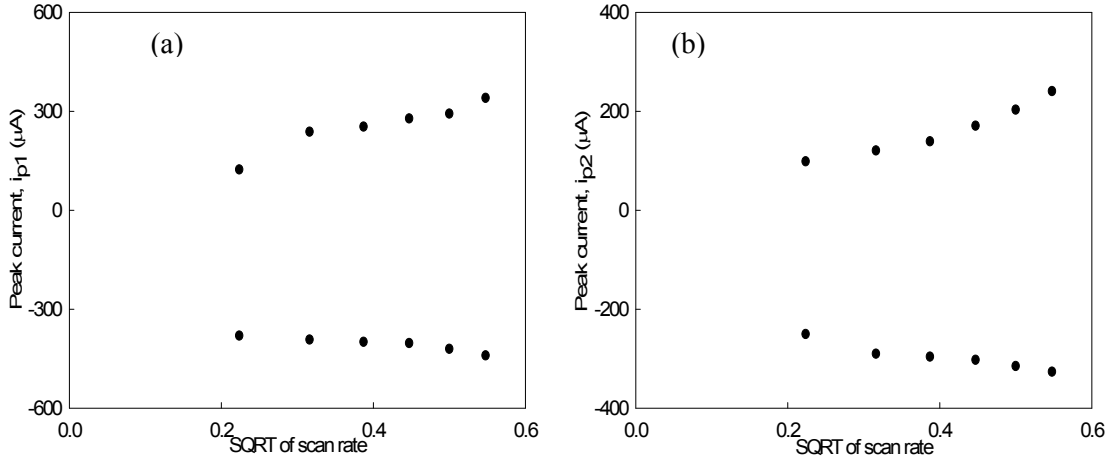

Fig 3.1.4 Variation of peak current with square root of scan rate for Cu(II) in 0.1 M KCl solution (a) first pair, (b) second pair of peaks.

Again the plot of log i_p against log ν (Fig 3.1.7) shows a linear relationship having slope more than unity, which demonstrate that adsorption occurs on the electrode during the process[3, 103].

Tafel plot (peak potential vs log ν) for the first and the second pair of peaks are shown in Fig 3.1.8. The curves express that the slopes of the Tafel plot are not zero. So the electrochemical process will be different from reversibility, which may be quasi-reversible.

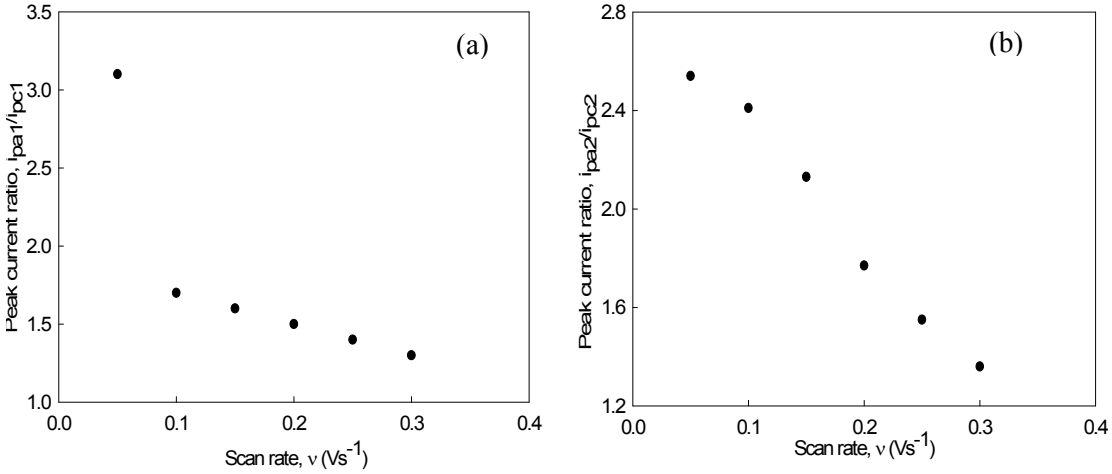

Fig 3.1.5 Variation of peak current ratio with scan rate for Cu(II) in 0.1 M KCl solution (a) first pair, (b) second pair of peaks.

Therefore from the above discussions there are some findings, such as: i) peak potential shifts with scan rate, ii) peak current ratio is not equal to unity, iii) the current function $i_p/v^{1/2}$ is independent of scan rate, iv) peak response broadens as scan rate increases, v) slope of Tafel plot is not equal to zero.

Considering all the above points it can be concluded that the electrochemical process involved in Cu(II) is quasi-reversible.

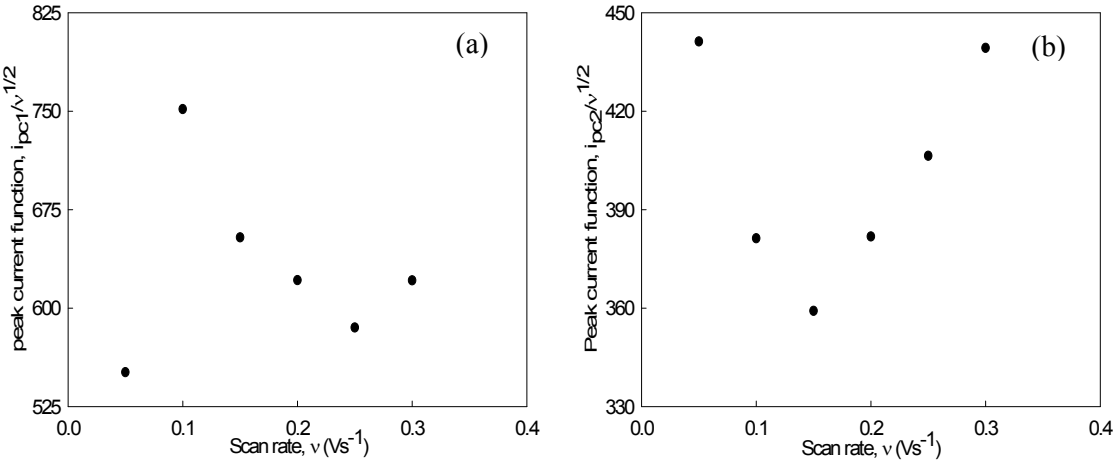

Fig 3.1.6 Variation of peak current function with scan rate for Cu(II) in 0.1 M KCl solution (a) first pair, (b) second pair of peaks.

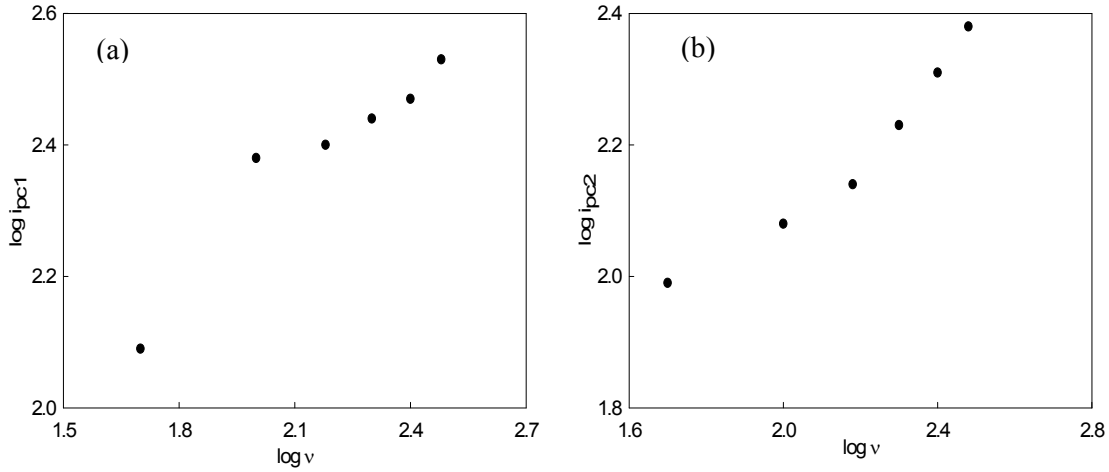

Fig 3.1.7 Plot of log i_p against log ν for Cu(II) in 0.1 M KCl solution (a) first pair, (b) second pair of peaks.

Moreover, the system is diffusion controlled as well as adsorptive controlled, which can be declared from the facts that a) in the forward scans, peak currents are proportional to the square root of scan rate, b) peak currents in both the regions (cathodic and anodic) increases linearly with square root of scan rate, c) slope of log i_p against log ν plot is more than unity.

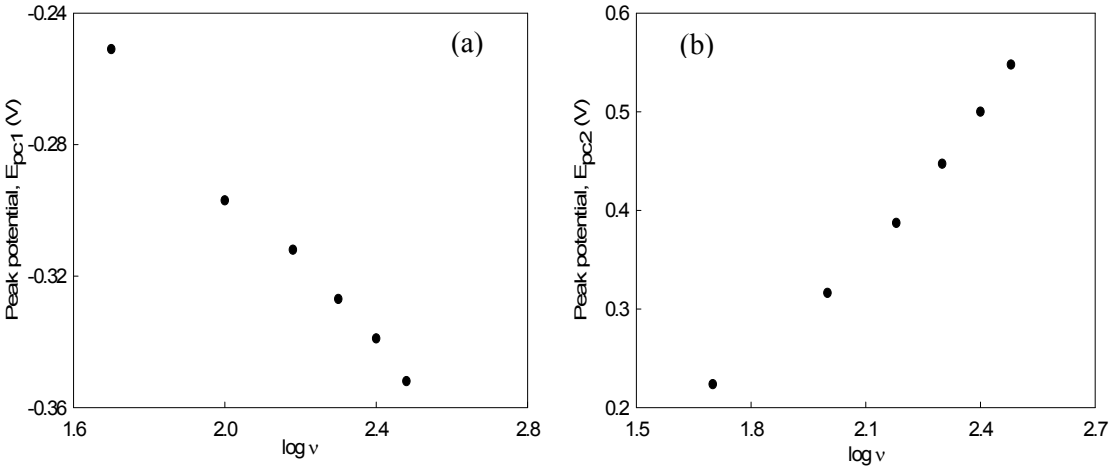

Fig 3.1.8 Variation of peak potential with log ν for Cu(II) in 0.1 M KCl solution (a) first pair, (b) second pair of peaks.

Redox behavior of Ciprofloxacin

The redox behaviour of Ciprofloxacin in 0.1M potassium chloride and at varying scan rate was also studied using cyclic voltammetric technique within the potential window from -2.300 V to 2.000 V at room temperature at glassy carbon electrode (GCE). A CV of the above system at scan rate 0.100 Vs^{-1} is given in Fig 3.1.9.

It shows peak in the cathodic region at about -0.791 V and in the anodic region at about 1.231 V. It was found that with increase of scan rate the peak in the cathodic region becomes broader and ultimately from 0.200 Vs^{-1} the peak is replaced by humplike shape. But the peak as well as the humplike shape shifts towards towards more negative potentials with increase in scan rate (Fig 3.1.10).

On the other hand, in the anodic region, the humplike shape becomes more prominent with the increase in scan rate and to some extent shifts towards more positive potential.

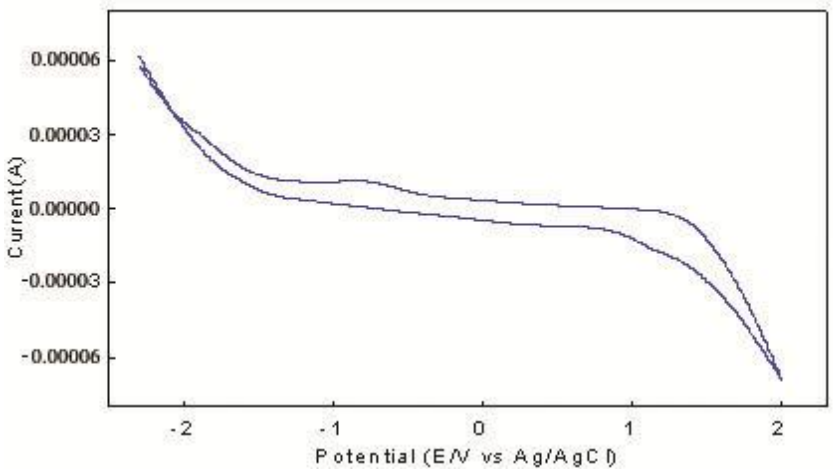

Fig 3.1.9 Cyclic voltammogram of Ciprofloxacin at scan rate 0.100 Vs^{-1} in 0.1M KCl solution.

Redox behavior of Cu(II)-Ciprofloxacin mixture in solution

The redox behaviour of Cu(II)-Ciprofloxacin 1:1 interaction was also studied in 0.1M potassium chloride and at varying scan rates using cyclic voltammetric technique within the potential window from -1.800 V to 2.000 V at room temperature at glassy carbon electrode (GCE). A CV of the above system at scan rate 0.100 Vs^{-1} is given in Fig 3.1.11.

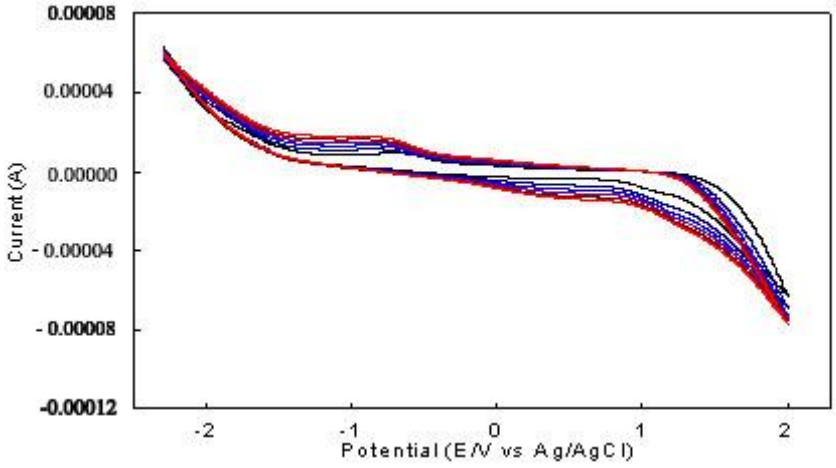

Fig 3.1.10 Scan rate variation of Ciprofloxacin in 0.1M KCl solution.

The CV shows three cathodic peaks (c_1, c_2 and c_3) at the potentials of -0.921 V, -0.211 V and -0.032 V and in the anodic region two peaks (a_1 and a_2) at 0.022 V and 0.331 V as well as a humplike shape.

The first cathodic may be due to the ligand (Ciprofloxacin) itself and the second as well as the third cathodic peaks are originated from the parent metal (Cu(II)) as in Fig 3.1.12.

Compared to the CV of Cu(II) together with that of Ciprofloxacin (Fig 3.1.12), it is found that after interaction, the second (c_2) and the third cathodic peak (c_3) moves less negative

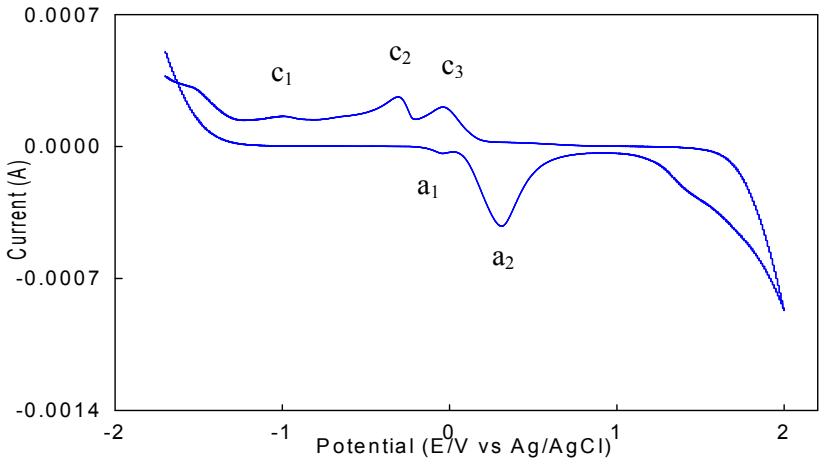

Fig 3.1.11 Cyclic voltammogram of Cu(II)-Ciprofloxacin 1:1 interaction in 0.1 M KCl solution at scan rate 0.100 Vs^{-1}

and less positive potential. But both the anodic peaks (a_1 and a_2) shifts towards less positive potential.

Therefore, it is observed that after interaction the number of peaks in both the regions are changed as well as the peak positions are also altered. These two facts implies that the interaction between Cu(II) and Ciprofloxacin is successful.

Fig 3.1.13 shows the voltammograms of Cu(II)-Ciprofloxacin 1:1 interaction at different scan rates. It shows that with the increase in scan rate the first cathodic peak (c_1) shifts towards more negative potential upto scan rate 0.100 Vs^{-1} and then vanishes. But the second (c_2) and the third (c_3) cathodic peaks shifts toward more negative potential with

increasing scan rates. But the both the anodic peaks shifts towards more positive potential with the increase in scan rate. Again the hump in the anodic region, is more prominent at the lower scan rates and ultimately diminishes at the higher scan rates. Moreover, with the increase in scan rate, almost all the peaks become broader. Such behavior has been ascribed to slower charge propagation, probably due to difference in salvation and or permeability.

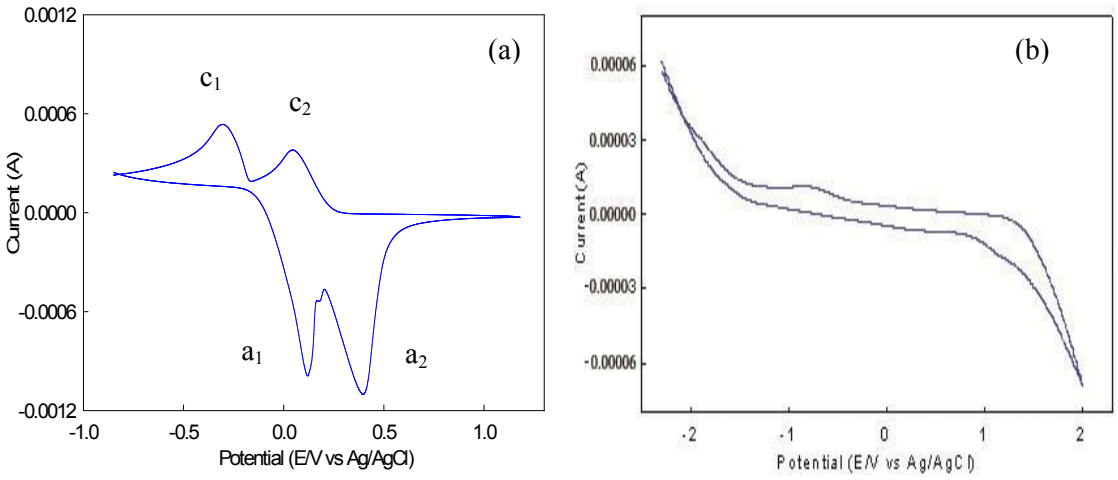

Fig 3.1.12 Cyclic voltammograms of (a) Cu(II) and (b) Ciprofloxacin at scan rate 0.100 Vs^{-1}.

Current-potential data for the system under consideration is recorded in Table 3.1.2. It is evident that after interaction, the peak separation becomes less to a considerable extent for the first pair of peaks but for the second pair the separation becomes a little bit less than Cu(II) before interaction.

The peak separation potential for the first pair of peaks (ΔE_{p1}) increases with the increase in scan rate, because the cathodic peak shifts towards negative and that of anodic towards positive. Here the cause responsible is the effect of iR drop. This fact is similar to the copper system before interaction. But for the second pair, it (ΔE_{p2}) decreases with the increase in scan rate with an exception as scan rate 0.300 Vs^{-1}. This bevaviour is absolutely different behavior from the fact happened in case of copper before interaction. Therefore it may be said that the above system indicate the limitation due to charge

transfer kinetics to some extent and simultaneously to some extent does not indicate the limitation due to charge transfer kinetics[35, 104] and are shown in the plot of ΔE_{p1} vs ν and ΔE_{p2} vs ν in Fig 3.1.14.

Again the forward scan peak currents (i_{pc2} and i_{pc3}) are proportional to the square root of the scan rate, which means the system to be diffusion controlled. Diffusion occurs only when a concentration gradient is set up. If the gradient arises from a constant rate of removal of the species across one face of the volume, then this constant flux makes the concentration of the diffusing species vary with distance and time[100]. Moreover with increasing $\nu^{1/2}$, the peak currents (Randle-Sevseik plot) for both cathodic and anodic

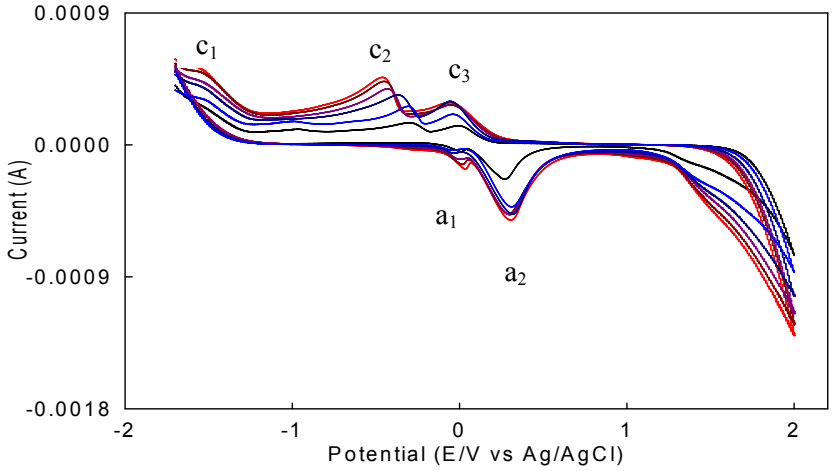

Fig 3.1.13 Cyclic voltammogram of Cu(II)-Ciprofloxacin 1:1 interaction in 0.1 M KCl solution at different scan rates.

Table 3.1.2 Current-potential data for Cu(II)-Ciprofloxacin 1:1 interaction in 0.1 M KCl solution at different scan rates.

Scan rate	SQRT of scan rate	Cathodic peak potential		Anodic peak potential	Cathodic peak current		Anodic peak current	Peak potential separation	Peak current ratio
ν (Vs^{1})		E_{pc1} (V) [-]	E_{pc2} (V) [-]	E_{pa1} (V)	i_{pc1} (μA)	i_{pc2} (μA)	i_{pa1} (μA) [-]	ΔE_{p1}= E_{pa1}- E_{pc2} (V)	i_{pa1}/ i_{pc2}
0.050	0.2236	0.902	0.206	0.105	34.12	105.21	60.21	0.311	0.57
0.100	0.3162	0.921	0.211	0.122	38.51	210.94	65.94	0.333	0.31
0.150	0.3872	-	0.218	0.135	-	280.17	67.08	0.353	0.24
0.200	0.4472	-	0.247	0.144	-	325.67	142.11	0.391	0.44

0.250	0.5000	-	0.249	0.156	-	371.15	195.78	0.405	0.53
0.300	0.5477		0.252	0.165	-	385.24	230.15	0.417	0.60

ν (Vs^{1})		E_{pc3} (V)	E_{pa2} (V)	i_{pc3} (μA)	i_{pa2} (μA) [-]	$\Delta E_{p2}= E_{pa2}- E_{pc3}$ (V)	i_{pa2}/ i_{pc3}
0.050	0.2236	0.019	0.283	128.21	295.15	0.264	2.30
0.100	0.3162	0.042	0.301	175.99	460.41	0.259	2.62
0.150	0.3872	0.069	0.305	250.41	480.14	0.236	1.92
0.200	0.4472	0.076	0.308	251.12	482.11	0.232	1.92
0.250	0.5000	0.080	0.311	252.05	484.84	0.231	1.92
0.300	0.5477	0.085	0.320	253.84	499.08	0.235	1.97

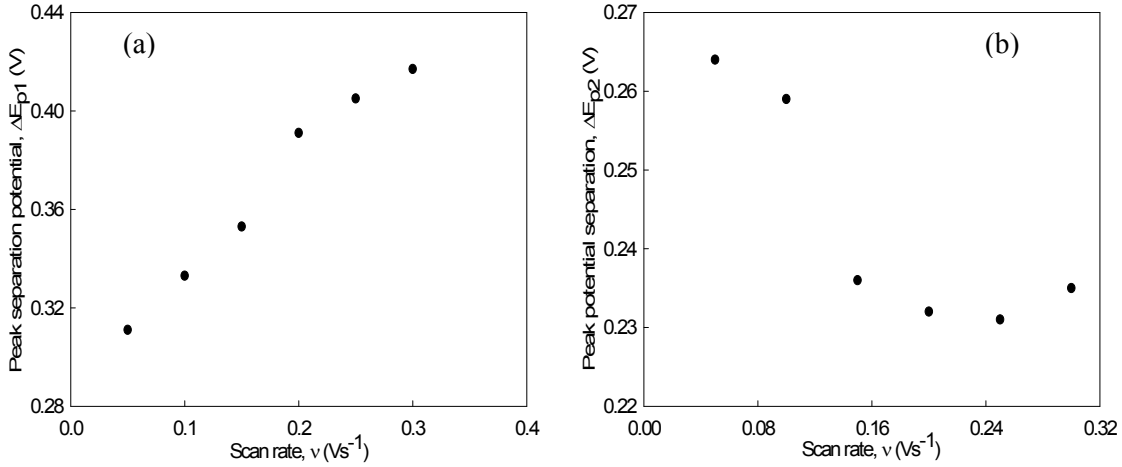

Fig 3.1.14 Variation of peak potential separation with scan rate for Cu(II)-Ciprofloxacin 1:1 interaction in 0.1M KCl solution (a) first pair (b) second pair of peaks.

peaks increases linearly (Fig 3.1.15), giving the conclusion that the processes are adsorptive controlled [35, 99].

The peak current ratio for the first pair of peaks are very much lower than unity. But for the second pair, the peak current ratio is very much higher than unity. Therefore it may said that system shows almost exceptional character from the reversible behavior[101, 102]. Fig 3.1.16 shows that the peak current ratio decreases with increasing scan rate for the first pair of peaks at the lower scan rates and then increases. But for the second pair, it increases at first, then a sudden decrease and then constant.

Again Fig 3.1.17 peak current function ($i_p/\nu^{1/2}$) for the first pair, decreases upto scan rate 0.150 Vs^{-1} then increases with increasing scan rate. But the second pair of peaks show three regions. Firstly, a decrease, then a sudden increase and after that decreases with increasing scan rates. Therefore, it does not indicate any clear conception about the electrochemical process.

Again the plot of log i_p against log ν shows a linear relationship for both pair of peaks. It is found that for both the pair of peaks the slope is more than unity (Fig 3.1.18). Therefore it may be said that the process is accompanied by adsorption[3, 103].

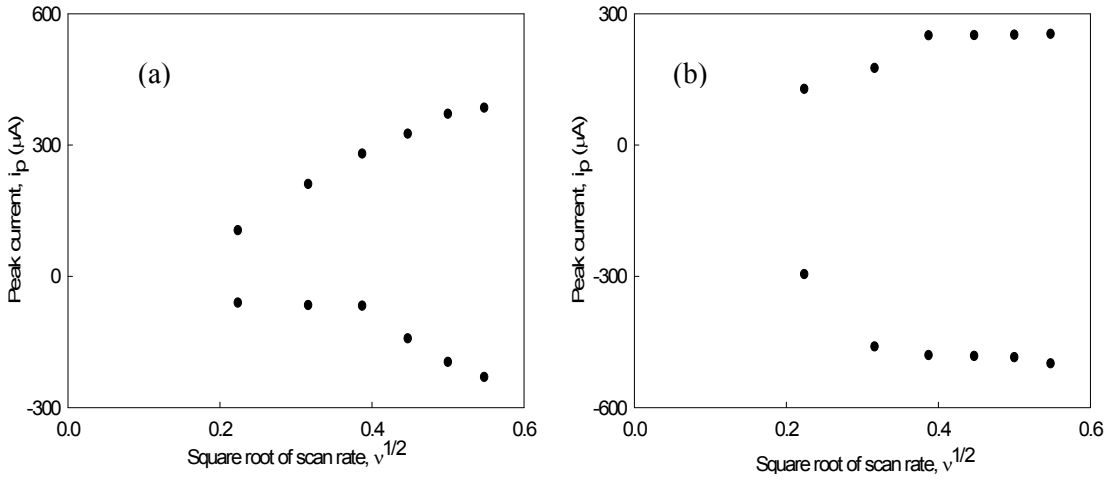

Fig 3.1.15 Variation of peak current with square root of scan rate for Cu(II)-Ciprofloxacin 1:1 interaction in 0.1M KCl solution. (a) first pair (b) second pair of peaks.

Tafel plot (peak potential vs log ν) for the first and the second pair of peaks are shown in Fig 3.1.19. The curves express that the slopes of the Tafel plot are not zero. So the electrochemical process will be different from reversibility.

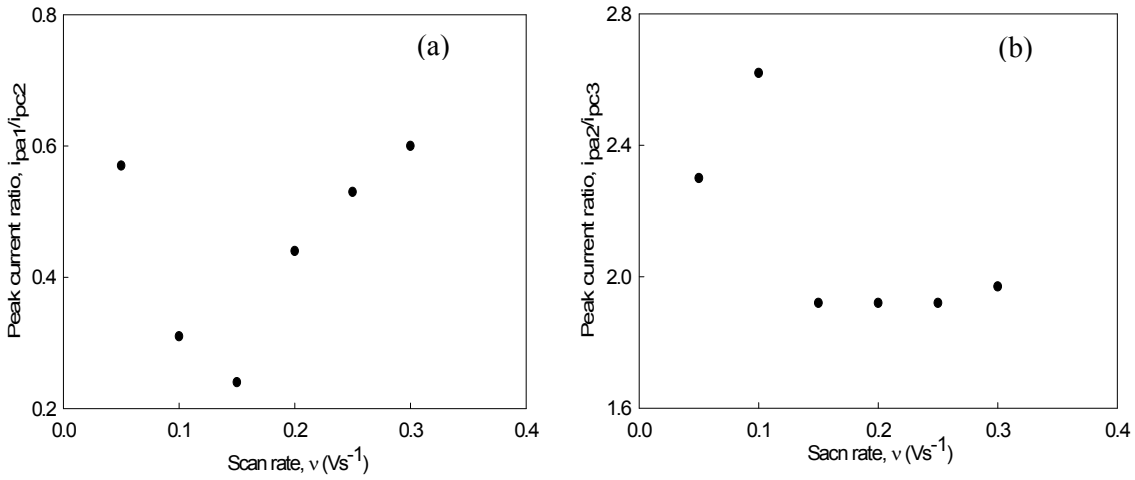

Fig 3.1.16 Variation of peak current ratio with scan rate for Cu(II)-Ciprofloxacin 1:1 interaction in 0.1M KCl solution (a) first pair (b) second pair of peaks.

Therefore from the above discussions there are some findings, such as: i) peak potential shifts with scan rate, ii) peak current ratio is not equal to unity, iii) the current function $i_p/v^{1/2}$ is independent of scan rate, iv) peak response broadens as scan rate increases, v) slope of Tafel plot is not equal to zero.

Considering all the above points it can be concluded that the electrochemical process involved in Cu(II)-Ciprofloxacin 1:1 interaction is quasi-reversible.

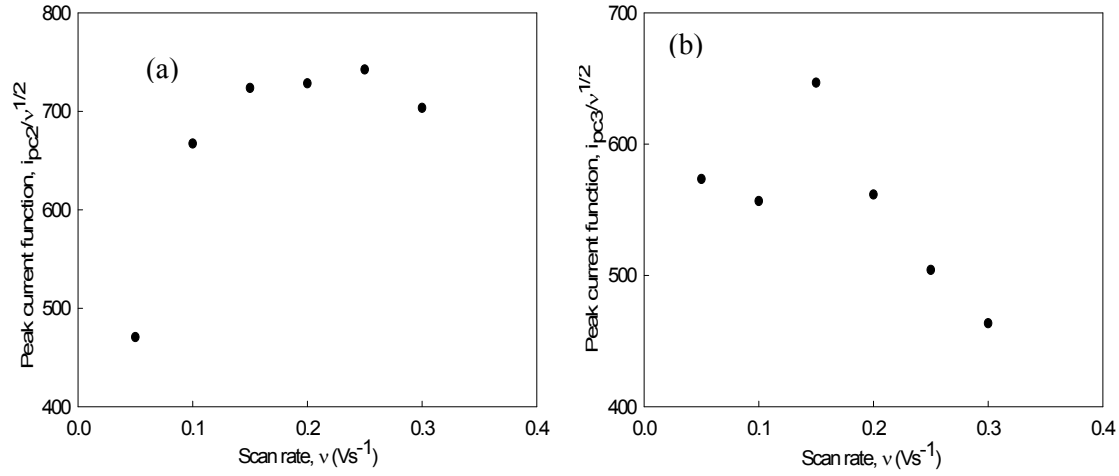

Fig 3.1.17 Variation of peak current function with scan rate for Cu(II)-Ciprofloxacin 1:1 interaction in 0.1M KCl solution. (a) first pair (b) second pair of peaks.

Moreover, the system is diffusion controlled as well as adsorptive controlled, which can be declared from the facts that a) in the forward scans, peak currents are proportional to the square root of scan rate, b) peak currents in both the regions (cathodic and anodic) increases linearly with square root of scan rate, c) slope of log i_p against log ν plot is more than unity.

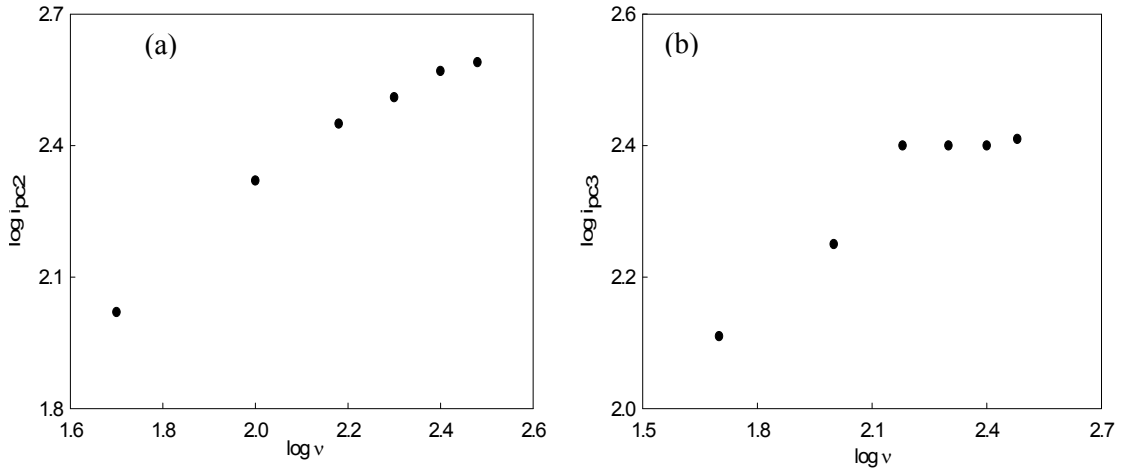

Fig 3.1.18 Plot of log i_p against logν for Cu(II)-Ciprofloxacin 1:1 interaction in 0.1M KCl solution (a) first pair (b) second pair of peaks.

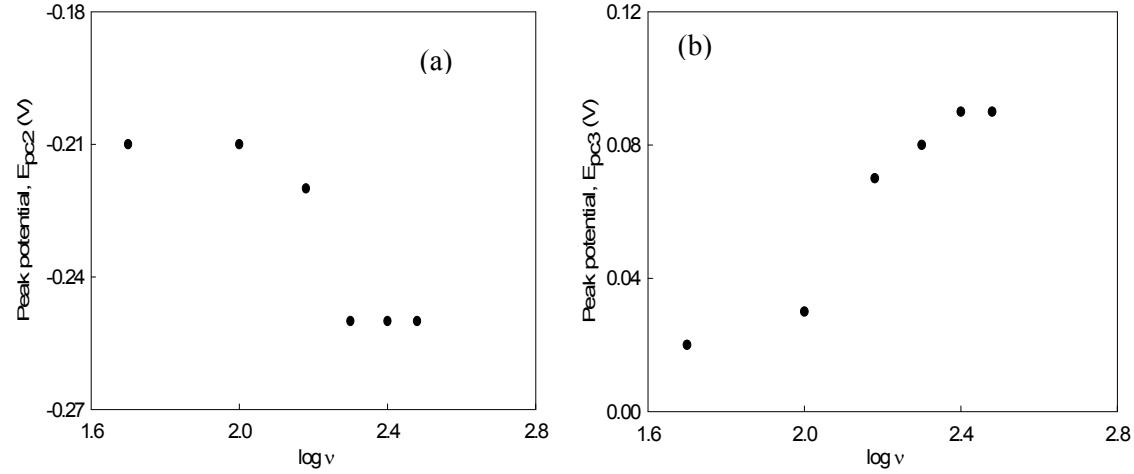

Fig 3.1.19 Variation of peak potential with logν for Cu(II)-Ciprofloxacin 1:1 interaction in 0.1M KCl solution (a) first pair (b) second pair of peaks.

3.1.2 Chronoamperometric and chronocoulometric study of Cu(II) and Cu(II)-Ciprofloxacin interaction

CA and CC study of Cu(II)

The Cu(II) system was also studied with chronoamperometric and chronocoulometric techniques which are double potential step processes. The chronoamperometric (CA) experiment gives a current versus time curve, which is known as current response or chronoamperogram. Such a current responses for Cu(II) are shown in Fig 3.1.20.

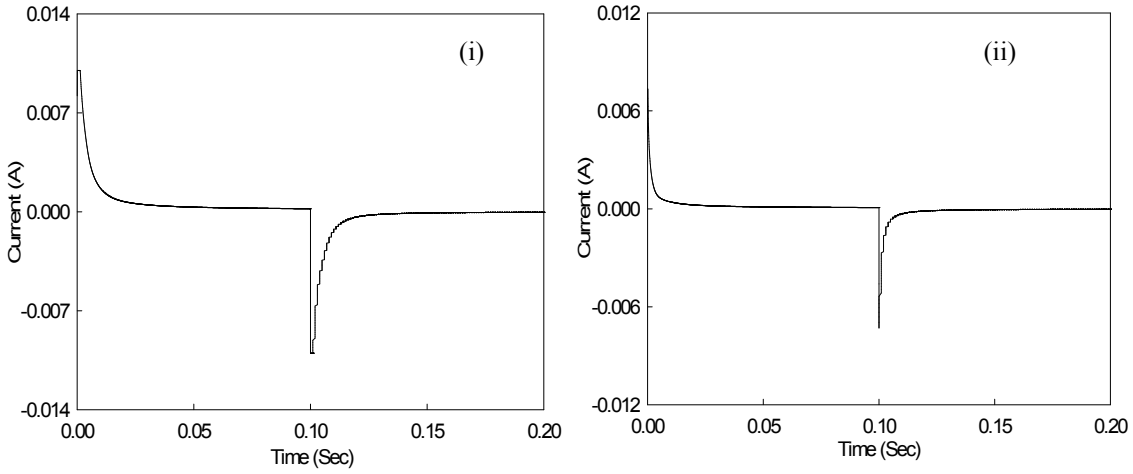

Fig 3.1.20 Current responses for Cu(II) in 0.1 M KCl solution (i) first and (ii) second pair of peaks.

It shows a current spike followed by a gradual decay in current. The spike is due to initial electrolysis of species at the electrode surface and the decay is due to diffusion of molecules to the electrode surface[101].

The forward step, that is, the transition from initial potential (E_1) to first step potential (E_2) at t=0, is that the electrode must instantly reduce the copper from higher oxidation state to lower one.

For a period τ, it causes a build up of the reduction product in the region near the electrode.

However, in the second phase of the experiment, after t= τ, the potential returns to E1, where only the oxidized form is stable at the electrode. The ionic radical produced by reduction cannot coexist there; hence a large anodic current follows as it begins to reoxidize, then the current declines in magnitude[35].

Chronocoulometry (CC) is the integrated form of the chronoamperometry. So that in CC the monitored response is charge. It is also known as chronocoulogram. Such a charge response is shown in Fig 3.1.21.

Here in this double potential step CC, the potential is stepped from an initial value to a second value and then back to the initial value. The step from initial to the second is termed as forward potential step whereas the step from the second to the initial value is termed as reverse step[35].

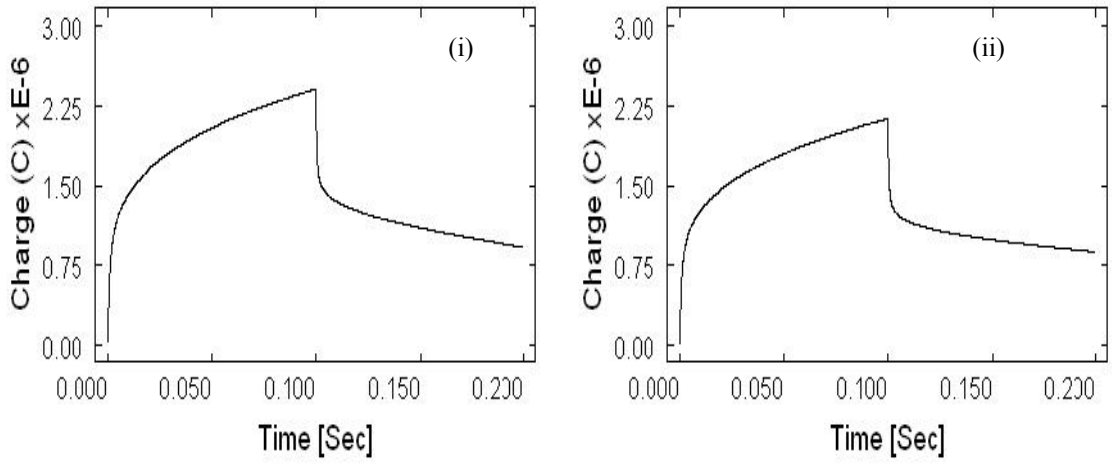

Fig 3.1.21 Charge responses for Cu(II) for in 0.1 M KCl solution (i) first and (ii) second pair of peaks.

Chronocoulometric response (Fig 3.1.22) shows that the charge at τ is about 2.482 μC for the first peak and 2.251 μC for the second peak. Now if Q value obtained from time less than τ is plotted versus $t^{1/2}$ and on the same graph $-Q_r$ is plotted versus $\theta = [\tau^{1/2} + (t- \tau)^{1/2} - t^{1/2}]$, there will be two straight lines which intersects each other at Q=0 axis with equal slope, if there is no adsorption of reactant or product[31]. Any deviation from such condition means adsorption. Such plots are shown in the Fig 3.1.23 (i) and (ii). This

shows that the plots Q vs $t^{1/2}$ and $-Q_r$ vs θ do not intersect each other at Q=0 axis. Moreover they do not have equal slopes. Therefore from this plot, it may be said that adsorption of reactant or products occur on the electrode.

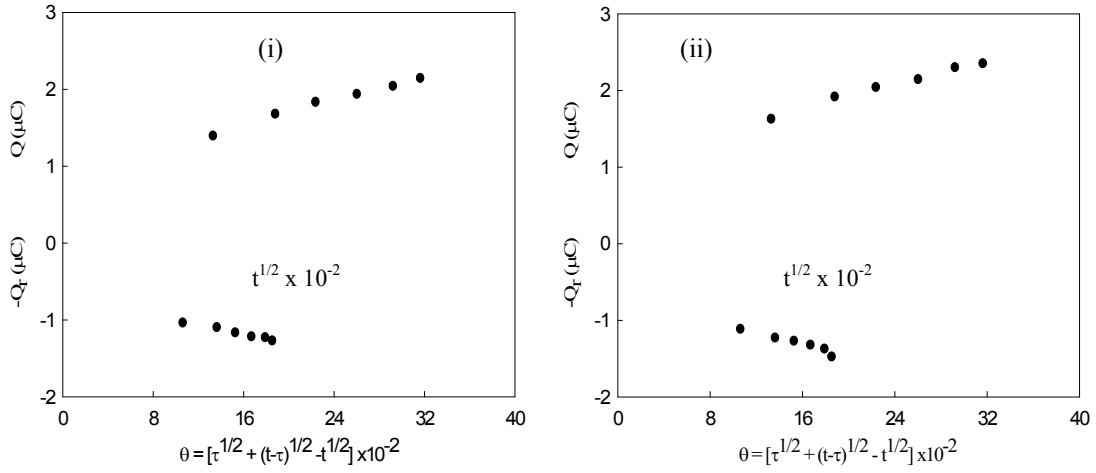

Fig 3.1.23 Plots of Q vs $t^{1/2}$ and $-Q_r$ vs θ for Cu(II) system in 0.1 M KCl solution (i) first and (ii) second pair of peaks.

CA and CC study of Cu(II)-Ciprofloxacin mixture in solution

Chronoamperometric study of Cu(II) system was also done after interaction with Ciprofloxacin. It was observed that there were three peaks after interaction in the cathodic region but in the anodic region, there are two. Therefore, after interaction there are two pair of peaks and CA study was also done correspondingly for each of the pair of peaks. The chroamperograms are shown in the Fig 3.1.24.

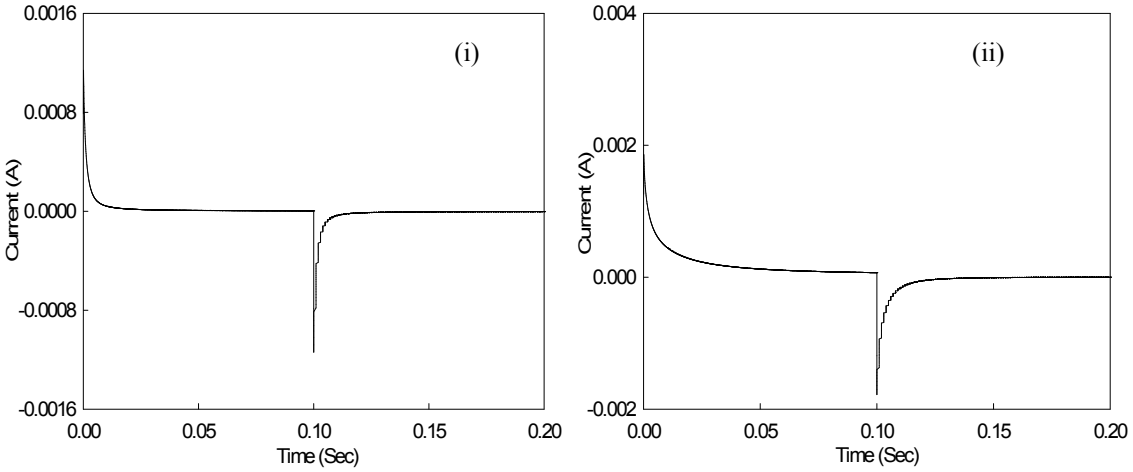

Fig 3.1.24 Current responses for Cu(II)-Ciprofloxacin 1:1 interaction in 0.1 M KCl solution (i) first pair and (ii) second pair of peaks.

It shows that the spike height after interaction with Ciprofloxacin is decreased for each of the pair of peaks (Figures 3.1.25 and 3.1.26) compared to that of Cu(II) before interaction with Ciprofloxacin. Since the spike height is proportional to the rate of electrolysis, this means that after interaction the rate of electrolysis has been decreased.

Chronocoulometry (CC) is the integrated form of the chronoamperometry. So that in CC the monitored response is charge. It is also known as chronocoulogram. Such charge responses are shown in Fig 3.1.27 (i) and (ii).

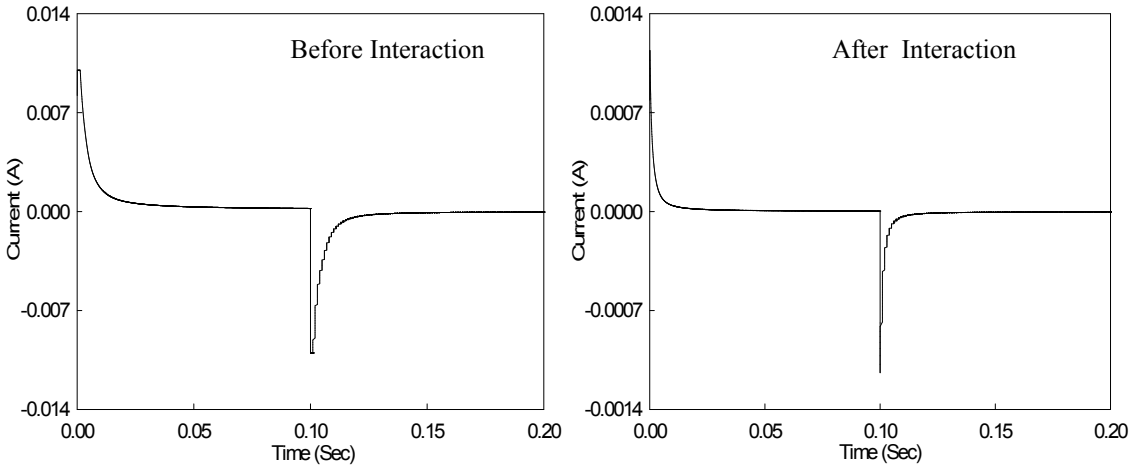

Fig 3.1.25 Current responses for Cu(II) in 0.1 M KCl solution (i) before and (ii) after interaction with Ciprofloxacin for first pair of peaks.

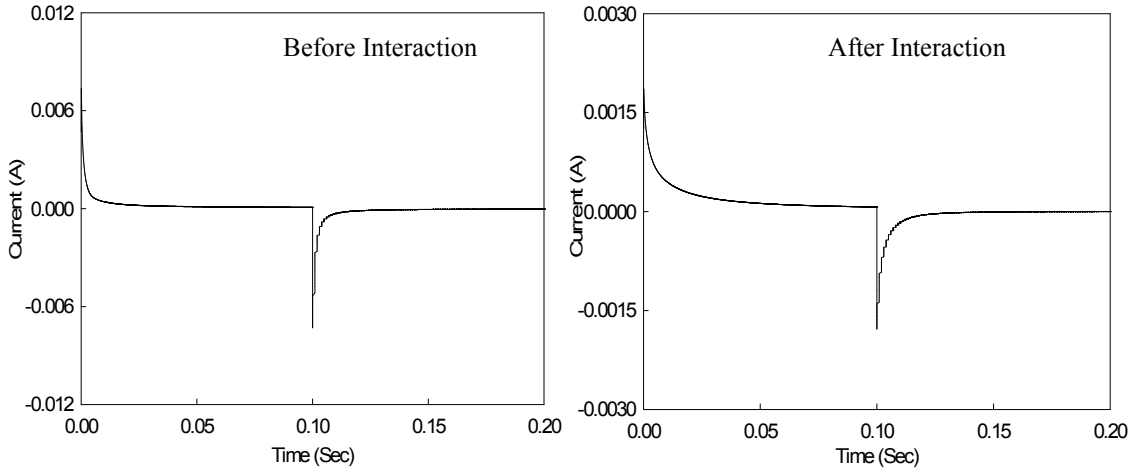

Fig 3.1.26 Current responses for Cu(II) in 0.1 M KCl solution (i) before and (ii) after interaction with Ciprofloxacin for second pair of peaks.

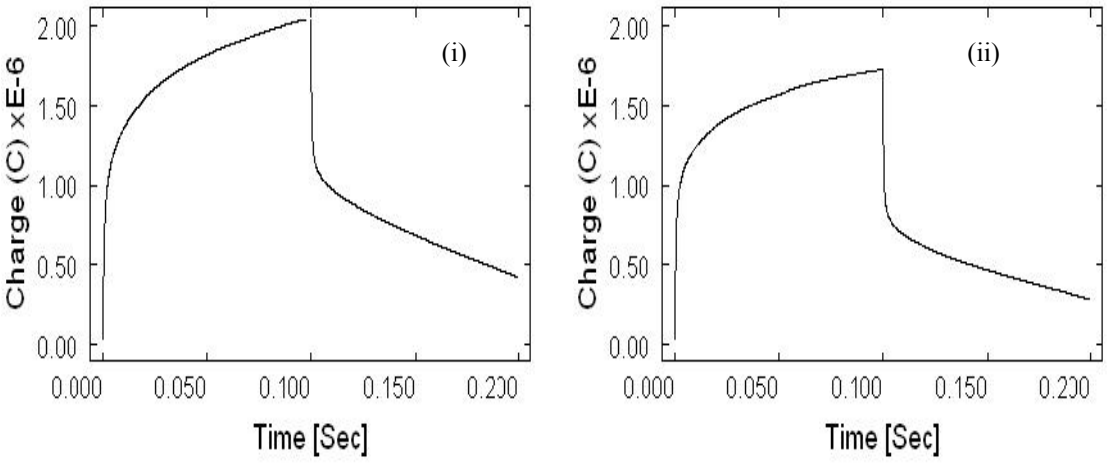

Fig 3.1.27 Charge responses for Cu(II)-Ciprofloxacin 1:1 interaction in 0.1 M KCl solution (i) first pair and (ii) second pair of peaks.

Chronocoulometric response (Fig 3.1.27) shows that the charge at τ is decreased after interaction with Ciprofloxacin. It was 2.482 μC for the first peak and 2.251 μC for the second peak in the absence of Ciprofloxacin, whereas it becomes 2.007 μC and 1.726 μC for the first and second pair of peaks respectively after interaction with Cipropfloxacin. Now if Q value obtained from time less than τ is plotted versus $t^{1/2}$ and on the same graph $-Q_r$ is plotted versus $\theta = [\tau^{1/2} + (t- \tau)^{1/2} - t^{1/2}]$, there will be two straight lines which intersects each other at Q=0 axis with equal slope, if there is no adsorption of reactant or

product. Any deviation from such condition means adsorption. Such plots are shown in the Fig 3.1.28 (i) and (ii). This shows that the plots Q vs $t^{1/2}$ and $-Q_r$ vs θ do not intersect each other at Q=0 axis. Moreover they do not have equal slopes. Therefore from this plot, it may be said that adsorption of reactant or products occur on the electrode.

Therefore the findings from the Chronoamperometric studiy is that after interaction the spike height is decreased, indicating towards a decrease in the rate of electrolysis. And from the Chronocoulometric study, it is observed that the charge at τ are decreased in all the cases. Both of these facts combinedly indicates towards successful interaction. And the observations from the plots Q vs $t^{1/2}$ and $-Q_r$ vs θ gives conclusion that adsorption of reactant or products occur on the electrode also after interaction.

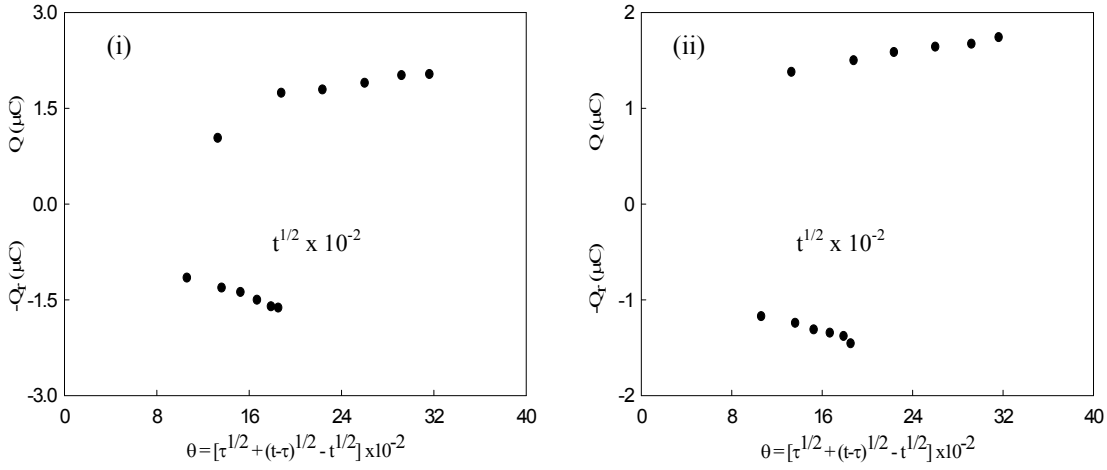

Fig 3.1.28 Plots of Q vs $t^{1/2}$ and $-Q_r$ vs θ for Cu(II)-Ciprofloxacin 1:1 interaction in 0.1 M KCl solution (i) first and (ii) second pair of peaks.

3.1.3 Cyclic voltammetric study of Mn(II) and Mn(II)-Ciproflofloxacin interaction at Glassy Carbon Electrode (GCE).

Redox behavior of Mn(II)

The redox behaviour of Mn(II) (in solution of $MnCl_2$) in 0.1M potassium chloride and at varying scan rate was studied using cyclic voltammetric technique within the potential window from -0.900 V to 1.500 V at room temperature at glassy carbon electrode (GCE). A CV of the above system at scan rate 0.100 Vs^{-1} is given in Fig 3.1.29.

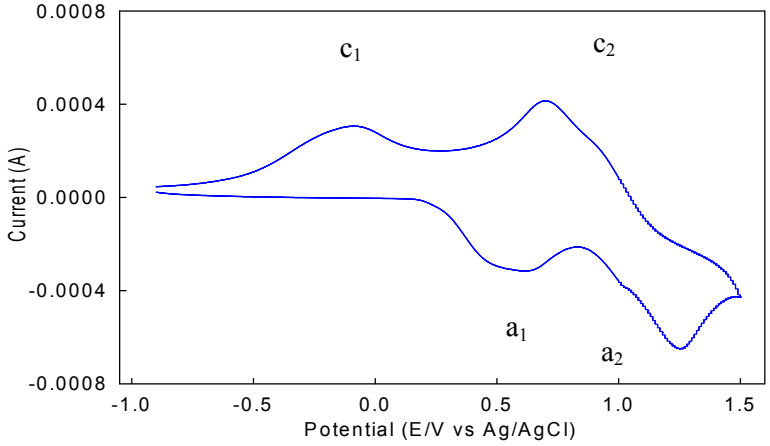

Fig 3.1.29 Cyclic voltammogram of Mn(II) in 0.1 M KCl at scan rate 0.100 Vs^{-1}

The CV shows two cathodic peaks (c_1 and c_2) at the potentials of -0.092 V and 0.693 V due to reduction of Mn(IV) to Mn(III) and Mn(III) to Mn(II) respectively and the same number of peaks in anodic region (a_1 and a_2) at 0.621 V and 1.402 V due to oxidation of Mn(II) to Mn(III) and Mn(III) to Mn(IV) respectively. The electrode reaction may be presented by the following equations:

Cathodic reaction: $Mn^{4+} + e \longrightarrow Mn^{3+}$

$Mn^{3+} + e \longrightarrow Mn^{2+}$

Anodic reaction: $Mn^{2+} - e \longrightarrow Mn^{3+}$

$Mn^{3+} - e \longrightarrow Mn^{4+}$

The overall reaction is: $Mn^{4+} \underset{-e}{\overset{+e}{\rightleftharpoons}} Mn^{3+} \underset{-e}{\overset{+e}{\rightleftharpoons}} Mn^{2+}$

Fig 3.1.30 shows the voltammograms of Mn(II) at different scan rates. It shows that with the increase in scan rate both the cathodic peaks shifts towards more negative potential. On the other hand, both the peaks in the anodic region shifts towards more positive potentials.

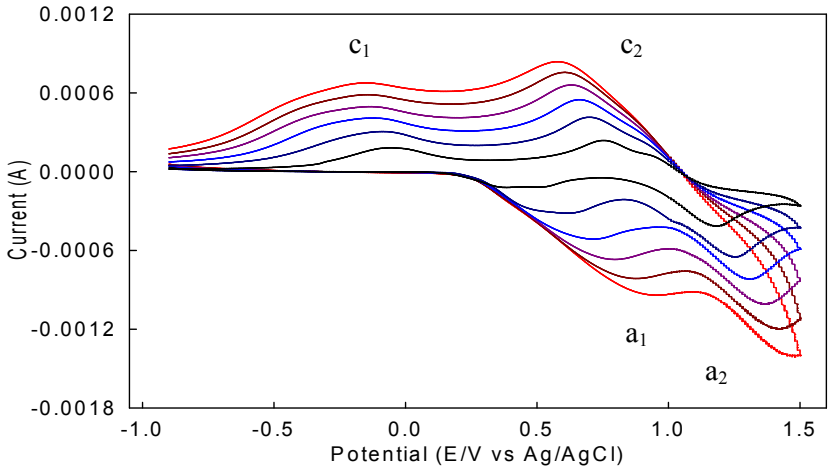

Fig 3.1.30 Cyclic voltammogram of Mn(II) in 0.1 M KCl at different scan rates.

It is found that with the increase in scan rate, almost all the peaks become broader. Such behavior has been ascribed to slower charge propagation, probably due to difference in salvation and or permeability. Table 3.1.3 gives the current-potential data for the above system.

The peak separation potential (Fig 3.1.31) for both the pair of peaks (ΔE_{p1} and ΔE_{p2}) increases with the increase in scan rate. Because the cathodic peak shifts towards negative and that of anodic towards positive. Here the cause responsible is the effect of iR drop. Moreover, it indicates the limitation due to charge transfer kinetics and are shown in the plot of ΔE_{p1} vs ν and ΔE_{p2} vs ν in Fig 3.1.31.

Again the forward scan peak currents (i_{pc1} and i_{pc2}) are proportional to the square root of the scan rate at all scan rates, which means the system to be diffusion controlled. Moreover with increasing $\nu^{1/2}$, the peak currents for both cathodic and anodic peaks as well as for both the pairs increase linearly (Fig 3.1.32), giving the conclusion that the processes are adsorptive controlled [35, 99].

Table 3.1.3 Current-potential data for Mn(II) in 0.1 M KCl solution at different scan rates.

Scan rate ν (Vs^{-1})	SQRT of scan rate	Cathodic peak potential E_{pc1} (V) [-]	Anodic peak potential E_{pa1} (V)	Cathodic peak current i_{pc1} (μA)	Anodic peak current i_{pa1} (μA) [-]	Peak potential separation $\Delta E_{p1}= E_{pa1}- E_{pc1}$ (V)	Peak current ratio i_{pa1}/ i_{pc1}
0.050	0.2236	0.054	0.372	182.12	160.25	0.426	0.88
0.100	0.3162	0.092	0.621	306.25	316.22	0.713	1.03
0.150	0.3872	0.120	0.720	409.56	514.18	0.840	1.26
0.200	0.4472	0.131	0.794	495.02	669.07	0.925	1.35
0.250	0.5000	0.154	0.885	586.81	814.91	1.039	1.39
0.300	0.5477	0.160	0.960	676.26	940.45	1.120	1.39
ν (Vs^{-1})		E_{pc2} (V)	E_{pa2} (V)	i_{pc2} (μA)	i_{pa2} (μA) [-]	$\Delta E_{p2}= E_{pa2}- E_{pc2}$ (V)	i_{pa2}/ i_{pc2}
0.050	0.2236	0.757	1.351	237.36	107.11	0.594	0.45
0.100	0.3162	0.693	1.402	414.51	215.25	0.709	0.52
0.150	0.3872	0.664	1.415	548.52	347.08	0.751	0.63
0.200	0.4472	0.627	1.423	660.07	479.82	0.796	0.73
0.250	0.5000	0.603	1.429	756.39	608.13	0.826	0.80
0.300	0.5477	0.580	1.437	837.22	733.42	0.857	0.88

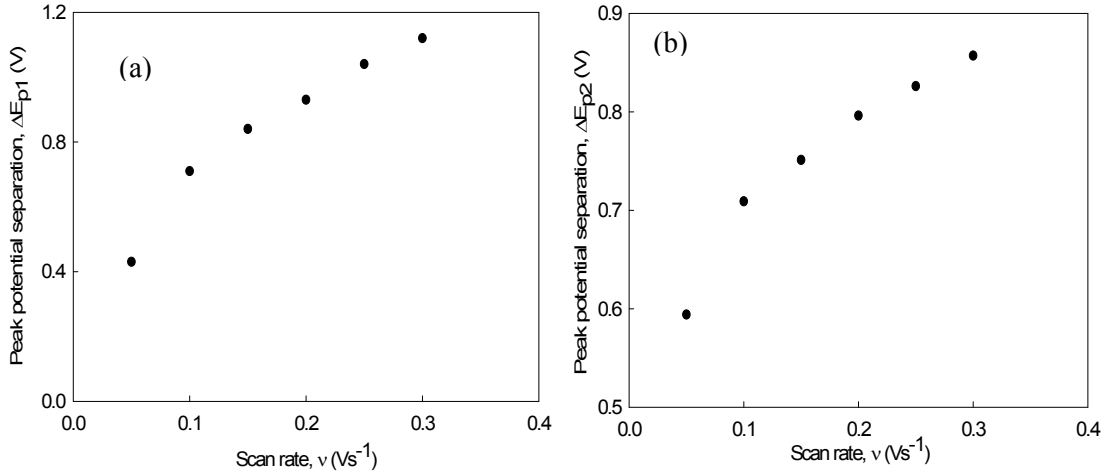

Fig 3.1.31 Variation of Peak potential separation with scan rate for Mn(II) in 0.1M KCl solution (a) first pair (b) second pair of peaks.

The peak current ratio for the first pair of peaks are almost unity at some scan rates and at some scan rates it is more than unity to some extent. But for the second pair, the peak current ratio is lower than unity to some extent at the lower scan rates and very much nearest to unity at higher scan rates. Therefore it may said that system shows exceptional character from the reversible behavior[101, 102].

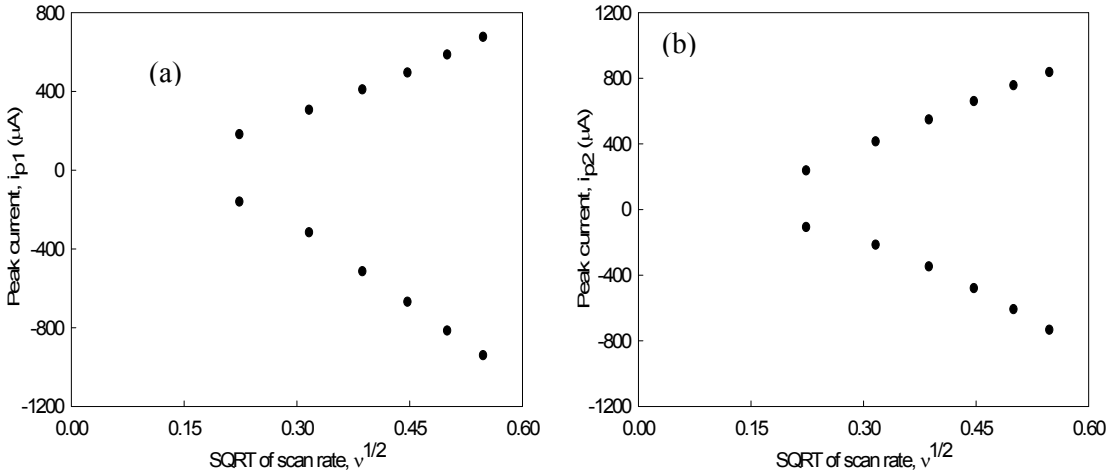

Fig 3.1.32 Variation of peak current with square root of scan rate for Mn(II) in 0.1 M KCl solution (a) first pair, (b) second pair of peaks.

Figures 3.1.33 and 3.1.34 show that the peak current ratio and peak current function ($i_p/\nu^{1/2}$) both increases with increasing scan rate. Both of these facts indicate that the electrochemical process under the investigation do not followed by any chemical process, i.e. it does not follow EC mechanism[101, 102].

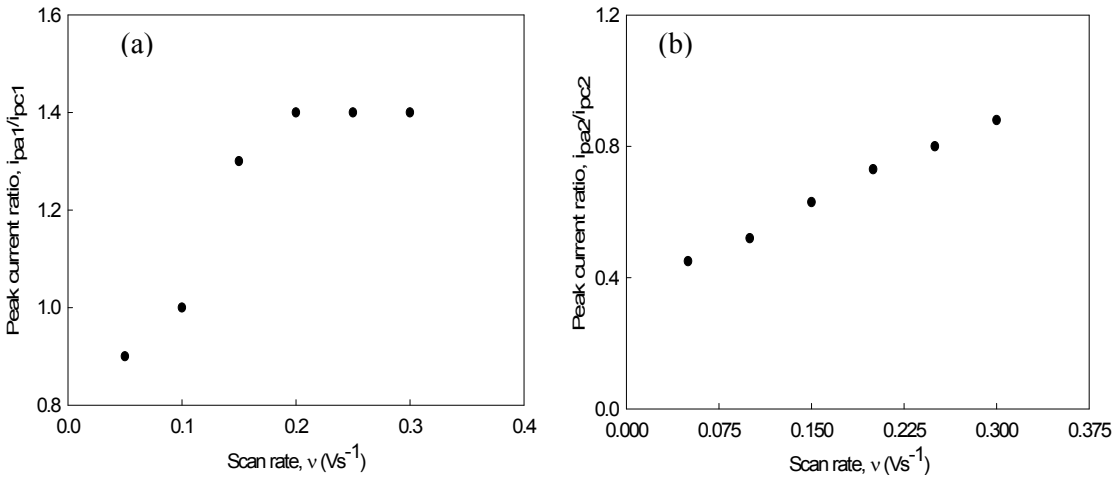

Fig 3.1.33 Variation of peak current ratio with scan rate for Mn(II) in 0.1 M KCl solution (a) first pair, (b) second pair of peaks.

Again the plot of log i_p against log ν shows a linear relationship having slope less than unity, indicating that the process is accompanied by diffusion[3, 103] (Fig 3.1.35).

Tafel plot (peak potential vs log ν) for the first and the second pair of peaks are shown in Fig 3.1.36. The curves express that the slopes of the Tafel plot are not zero. So the electrochemical process will not be reversible.

Therefore from the above discussions there are some findings, such as: i) peak potential shifts with scan rate, ii) peak current ratio is not equal to unity, iii) the current function $i_p/\nu^{1/2}$ is independent of scan rate, iv) peak response broadens as scan rate increases, v) slope of Tafel plot is not equal to zero.

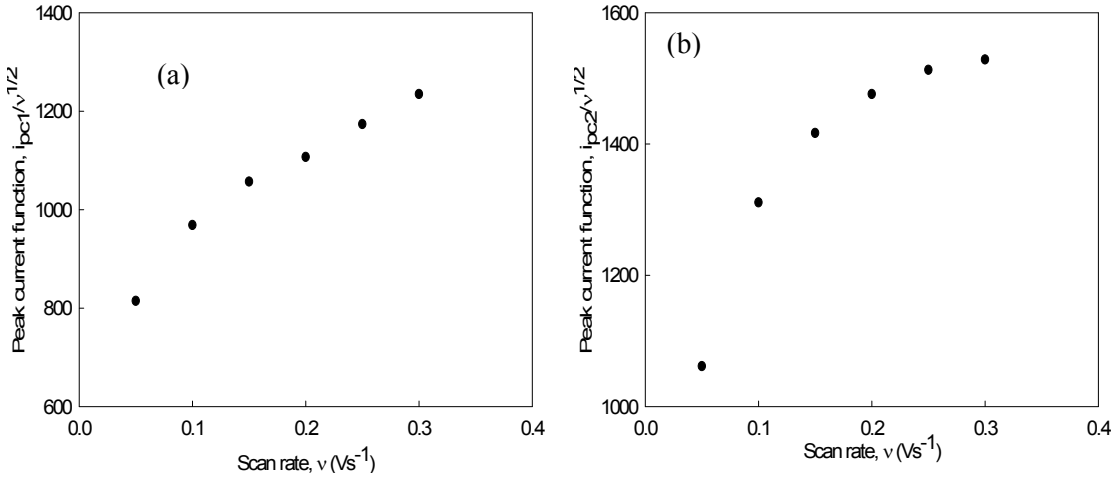

Fig 3.1.34 Variation of Peak current function with scan rate for Mn(II) in 0.1 M KCl solution (a) first pair, (b) second pair of peaks.

Considering all the above points it can be concluded that the electrochemical process involved in Mn(II) is quasi-reversible.

Moreover, the system is diffusion controlled as well as adsorptive controlled, which can be declared from the facts that a) in the forward scans, peak currents are proportional to the square root of scan rate, b) peak currents in both the regions (cathodic and anodic) increases linearly with square root of scan rate, c) slope of log i_p against log ν plot is less than unity.

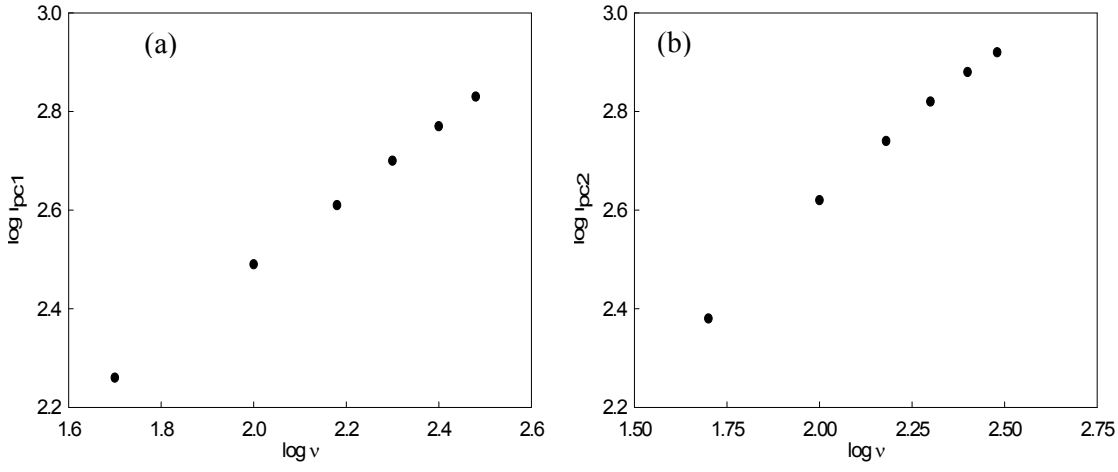

Fig 3.1.35 Plot of log i_p with log ν for Mn(II) in 0.1 M KCl solution (a) first pair, (b) second pair of peaks.

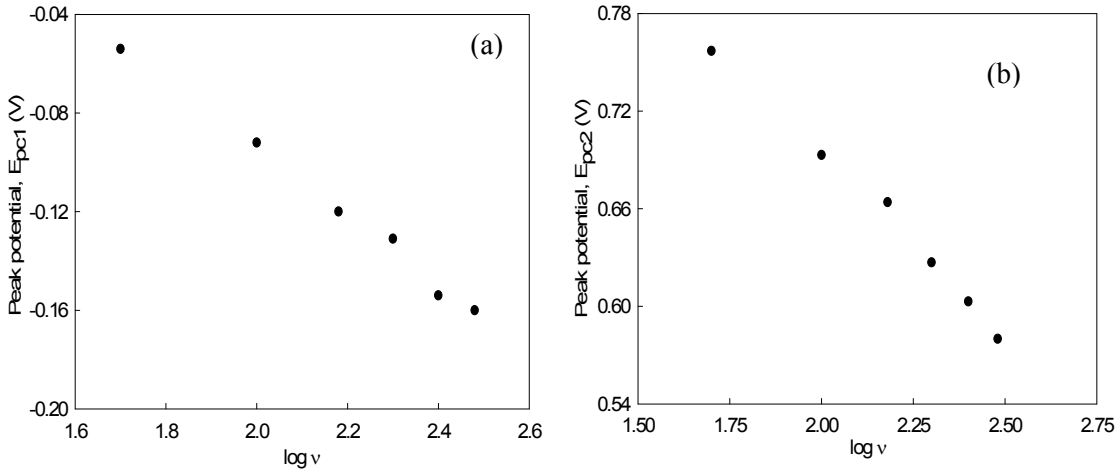

Fig 3.1.36 Variation of Peak potential with log ν for Mn(II) in 0.1 M KCl solution (a) first pair, (b) second pair of peaks.

Redox behavior of Mn(II)-Ciprofloxacin mixture in solution

The redox behaviour of Mn(II)-Ciprofloxacin 1:2 interaction was also studied in 0.1M potassium chloride and at varying scan rates using cyclic voltammetric technique within the potential window from -1.400 V to 2.000 V at room temperature at glassy carbon electrode (GCE). A CV of the above system at scan rate 0.100 Vs^{-1} is given in Fig 3.1.37.

The CV shows two cathodic peaks (c_1 and c_2) at the potentials of -0.181 V and 0.349 V and one (a_1) in the anodic region at 1.014 V. Compared to the CV of Mn(II), it is found that the first cathodic peak (c_1) shifts towards more negative as well as the second one (c_2) towards less positive potential. Therefore, it is observed that after interaction the number of peaks in the anodic region is changed as well as the peak positions are also altered. These two facts implies that the interaction between Mn(II) and Ciprofloxacin is successful.

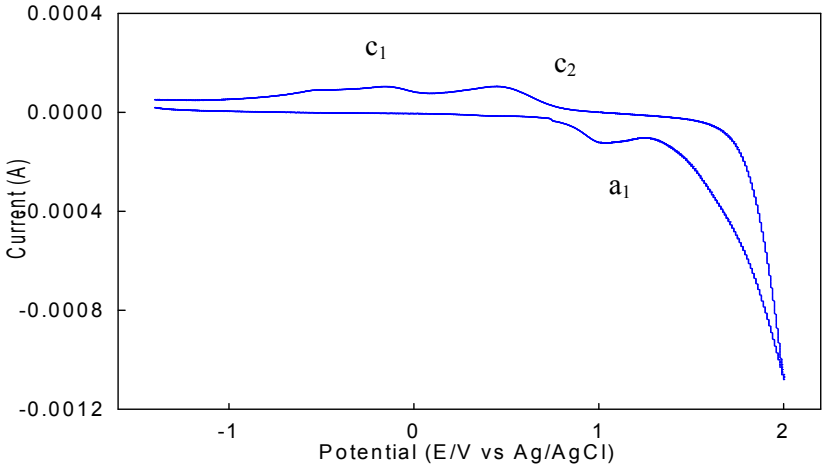

Fig 3.1.37 Cyclic voltammogram of Mn(II)-Ciprofloxacin 1:2 interaction in 0.1 M KCl at scan rate 0.100 Vs^{-1}.

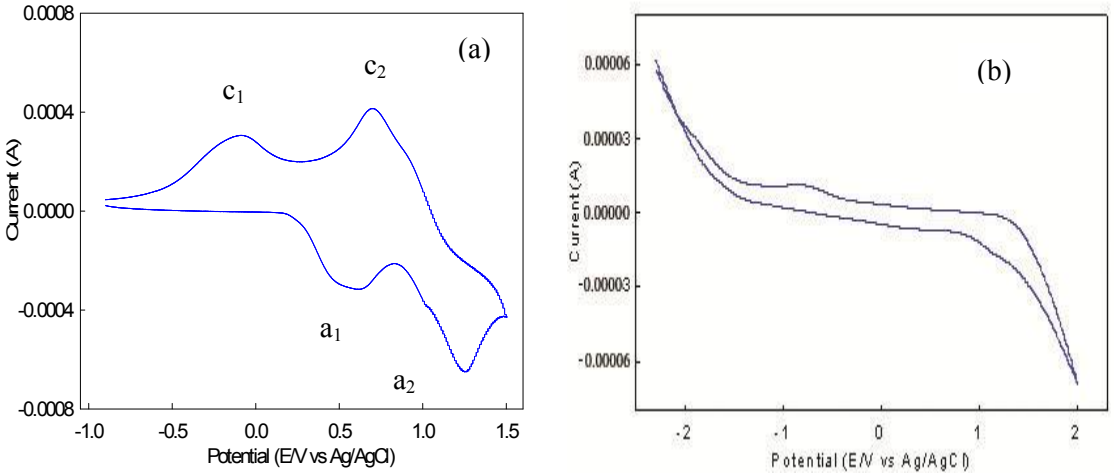

Fig 3.1.38 Cyclic voltammograms of (a) Mn(II) and (b) Ciprofloxacin at scan rate 0.100 Vs^{-1}.

Fig 3.1.39 shows the voltammograms of Mn(II)-Ciprofloxacin interaction at different scan rates. It shows that with the increase in scan rate the first cathodic peak shifts towards more negative potential but the second one towards more positive potential. Again in the anodic region, the peak shifts towards more positive potential with the increase in scan rate.

With the increase in scan rate, almost all the peaks become broader. Such behavior has been ascribed to slower charge propagation, probably due to difference in salvation and

or permeability. Current-potential data for the system under consideration is recorded in Table 3.1.4.

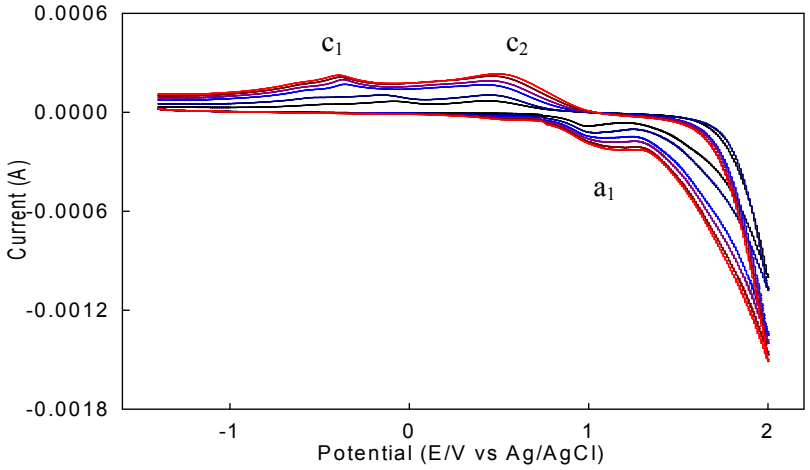

Fig 3.1.39 Cyclic voltammograms of Mn(II)-Ciprofloxacin 1:2 interaction in 0.1 M KCl solution at different scan rates.

Table 3.1.4 Current-potential data for Mn(II)-Ciprofloxacin 1:2 interaction in 0.1 M KCl at different scan rates.

Scan rate	SQRT of scan rate	Cathodic peak potential		Anodic peak potential	Cathodic peak current		Anodic peak current	Peak potential separation	Peak current ratio
ν (Vs^{-1})		E_{pc1} (V) [-]	E_{pc2} (V)	E_{pa} (V)	i_{pc1} (μA)	i_{pc2} (μA)	i_{pa} (μA) [-]	$\Delta E_p = E_{pa} - E_{pc2}$ (V)	i_{pa}/ i_{pc2}
0.050	0.2236	0.075	0.477	1.051	60.25	41.11	50.21	1.126	1.22
0.100	0.3162	0.089	0.482	1.084	86.22	52.21	52.32	1.173	1.00
0.150	0.3872	0.358	0.486	1.111	111.84	71.08	54.47	1.469	0.77
0.200	0.4472	0.362	0.491	1.153	137.35	82.45	57.04	1.515	0.69
0.250	0.5000	0.365	0.496	1.187	163.71	93.55	60.22	1.552	0.64
0.300	0.5477	0.369	0.501	1.211	180.25	104.15	61.04	1.580	0.59

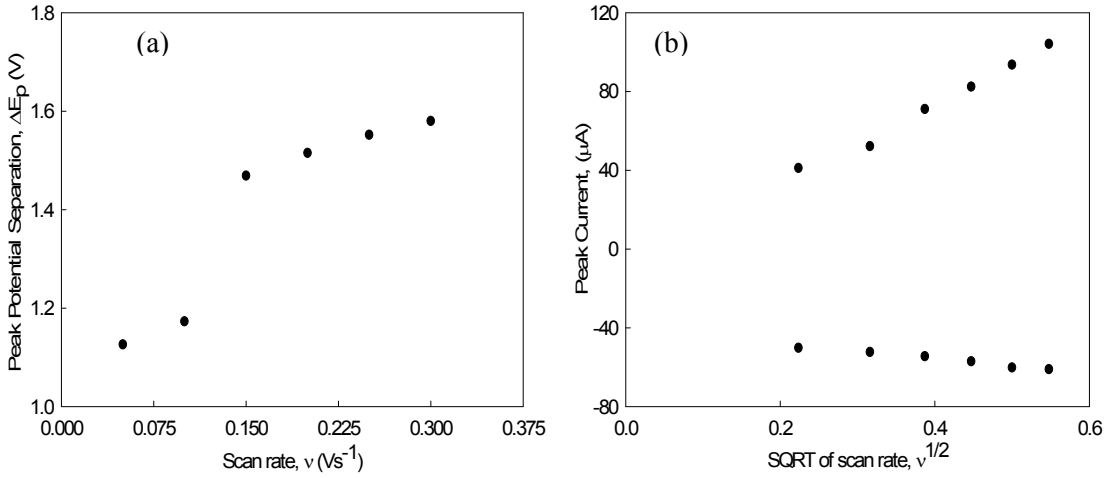

Fig 3.1.40 Variation of (a) peak potential separation with scan rate and (b) peak current with square root of scan rate for Mn(II)-Ciprofloxacin 1:2 interaction in 0.1M KCl solution.

The peak separation potential increases with the increase in scan rate (Fig 3.1.40(a)), indicating the limitation due to charge transfer kinetics.

Again the forward scan peak currents (i_{pc1} and i_{pc2}) are proportional to the square root of the scan rate at all the scan rates, which means the system to be diffusion controlled. Randle-Sevseik plot shows that with increasing $\nu^{1/2}$, the peak currents for both cathodic and anodic peaks increases linearly (Fig 3.1.40(b)), giving the conclusion that the processes are adsorptive controlled [35, 99].

The peak current ratios are almost unity at the lower scan rates and those are less than uity at higher scan rates. So, the system shows different character from reversible system to a little extent[101, 102].

Again the peak current ratio decreases with increasing scan rate (Fig 3.1.41(a)) and the peak current function ($i_p/\nu^{1/2}$) also decreases with increasing scan rate (Fig 3.1.41(b)). Both of these facts indicate that the electrochemical process under the investigation may have followed by any chemical process, i.e. it may follow EC mechanism[101, 102].

Again the plot of log i_p against log ν shows a linear relationship. It is found that the slope is less than unity, indicating that the process is accompanied by diffusion (Fig 3.1.42(a)).

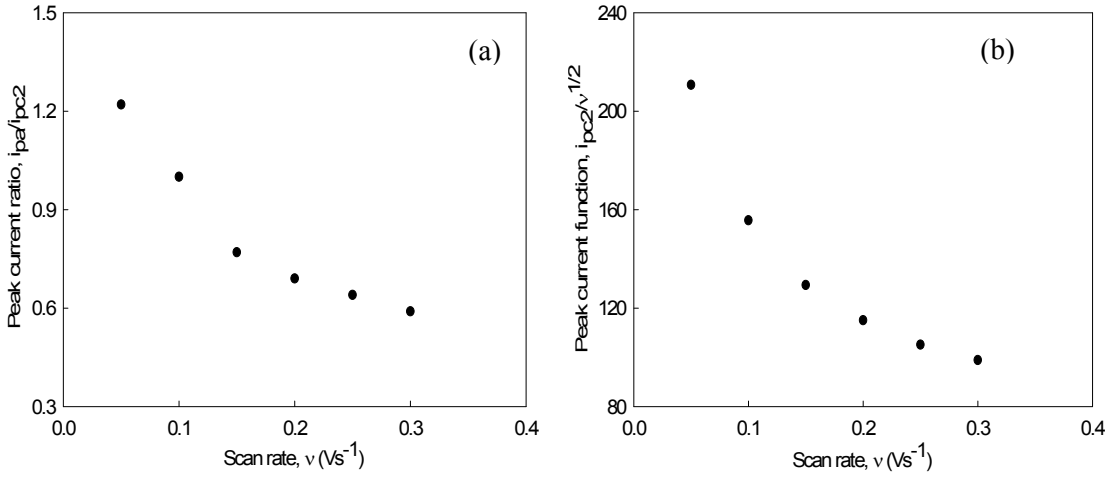

Fig 3.1.41 Variation of (a) peak current ratio with scan rate and (b) peak current function with scan rate for Mn(II)-Ciprofloxacin 1:2 interaction in 0.1M KCl solution.

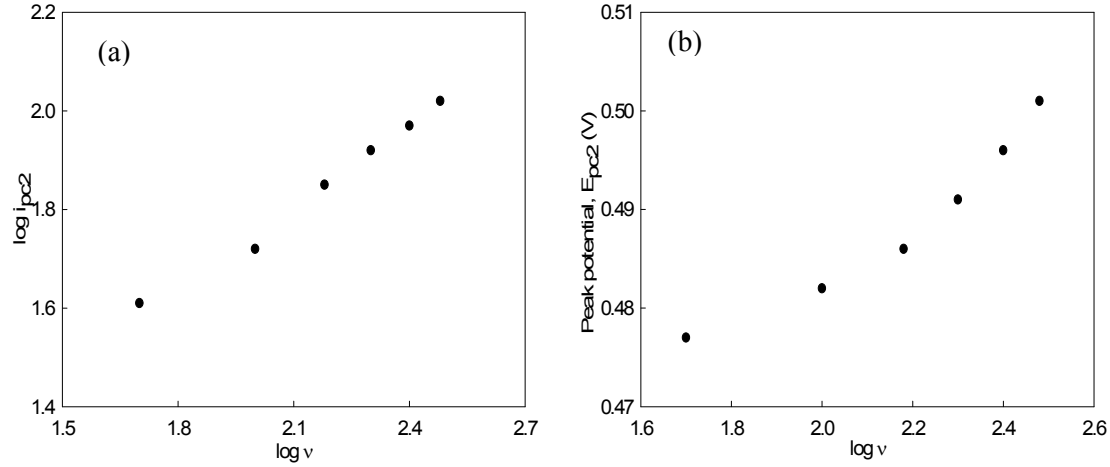

Fig 3.1.42 Variation of (a) log i_{pc2} with log ν and (b) peak potential with log ν for Mn(II)-Ciprofloxacin 1:2 interaction in 0.1 M KCl solution.

Tafel plot for the above system is shown in Fig 3.1.42(b). The curve express that the slope of the Tafel plot is not zero. So the electrochemical process exhibits character different from reversibility[3, 103].

Therefore from the above discussions there are some findings, such as: i) peak potential shifts with scan rate, ii) peak current ratio is not equal to unity, iii) the current function $i_p/\nu^{1/2}$ is independent of scan rate, iv) peak response broadens as scan rate increases, v) slope of Tafel plot is not equal to zero.

Considering all the above points it can be concluded that the electrochemical process involved in Mn(II)-Ciprofloxacin 1:2 interaction is quasi-reversible.

Moreover, the system is diffusion controlled as well as adsorptive controlled, which can be declared from the facts that a) in the forward scans, peak currents are proportional to the square root of scan rate, b) peak currents in both the regions (cathodic and anodic) increases linearly with square root of scan rate, c) slope of log i_p against log ν plot is less than unity.

3.1.4 Chronoamperometric and chronocoulometric study of Mn(II) and Mn(II)-Ciprofloxacin interaction

CA and CC study of Mn(II)

The Mn(II) system was also studied with chronoamperometric and chronocoulometric techniques which are also double potential step processes. The chronoamperometric (CA) experiment gives a current versus time curve, which are shown in Fig 3.1.43.

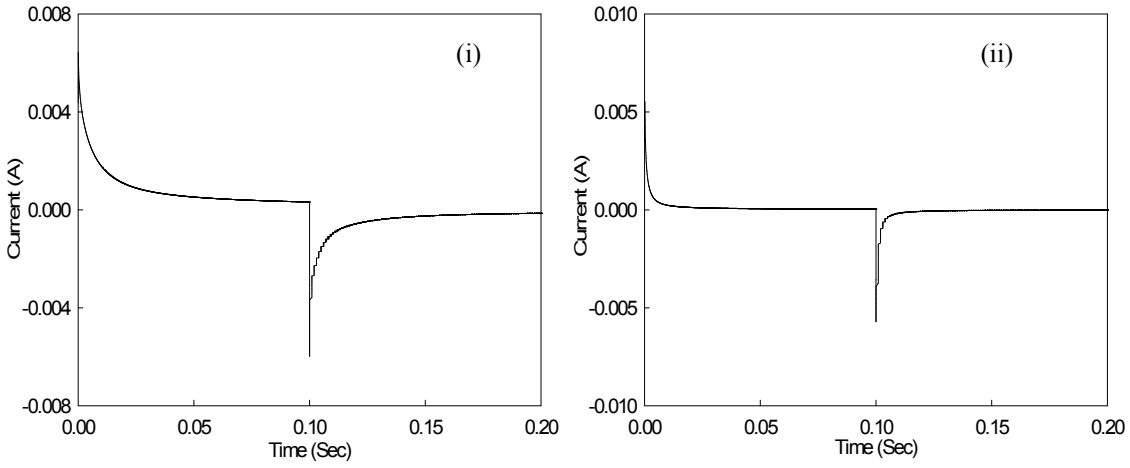

Fig 3.1.43 Current responses for Mn(II) in 0.1 M KCl solution (i) first and (ii) second pair of peaks.

It shows a current spike followed by a gradual decay in current. The spike is due to initial electrolysis of species at the electrode surface and the decay is due to diffusion of molecules to the electrode surface.

Chronocoulometry (CC) is the integrated form of the chronoamperometry. So that in CC the monitored response is charge. Such charge responses are shown in Fig 3.1.44.

Here in this double potential step CC, the potential is stepped from an initial value to a second value and then back to the initial value. The step from initial to the second is termed as forward potential step whereas the step from the second to the initial value is termed as reverse step[35].

Chronocoulometric response (Fig 3.1.44) shows that the charge at τ is about 2.211 μC for the first peak and 2.483 μC for the second peak.

Now if Q value obtained from time less than τ is plotted versus $t^{1/2}$ and on the same graph $-Q_r$ is plotted versus $\theta = [\tau^{1/2} + (t- \tau)^{1/2} - t^{1/2}]$, there will be two straight lines which intersects each other at Q=0 axis with equal slope, if there is no adsorption of reactant or product[31]. Any deviation from such condition means adsorption. Such plots are shown in the Figures 3.1.45 (i) and (ii).

This shows that the plots Q vs $t^{1/2}$ and $-Q_r$ vs θ do not intersect each other at Q=0 axis. Moreover they do not have equal slopes. Therefore from this plot, it may be said that adsorption of reactant or products occur on the electrode.

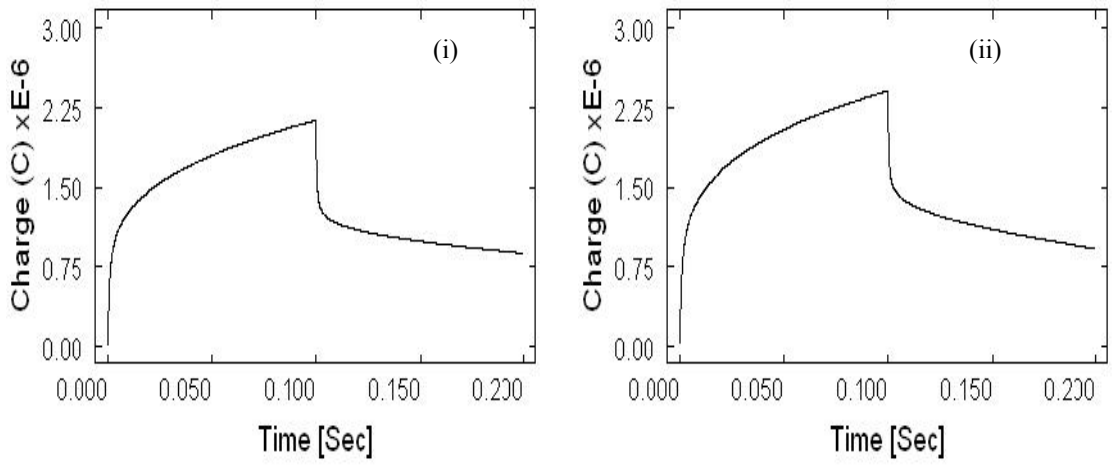

Fig 3.1.44 Charge responses for Mn(II) for in 0.1 M KCl solution (i) first and (ii) second pair of peaks.

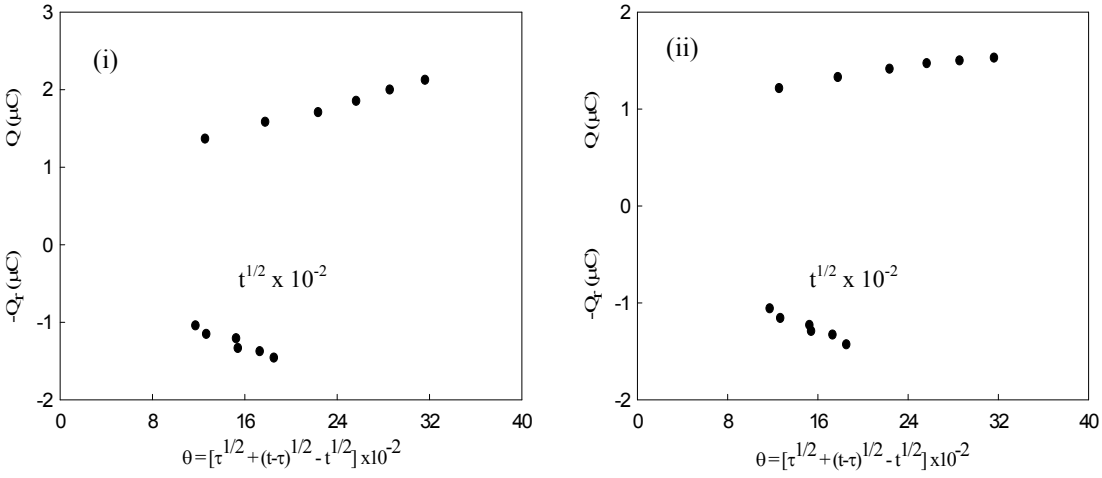

Fig 3.1.45 Plots of Q vs $t^{1/2}$ and $-Q_r$ vs θ for Mn(II) system in 0.1 M KCl solution (i) first and (ii) second pair of peaks.

CA and CC study of Mn(II)-Ciprofloxacin mixture in solution

Chronoamperometric study of Mn(II) system was also done after interaction with Ciprofloxacin. It was observed that there were two in the cahodic region after interaction and in the anodic region, there is only one. Therefore, after interaction there are only pair of peaks and CA study was also done correspondingly for that pair of peaks (which

corresponds to the second pair in case of Mn(II)). The chronoamperogram is shown in the Fig 3.1.46.

It shows that the spike height after interaction with Ciprofloxacin is decreased compared to that of Mn(II) (second pair) before interaction with Ciprofloxacin. Since the spike height is proportional to the rate of electrolysis, this means that after interaction the rate of electrolysis has been decreased (Fig 3.1.47).

Chronocoulometry (CC) is the integrated form of the chronoamperometry. So that in CC the monitored response is charge. It is also known as chronocoulogram. Such a charge response is shown in Fig 3.1.48.

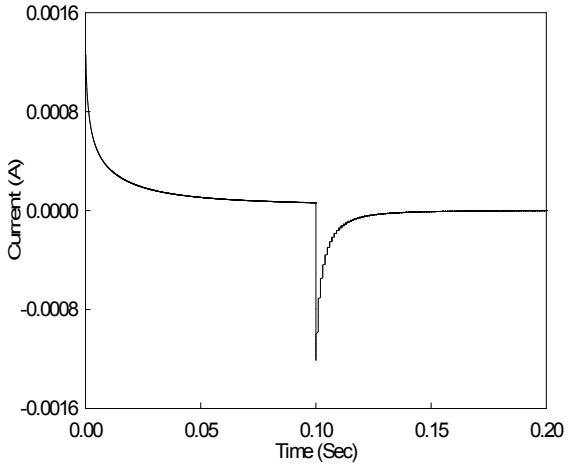

Fig 3.1.46 Current response for Mn(II)-Ciprofloxacin 1:2 interaction in 0.1 M KCl solution (corresponding to the second cathodic peak).

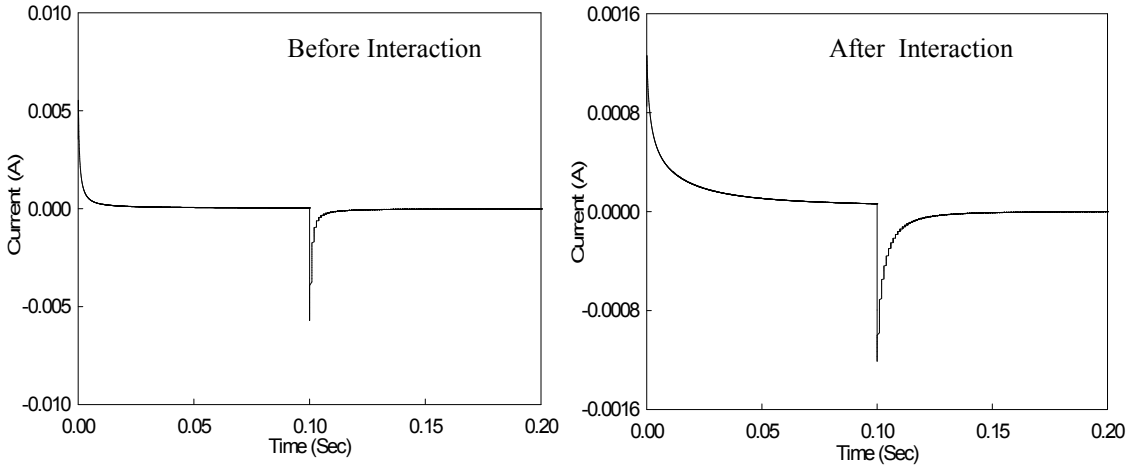

Fig 3.1.47 Current responses for Mn(II) in 0.1 M KCl solution (i) before and (ii) after interaction with Ciprofloxacin for second pair of peaks.

Chronocoulometric response (Fig 3.1.48) shows that the charge at τ is decreased after interaction with Ciprofloxacin. It was 2.211 μC for the first peak and 2.483 μC for the second peak in the absence of Ciprofloxacin, whereas it becomes 1.745 μC for the second pair of peaks after interaction with Cipropfloxacin.

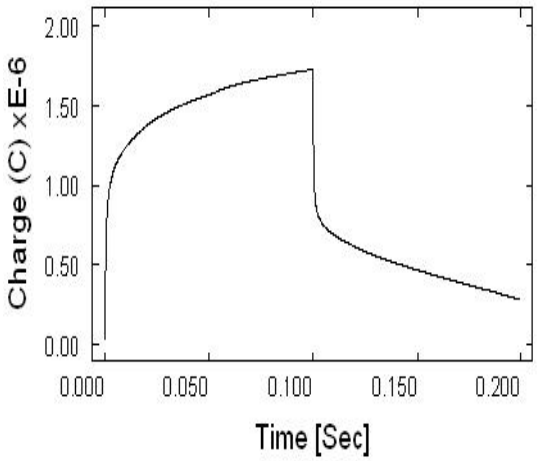

Fig 3.1.48 Charge response for Mn(II)-Ciprofloxacin 1:2 interaction in 0.1 M KCl solution (corresponding to the second cathodic peak).

Now if Q value obtained from time less than τ is plotted versus $t^{1/2}$ and on the same graph $-Q_r$ is plotted versus $\theta = [\tau^{1/2} + (t- \tau)^{1/2} - t^{1/2}]$, there will be two straight lines which intersects each other at Q=0 axis with equal slope, if there is no adsorption of reactant or product[31]. Any deviation from such condition means adsorption. Such a plot is shown in the Fig 3.1.49.

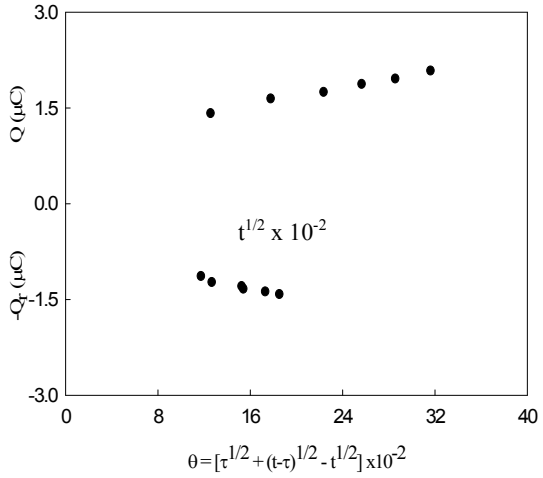

Fig 3.1.49 Plot of Q vs $t^{1/2}$ and $-Q_r$ vs θ for Mn(II)-Ciprofloxacin 1:2 interaction in 0.1 M KCl solution (corresponding to the second cathodic peak).

This shows that the plots Q vs $t^{1/2}$ and $-Q_r$ vs θ do not intersect each other at Q=0 axis. Moreover they do not have equal slopes. Therefore from this plot, it may be said that adsorption of reactant or products occur on the electrode.

Therefore the findings from the Chronoamperometric study is that after interaction the spike height is decreased, indicating towards a decrease in the rate of electrolysis. And from the Chronocoulometric study, it is observed that the charge at τ is also decreased. Both of these facts combinedly indicates towards successful interaction. And the observations from the plots Q vs $t^{1/2}$ and $-Q_r$ vs θ gives conclusion that adsorption of reactant or products occur on the electrode also after interaction.

3.1.5 Cyclic voltammetric study of Zn(II) and Zn(II)-Ciprofloxacin interaction at Glassy Carbon Electrode (GCE).

Redox behavior of Zn(II)

The redox behaviour of Zn(II) (in solution of $ZnCl_2$) in 0.1M potassium chloride and at varying scan rate was studied using cyclic voltammetric technique within the potential window from -1.700 V to -0.400 V at room temperature at glassy carbon electrode (GCE). A CV of the above system at scan rate 0.100 Vs^{-1} is given in Fig 3.1.50.

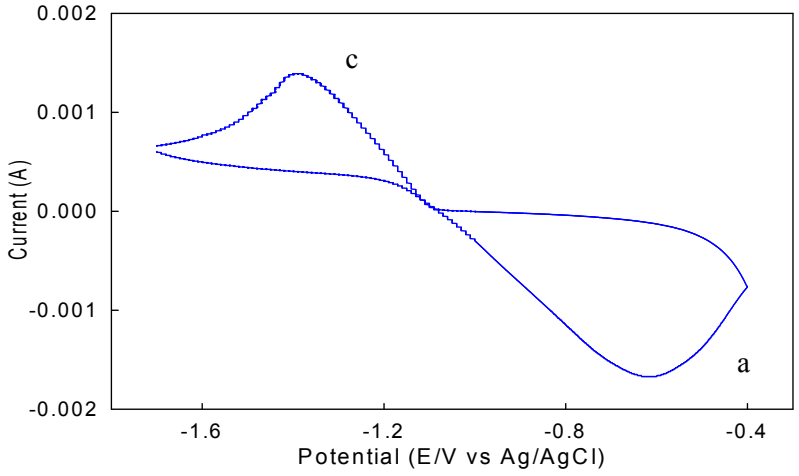

Fig 3.1.50 Cyclic voltammogram of Zn(II) in 0.1 M KCl solution at scan rate 0.100 Vs^{-1}.

The CV shows one cathodic peak (c) at the potential -1.381 V due to reduction of Zn(II) to Zn(0) and the same number of peak in the anodic (a) region at -0.611 V due to oxidation of Zn(0) to Zn(II). The electrode reaction may be presented by the following equations:

Cathodic reaction: $Zn^{2+} + 2e \longrightarrow Zn^{0}$

Anodic reaction: $Zn^{0} - 2e \longrightarrow Zn^{2+}$

The overall reaction is: $Zn^{2+} \underset{-2e}{\overset{+2e}{\rightleftharpoons}} Zn^{0}$

Fig 3.1.51 shows the voltammograms of Zn(II) at different scan rates. It is found that with the increase in scan rate the cathodic peak shifts towards more negative potential. On the other hand, the anodic peak shifts towards more positive potentials. That is, they moves towards opposite to each other with increasing scan rate. And Table 3.1.5 gives the current-potential data for the above system.

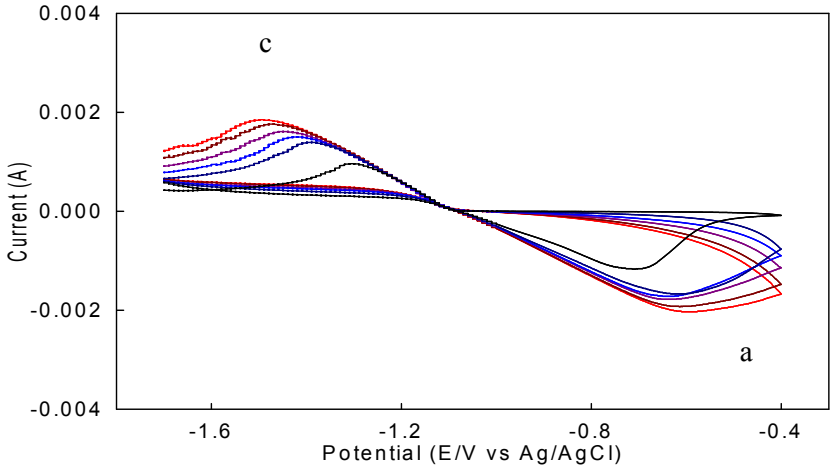

Fig 3.1.51 Cyclic voltammograms of Zn(II) in 0.1 M KCl at different scan rates.

It is found that with the increase in scan rate, almost all the peaks become broader. Such behavior has been ascribed to slower charge propagation, probably due to difference in salvation and or permeability.

The peak separation potential for the pair of peaks (ΔE_p) increases with the increase in scan rate, because the cathodic peak shifts towards negative and that of anodic towards positive. Here the cause responsible is the effect of iR drop. This fact further indicates the limitation due to charge transfer kinetics and is shown in the plot of ΔE_p vs ν (Fig 3.1.52(a).

Again the forward scan peak currents (i_{pc}) are proportional to the square root of the scan rate at all the pH values, which means the system to be diffusion controlled. Moreover with increasing $\nu^{1/2}$, the peak currents for both cathodic and anodic peaks increases linearly (Fig 3.1.52(b)), giving the conclusion that the processes are adsorptive controlled [35, 99].

Table 3.1.5 Current-potential data for Zn(II) in 0.1 M KCl at different scan rates.

Scan rate ν (Vs^{-1})	SQRT of scan rate	Cathodic peak potential E_{pc} (V)	Anodic peak potential E_{pa} (V)	Cathodic peak current i_{pc} (μA)	Anodic peak current i_{pa} (μA)	Peak potential separation $\Delta E_p = E_{pa} - E_{pc}$	Peak current ratio i_{pa}/ i_{pc}

		[-]	[-]		[-]	(V)	
0.050	0.2236	1.321	0.695	575.22	507.12	0.626	0.88
0.100	0.3162	1.381	0.611	787.40	705.62	0.770	0.90
0.150	0.3872	1.403	0.625	830.48	800.94	0.778	0.96
0.200	0.4472	1.442	0.609	875.95	940.71	0.833	1.07
0.250	0.5000	1.478	0.596	922.57	997.25	0.882	1.08
0.300	0.5477	1.516	0.581	973.15	1065.47	0.935	1.10

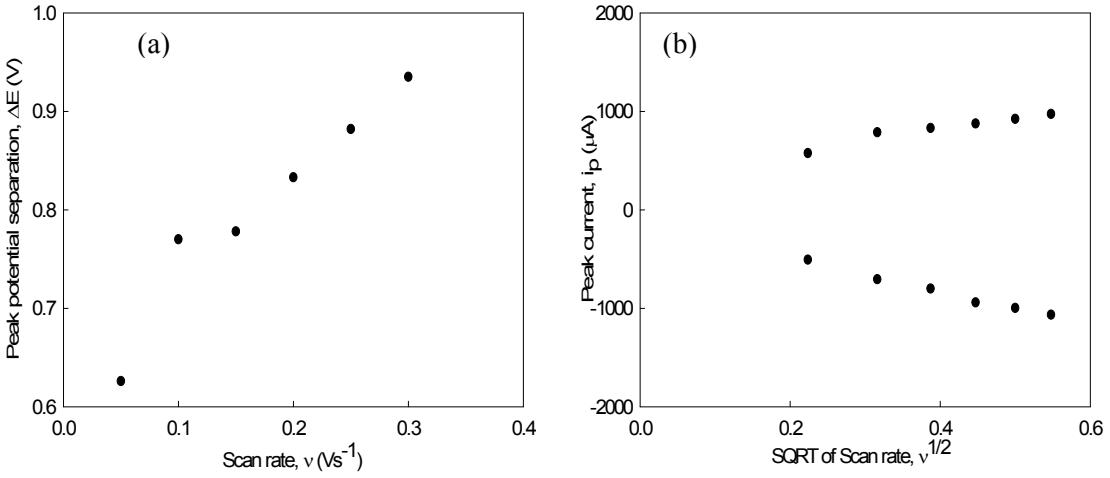

Fig 3.1.52 Variation of (a) Peak potential separation with scan rate and (b) Peak current with square root of scan rate for Zn(II) in 0.1 M KCl solution.

The peak current ratio for the pair of peaks is very much nearest to unity at all the scan rates. It is known that it is a strong evidence for reversibility. So, from this finding it may be concluded that the system may be reversible[101, 102].

A plot of peak current ratio against scan rate is given in Fig 3.1.53(a). It shows that the peak current ratio increases with increasing scan rate.

Fig 3.1.53(b) shows that peak current function ($i_p/\nu^{1/2}$) at first decreases with increasing scan rate. This fact indicates that the electrochemical process under the investigation is not followed by chemical process, i.e. it does not follow EC mechanism[101, 102].

Again the plot of log i_p against log ν shows a linear relationship having slope less than unity, indicating that the process is accompanied by diffusion[3, 103] (Fig 3.1.54(a)).

Tafel plot (peak potential vs log ν) for the pair of peaks are shown in Fig 3.1.54(b). The

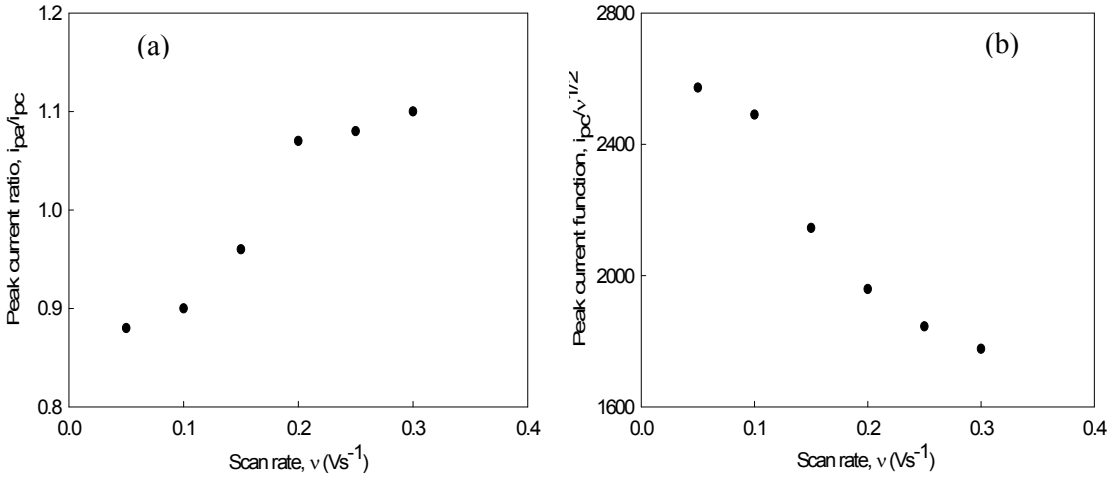

Fig 3.1.53 Variation of (a) peak current ratio and (b) peak current function with scan rate for Zn(II) in 0.1 M KCl solution.

curve express that the slope of the Tafel plot is not zero but very much nearest to zero. So the electrochemical process may be reversible.

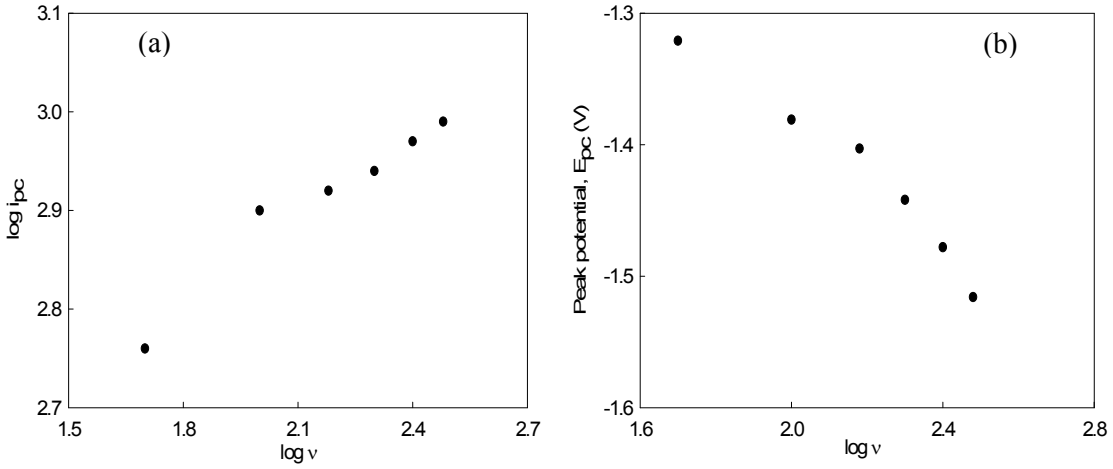

Fig 3.1.54 Variation of (a) log i_p and (b) peak potential with log ν for Zn(II) in 0.1 M KCl solution.

Therefore from the above discussions there are some findings, such as: i) peak potential shifts with scan rate to small extent, ii) peak current ratio is almost equal to unity, iii)

slope of Tafel plot is very nearest to zero. Considering all the above points it can be concluded that the electrochemical process involved in Zn(II) is near to reversible.

Moreover, the system is diffusion controlled as well as adsorptive controlled, which can be declared from the facts that a) in the forward scans, peak currents are proportional to the square root of scan rate, b) peak currents in both the regions (cathodic and anodic) increases linearly with square root of scan rate, c) slope of log i_p against log ν plot is less than unity.

Redox behavior of Zn(II)-Ciprofloxacin mixture in solution

The redox behaviour of Zn(II)-Ciprofloxacin 1:1 interaction was also studied in 0.1M potassium chloride and at varying scan rates using cyclic voltammetric technique within the potential window from -1.700 V to -0.400 V at room temperature at glassy carbon electrode (GCE). A CV of the above system at scan rate 0.100 Vs^{-1} is given in Fig 3.1.55.

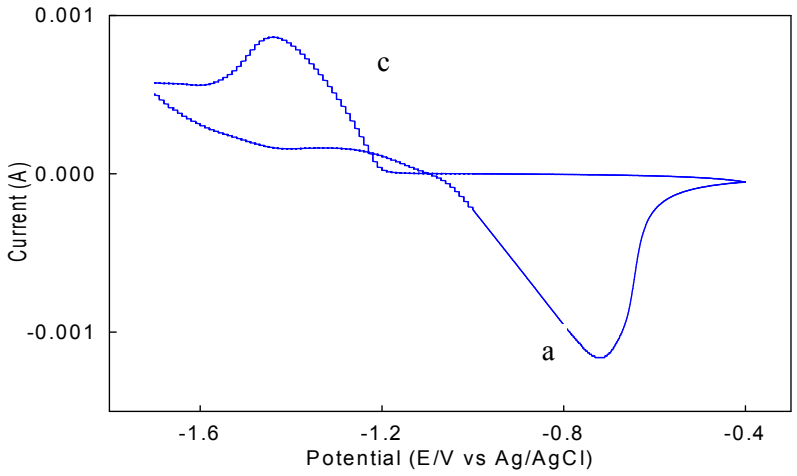

Fig 3.1.55 Cyclic voltammogram of Zn(II)-Ciprofloxacin 1:1 interaction in 0.1 M KCl solution at scan rate 0.100 Vs^{-1}.

The CV shows one cathodic peak at the potential -1.479 V as well as in the anodic region peak at -0.725 V. It is found that compared to the Zn(II) (before interaction), both the peaks shift towards more negative potentials. This fact indicates towards successful interaction.

Fig 3.1.57 shows the voltammograms of Zn(II)-Ciprofloxacin 1:1 interaction at different scan rates. It shows that with the increase in scan rate the cathodic peak shifts towards more negative potential. But the anodic peak move towards less negative potential with increasing scan rates.

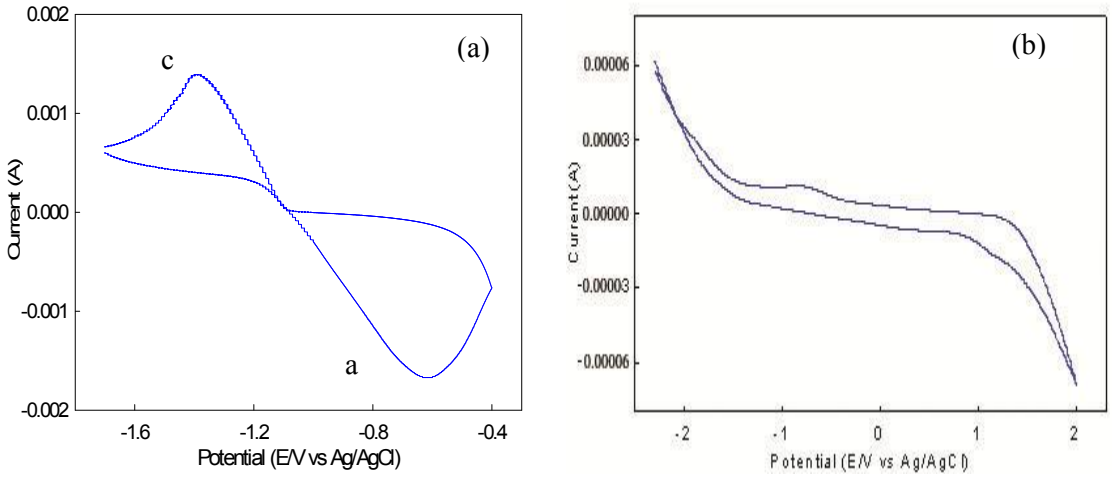

Fig 3.1.56 Cyclic voltammograms of (a) Zn(II) and (b) Ciprofloxacin before interaction in 0.1 M KCl at scan rate 0.100 Vs^{-1}.

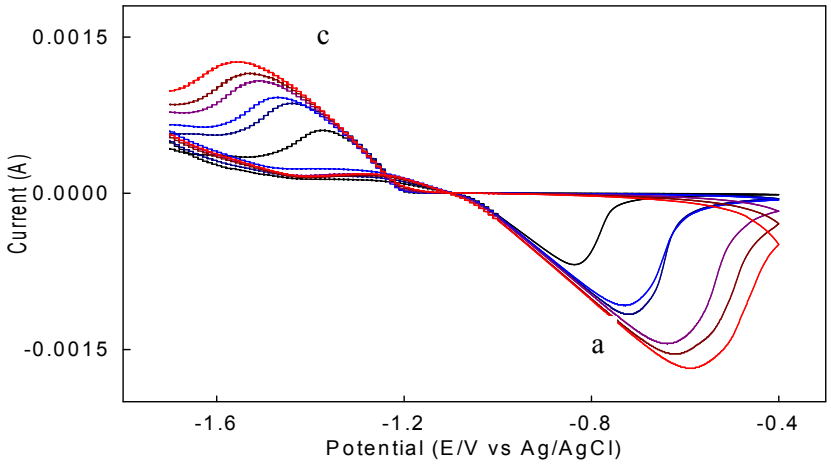

Fig 3.1.57 Cyclic voltammogram of Zn(II)-Ciprofloxacin 1:1 interaction in 0.1 M KCl at different scan rates.

Moreover, with the increase in scan rate, almost all the peaks become broader. Such behavior has been ascribed to slower charge propagation, probably due to difference in

salvation and or permeability. Current-potential data for the system under consideration is recorded in Table 3.1.6.

The peak separation potential for the pair of peaks (ΔE_p) increases with the increase in scan rate as the cathodic peak shifts towards negative and that of anodic towards less negative potential. Here the cause responsible is the effect of iR drop. This behaviour is similar to that of the Zn(II) system before interaction. Therefore it may be said that the

Table 3.1.6 Current-potential data for Zn(II)-Ciprofloxacin 1:1 interaction in 0.1 M KCl at different scan rates.

Scan rate ν (Vs^{-1})	SQRT of scan rate	Cathodic peak potential E_{pc} (V) [-]	Anodic peak potential E_{pa} (V) [-]	Cathodic peak current i_{pc} (μA)	Anodic peak current i_{pa} (μA) [-]	Peak potential separation $\Delta E_p = E_{pa} - E_{pc}$ (V) [-]	Peak current ratio i_{pa}/ i_{pc}
0.050	0.2236	1.329	0.842	344.14	580.51	0.487	1.69
0.100	0.3162	1.479	0.725	348.77	768.99	0.754	2.21
0.150	0.3872	1.484	0.711	352.48	785.65	0.773	2.23
0.200	0.4472	1.507	0.664	360.58	1050.25	0.843	2.91
0.250	0.5000	1.538	0.645	369.57	1090.50	0.893	2.95
0.300	0.5477	1.563	0.607	377.51	1130.18	0.956	2.99

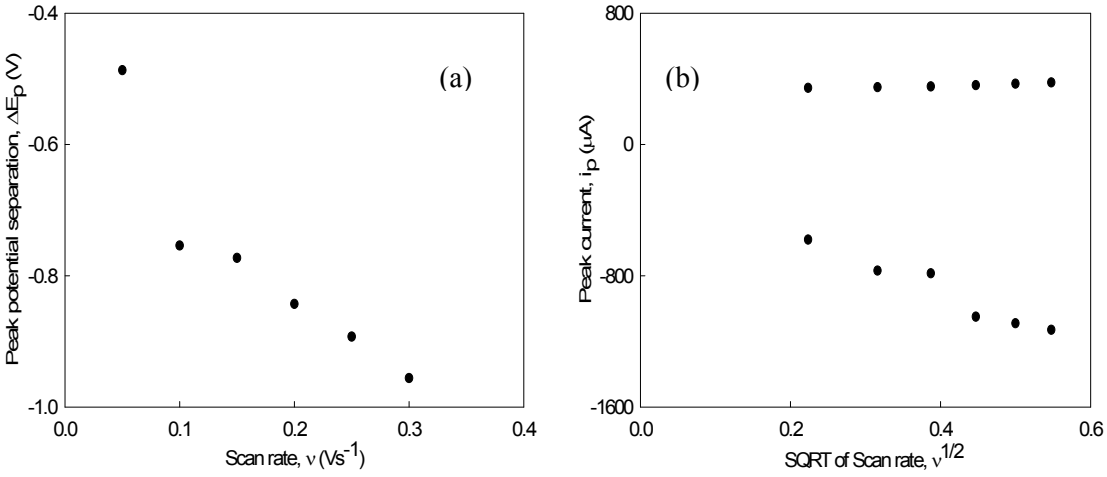

Fig 3.1.58 Variation of (a) peak potential separation with scan rate and (b) peak current with square root of scan rate for Zn(II)-Ciprofloxacin 1:1 interaction in 0.1 M KCl solution.

above system indicate the limitation due to charge transfer kinetics and is shown in the plot of ΔE_p vs ν in Fig 3.1.58(a).

Again the forward scan peak currents (i_{pc}) are proportional to the square root of the scan rate at all the scan rates, which means the system to be diffusion controlled. Moreover with increasing $\nu^{1/2}$, the peak currents for both cathodic and anodic peaks increases linearly[35, 99] (Fig 3.1.58(b)), giving the conclusion that the processes are adsorptive controlled.

The peak current ratios are very much higher than unity. Therefore it may be said that the system shows almost exceptional character from the reversible behavior[101, 102].

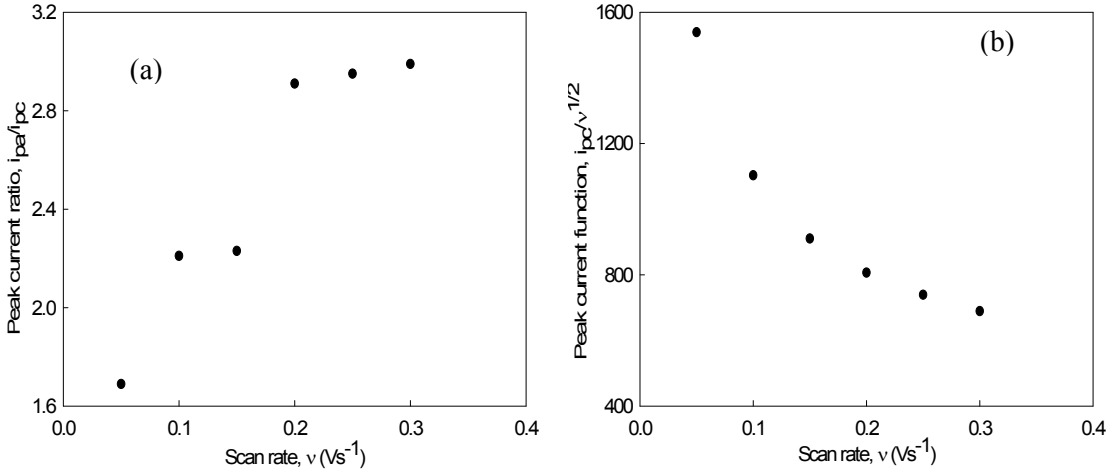

Fig 3.1.59 Variation of (a) peak current ratio and (b) peak current function with scan rate for Zn(II)-Ciprofloxacin 1:1 interaction in 0.1 M KCl solution.

Fig 3.1.59(a) shows that the peak current ratio increases with increasing scan rates. It shows two different regions of gradual increase. One upto scan rate 0.150 Vs^{-1} and the other above this scan rate.

Again peak current function ($i_{pc1}/\nu^{1/2}$) decreases with increasing scan rate (Fig 3.1.59(b)). Therefore, together both of these facts do not indicate any clear conception about the electrochemical process.

Plot of log i_{pc1} against log ν shows a linear relationship. It is found that the slope is less

than unity. Therefore it may be said that the process is accompanied by diffusion[3, 103] (Fig 3.1.60(a)).

Tafel plot (peak potential vs log ν) is shown in Fig 3.1.60(b). The curves express that the slopes of the Tafel plot is not zero. So the electrochemical process shows some exceptional character from reversibility.

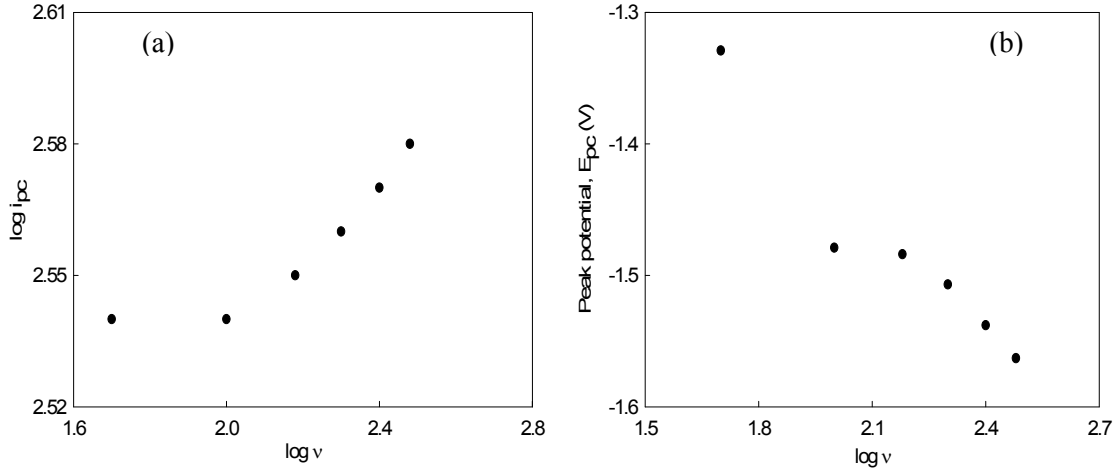

Fig 3.1.60 Variation of (a) log i_{pc1} and (b) peak potential with logν for Zn(II)-Ciprofloxacin 1:1 interaction in 0.1 M KCl solution.

Therefore from the above discussions there are some findings, such as: i) peak potential shifts with scan rate, ii) peak current ratio is not equal to unity, iii) the current function $i_p/\nu^{1/2}$ is independent of scan rate, iv) peak response broadens as scan rate increases, v) slope of Tafel plot is not equal to zero.

Considering all the above points it can be concluded that the electrochemical process involved in Zn(II)-Ciprofloxacin 1:1 interaction is quasi-reversible.

Moreover, the system is diffusion controlled as well as adsorptive controlled, which can be declared from the facts that a) in the forward scans, peak currents are proportional to the square root of scan rate, b) peak currents in both the regions (cathodic and anodic) increases linearly with square root of scan rate, c) slope of log i_p against log ν plot is less than unity.

3.1.6 Chronoamperometric and chronocoulometric study of Zn(II) and Zn(II)-Ciprofloxacin interaction

CA and CC study of Zn(II)

The Zn(II) system was also studied using chronoamperometric and chronocoulometric techniques which are also double potential step processes. The chronoamperometric (CA) experiment gives a current versus time curve, which is shown in Fig 3.1.61.

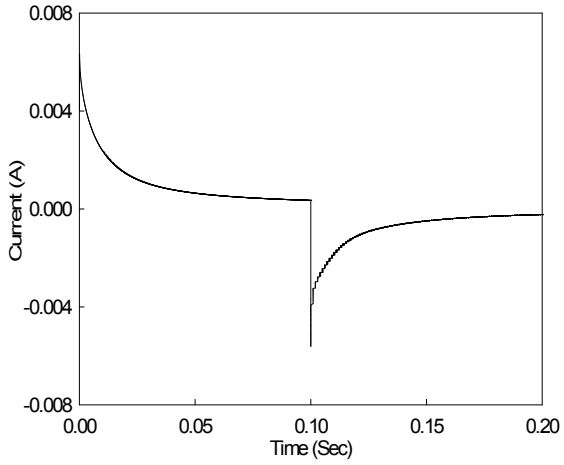

Fig 3.1.61 Current response for Zn(II) in 0.1 M KCl solution.

It shows a current spike followed by a gradual decay in current. The spike is due to initial electrolysis of species at the electrode surface and the decay is due to diffusion of molecules to the electrode surface[101].

Chronocoulometry (CC) is the integrated form of the chronoamperometry. So that in CC the monitored response is charge. Such charge responses are shown in Fig 3.1.62.

Here in this double potential step CC, the potential is stepped from an initial value to a second value and then back to the initial value. The step from initial to the second is termed as forward potential step whereas the step from the second to the initial value is termed as reverse step.[35]

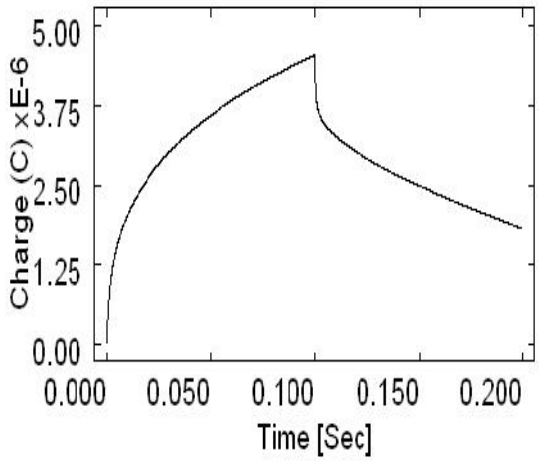

Fig 3.1.62 Charge responses for Zn(II) for in 0.1 M KCl solution.

Chronocoulometric response (Fig 3.1.62) shows that the charge at τ is about 4.659 μC. Now if Q value obtained from time less than τ is plotted versus $t^{1/2}$ and on the same graph $-Q_r$ is plotted versus $\theta = [\tau^{1/2} + (t- \tau)^{1/2} – t^{1/2}]$, there will be two straight lines which intersects each other at Q=0 axis with equal slope, if there is no adsorption of reactant or product[31]. Any deviation from such condition means adsorption. Such a plot is shown in the Fig 3.1.63.

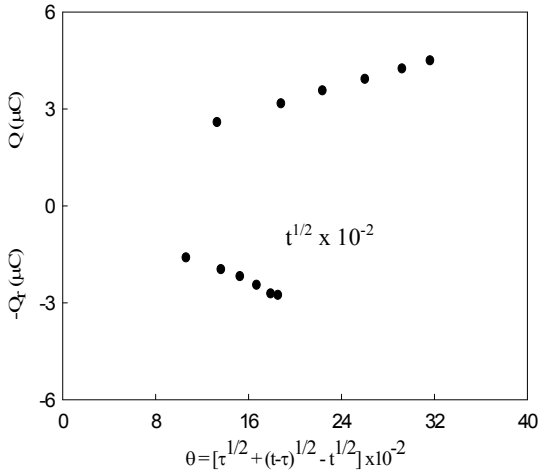

Fig 3.1.63 Plot of Q vs $t^{1/2}$ and $–Q_r$ vs θ for Zn(II) system in 0.1 M KCl solution.

This shows that the plots Q vs $t^{1/2}$ and $-Q_r$ vs θ do not intersect each other at Q=0 axis. Moreover they do not have equal slopes. Therefore from this plot, it may be said that adsorption of reactant or products occur on the electrode.

CA and CC study of Zn(II)-Ciprofloxacin mixture in solution

Chronoamperometric study of Zn(II) system was also done after interaction with Ciprofloxacin. It was observed that after interactionthe number of signals in cathodic as well as in the anodic region is unaltered, i.e there is only one peak in each region. But the positions and the shapes are changed. Therefore, after interaction there are only pair of peaks as in the system before interaction. And CA study was also done correspondingly for that pair of peaks. The chroamperogram is shown in the Fig 3.1.64.

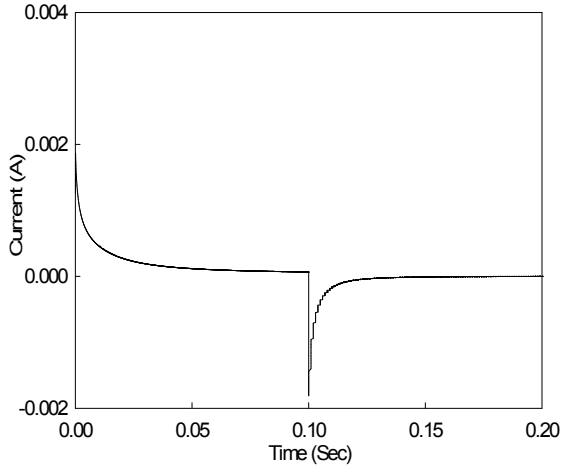

Fig 3.1.64 Current response for Zn(II)-Ciprofloxacin 1:1 interaction in 0.1 M KCl solution.

It shows that the spike height after interaction with Ciprofloxacin is decreased compared to that of Zn(II) before interaction with Ciprofloxacin. Since the spike height is proportional to the rate of electrolysis, this means that after interaction the rate of electrolysis has been decreased (Fig 3.1.65).

Chronocoulometry (CC) is the integrated form of the chronoamperometry. So that in CC the monitored response is charge. It is also known as chronocoulogram. Such a charge response is shown in Fig 3.1.66.

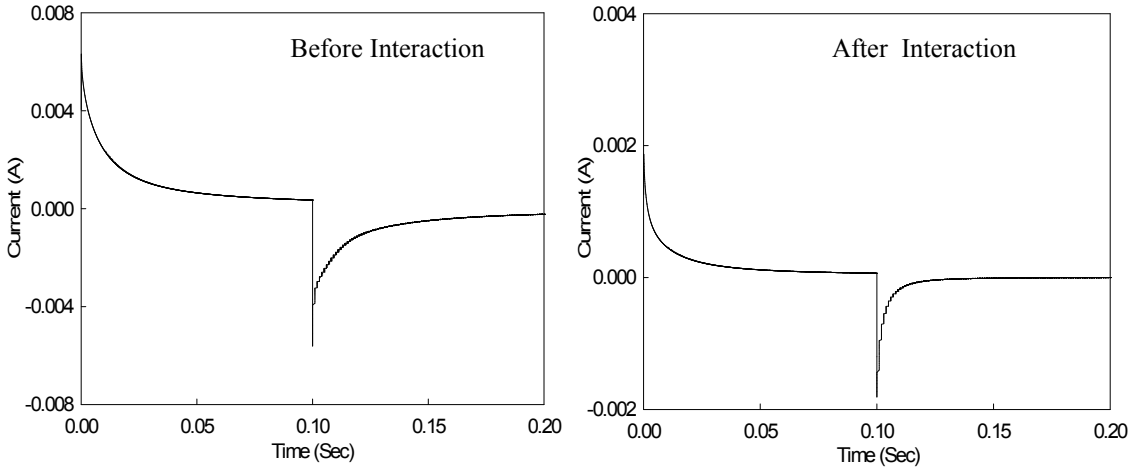

Fig 3.1.65 Current responses for Zn(II) in 0.1 M KCl solution (i) before and (ii) after interaction with Ciprofloxacin.

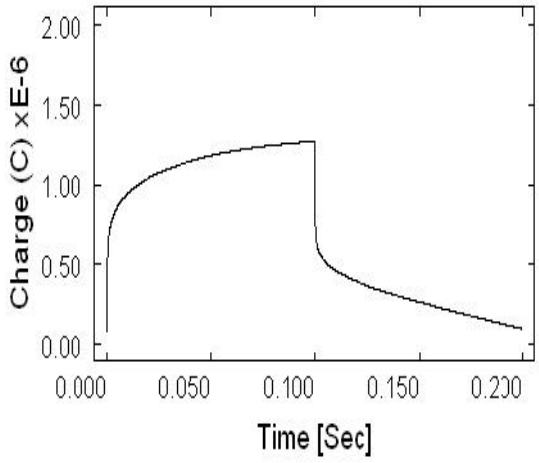

Fig 3.1.66 Charge response for Zn(II)-Ciprofloxacin 1:1 interaction in 0.1 M KCl solution.

Chronocoulometric response (Fig 3.1.66) shows that the charge at τ is decreased after interaction with Ciprofloxacin. It was 4.659 μC in the absence of ciprofloxacin, whereas it becomes 1.362 μC after interaction with Ciprofloxacin.

Now if Q value obtained from time less than τ is plotted versus $t^{1/2}$ and on the same graph $-Q_r$ is plotted versus $\theta = [\tau^{1/2} + (t- \tau)^{1/2} - t^{1/2}]$, there will be two straight lines which intersects each other at Q=0 axis with equal slope, if there is no adsorption of reactant or

product[31]. Any deviation from such condition means adsorption. Such a plot is shown in the Fig 3.1.67.

This shows that the plots Q vs $t^{1/2}$ and $-Q_r$ vs θ do not intersect each other at Q=0 axis. Moreover they do not have equal slopes. Therefore from this plot, it may be said that adsorption of reactant or products occur on the electrode.

Therefore the findings from the Chronoamperometric studiy is that after interaction the spike height is decreased, indicating towards a decrease in the rate of electrolysis. And from the Chronocoulometric study, it is observed that the charge at τ is also decreased. Both of these facts combinedly indicates towards successful interaction.

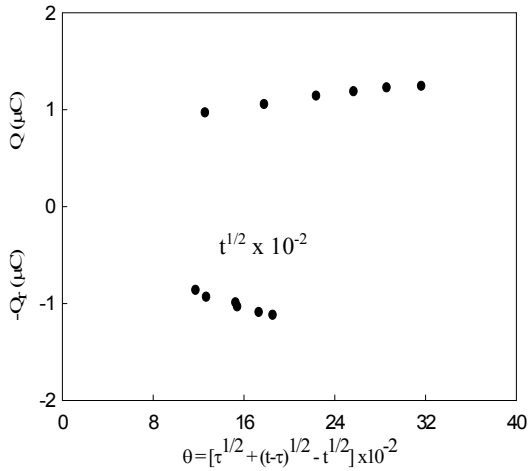

Fig 3.1.67 Plot of Q vs $t^{1/2}$ and $-Q_r$ vs θ for Zn(II)-Ciprofloxacin 1:1 interaction in 0.1 M KCl solution.

And the observations from the plots Q vs $t^{1/2}$ and $-Q_r$ vs θ gives conclusion that adsorption of reactant or products occur on the electrode also after interaction.

3.1.7 Cyclic voltammetric study of Cr(III), Ciprofloxacin and Cr(III)-Ciprofloxacin interaction at Platinum (Pt) Electrode.

Redox behavior of Cr(III)

The redox behaviour of Cr(III) (in solution of $CrCl_3$) in saturated potassium chloride at varying scan rate was studied using cyclic voltammetric technique within the potential window from 0.250 V to 1.700 V at room temperature at Platinum electrode (Fig 3.1.68).

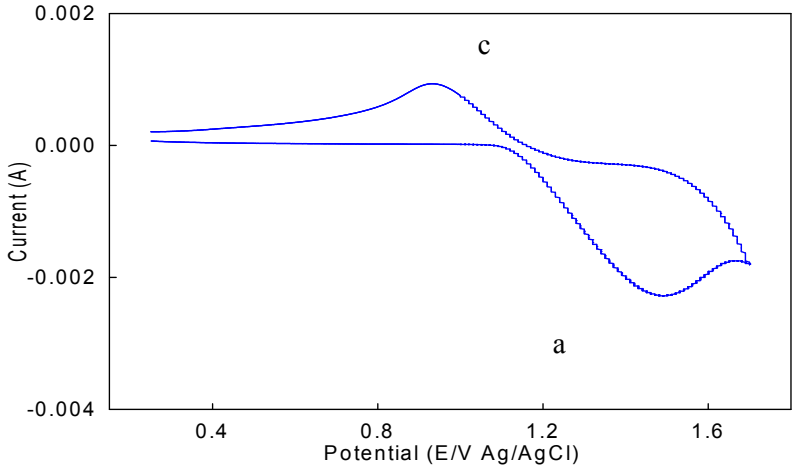

Fig 3.1.68 Cyclic voltammogram of Cr(III) in saturated KCl at scan rate 0.100 Vs^{-1}.

The CV shows one cathodic peak (c) at the potential 0.933 V due to reduction of Cr(III) to Cr(0) and the same number of peak in the anodic region (a) at 1.482 V due to oxidation of Cr(0) to Cr(III). Considering the peak separation value (0.549 V), the electrode reaction may be proposed by the following equations:

Cathodic reaction: $Cr^{3+} + e \longrightarrow Cr^{2+}$

Anodic reaction: $Cr^{2+} - e \longrightarrow Cr^{3+}$

The overall reaction is:

$$Cr^{3+} \underset{-e}{\overset{+e}{\rightleftharpoons}} Cr^{2+}$$

Fig 3.1.69 shows the voltammograms of Cr(III) at different scan rates. With the increase in scan rate the cathodic peak (c) shifts towards less positive potential. On the other hand, the anodic peak (a) shifts towards more positive potentials. That is, they moves towards opposite to each other with increasing scan rate. Table 3.1.7 gives the current-potential data for the above system.

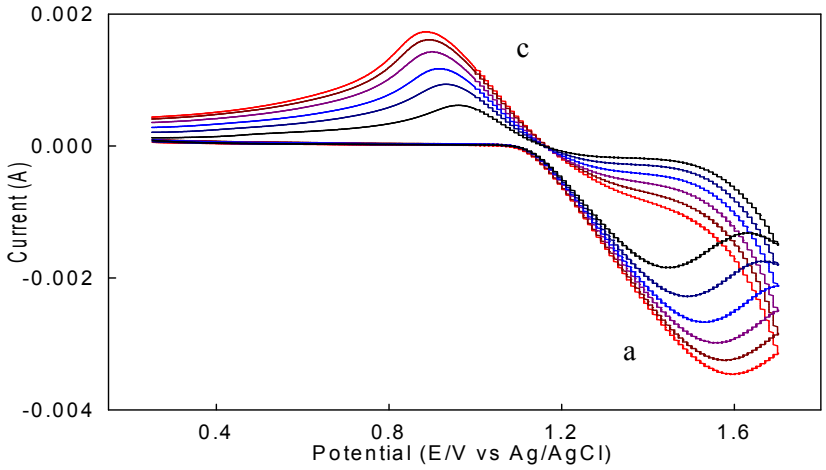

Fig 3.1.69 Cyclic voltammograms of Cr(III) in saturated KCl solution at different scan rates.

It is found that with the increase in scan rate, almost all the peaks become broader. Such behavior has been ascribed to slower charge propagation, probably due to difference in salvation and or permeability.

It is seen that with increasing scan rate (Table 3.1.7), the peak separation potential increases because the cathodic peak shifts towards less positive and that of anodic towards positive. Here the cause responsible is the effect of iR drop. This fact further indicates the limitation due to charge transfer kinetics and is shown in Fig 3.1.70(a).

Again the forward scan peak currents (i_{pc}) are proportional to the square root of the scan rate at all the scan rates, which means the system to be diffusion controlled. The peak currents in the cathodic region increases with increasing scan rate but the currents in the anodic region decreases with scan rate (Table 3.1.7). From the Randle-Sevseik plot (peak current vs square root of scan rate) for the above system, it was also found that the

cathodic peak currents increases linearly with the square root of scan rate (Fig 3.1.70(b)) although the situation is opposite in case of anodic peak current. Therefore, from these facts it cannot be demonstrated that the electrode process is adsorptive controlled[35, 99].

Table 3.1.7 Current-potential data for Cr(III) in saturated KCl at different scan rates.

Scan rate ν (Vs^{-1})	SQRT of scan rate	Cathodic peak potential E_{pc} (V)	Anodic peak potential E_{pa} (V)	Cathodic peak current i_{pc} (μA)	Anodic peak current i_{pa} (μA) [-]	Peak potential separation $\Delta E_p = E_{pa} - E_{pc}$ (V)	Peak current ratio i_{pa}/ i_{pc}
0.050	0.2236	0.961	1.443	530.11	1102.32	0.482	2.08
0.100	0.3162	0.933	1.482	640.33	1077.55	0.549	1.68
0.150	0.3872	0.902	1.531	710.74	1011.21	0.629	1.42
0.200	0.4472	0.891	1.566	850.97	988.17	0.675	1.16
0.250	0.5000	0.880	1.583	990.47	937.50	0.703	0.95
0.300	0.5477	0.873	1.594	1083.21	865.09	0.721	0.80

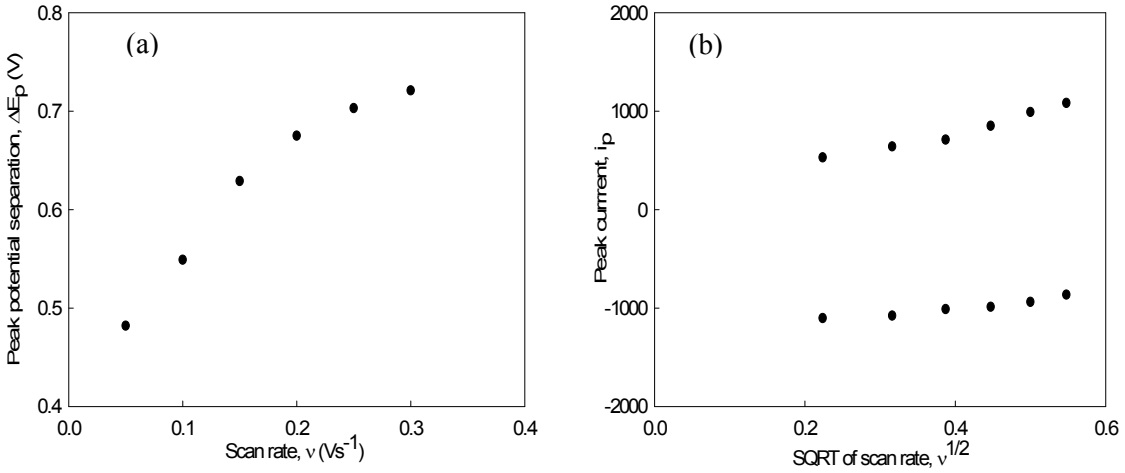

Fig 3.1.70 Variation of (a) peak potential separation with scan rate and (b) peak current with square root of scan rate for Cr(III) in saturated KCl solution.

The peak current ratio for the pair of peaks is more than unity at lower scan rates and decreases with increasing scan rate (Fig 3.1.71(a)). Again less than (or very nearest to) unity at higher scan rates. Therefore it may said that system shows different character from the reversible behavior at lower scan rates but almost reversible behavior at higher scan rates.

Fig 3.1.71(b) show that peak current function ($i_p/v^{1/2}$) at first decreases with increasing scan rate upto scan rate 0.150 Vs^{-1}. Then increases upto scan rate 0.250 Vs^{-1}. After that it is almost constant (Fig 3.1.71(b)). Both of these facts indicate that the electrochemical process under the investigation is partially followed by chemical process, i.e. it follows partial EC mechanism[101, 102].

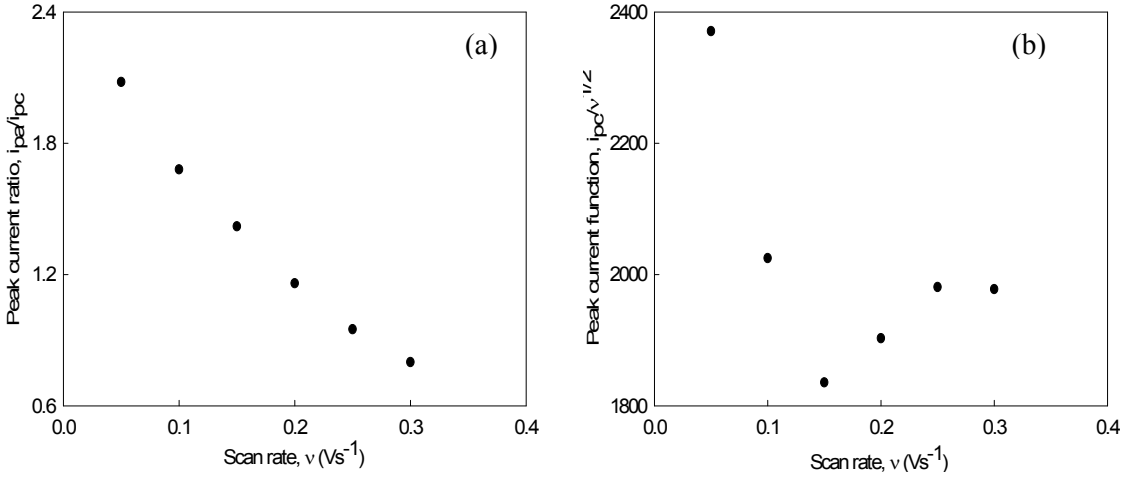

Fig 3.1.71 Variation of (a) peak current ratio and (b) peak current function with scan rate for Cr(III) in saturated KCl solution.

Again the plot of log i_p against log ν shows a linear relationship having slope less than unity, indicating that the process is accompanied by diffusion[3, 103] (Fig 3.1.72(a)). Tafel plot (peak potential vs log ν) for the pair of peaks are shown in Fig 3.1.72(b). The curve express that the slopes of the Tafel plot are not zero but much nearer to zero. So the

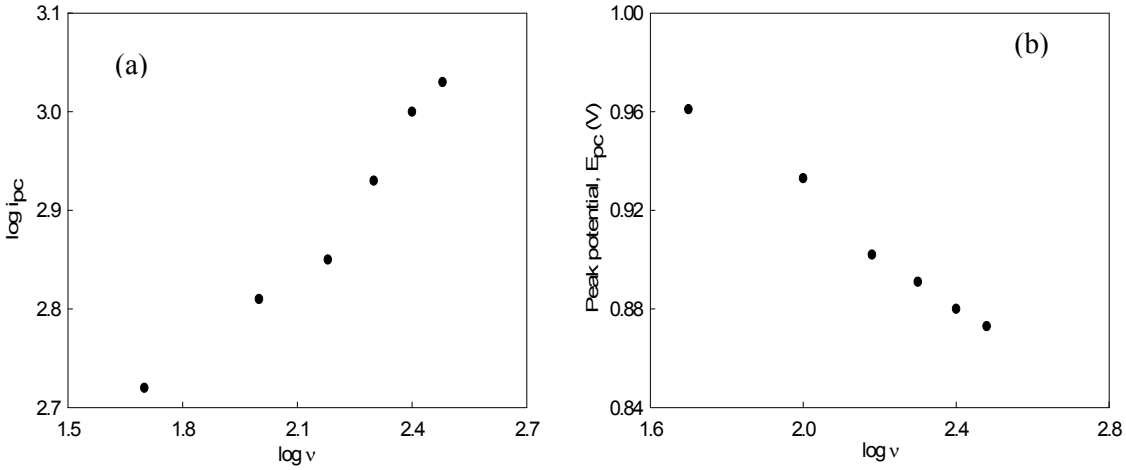

Fig 3.1.72 Variation of (a) log i_p and (b) peak potential with log ν for Cr(III) in saturated KCl solution.

electrochemical process will be a little bit different from reversible behavior. Therefore from the above discussions there are some findings, such as: i) peak potential shifts with scan rate to small extent, ii) peak current ratio is almost equal to unity, iii) slope of Tafel plot is very nearest to zero.

Considering all the above points it can be concluded that the electrochemical process involved in Cr(III) is near to reversible.

Moreover, the system is diffusion controlled as well as adsorptive controlled, which can be declared from the facts that a) in the forward scans, peak currents are proportional to the square root of scan rate, b) peak currents in both the regions (cathodic and anodic) increases linearly with square root of scan rate, c) slope of log i_p against log ν plot is less than unity.

Redox behavior of Ciprofloxacin (at Platinum electrode)

The redox behaviour of Ciprofloxacin in saturated potassium chloride and at varying scan rate was also studied using cyclic voltammetric technique within the potential window

from -0.900 V to 1.400 V at room temperature at Platinum electrode. A CV of the above system at scan rate 0.100 Vs^{-1} is given in Fig 3.1.73.

It shows two cathodic peaks at -0.079 V and at 1.095 V as well as the same number of peaks in the anodic region at -0.672 V and at 1.382 V. there is also a humplike shape in the cathodic region.

Responses for all the peaks are very much weak. It is found that with the increase in scan rate, both the first cathodic and the first anodic peaks shift towards less negative potentials. Exceptional behavior was observed in case of second cathodic peak. It does not show any significant change with scan rate. And the second anodic peak moves towards less positive potential to a very little extent with the increase in scan rate.

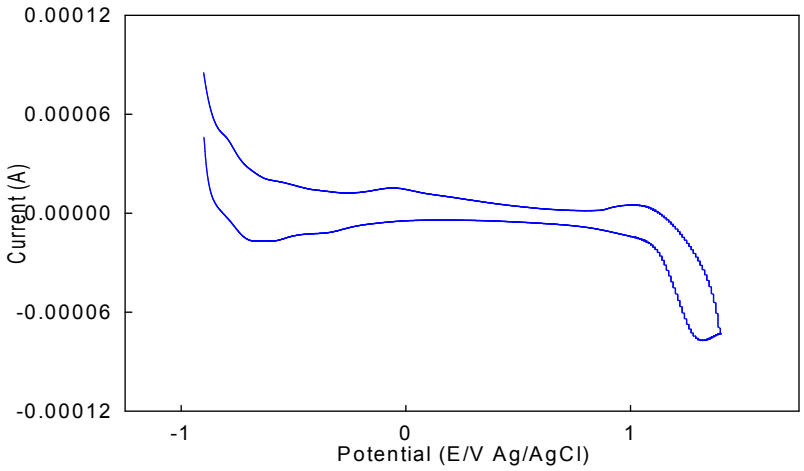

Fig 3.1.73 Cyclic voltammogram of Ciprofloxacin at scan rate 0.100 Vs^{-1} in saturated KCl solution.

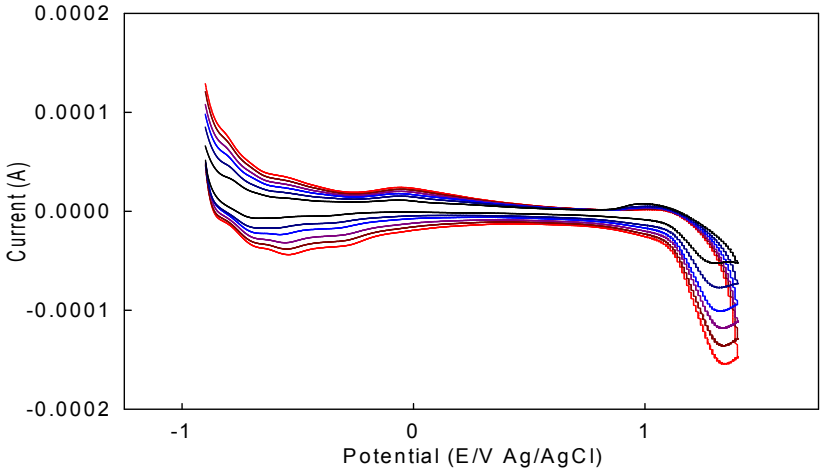

Fig 3.1.74 Scan rate variation of Ciprofloxacin in saturated KCl solution.

Again another character was noted in the scan rate variation. The fact is that with the change in scan rate, some humplike shapes develop in both the regions which also becomes more prominent at higher scan rates. The first peak both in the cathodic and the anodic regions also becomes broader with increasing scan rates.

Redox behavior of Cr(III)-Ciprofloxacin mixture in solution

The redox behaviour of Cr(III)-Ciprofloxacin 1:2 interaction was also studied in saturated potassium chloride and at varying scan rates using cyclic voltammetric technique within the potential window from -1.000 V to 1.700 V at room temperature at Platinum electrode. A CV of the above system at scan rate 0.100 Vs^{-1} is given in Fig 3.1.75.

The CV shows three cathodic peaks (c_1, c_2 and c_3) at the potentials of -0.711 V, 0.376 V and 0.898 V as well as in the anodic region two peaks (a_1 and a_2) at -0.531 V and 1.331 V. It also contains humplike shapes in both the regions. The first cathodic (c_1) and anodic peaks (a_1) may be due to the ligand (Ciprofloxacin) and the third cathodic (c_3) as well as the second anodic peak (a_2) may be due to Cr(III).

Compared to the CV of Cr(III) before interaction, it is found that peaks (c_3 and a_2) in both the region shifts towards less positive potential.

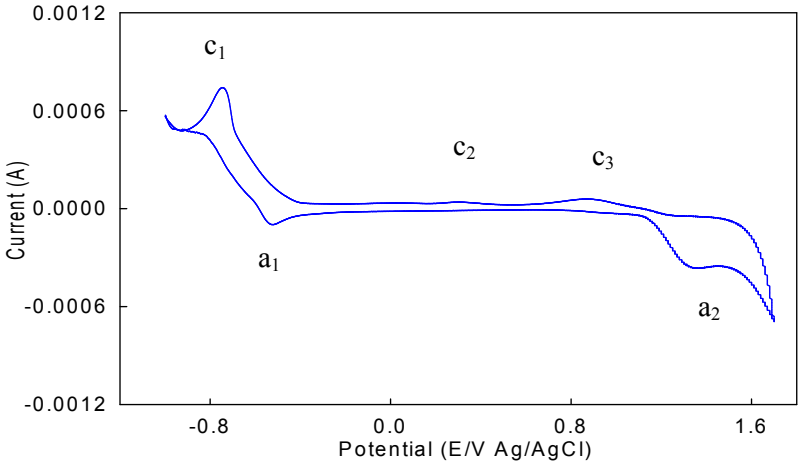

Fig 3.1.75 Cyclic voltammogram of 1:2 interaction of Cr(III)-ciprofloxacin in saturated KCl at scan rate 100 mVs^{-1}

Therefore it is found that after interaction the number of peaks are changed in both the region and also the peak positions are altered. All these facts gives clear indication about successful interaction.

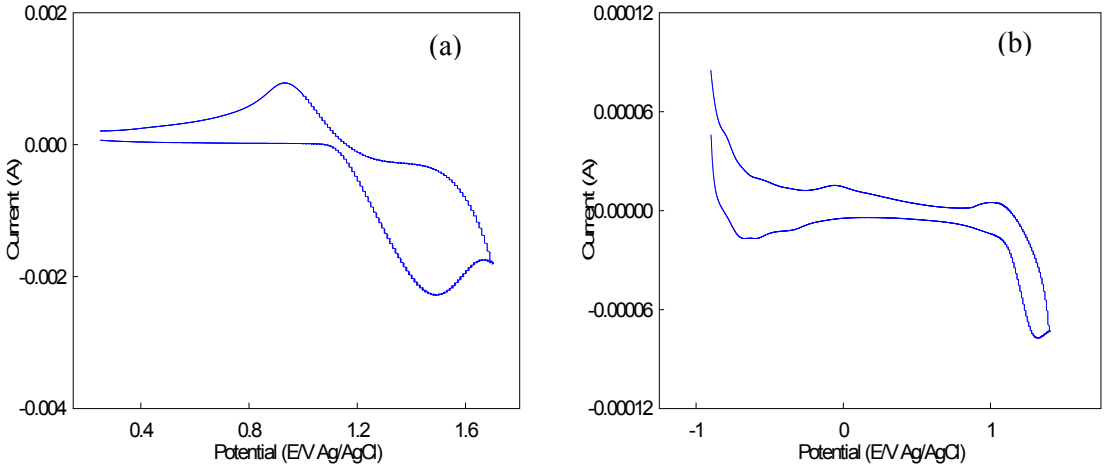

Fig 3.1.76 Cyclic voltammogram of uncoordinated (a) Cr(III) (b) Ciprofloxacin in saturated KCl at scan rate 100 mVs^{-1}

Fig 3.1.77 shows the voltammograms of Cr(III)-Ciprofloxacin 1:2 interaction at different scan rates. It shows that with the increase in scan rate all the cathodic peaks and the second anodic peak shift towards same direction (i.e. peak c_1 to more negative potential, c_2 and a_2 to less positive potential). But the first anodic peak towards more positive potential. Again in the anodic region the second peak disappears at the higher scan rates. At the higher scan rates, it is replaced by hump.

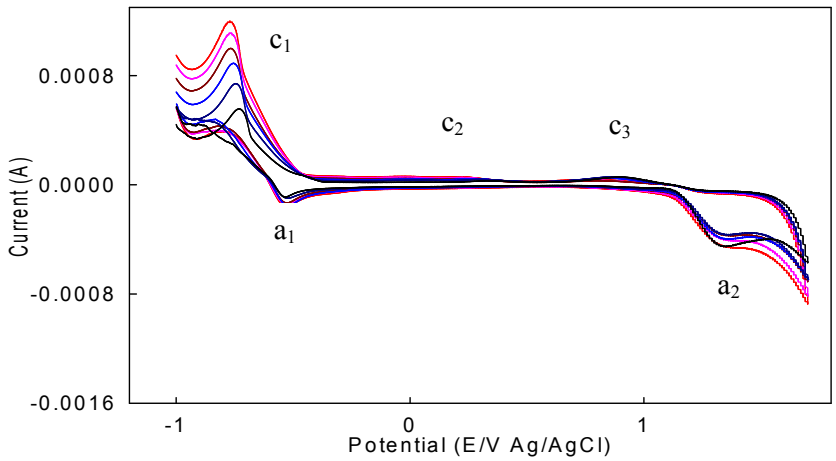

Fig 3.1.77 Cyclic voltammogram of 1:2 interaction of Cr(III)-Ciprofloxacin in saturated KCl at different scan rates.

Moreover, with the increase in scan rate, almost all the peaks become broader. Such behavior has been ascribed to slower charge propagation, probably due to difference in salvation and or permeability. Current-potential data for the system under consideration is recorded in Table 3.1.8.

It is evident that after complexation, the peak separation becomes less to a considerable extent. The peak separation potential for the pair of peaks (ΔE_p) decreases with the increase in scan rate. This behaviour is not similar to that of the uncoordinated chromium. Therefore it may be said that the above system does not indicate the limitation due to charge transfer kinetics and is shown in the plot of ΔE_p vs ν in Fig 3.1.78(a).

The peak currents for all the peaks increases with increasing scan rates (Table 3.1.8). From the Randle-Sevseik plot (peak current vs square root of scan rate) for the above system, it was also found that all the peak currents increases linearly with the square root of scan rate (Fig 3.1.78(b)). All of these facts demonstrate that the electrode process may be diffusion controlled[35, 99].

Table 3.1.8 Current-potential data of the 1:2 interaction of Cr(III)-Ciprofloxacin in saturated KCl at different scan rates.

Scan rate	SQRT of scan rate	Cathodic peak potential		Anodic peak potential		Cathodic peak current		Anodic peak current		Peak potential separation	Peak current ratio
ν (Vs^1)		E_{pc1} (V) [-]	E_{pc3} (V)	E_{pa1} (V) [-]	E_{pa2} (V)	i_{pc1} (μA)	i_{pc3} (μA)	i_{pa1} (μA) [-]	i_{pa2} (μA) [-]	$\Delta E_p = E_{pa2} - E_{pc3}$ (V)	i_{pa2}/ i_{pc3}
0.050	0.2236	0.702	0.901	0.535	1.356	270.25	37.75	200.65	60.26	0.455	1.60
0.100	0.3162	0.711	0.898	0.531	1.331	312.87	38.25	201.08	90.15	0.433	2.36
0.150	0.3872	0.722	0.894	0.525	1.307	360.18	40.18	229.57	91.55	0.413	2.28
0.200	0.4472	0.731	0.890	0.519	-	392.09	41.66	238.84	-	-	-
0.250	0.5000	0.740	0.887	0.515	-	431.83	43.08	244.09	-	-	-
0.300	0.5477	0.749	0.885	0.510	-	450.22	45.25	250.87	-	-	-

The peak current ratios are very much higher than unity. Therefore it may be said that the system shows almost exceptional character from the reversible behavior[101, 102]. Fig 3.1.79 shows that the plot of peak current ratio with scan rate.

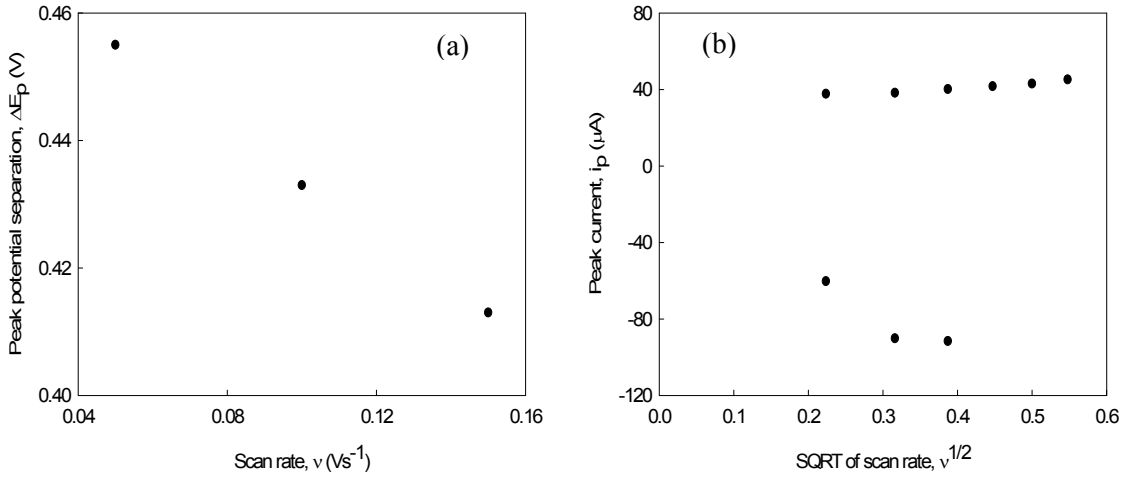

Fig 3.1.78 Variation of (a) peak potential separation with scan rate and (b) peak current with square root of scan rate for Cr(III)-Ciprofloxacin 1:2 interaction in saturated KCl solution.

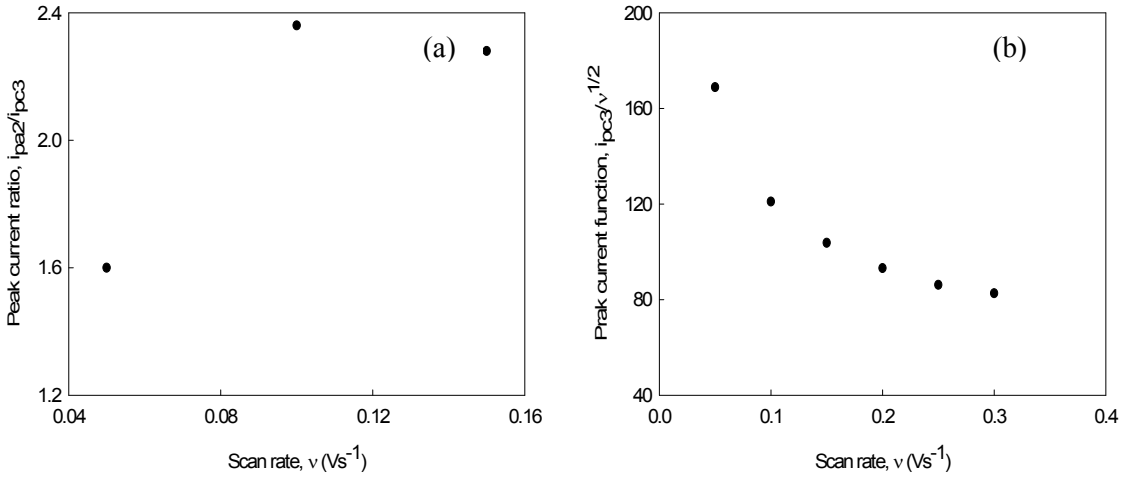

Fig 3.1.79 Variation of (a) peak current ratio and (b) peak current function with scan rate for Cr(III)-Ciprofloxacin 1:2 interaction in saturated KCl solution.

Again peak current function ($i_{pc1}/\nu^{1/2}$) decreases with increasing scan rate. Therefore, it does not indicate any clear conception about the electrochemical process.

Plot of log i_{pc1} against log ν shows a linear relationship. It is found that the slope is less than unity. Therefore it may be said that the process is accompanied by diffusion[3, 103] (Fig 3.1.80).

Tafel plot (peak potential vs log ν) is shown in Fig 3.1.80. The curves express that the slopes of the Tafel plot are not zero. So the electrochemical process will be irreversible.

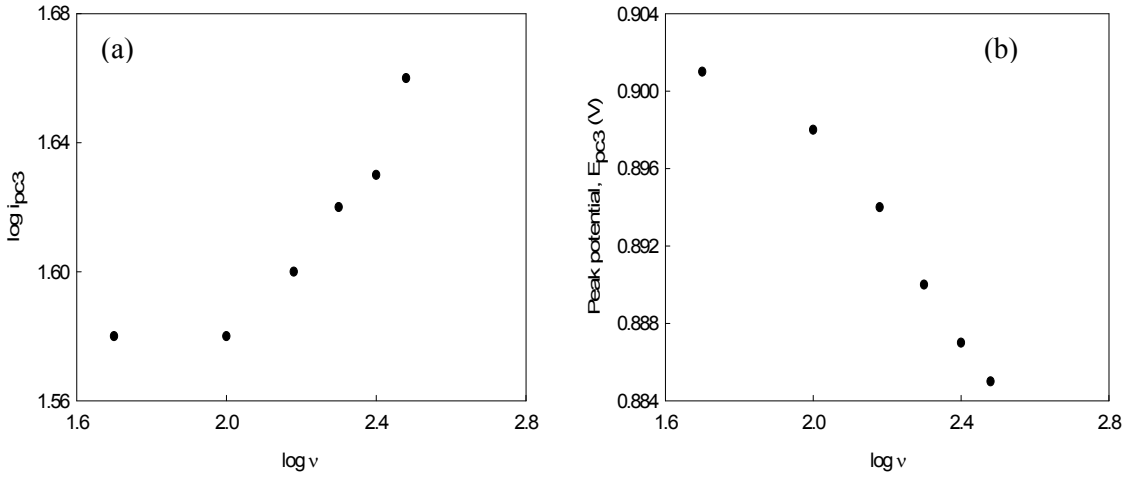

Fig 3.1.80 Variation of (a) log i_{pc1} and (b) peak potential with logν for Cr(III)-Ciprofloxacin 1:2 interaction in saturated KCl solution.

Therefore from the above discussions there are some findings, such as: i) peak potential shifts with scan rate, ii) peak current ratio is not equal to unity, iii) the current function $i_p/\nu^{1/2}$ is independent of scan rate, iv) peak response broadens as scan rate increases, v) slope of Tafel plot is not equal to zero and vi) the peak in the anodic region is absent at higher scan rates.

Considering all the above points it can be concluded that the electrochemical process involved in Cr(III)-Ciprofloxacin 1:2 interaction is irreversible.

Moreover, the system is diffusion controlled as well as adsorptive controlled, which can be declared from the facts that a) in the forward scans, peak currents are proportional to the square root of scan rate, b) peak currents in both the regions (cathodic and anodic) increases linearly with square root of scan rate, c) slope of log i_p against log ν plot is less than unity.

3.1.8 Chronoamperometric and chronocoulometric study of Cr(III) and Cr(III)-Ciprofloxacin interaction

The chronoamperometric as well as chrocoulomeric study of Cr(III) and the Cr(III)-Ciprofloxacin interaction was studied in some modified environment. As like Cyclic voltammetric study of the above system, the present study was also accomplish in saturated potassium chloride and using Platinum electrode as working electrode.

CA and CC study of Cr(III)

The Cr(III) system was also studied using chronoamperometric and chronocoulometric techniques which are also double potential step processes. The chronoamperometric (CA) experiment gives a current versus time curve, which is shown in Fig 3.1.81.

It shows a current spike followed by a gradual decay in current. The spike is due to initial electrolysis of species at the electrode surface and the decay is due to diffusion of molecules to the electrode surface[101].

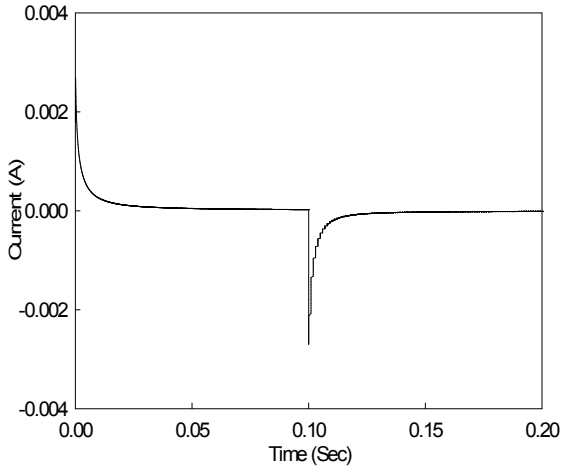

Fig 3.1.81 Current responses for Cr(III) in saturated KCl solution.

Chronocoulometry (CC) is the integrated form of the chronoamperometry. So that in CC the monitored response is charge. Such charge responses are shown in Fig 3.1.81.

Here in this double potential step CC, the potential is stepped from an initial value to a second value and then back to the initial value. The step from initial to the second is

termed as forward potential step whereas the step from the second to the initial value is termed as reverse step[35].

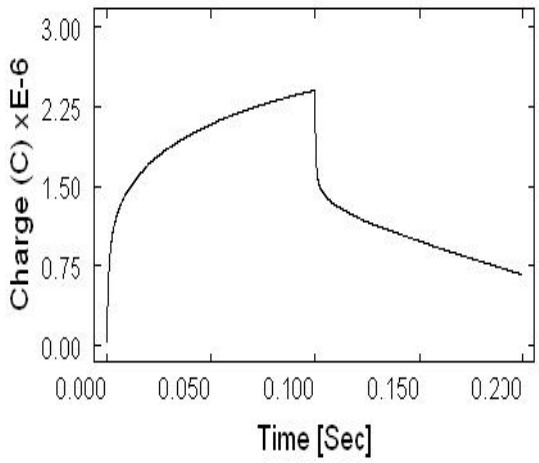

Fig 3.1.81 Charge response for Cr(III) in saturated KCl solution.

Chronocoulometric response (Fig 3.1.81) shows that the charge at τ is about 2.459 μC. Now if Q value obtained from time less than τ is plotted versus $t^{1/2}$ and on the same graph $-Q_r$ is plotted versus $\theta = [\tau^{1/2} + (t- \tau)^{1/2} - t^{1/2}]$, there will be two straight lines which intersects each other at Q=0 axis with equal slope, if there is no adsorption of reactant or product[31]. Any deviation from such condition means adsorption. Such a plot is shown in the Fig 3.1.82.

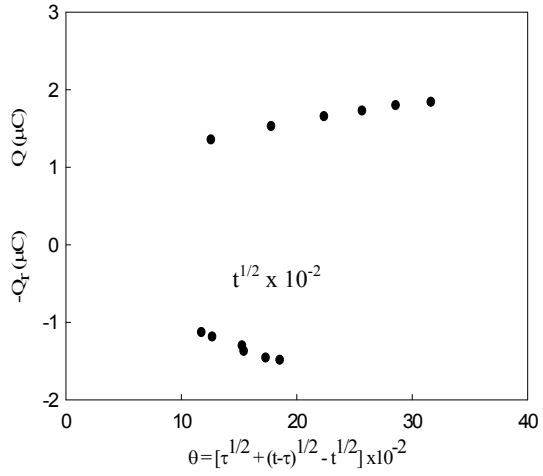

Fig 3.1.82 Plots of Q vs $t^{1/2}$ and $-Q_r$ vs θ for Cr(III) system in saturated KCl solution.

This shows that the plots Q vs $t^{1/2}$ and $-Q_r$ vs θ do not intersect each other at Q=0 axis. Moreover they do not have equal slopes. Therefore from this plot, it may be said that adsorption of reactant or products occur on the electrode.

CA and CC study of Cr(III)-Ciprofloxacin mixture in solution

Chronoamperometric study of Cr(III) system was also done after interaction with Ciprofloxacin. It was observed that after interaction the number of signals in cathodic region has become three but in the anodic region it is two. Moreover a comparison with the cyclic voltammigrams of Cr(III) and Ciprofloxacin implies that the second pair of peaks (combination of third cathodic and the second anodic peak) is the indication of the metallic part. So, CA study was accomplished considering this pair of peaks. The chroamperogram is shown in the Fig 3.1.83.

It shows that the spike height after interaction with Ciprofloxacin is decreased compared to that of Cr(III) before interaction with Ciprofloxacin. Since the spike height is proportional to the rate of electrolysis, this means that after interaction the rate of electrolysis has been decreased (Fig 3.1.84).

Chronocoulometry (CC) is the integrated form of the chronoamperometry. So that in CC the monitored response is charge. It is also known as chronocoulogram. Such a charge response is shown in Fig 3.1.85.

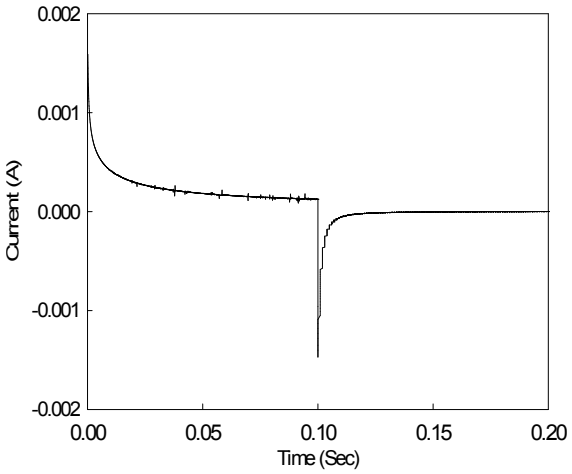

Fig 3.1.83 Current response for Cr(III)-Ciprofloxacin 1:2 interaction in saturated KCl solution.

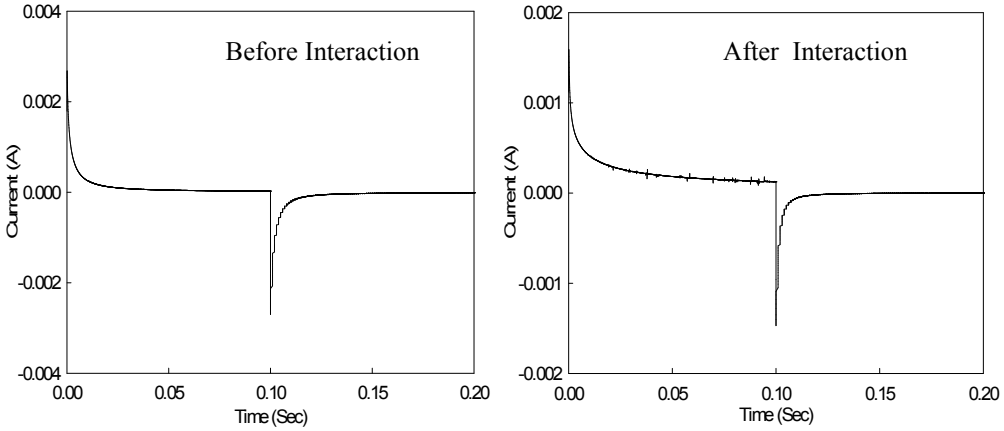

Fig 3.1.84 Current responses for Cr(III) in saturated KCl solution (i) before and (ii) after interaction with Ciprofloxacin.

Chronocoulometric response (Fig 3.1.85) shows that the charge at τ is decreased after interaction with Ciprofloxacin. It was 2.459 μC in the absence of ciprofloxacin, whereas it becomes 1.497 μC after interaction with Ciprofloxacin.

Now if Q value obtained from time less than τ is plotted versus $t^{1/2}$ and on the same graph $-Q_r$ is plotted versus $\theta = [\tau^{1/2} + (t- \tau)^{1/2} - t^{1/2}]$, there will be two straight lines which intersects each other at Q=0 axis with equal slope, if there is no adsorption of reactant or product[31]. Any deviation from such condition means adsorption. Such a plot is shown in Fig 3.1.86.

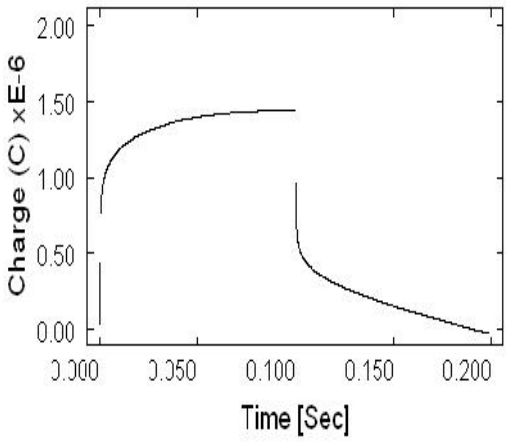

Fig 3.1.85 Charge response for Cr(III)-Ciprofloxacin 1:2 interaction in saturated KCl solution.

This shows that the plots Q vs $t^{1/2}$ and $-Q_r$ vs θ do not intersect each other at Q=0 axis. Moreover they do not have equal slopes. Therefore from this plot, it may be said that adsorption of reactant or products occur on the electrode.

Therefore the findings from the Chronoamperometric studiy is that after interaction the spike height is decreased, indicating towards a decrease in the rate of electrolysis. And from the Chronocoulometric study, it is observed that the charge at τ is also decreased. Both of these facts combinedly indicates towards successful interaction.

And the observations from the plots Q vs $t^{1/2}$ and $-Q_r$ vs θ gives conclusion that adsorption of reactant or products occur on the electrode also after interaction.

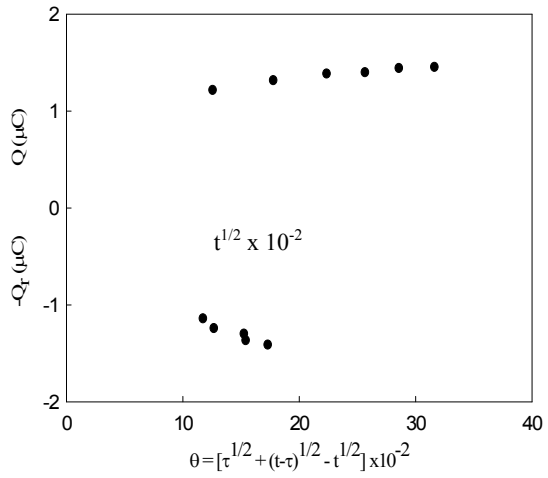

Fig 3.1.86 Plot of Q vs $t^{1/2}$ and $-Q_r$ vs θ for Cr(III)-Ciprofloxacin 1:2 interaction in saturated KCl solution.

4 CONCLUSION

1. The findings from the cyclic voltammetric studies of different metal ions are very important.

   (i) Scan rate variation of Cu(II), Mn(II), Zn(II) and Cr(III) systems shows that the cathodic peaks shifts towards more negative potentials and the anodic peaks moves towards more positive potential. Moreover the peak response broadens as scan rate increases for all the metal ions systems. Such behavior has been ascribed to slower charge propagation, probably due to difference in salvation and or permeability.

   (ii) Slope of Tafel plots are not equal to zero for Cu(II), Mn(II) and Zn(II) bur for Cr(III) it is almost zero. The peak current ratios for Cu(II) and Mn(II) are not equal to unity but for the other two systems such as Zu(II) and Cr(III) those are almost unity. All the above points conclude that the electrochemical process involved in Cu(II) and Mn(II) are quasi-reversible and for Zn(II) as well as Cr(III) are near to reversible.

   (iii) All the systems (Cu(II), Mn(II), Zn(II) and Cr(III)) exhibit some common characters such as, the proportionality of peak current in the forward scans with the square root of scan rate, linear increase of peak currents in both the regions (cathodic and anodic) with square root of scan rate and the values of slopes of log i_p against log ν plot. These findings together gives the conclusion that the systems are diffusion controlled as well as adsorptive controlled.

2. The cyclic voltammetric studies of the Metal-Ciprofloxacin *interactions in solution* also give some important findings similar to those of metal ion solutions in absence of ligand.

   (i) Scan rate variation of Cu(II)-Ciprofloxacin interaction exhibits that all the cathodic peaks shift towards more negative potentials. But the anodic peaks moves towards more positive potential. Similar is the case for Zn(II)-Ciprofloxacin interaction. But Mn(II) and Cr(III)-Ciprofloxacin interactions do not show any distinct characteristics.

(ii) Broadening of peak response occurs as scan rate increases for interaction of Ciprofloxacin with Mn(II), Zn(II) and Cr(III). Such behavior has been ascribed to slower charge propagation, probably due to difference in salvation and or permeability.

(iii) Slope of Tafel plots are not equal to zero for Cu(II), Mn(II), Zn(II) Ciprofloxacin interaction, but it is almost zero for Cr(III). The peak current ratios for all the interactions are not equal to unity. All the above points conclude that the electrochemical process involved in three of the above interactions (Cu(II), Mn(II) and Zn(II)-Cprofloxacin) are quasi-reversible and for Cr(III)-Ciprofloxacin interaction is irreversible.

(iv) All the systems (Cu(II), Mn(II), Zn(II) and Cr(II)) are diffusion controlled as well as adsorptive controlled, which can be declared from different facts such that the proportionality of peak current in the forward scans to the square root of scan rate, linear increase of peak currents in both the regions (cathodic and anodic) with square root of scan rate and the slopes of log i_p against log ν plot.

3. Chronoamperometric as well as chronocoulometric study for all the metals and their interactions with ciprofloxacin give almost same type of findings. The findings from the Chronoamperometric study are

   (i) after interaction the spike height is decreased, indicating towards a decrease in the rate of electrolysis. And from the Chronocoulometric study, it is observed that the charge at τ are decreased in all the cases. Both of these facts combinedly indicates towards successful interaction.

   (ii) the observations from the plots Q vs $t^{1/2}$ and $-Q_r$ vs θ gives conclusion that adsorption of reactant or products occur on the electrode also after interaction.

4. The redox process involved in Cu(II) and Mn(II) systems are double step redox processes involving the total of two electrons (one electron involved in each step).

   But Zn(II) and Cr(II) redox processes are single step redox processes, the former involving two and the later with one electrons.

5 EXPERIMENTAL

Materials, Methods and Equipments

Few metal compounds using Ciprofloxacin, a quinolone derivative and few biologically important metal ions were prepared and characterized using different physic-chemical methods. The sources of different chemicals, the instruments and brief description of the methods are given below.

5.1 Chemicals

Preparation of the complexes were accomplished by the reaction between Ciprofloxacin Hydrochloride (Dr. Reddy's Laboratory, India) and the chloride salts of Chromium, Manganese, Nickel, Copper and Zinc (all of MERCK, Germany). Cleaning of the electrodes and all the solutions were prepared using de-ionized water. 99.997% Nitrogen was used for purging purpose.

5.2 Electronic Spectral Analysis

The visible and ultraviolet regions of the spectrum, that is 190—800 nm are those in which electronic excitation usually occurs. Light of these wavelengths may be absorbed by a complex and electronic spectra can be measured. The electronic spectral bands are very broad, these spectra are not often used as "finger prints" or in looking for functional groups as is done in infrared spectroscopy.

Energy absorbed in the UV region are due to the electronic energy of the compound resulting from the transition of electrons in the molecule. The transition is manifest because of the excitation of electrons from filled molecular orbital (usually non-bonding or bonding π orbital) to the next higher energy level (an antibonding π^* orbital) .

The electronic spectra of the compounds were recorded using UV-visible spectrophotometer, Model UV-160 A, in the wave length range 200—1100 nm. Sampling was done as follows. At first, water was used in the quartz cells for baseline

correction. Then saturated solutions of the compounds, metal salts and the ligand was scanned.

Fig 5.1 A UV-visible spectrophotometer.

5.3 Infra-red Spectral Analysis

The compounds having covalent bonds will be found to absorb various frequencies of electromagnetic radiation in the infrared (IR) region of the spectrum. The IR spectra originate from the different modes of vibration of a molecule due to the absorption of radiation energy in the IR region. However, it is essential that a change in dipole moment occurs during the vibration. In the absorption process, those frequencies of IR radiation will be absorbed which match the natural vibrational frequencies of the

Fig 5.2 A FTIR Spectrophotometer.

molecules. Since every different type of bond has a different frequency of vibration, and since the same type of bond in two different compounds is in a different

environment, no two molecules of different structure will have exactly the same infrared absorption pattern. This is why IR spectrum is a very authentic identity of the compounds which are IR active. Another more important use of the IR spectrum is that it gives structural information about a molecule can be identified.

Infra-red spectra of the compounds were recorded on a Shimadzu (Japan), Infra-red spectrophotometer of model IR-470 in the range 500—4000 cm^{-1} using KBr pellets. The sample (solid substance) is ground with KBr 1:100 by weight and is made into a pellet pressing it under high pressures (eight ton). Grinding is usually done in agate mortar and pastel.

5.4 Near Infra-red Spectral Analysis

Near-infrared spectroscopy (NIRS) is a spectroscopic method that uses the near-infrared region of the electromagnetic spectrum (from about 800 nm to 2500 nm). Typical applications include pharmaceutical, medical diagnostics (including blood sugar and pulse oximetry), food and agrochemical quality control, and combustion research, as well as research in functional neuroimaging, sports medicine & science, elite sports training, ergonomics, rehabilitation, neonatal research, brain computer interface, urology (bladder contraction) and neurology (neurovascular coupling).

Fig 5.3 A typical Near Infrared Spectrophotometer

NIR spectra of the complexes were recorded on a Near-infrared spectrophotometer in the range 4000—10000 cm^{-1} (from about 800 nm to 2500 nm). Sample was directly introduced to the analyzer to obtain the spectrum.

5.5 Melting Point

The melting of a solid is a temperature at which it changes state from solid to liquid. At the melting point the solid and liquid exist in equilibrium. The melting point of a substance depends (usually slightly) on pressure and is usually specified at standard pressure. Melting generally occurs over a temperature range, which is termed as melting range.

Fig 5.4 A typical Melting point Apparatus.

The melting points of the compounds were recorded in a MEL-TEMP-(II) heating device, with a FLUKE 51Kj thermometer, made in USA in the range 0˚C--1400˚C.

5.6 Solubility

Solubility is the property of a solid, liquid or gaseous chemical substance called solute to dissolve in a solid, liquid or gaseous solvent to form a homogeneous solution of the solute in the solvent. According to an IUPAC definition, solubility is the analytical composition of a saturated solution expressed as a proportion of a designated solute in a designated solvent.

The solubility of all the compounds were examined (qualitatively) in water, hot water and some common organic solvents such as methanol, acetronitrile, dimethyl formamide and dimethyl sulfoxide.

5.7 Conductivity

A solution will conduct electricity if it contains ions that are free to move. The ionic solids posses that property when they are in solution. These solids are called electrolytes and the power of electrolytes to conduct electrical current is termed as conductivity. On the other hand, most of the covalent and co-ordinate compounds are bad conductors of electricity, since they do not contain charge particles (i.e. ions) or electrons to carry the current. Thus whether a compound is completely ionic, covalent/coordinate or possesses some ionic character, may be known from the conductivity measurement in solution.

Fig 5.5 A typical conductance meter.

A TOA conductivity meter CM-5S (Shimadzu, Japan) was used to measure the conductance of the complexes. Cell constant of the cell used in the measurement is 0.954. Specific conductance of pure solvent (de-ionized water) used in the experiment was 2.9x1 μs/cm. Aqueous solution of the compounds were prepared and then the conductivity was measured. All the measurements were done in the room temperature.

5.8 DSC (Differrential Scanning Calorimetry) Analysis

Differential scanning calorimetry or DSC is a thermoanalytical technique in which the difference in the amount of heat required to increase the temperature of a sample and reference is measured as a function of temperature. Both the sample and reference are maintained at nearly the same temperature throughout the experiment. Generally, the temperature program for a DSC analysis is designed such that the sample holder temperature increases linearly as a function of time. The reference sample should have a well-defined heat capacity over the range of temperatures to be scanned.

Fig 5.6 A typical Differential scanning calorimeter

5.9 Preparation and Formulation of Metal-Ciprofloxacin Compounds

Five compounds of Ciprofloxacin with different metals were prepared. These compounds were prepared using Ciprofloxacin and metal chlorides as the starting materials.

5.9.1 Cr(III)-Ciprofloxacin compound

A little portion of Chloride salt of Chromium (271.69 mg) was dissolved quantitatively in a minimum volume of water. Similarly Ciprofloxacin (762.12 mg) was also dissolved in a little portion of water quantitatively. Then the solutions were mixed to a metal to ligand molar ratio of 1:2. The resulting solution was then filtered and kept for slow evaporation in an open space in the normal laboratory condition. Approximately after 20 days, light greenish Cr(II)-Ciprofloxacin compound (804.26 mg) was found. It was then filtered and the product was collected, washed and dried.

$$CrCl_3 + 2C_{17}H_{18}FN_3O_3 \longrightarrow CrCl_3.2(C_{17}H_{18}FN_3O_3)$$

Yield : 78.04 % (on metal **basis)**

	Metal %	C %	N %	H %
Calculated data of $CrCl_3.2(C_{17}H_{18}FN_3O_3)$	6.34	49.74	10.24	4.89
Experimental data	6.59	50.24	10.32	5.48

5.9.2 Mn(II)-Ciprofloxacin compound

Manganese Chloride (163.01 mg) was dissolved quantitatively in water and the same was also done for ciprofloxacin (767.25 mg). After that these two solutions were mixed to a metal to ligand molar ratio of 1:2. The filtered solution was then heated slightly on a water bath, so that it becomes concentrated. Then it was kept in the normal laboratory condition. After about 5-6 hours, very light pink transparent crystalline products (720.11 mg) were isolated from the mother liquer. Then it was washed, dried and collected for preservation and characterization.

$$MnCl_2 + 2C_{17}H_{18}FN_3O_3 \longrightarrow MnCl_2.2(C_{17}H_{18}FN_3O_3)$$

Yield : 71.40 % (on metal basis)

	Metal %	C %	N %	H %
Calculated data of $MnCl_2.2(C_{17}H_{18}FN_3O_3)$	6.97	51.79	10.66	4.57
Experimental data	6.75	51.03	10.48	5.53

5.9.3 Ni(II)-Ciprofloxacin compound

A specified amount of Nickel Chloride (240.51 mg) was dissolved in a minimum volume of water. Again Ciprofloxacin (770.09 mg) was also dissolved in minimum volume of water. Then both the solutions were mixed so that there were a metal to ligand molar ratio be 1:2. It was then filtered and kept for slow evaporation under normal laboratory condition. After about one week pale bluewish product (713.21 mg) was found, which was then washed, dried and preserved.

$$NiCl_2 + 2C_{17}H_{18}FN_3O_3 \longrightarrow NiCl_2.2(C_{17}H_{18}FN_3O_3)$$

Yield : 65.10 % (on metal basis)

	Metal %	C %	N %	H %
Calculated data of $NiCl_2.2(C_{17}H_{18}FN_3O_3)$	7.41	51.55	10.61	4.55

Experimental data	7.87	51.28	10.54	5.54

5.9.4 Cu(II)-Ciprofloxacin compound

Copper Chloride (173.61 mg) and Ciprofloxacin (346.51 mg) were dissolved in a minimum volume of water separately and was mixed in the molar ratio 1:1. The resulting solution was then heated on a water bath and the concentrated solution was kept overnight. Crystalline intense blue products (421.77 mg) were isolated from the mother liquor. It was then washed and collected for futher use.

$$CuCl_2 + C_{17}H_{18}FN_3O_3 \longrightarrow CuCl_2.(C_{17}H_{18}FN_3O_3)$$

Yield : 90.65 % (on metal basis)

	Metal %	C %	N %	H %
Calculated data of $CuCl_2.(C_{17}H_{18}FN_3O_3)$	15.62	43.85	9.03	4.87
Experimental data	16.90	44.11	9.05	5.33

5.9.5 Zn(II)-Ciprofloxacin compound

Quantitative amount of Zinc Chloride (137.58 mg) was dissolved in minimum volume of water. Similar work was done for ciprofloxacin (349.51 mg). Then these were mixed to a molar ratio of 1:1. The filtered mixture was then warmed on a water bath to concentrate the content. White product (403.11 mg) was found immediately after cooling. It was then washed, dried and preserved.

$$ZnCl_2 + C_{17}H_{18}FN_3O_3 \longrightarrow ZnCl_2.(C_{17}H_{18}FN_3O_3)$$

Yield : 86.27 % (on metal basis)

	Metal %	C %	N %	H %
Calculated data of $ZnCl_2.(C_{17}H_{18}FN_3O_3)$	13.99	43.66	8.99	4.25
Experimental data	14.25	42.67	8.76	4.48

5.10 Elemental Analysis

5.10.1 Carbon, hydrogen and nitrogen micro analysis

Micro analytical data of carbon, hydrogen and nitrogen of the metal-ciprofloxacin compounds were obtained from Kyushu University, Japan. The analysis were done on a Automatic Micro Analyzer.

5.10.2 Metal analysis

Metal analysis of the compounds were done by titrimetric methods especially complexometric and iodometric methods. The metal contents were calculated from the equivalence relationship. The methods employed for metal quantification is stated specifically below.

Chromium analysis: About 0.2 g of the sample was weighed and taken in a conical flask. 50 mL of water and 3 mL of concentrated sulphuric acid was added to it. Again 1.5 g of solid potassium bromate was added and boiled for 10 minutes. 5 g of ammonium sulphate was dissolved in a small volume of water and added to the hot solution, in which chromium was present as chromic acid. The whole content was then boiled until all excess bromine had been volatilized. Then 10 mL of 1N HCl solution was added and again boiled until starch-iodine paper was not stained when held in the steam. The liquid was then cooled, 5 mL of concentrated HCl and 10 mL of 10% KI solution was also added. The liberated iodine was then titrated with standard thiosulphate solution.

Manganese analysis: An accurately weighed amount of Mn(II)-Ciprofloxacin compound was dissolved in 200 mL of water. 10 mg of ascorbic acid was added to it and titration was started by adding 25 mL of 0.05 M EDTA. Then 10 mL ammonia-ammonium chloride buffer and 0.15 mL Eriochrome Black T indicator was added to it. The titration was then completed using 0.05 M EDTA solution to a blue end point.

Nickel analysis: About 0.173 g of the prepared Ni(II)-Ciprofloxacin compound was weighed and was dissolved in 1-2 mL 6M HCl and diluted to 100 mL in a volumetric flask. 10 mL of this solution was taken in a conical flask and diluted to 50 mL with distilled water. A pinch (0.05 g) of murexide-NaCl mixture followed by 4-5 mL 1M NH_4Cl solution was added to it. Concentrated NH_3 was added to the mixture drop wise until the colour of the solution changes to yellow (pH-7). It was then titrated with 0.01M EDTA solution until the end point was approached. The solution was then rendered alkaline with 4-5 mL concentrated NH_3 and the titration was continued till

the colour changed from yellow to bluish-violet. The titration was repeated two times more.

Copper analysis: A quantitative amount of Cu(II)-Ciprofloxacin compound was taken in a 250 mL volumetric flask and made upto volume by water. 25 mL of that solution was taken in a conical flask and diluted with an equal volume of water. 5 mL of concentrated ammonia solution and 5 drops of the indicator (0.5% aqueous solution of Fast Sulphon Black F) solution was added to that. It was then titrated with standard

EDTA solution until the colour changes from blue to a dark green.

Zinc analysis: An accurately weighted amount of Zn(II)-Ciprofloxacin compound was dissolved in 100 mL of water. 2 mL of ammonia-ammonium chloride buffer (pH-10) and a few drops of Eriochrome Black T indicator was added to it. The solution was thed titrated with 0.1 M EDTA until the solution is deep blue in colour.

6 RESULTS AND DISCUSSION

6.1 Characterization of the Metal-Ciprofloxacin Compounds

6.1.1 Formulation

Elemental analysis is the prime tools for the formulation of any chemical species. To determine different elements present in the sample, highly sophisticated instruments were used. The formulation of the prepared compounds were done on the basis of elemental analysis, metal analysis as well as spectral analytical results.

Elemental and metal analysis

Elemental analysis is a process where a sample of some materials is analyzed for its elemental and sometimes isotopic composition. Elemental analysis can be qualitative (determining what materials are present) and may be quantitative (determining how much of each are present). Elemental analysis falls within the ambit of analytical chemistry.

The microanalytical data(experimental) of Carbon, Nitrogen, Hydrogen and metal are given in Table 6.1.1. Again the calculated data for the elemental analysis of carbon, hydrogen and nitrogen as well as hypothetical formula for Metal-Ciprofloxacin compounds of different ratios [(1:1) and (1:2)] are also mentioned in the Table 6.1.1. Experimental data were compared with the calculated datas and found that they are in good agreement. The comparison shows that Chromium, Manganese and Nickel form compounds with Ciprofloxacin to a ratio of 1:2 and on the other hand Copper and Zinc to a ratio of 1:1. Thus the empirical formula for the Metal-Ciprofloxacin compounds is given in Table 6.1.1.

The compounds were also analyzed to estimate the metals quantitatively. This task was done titrimetrically. The experimental and calculated data are given in the Table 6.1.1. It is found that the experimental data are also in good agreement with those of the calculated data and thus support the empirical formula of the compounds.

6.1.2 Spectral analysis of the ligands and their compounds

The study of the spectral properties of compounds provides information about the

metal-ligand bonds. The absorption spectrum of Ciprofloxacin compounds and their characteristic bands are discussed below.

Table 6.1.1 The % of C, N, H and M (metal) in the compounds of Ciprofloxacin.

Compound	Formula	M.W.	Experimental Data (Calculated Data)			
			% Metal	% C	% N	% H
Cr(III)-Ciprofloxacin	$CrCl_3.2(C_{17}H_{18}N_3O_3F)$	820.35	6.59 (6.34)	50.24 (49.74)	10.32 (10.24)	5.48 (4.89)
Mn(II)-Ciprofloxacin	$MnCl_2.2(C_{17}H_{18}N_3O_3F)$	787.84	6.75 (6.97)	51.03 (51.79)	10.48 (10.66)	5.53 (4.57)
Ni(II)-Ciprofloxacin	$NiCl_2.2(C_{17}H_{18}N_3O_3F)$	791.59	7.87 (7.41)	51.28 (51.55)	10.54 (10.61)	5.54 (4.55)
Cu(II)-Ciprofloxacin	$CuCl_2.(C_{17}H_{18}N_3O_3F)$	465.25	16.90 (15.62)	44.11 (43.85)	9.05 (9.03)	5.33 (4.87)
Zn(II)-Ciprofloxacin	$ZnCl_2.(C_{17}H_{18}N_3O_3F)$	467.28	14.25 (13.99)	42.67 (43.66)	8.76 (8.99)	4.48 (4.25)

6.1.2.1 Infra-red spectral analysis

The compounds having covalent bonds will be found to absorb various frequencies of electromagnetic radiation in the infrared (IR) region of the spectrum. The IR spectra originate from the different modes of vibration of a molecule due to the absorption of radiation energy in the IR region. However, it is essential that a change in dipole moment occurs during the vibration. In the absorption process, those frequencies of IR radiation will be absorbed which match the natural vibrational frequencies of the molecules. Since every different type of bond has a different frequency of vibration, and since the same type of bond in two different compounds is in a different environment, no two molecules of different structure will have exactly the same infrared absorption pattern. This is why IR spectrum is a very authentic identity of the compounds which are IR active. Another more important use of the IR spectrum is that it gives structural information about a molecule can be identified.

The IR spectrum of a compound molecule consists of a number of group frequencies, which are highly useful in identifying the functional groups present in the compound. This achieved by comparing the number, position and intensities of various absorption bands observed with those reported in group frequency charts and related papers

published in different journals. In the present study, the infra-red spectral investigations was carried out to obtain information regarding the nature of the bonds between the metal ion and the ligands, the effects of hydrogen bonding and finally an overall view of the molecular structure. Shifts, splits and other minor changes in the bands with respect to ligands molecule are associated with the structural changes that occur in it during compound formation[105].

6.1.2.2 IR spectra of Ciprofloxacin and its compounds

The IR spectrum of Ciprofloxacin and Metal-Ciprofloxacin compounds are shown in Figures 6.1.1 to 6.1.6. the relative intensity and tentative band assignment of the various absorption bands are listed in Tables 6.1.2 to 6.1.7. The tentative band assignment have been made on the basis of some standard literature. The abbreviation and symbols used for discussing the IR spectra are listed below:

v = very	sym = symmetric
sh = shoulder	asym = asymmetric
m = medium	ν = stretching frequency
s = strong	δ = bending
b = broad	arom = aromatic
w = weak	

IR Spectrum of Ciprofloxacin: The IR spectrum of Ciprofloxacin is given in Fig 6.1.1. The frequencies of the bands are listed in Table 6.1.2. with relative intensities and tentative assignments.

Ciprofloxacin exhibits a strong band at 3530 cm^{-1} due to O-H stretching vibration as a result of H-bonding. The peak with very strong intensity at 1709 cm^{-1} is assigned due to ketonic ν(>C=O). Again very strong intensity is observed at 1610 cm^{-1} which is for ν_{arom}(C=C). The ν(C-F) frequency is observed at 1449 cm^{-1}. And a very strong response at 1273 cm^{-1} is found, which may be due to carboxylic ν(C-O)[105]. The vibretions for the out of plane bending modes of aromatic C-H is appeared at 740 cm^{-1}.

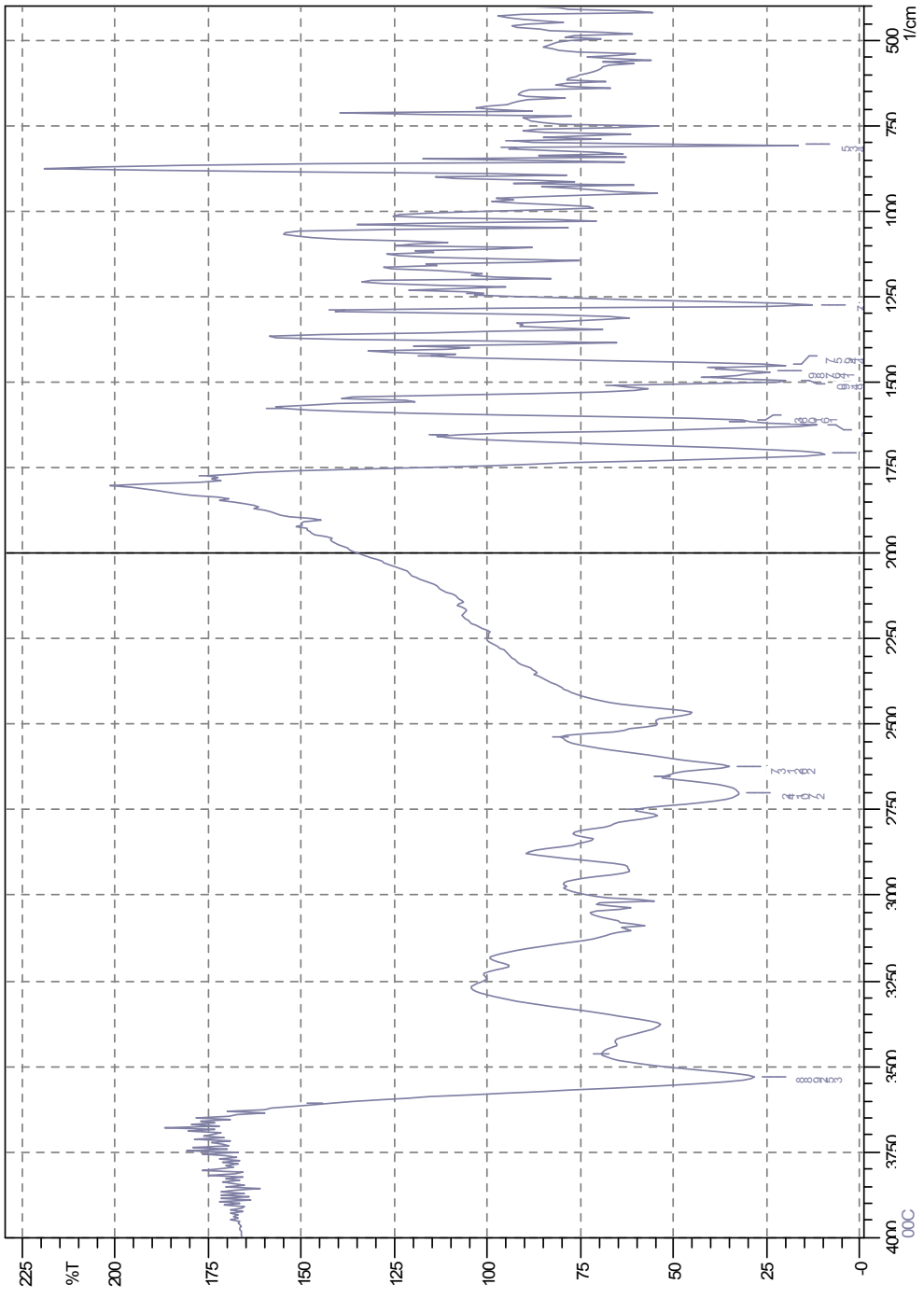

Fig 6.1.1 Infrared spectrum of Ciprofloxacin.

Table 6.1.2 Assignment for IR bands of Ciprofloxacin.

Wave no. (cm^{-1})	Relative Intesity	Tentative band assignment
3530	s	ν(O-H) H-bonded
3369	wb	
3095	wb	
3025	vwsh	
3010	vw	
2910	wsh	
2750	vw	
2701	wsh	
2621	vb	
2500	wsh	
2465	w	
1709	vs	ν(>C=O) Ketonic
1610	vs	ν_{arom}(C=C)
1495	ssh	
1467	sh	
1449	s	ν(C-F)
1370	w	
1350	vw	
1273	vs	ν(C-O) Carboxylic
1170	vwsh	
1145	vw	
1050	w	
998	vwb	
950	vw	
740	s	δ (C-H) Aromatic out of plane bend
650	vw	

IR spectrum of Cr(III)-Ciprofloxacin compound: The IR spectrum of Cr(III)-Ciprofloxacin compound is given in Fig 6.1.2. The frequencies of the bands are listed in Table 6.1.3 with relative intensities and tentative assignments.

This Cr(III)-Ciprofloxacin compound exhibits a strong broad band in the range 3590—3120 cm^{-1} due to O-H stretching vibration. The broad band in the range 2850—2590 cm^{-1} may be due to ν(O-H) involved with Carboxylic acid. Again very strong intensity is observed at 1609 cm^{-1} which is for ν_{arom}(C=C). A strong response at 1530 cm^{-1} is due to ν(N-H) bending. The ν(C-F) frequency is observed at 1480 cm^{-1}. And a very strong response at 1305 cm^{-1} is found, which may be due to carboxylic

ν(C-O). Another peak at 1280 cm^{-1} is observed due to ν(C-N). The vibrations for the out of plane bending mode of aromatic C-H is appeared at 752 cm^{-1}. The peak at 658 cm^{-1} may be due to ν(Cr-N)[105].

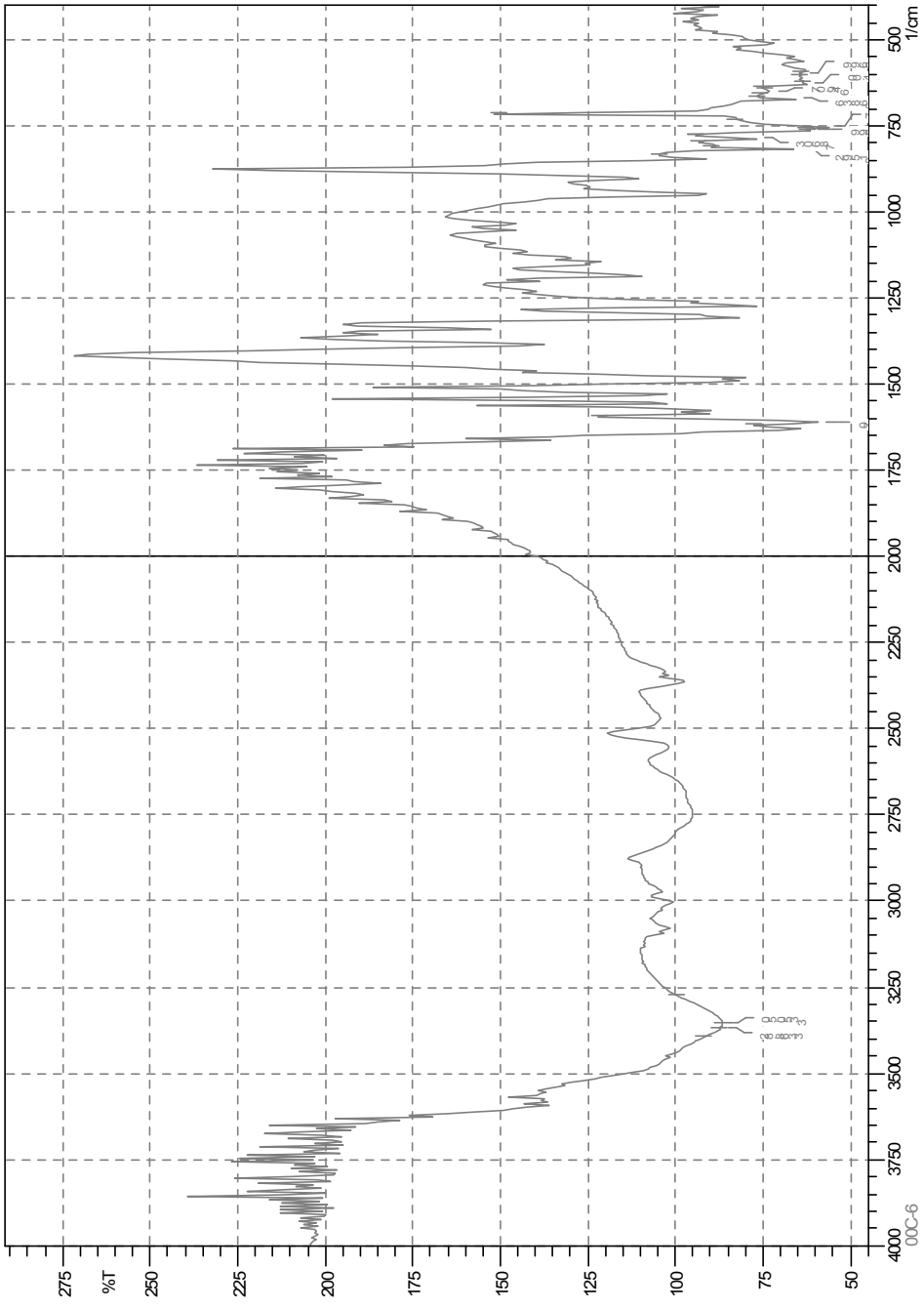

Fig 6.1.2 Infrared spectrum of Cr(III)-Ciprofloxacin compound.

Table 6.1.3 Assignment for IR bands of Cr(III)-Ciprofloxacin compound.

Wave no. (cm^{-1})	Relative Intesity	Tentative band assignment
3590--3120	sb	ν(O-H) H-bonded
3088	vwsh	
3000	vw	
2850--2590	mb	ν(O-H) Carboxylic
2550	wb	
2335	msh	
1609	vs	ν_{arom}(C=C)
1560	ssh	
1530	s	ν(N-H) bending
1498	ssh	
1480	sh	ν(C-F)
1395	ssh	
1345	vw	
1305	s	ν(C-O) Carboxylic
1280	ssh	ν(C-N)
1205	wsh	
1168	vwb	
1055	wsh	
950	s	
840	w	
805	sh	
752	ms	δ (C-H) Aromatic out of plane bend
658	ms	ν(Cr-N)

IR spectrum of Mn(II)-Ciprofloxacin compound: IR spectrum for Mn(II)-Ciprofloxacin compound is given in Fig 6.1.3. The frequencies of the bands are listed in Table 6.1.4 with relative intensities and tentative assignments.

The compound exhibits a broad band in the range 3650—3250 cm^{-1} due to both free and hydrogen bonded O-H stretching vibration. Compared to Ciprofloxacin ν(>C=O) shows a shift at 1757 cm^{-1}, suggesting that the >C=O group of Ciprofloxacin moity is also involved in hydrogen bonding. A very strong intensity is observed at 1620 cm^{-1} which is for ν_{arom}(C=C). Another response at 1535 cm^{-1} is due to ν(N-H) bending. The ν(C-F) frequency is observed at 1475 cm^{-1}. At 1370 cm^{-1} the response may be due to

ν(-CH_3) bending. And a very strong response at 1305 cm^{-1} is found, which may be due to carboxylic ν(C-O). Another peak at 1287 cm^{-1} is observed due to ν(C-N). The vibrations for the out of plane bending mode of aromatic C-H is appeared at 752 cm^{-1}. The peak at 665 cm^{-1} may be due to ν(Mn-N)[105].

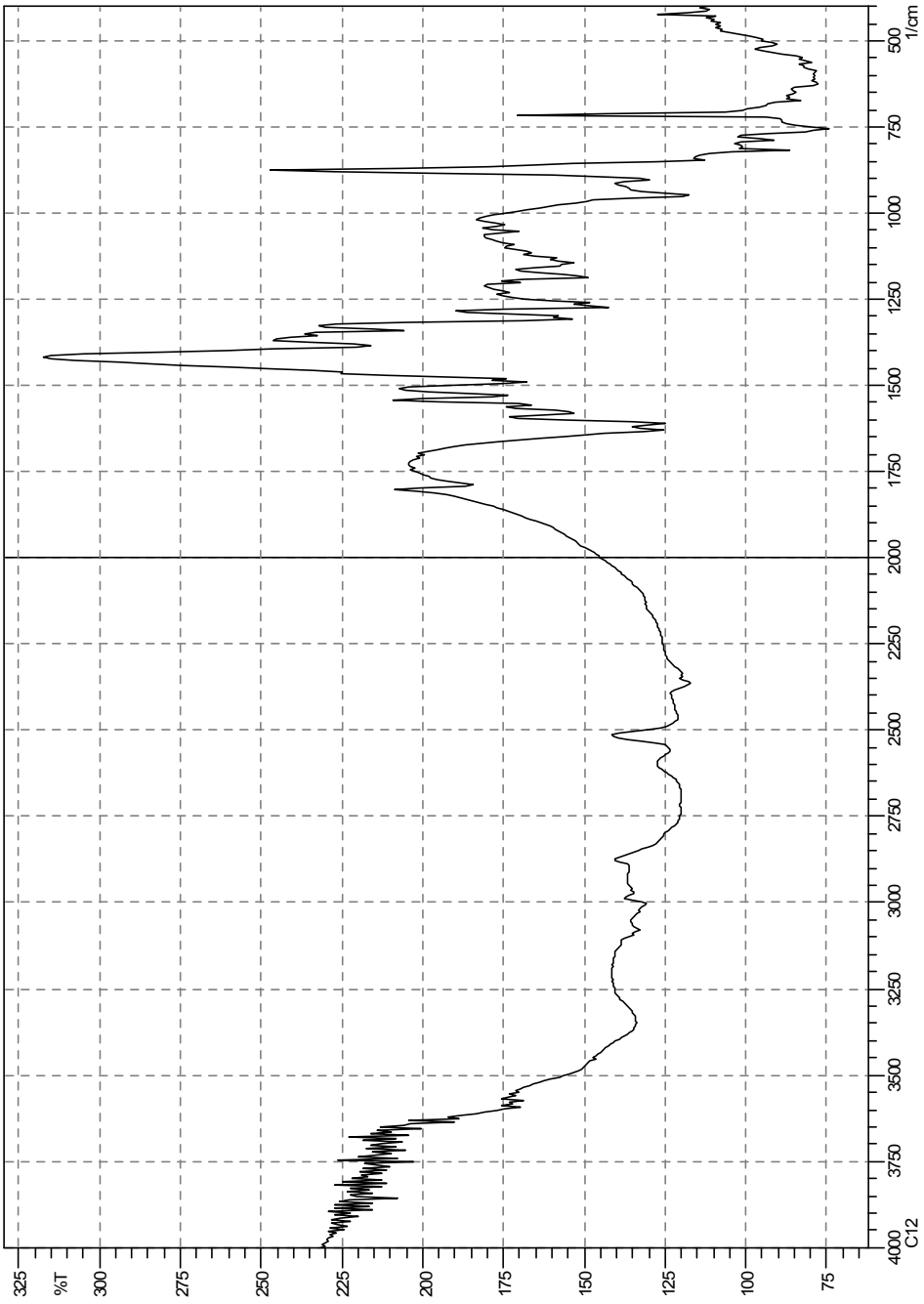

Fig 6.1.3 Infrared spectrum of Mn(II)-Ciprofloxacin compound.

Table 6.1.4 Assignment for IR bands of Mn(II)-Ciprofloxacin compound.

Wave no. (cm^{-1})	Relative Intesity	Tentative band assignment

3650--3250	sb	ν(O-H) Free & H-bonded
3010	vw	
2910	vw	
2890	vw	
2395	ms	
2380	wsh	
1757	vs	ν(>C=O) Ketonic
1620	vs	ν_{arom}(C=C)
1535	sh	ν(N-H) bending
1496	ssh	
1475	s	ν(C-F)
1370	ssh	ν(-CH_3) bending
1350	vw	
1305	vs	ν(C-O) Carboxylic
1287	s	ν(C-N)
1160	vwsh	
1055	ms	
1042	sh	
945	ms	
835	ms	
752	s	δ (C-H) Aromatic out of plane bend
655	s	ν(Mn-N)

IR spectrum of Ni(II)-Ciprofloxacin compound: IR spectrum for Ni(II)-Ciprofloxacin compound is given in Fig 6.1.4. The frequencies of the bands are listed in Table 6.1.5 with relative intensities and tentative assignments.

A broad band in the range 3040—2970 cm^{-1} was found due to both free and hydrogen bonded O-H stretching vibration. Compared to Ciprofloxacin ν(>C=O) shows a shift at 1797 cm^{-1}, suggesting that the >C=O group of Ciprofloxacin moity is also involved in hydrogen bonding. At 1625 cm^{-1} a very strong intensity is observed which is for ν_{arom}(C=C). Another response at 1510 cm^{-1} is due to ν(N-H) bending. The ν(C-F) frequency is observed at 1490 cm^{-1}. At 1390 cm^{-1} the response may be due to ν(-CH_3) bending. Another peak at 1272 cm^{-1} is observed due to ν(C-N). The vibrations for the out of plane bending mode of aromatic C-H is appeared at 675 cm^{-1}. The peak at 630 cm^{-1} may be due to ν(Ni-N)[105].

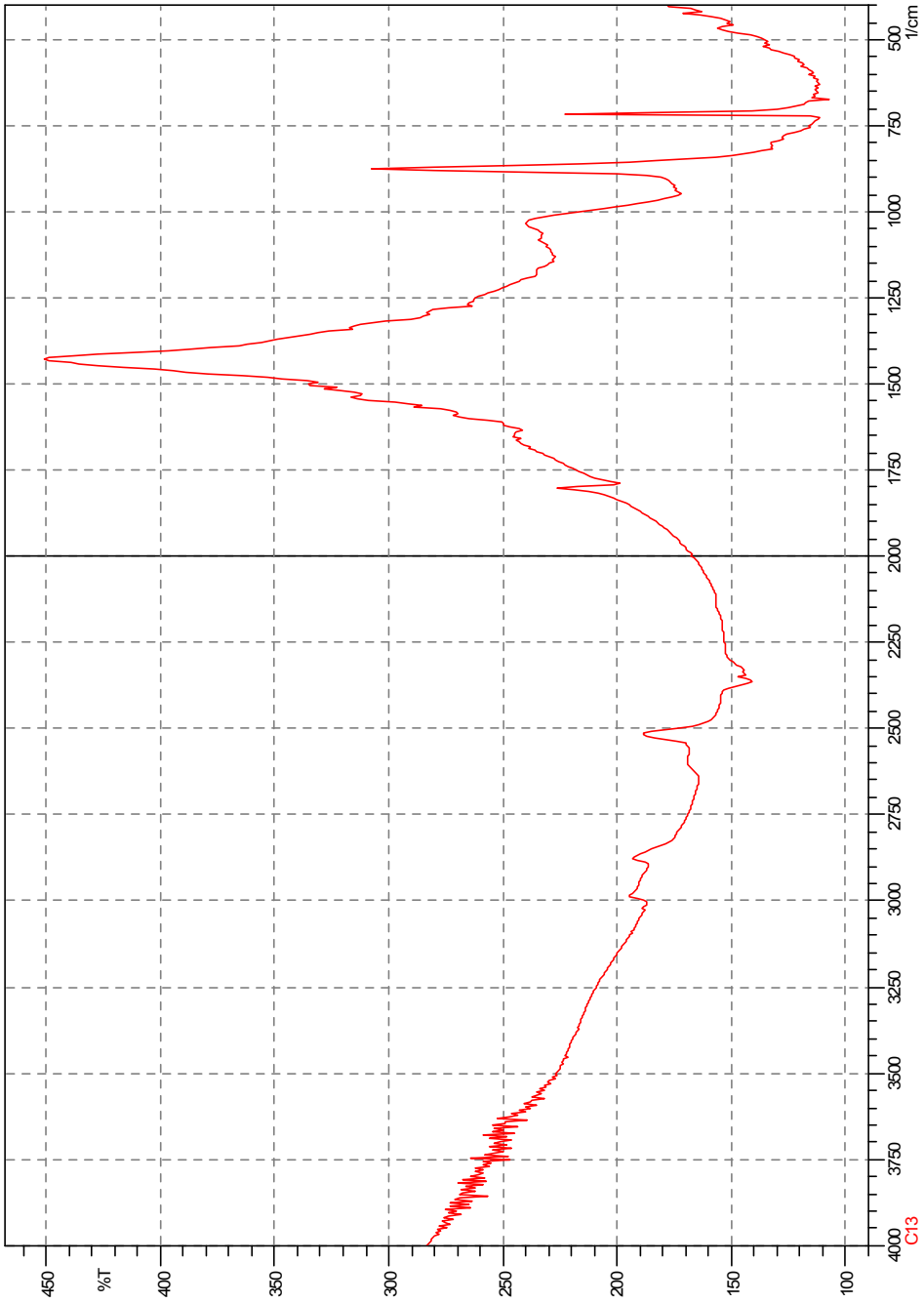

Fig 6.1.4 Infrared spectrum of Ni(II)-Ciprofloxacin compound.

Table 6.1.5 Assignment for IR bands of Ni(II)-Ciprofloxacin compound.

Wave no. (cm^{-1})	Relative Intesity	Tentative band assignment
3040--2970	sb	ν(O-H) Free & H-bonded
2896	vw	
2355	w	
2330	wsh	
1797	vs	ν(>C=O) Ketonic
1625	vs	ν_{arom}(C=C)
1560	sh	
1510	ssh	ν(N-H) bending
1490	s	ν(C-F)
1272	s	ν(C-N)
1155	vwsh	
935	ms	
675	s	δ (C-H) Aromatic out of plane bend
630	msh	ν(Ni-N)

IR spectrum of Cu(II)-Ciprofloxacin compound: The IR spectrum of Cu(II)-Ciprofloxacin compound is given in Fig 6.1.5. The frequencies of the bands are listed in Table 6.1.6 with relative intensities and tentative assignments.

This Cu(II)-Ciprofloxacin compound exhibits a strong broad band in the range 3555—3157 cm^{-1} due to O-H stretching vibration. Compared to Ciprofloxacin ν(>C=O) shows a down field shift at 1628 cm^{-1}, suggesting that the >C=O group of Ciprofloxacin moity is also involved in hydrogen bonding. Again very strong intensity is observed at 1578 cm^{-1} which is for ν_{arom}(C=C). A strong response at 1540cm^{-1} is due to ν(N-H) bending. The ν(C-F) frequency is observed at 1478 cm^{-1}. And a very strong response at 1310 cm^{-1} is found, which may be due to carboxylic ν(C-O). Another peak at 1295 cm^{-1} is observed due to ν(C-N). The vibrations for the out of plane bending mode of aromatic C-H is appeared at 752 cm^{-1}. The peak at 668 cm^{-1} may be due to ν(Cu-N)[105].

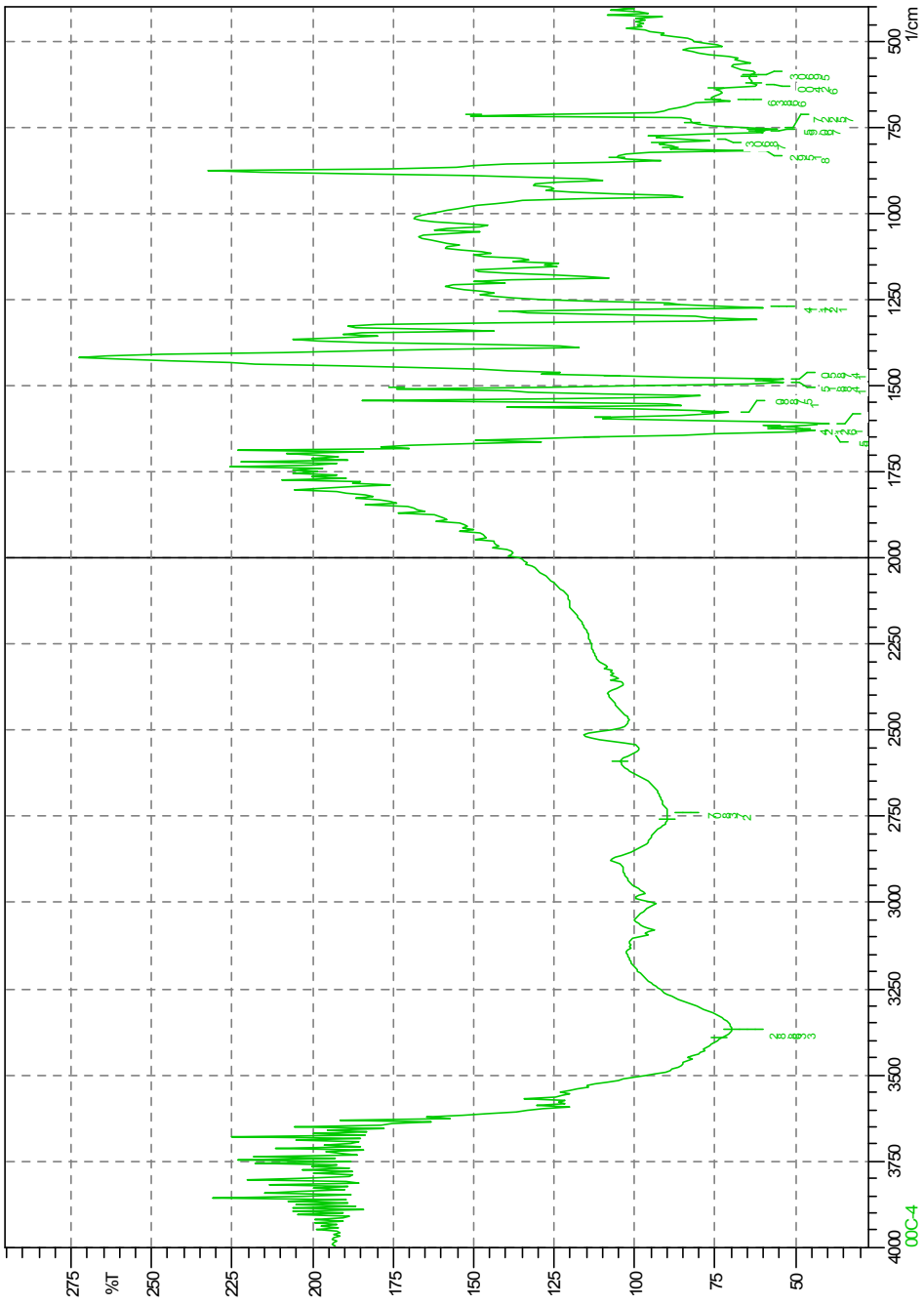

Fig 6.1.5 Infrared spectrum of Cu(II)-Ciprofloxacin compound.

Table 6.1.6 Assignment for IR bands of Cu(II)-Ciprofloxacin compound.

Wave no. (cm^{-1})	Relative Intesity	Tentative band assignment
3555--3157	sb	ν(O-H) H-bonded
3080	wb	
3000	vwsh	
2970	vw	
2555	vb	
2460	wb	
1628	vs	ν(>C=O) Ketonic
1578	vs	ν_{arom}(C=C)
1557	ssh	
1540	s	ν(N-H) bending
1478	sb	ν(C-F)
1370	w	
1350	vw	
1310	s	ν(C-O) Carboxylic
1295	ssh	ν(C-N)
1271	wsh	
1145	vwb	
1050	vwb	
950	w	
786	W	
761	w	
752	ms	δ (C-H) Aromatic out of plane bend
668	ms	ν(Cu-N)

IR spectrum of Zn(II)-Ciprofloxacin compound: The IR spectrum of Zn(II)-Ciprofloxacin compound is given in Fig 6.1.6. The frequencies of the bands are listed in Table 6.1.7 with relative intensities and tentative assignments.

Zn(II)-Ciprofloxacin compound exhibits a band at 3510 cm^{-1} due to both free and hydrogen bonded O-H stretching vibration. Another strong broad band in the range 3200—2900 cm^{-1} may be due to ν(O-H) of carboxylic acid. Compared to Ciprofloxacin ν(>C=O) shows a down field shift at 1725cm^{-1}, suggesting that the >C=O group of Ciprofloxacin moity is also involved in hydrogen bonding. Again very strong intensity is observed at 1635 cm^{-1} which is for ν_{arom}(C=C). A strong response at 1498 cm^{-1} is due to ν(N-H) bending. The ν(C-F) frequency is observed at 1480 cm^{-1}. And a very strong response at 1310 cm^{-1} is found, which may be due to carboxylic ν(C-O). Another peak at 1290 cm^{-1} is observed due to ν(C-N). The vibrations for the out of plane bending mode of aromatic C-H is appeared at 775 cm^{-1}. The peak at 690 cm^{-1} may be due to ν(Zn-N)[105].

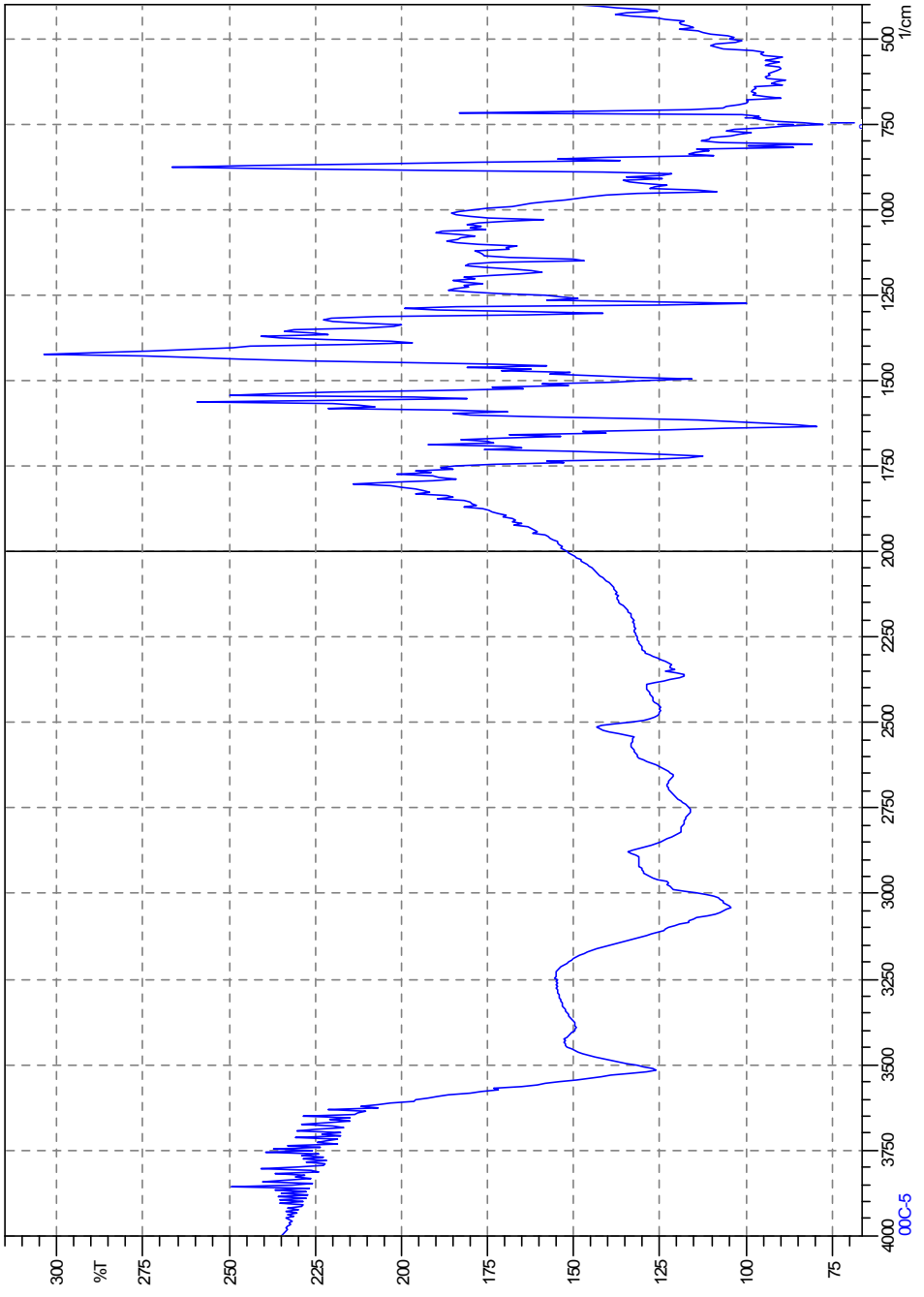

Fig 6.1.6 Infrared spectrum of Zn(II)-Ciprofloxacin compound.

Table 6.1.7 Assignment for IR bands of Zn(II)-Ciprofloxacin compound.

Wave no. (cm^{-1})	Relative Intesity	Tentative band assignment
3510	sw	ν(O-H) Free & H-bonded
3400	w	
3200--2900	sb	ν(O-H) Carboxylic acid
2752	wsh	
2620	vw	
2478	w	
2350	wb	
1725	vs	ν(>C=O) Ketonic
1635	vs	ν_{arom}(C=C)
1498	s	ν(N-H) bending
1480	sb	ν(C-F)
1400	sh	
1350	vw	
1310	s	ν(C-O) Carboxylic
1290	ssh	ν(C-N)
1250	wsh	
1110	w	
1100	W	
1023	ms	
910	msh	
870	ms	
750	w	
775	ms	δ (C-H) Aromatic out of plane bend
690	ms	ν(Zn-N)

6.1.2.3 Electronic Spectral Analysis

The visible and ultraviolet regions of the spectrum, that is 190—800 nm are those in which electronic excitation usually occurs. Light of these wavelengths may be absorbed by a complex and electronic spectra can be measured. The electronic spectral bands are very broad, these spectra are not often used as "finger prints" or in looking for functional groups as is done in infrared spectroscopy.

Energy absorbed in the UV region are due to the electronic energy of the compound resulting from the transition of electrons in the molecule. The transition is manifest because of the excitation of electrons from filled molecular orbital (usually non-

bonding or bonding π orbital) to the next higher energy level (an antibonding π^* orbital). The different possibilities of the electronic absorption spectra are discussed below:

i) Spectra associated principally with the ligand.
ii) Spectra involving electronic transition between the metal and the ligands, charge transfer spectra.
iii) Spectra associated with the metal induced by the presence of the ligands; d-d transition ion.
iv) Spectra associated with the counter ion.

These possible interactions can be classified as n→π*, n→σ*, π→π*, σ→π*, σ→σ* and may be shown by the energy diagram (Fig 6.1.7)

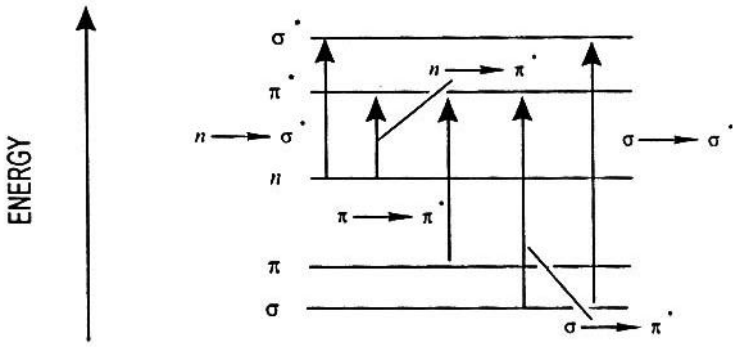

Fig 6.1.7 Electronic Energy levels and transitions.

Ligand spectra: Ligands such as water or organic molecules possess characteristics absorption bands that are normally in the ultra-violet.

n→π* transition: these transitions can occur in molecules containing donor atoms that are involved in π-bonding. Such molecules are aldehydes and ketones which contain the >C=O group.

n→σ* transition: When atoms in molecules contain lone-pair electrons that are not involved in bonding posses the transition of lowest energy is n→σ*.this transition is found in molecules such as water, alcohols, amines and alkyl halides.

π→π* transition: Molecules possessing double or triple bonds involve with π→π* transition. Such transitions occur in olefins, dienes and aromatic systems.

σ→π* transition: Transition corresponding to electron jump from bonding σ-orbital to anti-bonding π* orbital. Carbonyl compounds posses this type of transition.

σ→σ* transition: Transition involving electron jump from lowest occupied bonding σ orbital to highest unoccupied anti-bonding σ* orbital. In alkanes this type of transition occurs[106].

Counter-ion Spectra: A complex ion must be associated with a counter-ion; a knowledge of the spectrum of this counter-ion must be known in order to interpret the spectrum due to the complex ion.

Charge-transfer spectra: These spectra arise from transitions between orbitals that are principally those of the metal and orbitals that are largely ligand orbitals.

Ligand-field spectra: These arise from transitions between the d orbitals of the metal that have been split in a ligand field; they are also known as d-d spectra.

Therefore, the particular spectrum expressed by a compound is dependent upon the energy of the d-orbitals, their degeneracy and the number of electrons distributed in them. These outlines inturn governed by the oxidation state of the metal, the number and kind of ligand and the geometry of the complex. Transition metal complexes are generally coloured and this colour comes from absorption of light in the visible region. Absorption of light causes transition of d-electrons from lower to a higher energy level[106].

6.1.2.4 UV Spectra of Ciprofloxacin and its metal compounds

The UV-visible spectra Ciprofloxacin and Metal-Ciprofloxacin compounds are shown in Figures 6.1.8, 6.1.9, 6.1.10, 6.1.11, 6.1.12 as well as 6.1.13 and their absorption bands for various transition are given in Table 6.1.8. (parent metal compounds) and in Table 6.1.9. (Ciprofloxacin and Metal-Ciprofloxacin compounds) The tentative band assignments have been made on the basis of some standard literature.

Table 6.1.8 Absorption bands of parent metal compounds.

Parent metals	Absorption bands

Cr(III)	642, 410
Mn(II)	410, 270
Ni(II)	710, 660, 399, 298, 225
Cu(II)	798
Zn(II)	No characteristic bands.

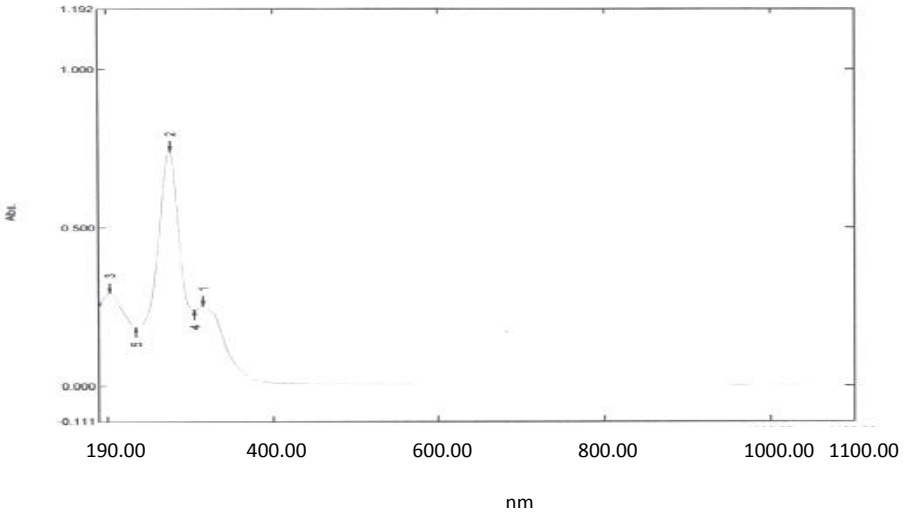

Fig 6.1.8 Ultraviolet spectrum for Ciprofloxacin.

Table 6.1.9 Absorption bands of Ciprofloxacin and Metal-Ciprofloxacin compounds.

Compounds	d→d	n→π*	π→π*	n→σ*
Ciprofloxacin		325	276	210
Cr(III)-Ciprofloxacin	432	310	280	
Mn(II)-Ciprofloxacin		302	285	
Ni(II)-Ciprofloxacin	395	315	265	
Cu(II)-Ciprofloxacin	807	305	278	
Zn(II)-Ciprofloxacin		302	270	

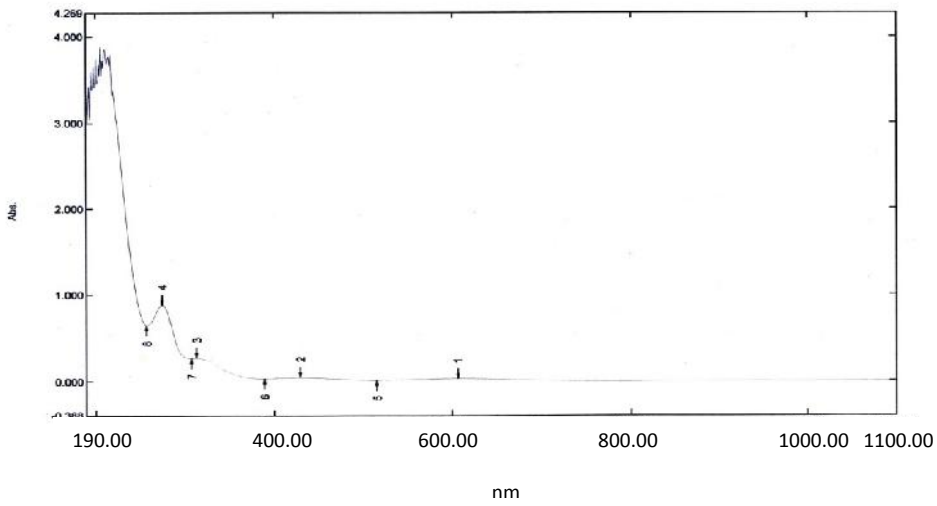

Fig 6.1.9 Ultraviolet spectrum of Cr(III)-Ciprofloxacin compound.

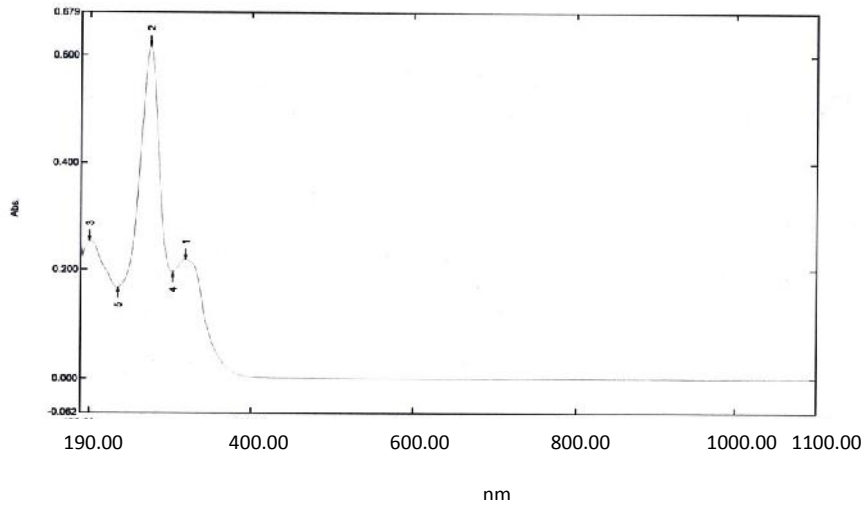

Fig 6.1.10 Ultraviolet spectrum of Mn(II)-Ciprofloxacin compound.

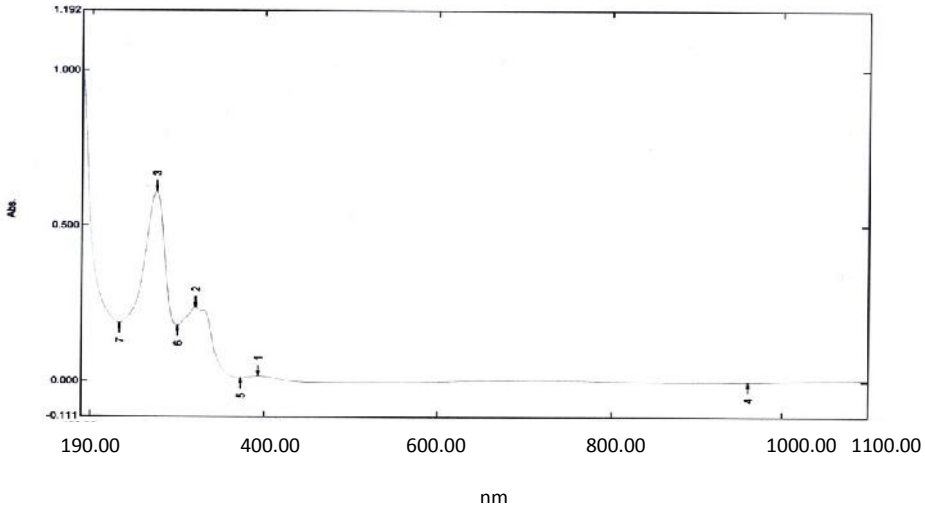

Fig 6.1.11 Ultraviolet spectrum of Ni(II)-Ciprofloxacin compound.

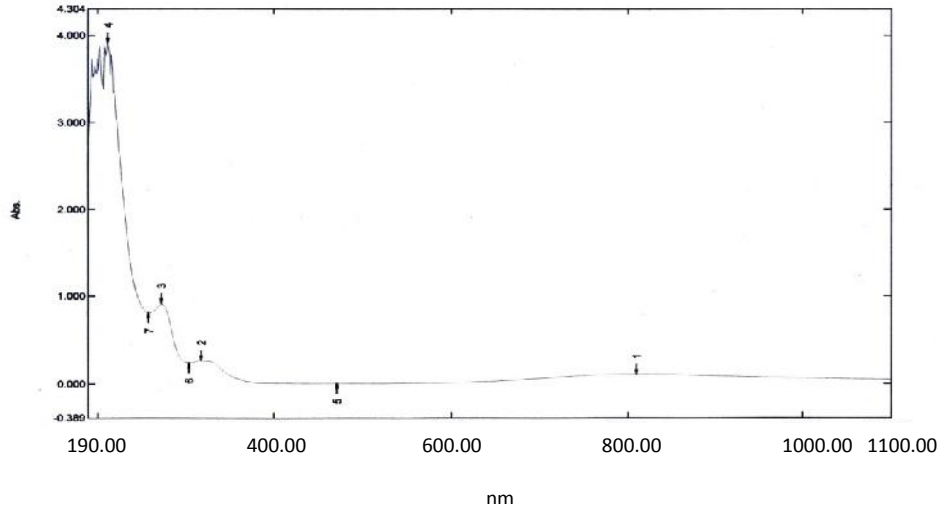

Fig 6.1.12 Ultraviolet spectrum of Cu(II)-Ciprofloxacin compound.

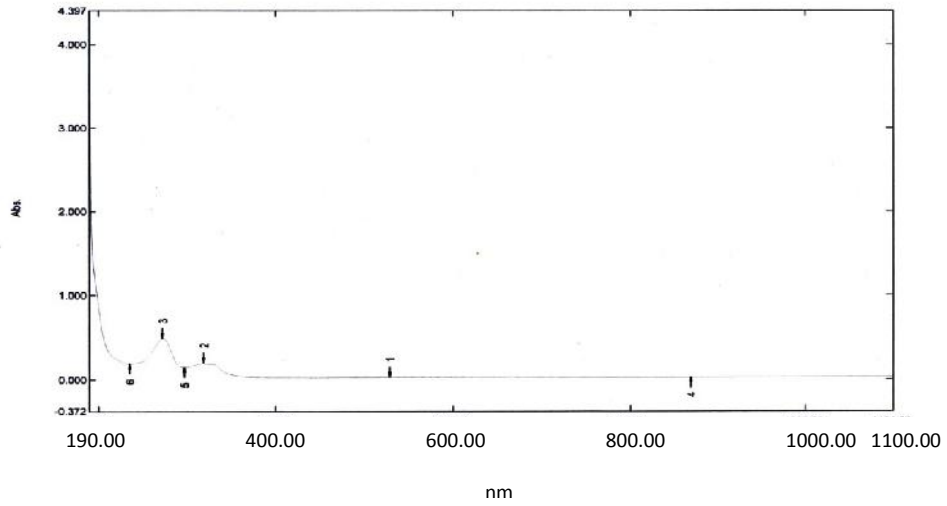

Fig 6.1.13 Ultraviolet spectrum of Zn(II)-Ciprofloxacin compound.

The ultra-violet radiations cover the wavelength range from 200-350 nm and the visible radiations which cover the wavelength 350-800nm. The parent metal compounds show absorption bands at different wave lengths most of which are in the visible range. These are due to d→d electron transition in metals and other types of transition found in the ultra-violet ranges are due to the anionic part of the compounds.

The ligand Ciprofloxacin showed an intense absorption band at 210, 276 and 325 nm resulting from n→σ*, π→π* and n→π* electron transitions of electron releasing substituent F on the aromatic ring, double bonds present in aromatic ring and the heterocyclic molecules as well as the non bonding electron present in >C=O group and on N atom. Specially heterocyclic molecule showed a combination of π→π* and n→π* electron transitions.

In the Cr(II), Mn(II), Ni(II), Cu(II) and Zn(II)-Ciprofloxacin compounds π→π* transition occurred at 280, 285, 265, 278 and 270 nm respectively and n→π* transition occurred at 310, 302, 315, 305 and 302 nm respectively. None of these compounds exhibit n→σ* transition. d→d electron transition occurred except manganese and zinc compound at 432, 395 and 807 nm respectively. The zinc compound does not show d→d transition because Zn contain d^{10} electrons[106].

6.1.2.5 Near-infrared spectroscopy (NIRS)

Near-infrared spectroscopy (NIRS) is a spectroscopic method that uses the near-infrared region of the electromagnetic spectrum (from about 800 nm to 2500 nm). Typical applications include pharmaceutical, medical diagnostics (including blood sugar and pulse oximetry), food and agrochemical quality control, and combustion research, as well as research in functional neuroimaging, sports medicine & science, elite sports training, ergonomics, rehabilitation, neonatal research, brain computer interface, urology (bladder contraction) and neurology (neurovascular coupling).

History of NIR: The discovery of near-infrared energy is ascribed to Herschel in the 19th century, but the first industrial application began in the 1950s. In the first applications, NIRS was used only as an add-on unit to other optical devices that used other wavelengths such as ultraviolet (UV), visible (Vis), or mid-infrared (MIR) spectrometers. In the 1980s, a single unit, stand-alone NIRS system was made available, but the application of NIRS was focused more on chemical analysis. With the introduction of light-fiber optics in the mid-1980s and the monochromator-detector developments in early-1990s, NIRS became a more powerful tool for scientific research.

This optical method can be used in a number of fields of science including physics, physiology, or medicine. It is only in the last few decades that NIRS began to be used as a medical tool for monitoring patients.

Properties of Infrared-Near-Infrared energy: Light has both particle and wave properties; quantum theory tells us that the energy of a light particle or photon E_p is given by

$$E_p = h\nu$$

Where h = Planck's constant (6.6256×10^{-27} erg-sec), and ν is the frequency of light (or the numberof vibrations per second or in units of sec^{-1}). Thus the energy for any specific photon can be quantified , and it is this energy that interacts with the vibrating

bonds within near-infrared active molecules[107]. The subsequent values for wavelength, wavenumber and frequency for both the visible and the extended near-infrared regions are shown in Table 6.1.10.

Table 6.1.10 Equivalent wavelength, wavenumber and frequency values for the visible and near-infrared spectral regions.

Region	Wavelength			Wavenumber	Frequency
	(cm)	(μm)	(nm)	(cm^{-1})	(Hertz)
Visible	$3.5x10^{-5}$ to $7.8x10^{-5}$	0.35-0.78	350-780	28,571 to 12,821	$8.563x10^{14}$ to $3.842x10^{14}$
Extended Near Infrared	$7.8x10^{-5}$ to $3.0x10^{-4}$	0.78-3.00	780-3000	12,821 to 3333	$3.842x10^{14}$ to $9.989x10^{13}$

Types of Near-Infrared absorbtions bands: Infrared energy is the electromagnetic energy of molecular vibration. The energy band is defined for convenience as the near-infrared covering 12,821 to 4000 cm^{-1} (780-2500 nanometers); the infrared (or mid-infrared) as 4000 to 400 cm^{-1} (2500-25,000 nm; and the far-infrared (or terahertz) from 400 to 10 cm^{-1} (25,000-1,000,000 nm). Table illustrates the region of the EMR (electromagnetic radiation) spectrum referred to as the NIR region. The Table 6.1.11 shows the molecular interactions associated with the energy frequencies (or corresponding wavelengths) of the various regions.

Table 6.1.11 Spectroscopic regions of interest for chemical analysis.

Region	Wavenumbers/ (Wavelength)	Characteristic Measured
Ultraviolet	52,632-27,778 cm^{-1} (190-360 nm)	Electronic transitions; delocalized Pi electrons
Visible	27,778-12,821 cm^{-1} (360-780 nm)	Electronic transitions; color measurements
Near-Infrared (NIR)	14,493-3333 cm^{-1} (690-3000 nm) or 12,821-4000 cm^{-1} (780-2500 nm)	Overtone and combination bands of fundamental molecular vibrations, especially stretching and bending (some deformation as well)
Infrared (IR)	4000-400 cm^{-1} (2500-25,000 nm)	Fundamental molecular vibrations; stretching, bending, wagging, scissoring
Far-Infrared (FIR or Tetrahertz)	400-10 cm^{-1} ($2.5x10^{4}$-10^{6} nm)	Molecular rotation

Specific molecular bonds most active in the NIR are listed here, with X-H bonds being the more active and intense.

C=O from aldehyde, amides, carboxylic acids, esters, ketones

C-H from aldehydes, alkanes, alkenes, alkynes, aromatic compounds

C-N from amines (alkyl), amines (aromatic)

C-O from alcohols, ethers and esters

N-H from amides, amines

NO_2 from nitro groups

O-H from alcohols (no hydrogen bonding) and alcohols (with hydrogen bonding), carboxylic acids[108]

Theory of NIR: Near-infraredspectroscopy is based on molecular overtone and combination vibrations. Such transitions are forbidden by the selection rules of quantum mechanics. As a result, the molar absorptivity in the near IR region is typically quite small. One advantage is that NIR can typically penetrate much farther into a sample than mid infrared radiation. Near-infrared spectroscopy is, therefore, not a particularly sensitive technique, but it can be very useful in probing bulk material with little or no sample preparation.

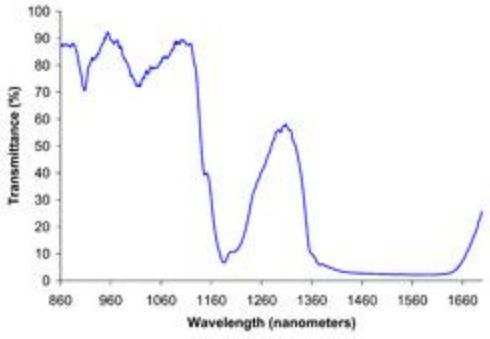

Fig 6.1.14 Near infrared spectrum of liquid ethanol.

The molecular overtone and combination bands seen in the near IR are typically very broad, leading to complex spectra; it can be difficult to assign specific features to specific chemical components. Multivariate (multiple variables) calibration techniques (e.g., principal components analysis, partial least squares, or artificial neural networks) are often employed to extract the desired chemical information. Careful development of a set of calibration samples and application of multivariate calibration techniques is essential for near-infrared analytical methods.

Instrumentation for NIR: Instrumentation for near-IR (NIR) spectroscopy is similar to instruments for the UV-visible and mid-IR ranges. There is a source, a detector, and a dispersive element (such as a prism, or, more commonly, a diffraction grating) to allow the intensity at different wavelengths to be recorded. Fourier transform NIR instruments using an interferometer are also common, especially for wavelengths above ~1000 nm. Depending on the sample, the spectrum can be measured in either reflection or transmission.

Common incandescent or quartz halogen light bulbs are most often used as broadband sources of near-infrared radiation for analytical applications. Light-emitting diodes (LEDs) are also used; they offer greater lifetime and spectral stability and reduced power requirements.

The type of detector used depends primarily on the range of wavelengths to be measured. Silicon-based CCDs are suitable for the shorter end of the NIR range, but are not sufficiently sensitive over most of the range (over 1000 nm). InGaAs and PbS devices are more suitable though less sensitive than CCDs. In certain diode array (DA) NIRS instruments, both silicon-based and InGaAs detectors are employed in the same instrument. Such instruments can record both UV-visible and NIR spectra 'simultaneously'.

Instruments intended for chemical imaging in the NIR may use a 2D array detector with an acousto-optic tunable filter. Multiple images may be recorded sequentially at different narrow wavelength bands.

Many commercial instruments for UV/vis spectroscopy are capable of recording spectra in the NIR range (to perhaps ~900 nm). In the same way, the range of some mid-IR instruments may extend into the NIR. In these instruments, the detector used for the NIR wavelengths is often the same detector used for the instrument's "main" range of interest.

Applications of NIR: The primary application of NIRS to the human body uses the fact that the transmission and absorption of NIR light in human body tissues contains information about hemoglobin concentration changes. When a specific area of the brain is activated, the localized blood volume in that area changes quickly. Optical imaging can measure the location and activity of specific regions of the brain by

continuously monitoring blood hemoglobin levels through the determination of optical absorption coefficients.

Typical applications of NIR spectroscopy include the analysis of foodstuffs, pharmaceuticals, combustion products and a major branch of astronomical spectroscopy.

i) Astronomical spectroscopy: Near-infrared spectroscopy is used in astronomy for studying the atmospheres of cool stars where molecules can form. The vibrational and rotational signatures of molecules such as titanium oxide, cyanide, and carbon monoxide can be seen in this wavelength range and can give a clue towards the star's spectral type. It is also used for studying molecules in other astronomical contexts, such as in molecular clouds where new stars are formed. The astronomical phenomenon known as reddening means that near-infrared wavelengths are less affected by dust in the interstellar medium, such that regions inaccessible by optical spectroscopy can be studied in the near-infrared. Since dust and gas are strongly associated, these dusty regions are exactly those where infrared spectroscopy is most useful. The near-infrared spectra of very young stars provide important information about their ages and masses, which is important for understanding star formation in general.

ii) Agriculture:Near-infrared spectroscopy is widely applied in agriculture for determining the quality of forages, grains, and grain products, oilseeds, coffee, tea, spices, fruits, vegetables, surgarcane, beverages, fats, and oils, dairy products, eggs, meat, and other agricultural products. It is widely used to quantify the composition of agricultural products because it meets the criteria of being accurate, reliable, rapid, non-destructive, and inexpensive.

iii) Remote monitoring: Techniques have been developed for NIR spectroscopic imaging. Hyperspectral imaging has been applied for a wide range of uses, including the remote investigation of plants and soils. Data can be collected from instruments on airplanes or satellites to assess ground cover and soil chemistry.

iv) Materials Science: Techniques have been developed for NIR spectroscopy of microscopic sample areas for film thickness measurements, research into the optical

characteristics of nanoparticles and optical coatings for the telecommunications industry.

v) Medical uses: Medical applications of NIRS center on the non-invasive measurement of the amount and oxygen content of hemoglobin, as well as the use of exogenous optical tracers in conjunction with flow kinetics.

NIRS can be used for non-invasive assessment of brain function through the intact skull in human subjects by detecting changes in blood hemoglobin concentrations associated with neural activity, e.g., in branches of Cognitive psychology as a partial replacement for fMRI techniques. NIRS can be used on infants, and NIRS is much more portable than fMRI machines, even wireless instrumentation is available, which enables investigations in freely moving subjects. However, NIRS cannot fully replace fMRI because it can only be used to scan cortical tissue, where fMRI can be used to measure activation throughout the brain. Special public domain statistical toolboxes for analysis of stand alone and combined NIRS/MRI measurement have been developed (NIRS-SPM).

The application in functional mapping of the human cortex is called diffuse optical tomography (DOT), near infrared imaging (NIRI) or functional NIRS (fNIR). The term diffuse optical tomography is used for three-dimensional NIRS. The terms NIRS, NIRI and DOT are often used interchangeably, but they have some distinctions. The most important difference between NIRS and DOT/NIRI is that DOT/NIRI is used mainly to detect changes in optical properties of tissue simultaneously from multiple measurement points and display the results in the form of a map or image over a specific area, whereas NIRS provides quantitative data in absolute terms on up to a few specific points. The latter is also used to investigate other tissues such as, e.g., muscle, breast and tumors. NIRS can be used to quantify blood flow, blood volume, oxygen consumption, reoxygenation rates and muscle recovery time in muscle.

By employing several wavelengths and time resolved (frequency or time domain) and/or spatially resolved methods blood flow, volume and absolute tissue saturation (StO_2 or Tissue Saturation Index (TSI)) can be quantified. Applications of oximetry by NIRS methods include neuroscience, ergonomics, rehabilitation, brain computer

interface, urology, the detection of illnesses which affect the blood circulation (e.g., peripheral vascular disease), the detection and assessment of breast tumors, and the optimization of training in sports medicine.

The use of NIRS in conjunction with a bolus injection of indocyanine green (ICG) has been used to measure cerebral blood flow and cerebral metabolic rate of oxygen consumption.[109] It has also been shown that CMRO2 can be calculated with combined NIRS/MRI measurements. NIRS is starting to be used in pediatric critical care, to help deal with cardiac surgery post-op. Indeed, NIRS is able to measure venous oxygen saturation (SVO2), which is

determined by the cardiac output, as well as other parameters (FiO2, hemoglobin, oxygen uptake). Therefore, following the NIRS gives critical care physicians a notion of the cardiac output. NIRS is liked by patients, because it is non-invasive, is painless, and uses non-ionizing radiation.

Optical Coherence Tomography (OCT) is another NIR medical imaging technique capable of 3D imaging with high resolution on par with low-power microscopy. Using optical coherence to measure photon pathlength allows OCT to build images of live tissue and clear examinations of tissue morphology. Due to technique differences OCT is limited to imaging 1–2 mm below tissue surfaces, but despite this limitation OCT has become an established medical imaging technique especially for imaging of the retina and anterior segments of the eye. The instrumental development of NIRS/NIRI/DOT/OCT has proceeded tremendously during the last years and, in particular, in terms of quantification, imaging and miniaturization.[137]

vi) Particle measurement: NIR is often used in particle sizing in a range of different fields, including studying pharmaceutical and agricultural powders.

vii) Industrial uses: As opposed to NIRS used in optical topography, general NIRS used in chemical assays does not provide imaging by mapping. For example, a clinical carbon dioxide analyzer requires reference techniques and calibration routines to be able to get accurate CO_2 content change. In this case, calibration is performed by adjusting the zero control of the sample being tested after purposefully supplying 0% CO_2 or another known amount of CO_2 in the sample. Normal compressed gas from

distributors contains about 95% O_2 and 5% CO_2, which can also be used to adjust %CO_2 meter reading to be exactly 5% at initial calibration.

6.1.2.6 NIR spectrum of Ciprofloxacin and its compounds

The NIR spectrum of Ciprofloxacin (Fig 6.1.15) and Metal-Ciprofloxacin compounds are shown in Figures 6.1.16 to 6.1.20 the spectra structure and material type of the various absorption bands are listed in Tables 6.1.12 to 6.1.17.

NIR spectrum of Ciprofloxacin: The NIR spectrum of Ciprofloxacin compounds is given in Fig 6.1.15. The frequencies of the bands are listed in Table 6.1.12 with relative intensities and tentative assignments.

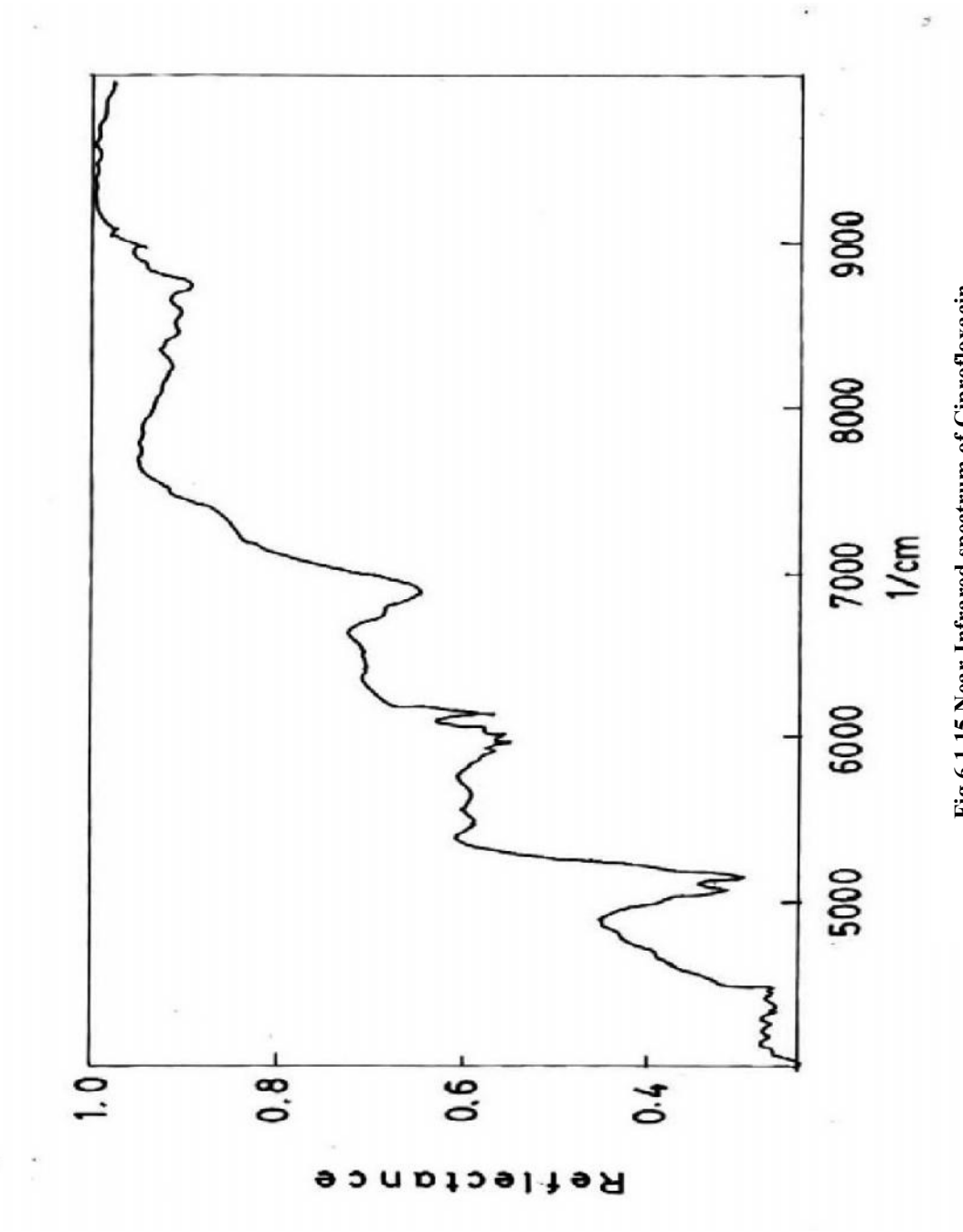

Fig 6.1.15 Near-Infrared spectrum of Ciprofloxacin .

Table 6.1.12 Assignment for NIR bands of Ciprofloxacin.

Wave no. (cm^{-1})	Spectra structure	Material type

4200	C-H, C-C	Combination
4270	C-H, (-CH_3)	Hydrocarbon
4390	C-H, (-CH_3)	Hydrocarbon
5076	N-H stretching & N-H bending	Combination
5200	C=O, (C=OOH)	Acid, carboxylic
5476	O-H & C-H stretching	Combination
5678	C-H, (-CH_3)	Aromatic
5840	C-H, (-CH_3)	Hydrocarbon
5950	-X	Halogenated
6075	C-H, (-CH_3)	Hydrocarbon
6190	N-H	N-H in plane bending
6800	N-H	Symmetric & asymmetric combination
6950	C-H combination, Ar.C-H	Hydrocarbon, Aromatic
8490	C-H, (-CH_3)	Hydrocarbon
8550	C-H	Adjacent C=C
8780	Ar.C-H	Aromatic C-H

Ciprofloxacin exhibits a sharp band at about 5076 cm^{-1} due to a combination of N-H stretching and bending. A weak band at about 4200 cm^{-1} due to a combination of C-H and C-C. It exhibits another sharp band at 5200 cm^{-1} which may be due to the C=O originating from carboxylic group. At 5476 cm^{-1} there is an band due to a combination of O-H and C-H stretching. There are bands at 4270 cm^{-1}, 4390 cm^{-1}, 5840 cm^{-1}, 6075 cm^{-1} and 8490 cm^{-1} originating from C-H of $–CH_3$ in hydrocarbon parts and at 5678 cm^{-1} originating from C-H of $–CH_3$ in aromatic part as well as at 8780 cm^{-1} due to Ar.C-H (aromatic C-H). Again a broad band at 6950 cm^{-1} exhibits a combination of C-H (hydrocarbon) and Ar.C-H (aromatic). In addition to this a band at 8550 cm^{-1} signifies the presence of C-H due to adjacent C=C. A sharp band at 6190 cm^{-1} represents the N-H in plane bending and comperatively weak band at 6800 cm^{-1} is due the combination of symmetric asymmetric N-H. At 5950 cm^{-1} a small but sharp band declairs the existence of bond with halogen (X).

NIR spectrum of Cr(III)-Ciprofloxacin compound: The NIR spectrum of Cr(III)-Ciprofloxacin compound is given in Fig 6.1.16. The frequencies of the bands are listed in Table 6.1.13 with relative intensities and tentative assignments.

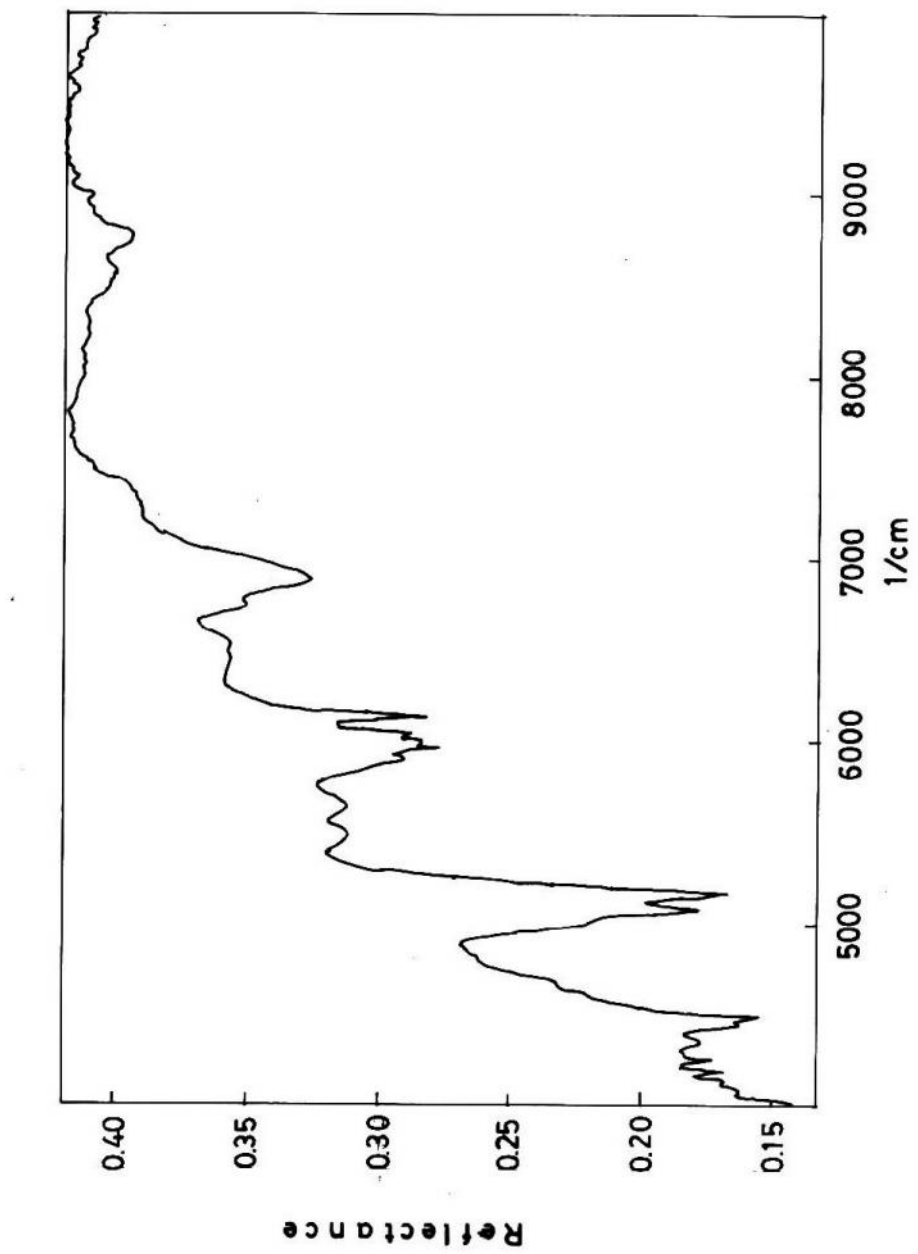

Fig 6.1.16 Near-Infrared spectrum of Cr(III)-Ciprofloxacin compound .

Cr(III)-Ciprofloxacin compound shows a medium but sharp band at about 4200 cm^{-1} due to a combination of C-H and C-C. At 4590 an almost sharp band is found as a

result of N-H, C-N and C=O combination. It exhibits another sharp band at 5190 cm^{-1} which may be due to the C=O originating from carboxylic group. At 5510 cm^{-1} there is a band due to a combination of O-H and C-H stretching. There are bands at 4280 cm^{-1}, 4350 cm^{-1}, 5860 cm^{-1} and 6125 cm^{-1} originating from C-H of $–CH_3$ in hydrocarbon parts and at 5710 cm^{-1} originating from C-H of $–CH_3$ in aromatic part as well as at 8740 cm^{-1} due to Ar.C-H (aromatic C-H). In addition to this a band at 8580 cm^{-1} signifies the presence of C-H due to adjacent C=C. A sharp band at 5050 cm^{-1} represents the combination of N-H both stretching and bending and also another sharp band at 6890 cm^{-1} is due the combination of symmetric asymmetric N-H. At 5990 cm^{-1} a small but sharp band declairs the existence of bond with halogen (X).

Table 6.1.13 Assignment for NIR bands of Cr(III)-Ciprofloxacin Compound.

Wave no. (cm^{-1})	Spectra structure	Material type
4200	C-H, C-C	Combination
4280	C-H, ($-CH_3$)	Hydrocarbon
4350	C-H, ($-CH_3$)	Hydrocarbon
4590	N-H, C-N & C=O	Combination
5050	N-H stretching & N-H bending	Combination
5190	C=O, (C=OOH)	Acid, carboxylic
5510	O-H & C-H stretching	Combination
5710	C-H, ($-CH_3$)	Aromatic
5860	C-H, ($-CH_3$)	Hydrocarbon
5990	-X	Halogenated
6125	C-H, ($-CH_3$)	Hydrocarbon
6890	N-H	Symmetric & asymmetric combination
8580	C-H	Adjacent C=C
8740	Ar.C-H	Aromatic C-H

NIR spectrum of Mn(II)-Ciprofloxacin compound: The NIR spectrum of Mn(II)-Ciprofloxacin compound is given in Fig 6.1.17. The frequencies of the bands are listed in Table 6.1.14 with relative intensities and tentative assignments.

Mn(II)-Ciprofloxacin compound exhibits a medium but sharp band at about 4150 cm^{-1} due to a combination of C-H and C-C. At 4500 an almost sharp band is found as a result of N-H, C-N and C=O combination. It exhibits another sharp band at 5180 cm^{-1} which may be due to the C=O originating from carboxylic group. At 5570 cm^{-1} there is a band due to a combination of O-H and C-H stretching. There are bands at 4200

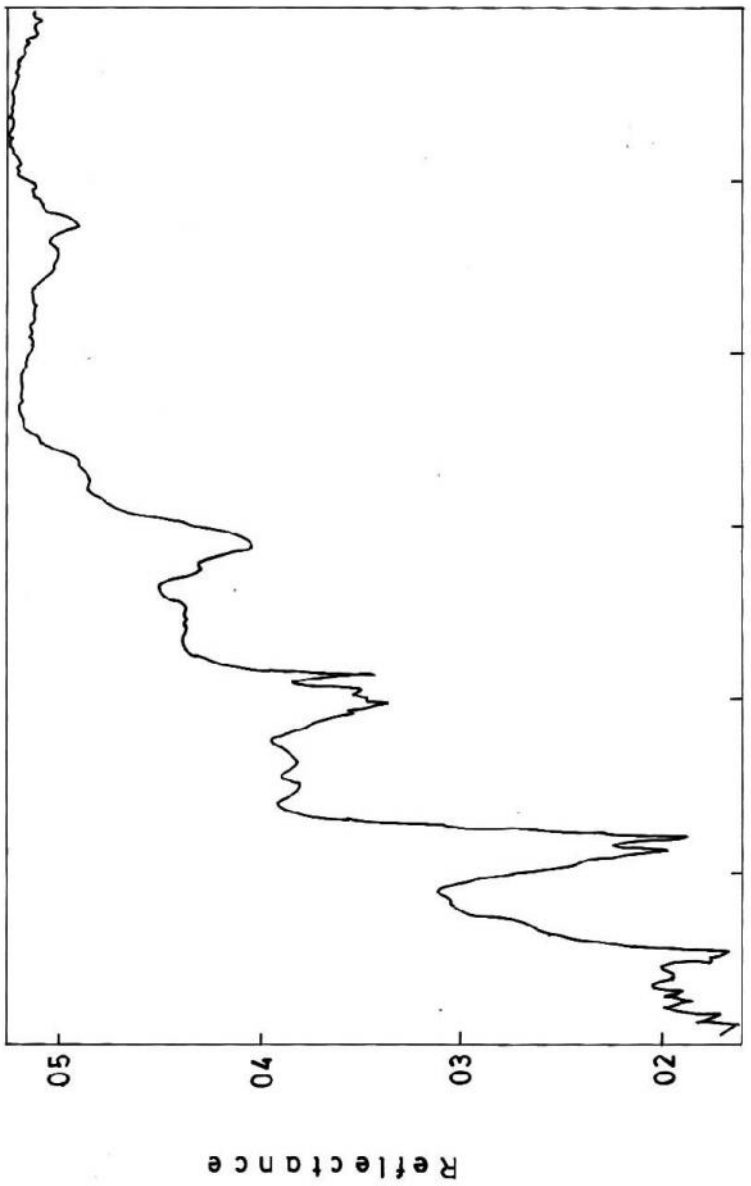

Fig 6.1.17 Near-Infrared spectrum of Mn(II)-Ciprofloxacin compound .

cm^{-1}, 4285 cm^{-1}, 5905 cm^{-1} and 6090 cm^{-1} originating from C-H of $–CH_3$ in hydrocarbon parts and at 5690 cm^{-1} originating from C-H of $–CH_3$ in aromatic part as

well as at 8760 cm^{-1} due to Ar.C-H (aromatic C-H). In addition to this a band at 6198 cm^{-1} signifies the presence of C-H due to adjacent C=O. A sharp band at 5035 cm^{-1} represents the combination of N-H both stretching and bending and also two another bands at 6760 cm^{-1} and 6941cm^{-1} are due to the combination of symmetric asymmetric N-H. At 5996 cm^{-1} as well as 6000 cm^{-1} two weak but sharp bands declear the existence of bond with halogen (X).

Table 6.1.14 Assignment for NIR bands of Mn(II)-Ciprofloxacin Compound.

Wave no. (cm^{-1})	Spectra structure	Material type
4150	C-H, C-C	Combination
4200	C-H, ($-CH_3$)	Hydrocarbon
4285	C-H, ($-CH_3$)	Hydrocarbon
4500	N-H, C-N & C=O	Combination
5035	N-H stretching & N-H bending	Combination
5180	C=O, (C=OOH)	Acid, carboxylic
5570	O-H & C-H stretching	Combination
5690	C-H, ($-CH_3$)	Aromatic
5905	C-H, ($-CH_3$)	Hydrocarbon
5996	-X	Halogenated
6000	-X	Halogenated
6090	C-H, ($-CH_3$)	Hydrocarbon
6198	C-H	Adjacent C=O
6760	N-H	Symmetric & asymmetric combination
6941	N-H	Symmetric & asymmetric combination
8760	Ar.C-H	Aromatic C-H

NIR spectrum of Ni(II)-Ciprofloxacin compound: The NIR spectrum of Ni(II)-Ciprofloxacin compound is given in Fig 6.1.18. The frequencies of the bands are listed in Table 6.1.15 with relative intensities and tentative assignments.

Ni(II)-Ciprofloxacin compound exhibits a medium but sharp band at about 4170 cm^{-1} due to a combination of C-H and C-C. At 4495 an almost sharp band is found as a result of N-H, C-N and C=O combination. It exhibits another sharp band at 5185 cm^{-1} which may be due to the C=O originating from carboxylic group. At 5555 cm^{-1} there is a band due to a combination of O-H and C-H stretching. There are bands at 4245 cm^{-1}, 4350 cm^{-1}, 5965 cm^{-1} and 6095 cm^{-1} originating from C-H of $-CH_3$ in hydrocarbon parts and at 5680 cm^{-1} originating from C-H of $-CH_3$ in aromatic part as well as at 8758 cm^{-1} due to Ar.C-H (aromatic C-H). In addition to this a band at 6200

cm^{-1} signifies the presence of C-H due to adjacent C=O. A sharp band at 5055 cm^{-1} represents the combination of N-H both stretching and bending and also two another bands at 6740 cm^{-1} and 6905 cm^{-1} are due to the combination of symmetric asymmetric N-H. At 5996 cm^{-1} as well as 6000 cm^{-1} two weak but sharp bands declear the existence of bond with halogen (X).

Table 6.1.15 Assignment for NIR bands of Ni(II)-Ciprofloxacin Compound.

Wave no. (cm^{-1})	Spectra structure	Material type
4170	C-H, C-C	Combination
4245	C-H, ($-CH_3$)	Hydrocarbon
4350	C-H, ($-CH_3$)	Hydrocarbon
4495	N-H, C-N & C=O	Combination
5055	N-H stretching & N-H bending	Combination
5185	C=O, (C=OOH)	Acid, carboxylic
5555	O-H & C-H stretching	Combination
5680	C-H, ($-CH_3$)	Aromatic
5965	C-H, ($-CH_3$)	Hydrocarbon
5996	-X	Halogenated
6000	-X	Halogenated
6095	C-H, ($-CH_3$)	Hydrocarbon
6200	C-H	Adjacent C=O
6740	N-H	Symmetric & asymmetric combination
6905	N-H	Symmetric & asymmetric combination
8758	Ar.C-H	Aromatic C-H

NIR spectrum of Cu(II)-Ciprofloxacin compound: The NIR spectrum of Cu(II)-Ciprofloxacin compound is given in Fig 6.1.19. The frequencies of the bands are listed in Table 6.1.16 with relative intensities and tentative assignments.

Cu(II)-Ciprofloxacin compound exhibits a very weak band at about 4160 cm^{-1} due to a combination of C-H and C-C. At 4511 cm^{-1} an almost sharp band is found as a result of N-H, C-N and C=O combination. It exhibits another sharp band at 5210 cm^{-1} which may be due to the C=O originating from carboxylic group. At 4410 cm^{-1}, 4415 cm^{-1}, 5090 cm^{-1} and 5515 cm^{-1} there are weak bands which are due to a combination of O-H and C-H stretching. There are bands at 4392 cm^{-1} and 6090 cm^{-1} originating from C-H of $-CH_3$ in hydrocarbon parts and at 4380 cm^{-1} originating from C-H of $-CH_3$ in aromatic part as well as at 6990 cm^{-1} due to a combination of C-H (hydrocarbon) and Ar.C-H (aromatic C-H). In addition to this a band at 7460 cm^{-1} signifies the presence

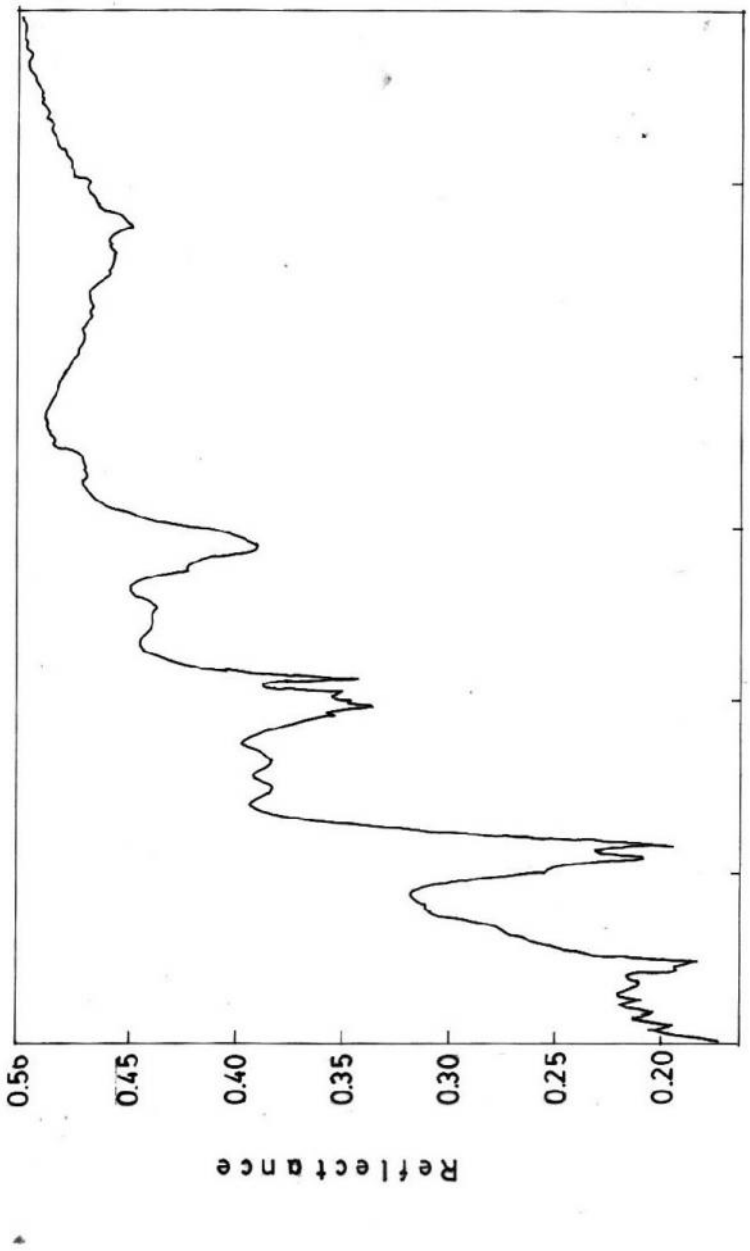

Fig 6.1.18 Near-Infrared spectrum of Ni(II)-Ciprofloxacin compound .

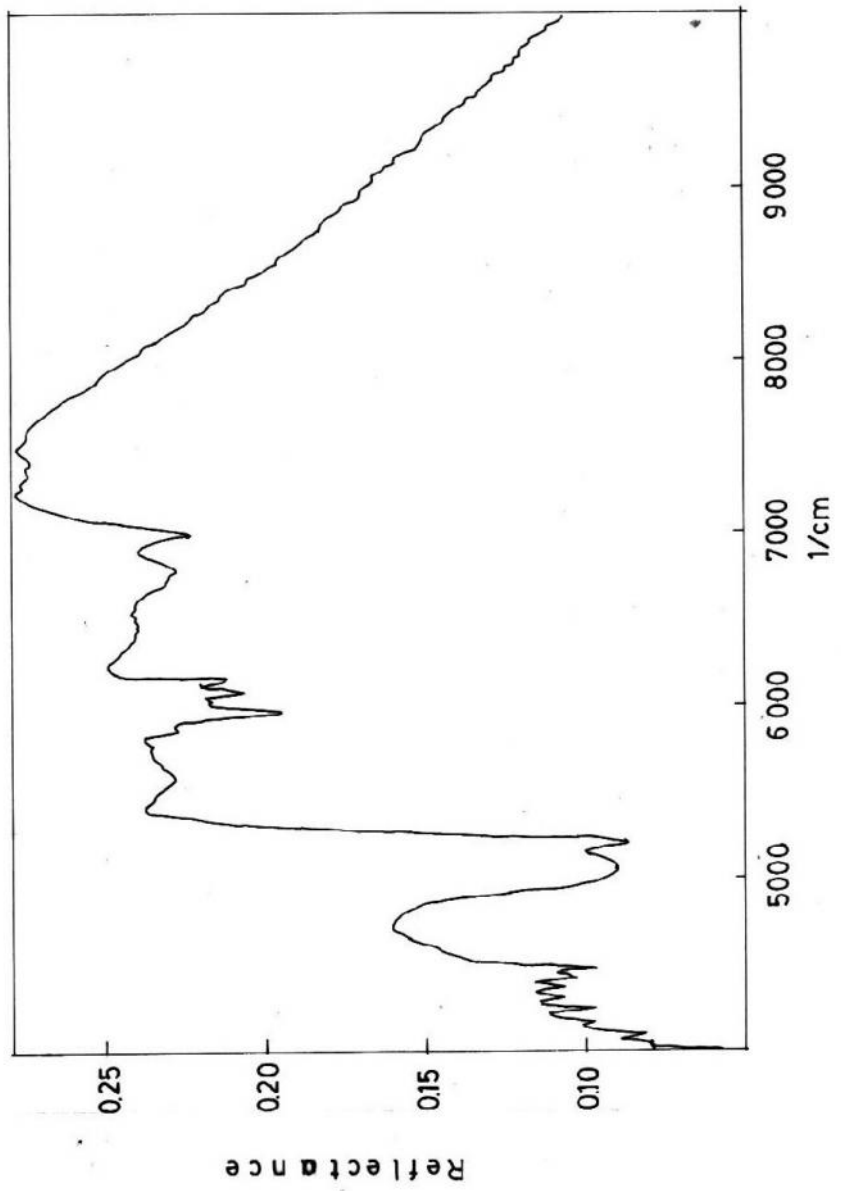

Fig 6.1.19 Near-Infrared spectrum of Cu(II)-Ciprofloxacin compound .

Table 6.1.16 Assignment for NIR bands of Cu(II)-Ciprofloxacin Compound.

Wave no. (cm^{-1})	Spectra structure	Material type
4160	C-H, C-C	Combination
4380	Ar.C-H	Aromatic
4392	C-H, ($-CH_3$)	Hydrocarbon
4410	O-H & C-H	Combination
4455	O-H & C-H	Combination
4511	N-H, C-N & C=O	Combination
5090	O-H & C-H	Combination
5210	C=O, (C=OOH)	Acid, carboxylic
5515	O-H & C-H stretching	Combination
5953	-X	Halogenated
6090	C-H, ($-CH_3$)	Hydrocarbon
6200	N-H	Symmetric & asymmetric combination
6750	N-H	Symmetric & asymmetric combination
6990	C-H, Ar.C-H	Combination
7460	C-H, ($-CH_3$)	Terminal

of C-H due to terminal CH_3 group. Two another bands at 6200 cm^{-1} and 6750 cm^{-1} are due to the combination of symmetric asymmetric N-H. At 5953 cm^{-1} weak but sharp bands declear the existence of bond with halogen (X).

NIR spectrum of Zn(II)-Ciprofloxacin compound: The NIR spectrum of Zn(II)-Ciprofloxacin compound is given in Fig 6.1.20. The frequencies of the bands are listed in Table 6.1.17 with relative intensities and tentative assignments.

Zn(II)-Ciprofloxacin compound exhibits a very weak band at about 4520 cm^{-1} an almost sharp band is found as a result of N-H, C-N and C=O combination. It exhibits another sharp band at 5140 cm^{-1} which may be due to the C=O originating from carboxylic group. At 4410 cm^{-1} there a sharp band which is due to a combination of O-H and C-H stretching. There are bands at 4300 cm^{-1}, 6135 cm^{-1} and 7310 cm^{-1} originating from C-H of $–CH_3$ in hydrocarbon parts and at 4360 cm^{-1} and 8705 cm^{-1} originating from C-H of $–CH_3$ in aromatic part. Two another bands at 6200 cm^{-1}, 6640 cm^{-1} and 6798 cm^{-1} are due to the combination of symmetric asymmetric N-H. At 6135 cm^{-1} weak but sharp bands declare the existence of bond with halogen (X).

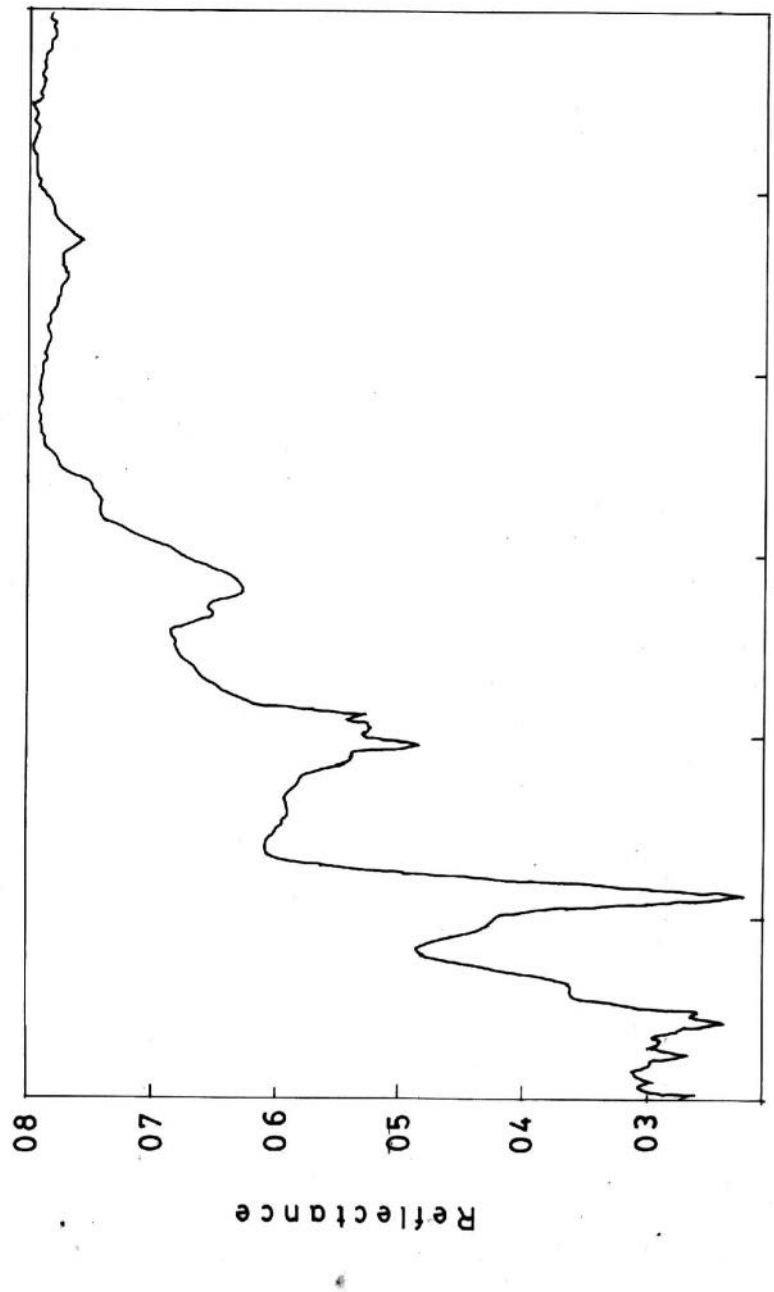

Fig 6.1.20 Near-Infrared spectrum of Zn(II)-Ciprofloxacin compound .

Table 6.1.17 Assignment for NIR bands of Zn(II)-Ciprofloxacin Compound.

Wave no. (cm^{-1})	Spectra structure	Material type
4300	C-H, ($-CH_3$)	Hydrocarbon
4360	Ar.C-H	Aromatic C-H
4410	O-H & C-H	Combination
4520	N-H, C-N & C=O	Combination
5140	C=O, (C=OOH)	Acid, carboxylic
5975	-X	Halogenated
6135	C-H	Hydrocarbon
6200	N-H	Symmetric & asymmetric combination
6640	N-H	Symmetric & asymmetric combination
6798	N-H	Symmetric & asymmetric combination
7310	C-H, ($-CH_3$)	Hydrocarbon
8705	Ar.C-H	Aromatic C-H

6.1.3 Physical Properties

6.1.3.1 Solubility

Solubility is the property of a solid, liquid or gaseous chemical substance called solute to dissolve in a solid, liquid or gaseous solvent to form a homogeneous solution of the solute in the solvent. According to an IUPAC definition, solubility is the analytical composition of a saturated solution expressed as a proportion of a designated solute in a designated solvent.

The solubility of a substance fundamentally depends on the used solvents as well as on temperature and pressure. The extent of the solubility of a substance in a specific solvent is measured as the saturation concentration, where adding more solute does not increase the concentration of the solution. Most often, the solvent is a liquid, which can be a pure substance or a mixture.

The extent of solubility ranges widely, from infinitely soluble (fully miscible) such as ethanol in water, to poorly soluble, such as silver chloride in water. The term insoluble is often applied to poorly or very poorly soluble compounds.

The solubility of one substance in another is determined by the balance of intermolecular forces between the solvent and solute, and the entropy change that accompanies the salvation. Factors such as temperature and pressure will alter this balance, thus changing the solubility.

Solubility may also strongly depend on the presence of other species dissolved in the solvent, for example, complex forming anions (ligands) in liquids. Solubility will also depend on the excess or deficiency of a common ion in the solution, a phenomenon known as the common ion effect. To a lesser extent, solubility will depend on the ionic strength of solutions. The last two effects can be quantified using the equation for solubility equilibrium.

The solubility of the Metal-Ciprofloxacin compounds were investigated qualitatively at room temperature using some common organic solvents and water. And the findings are tabulated below:

Table 6.1.18 Solubility of Metal-Ciprofloxacin compounds in some common organic solvents.

Compounds	Water		Organic Solvents			
	Normal	Hot	DMF	DMSO	Methanol	Acetonitrile
Cr(III)-Cipro	Soluble	Soluble	Slightly soluble	Very Slightly soluble	Slightly soluble	Insoluble
Mn(II)-Cipro	Soluble	Soluble	Very Slightly soluble	Very Slightly soluble	Soluble	Insoluble
Ni(II)-Cipro	Slightly soluble	Soluble	Soluble	Insoluble	Soluble	Insoluble
Cu(II)-Cipro	Very slightly soluble	Slightly soluble	Insoluble	Slightly soluble	Insoluble	Insoluble
Zn(II)-Cipro	Slightly soluble	Soluble	Soluble	Very Slightly soluble	Insoluble	Insoluble

The above findings show that Cr(III)-Ciprofloxacin compound is slightly soluble in methanol and DMF and very slightly soluble in DMSO. It is insoluble in acetonitrile but soluble in water in bot condition (normal and cold water). Mn(II)-Ciprofloxacin compound is soluble in water as well as methanol and insoluble in acetonitrile. But it is very slightly soluble in DMSO and DMF. Ni(II)-Ciprofloxacin compound is soluble in hot water, DMF and methanol. And insoluble in DMSO and Acetonitrile. Cu(II)-

Ciprofloxacin compound is almost insoluble (slightly soluble in DMSO) in some common organic solvents. Similar is the case in water. It is slightly soluble in hot water. Zn(II)-Ciprofloxacin compound is soluble in hot water and DMF. It is very slightly soluble in DMSO, whereas insoluble in methanol and acetonitrile.

6.1.3.2 Melting Point

The melting of a solid is a temperature at which it changes state from solid to liquid.

At the melting point the solid and liquid exist in equilibrium. The melting point of a substance depends (usually slightly) on pressure and is usually specified at standard pressure. Melting generally occurs over a temperature range, which is termed as melting range.

The melting range of a pure solid organic is the temperature range at which the solid is in equilibrium with its liquid. As heat is added to a solid, the solid eventually changes to a liquid. This occurs as molecules acquire enough energy to overcome the intermolecular forces previously binding them together in an orderly crystalline lattice. Melting does not occur instantaneously, because molecules must absorb the energy and then physically break the binding forces. Typically the outside of a crystal will melt faster than the inside, because it takes time for heat to penetrate. The melting range of a compound is one of the characteristic properties of a pure solid. The melting range is defined as the span of temperature from the point at which the crystals first begin to liquefy to the point at which the entire sample is liquid. Most pure organics melt over a narrow temperature range of 1-2ºC, if heated slowly enough. The molecular compounds (mostly of covalent nature) melt at relatively low temperature, in contrast with the ionic compounds having high melting points. Impure samples will normally have melting ranges that are both larger (>1ºC) and begin lower. A list of the melting ranges found from the observation of the Metal-Ciprofloxacin compounds in the following study is tabulated below.

Table 6.1.19 Melting ranges for the Metal-Ciprofloxacin compoundss.

Compound	Melting Point
Cr(III)-Ciprofloxacin	315-318
Mn(II)-Ciprofloxacin	316-328
Ni(II)-Ciprofloxacin	330-338
Cu(II)-Ciprofloxacin	238-242
Zn(II)-Ciprofloxacin	306-312

The melting range data shows that all of these compounds are unstable and decomposes at temperatures before melting.

6.1.3.3 Conductivity measurement

A solution will conduct electricity if it contains ions that are free to move. The ionic solids posses that property when they are in solution. These solids are called electrolytes and the power of electrolytes to conduct electrical current is termed as conductivity. On the other hand, most of the covalent and co-ordinate compounds are bad conductors of electricity, since they do not contain charge particles (i.e. ions) or electrons to carry the current. Thus whether a compound is completely ionic, covalent/coordinate or possesses some ionic character, may be known from the conductivity measurement in solution.

Specific conductivity is the reciprocal of the specific resistance of a solution measured between two electrodes 1 cm^2 in area and 1 cm apart. Conductivity is thus measured by placing two electrodes (with opposite electrical charge) in the water. For a known electrical current, the voltage drop across the electrodes reveals the water's resistance. Since the resistance of aqueous solution changes with temperature (resistance drops with increasing temperature), the resistance is corrected to the resistance of the solution at 25 ºC.

Molar conductivity is defined as the conductivity of an electrolyte solution divided by the molar concentration of the electrolyte, and so measures the efficiency with which a given electrolyte conducts electricity in solution. Its units are siemens per meter per molarity, or siemens meter-squared per mole. The usual symbol is a Capital lambda, Λ, or Λ_m.

From the definition molar conductance is given by

$$\Lambda_m = \frac{\kappa \times 1000}{M}$$

Where κ is the measured conductivity and M is the number of moles of the electrolyte present in 1000 cm^3 of the solution. The experimental results for specific conductance are listed in Tables 6.1.20 to 6.1.24.

The Tables show that the specific conductance for the compounds are higher than that of the solvent (de-ionized water). It is found that in all the cases, specific conductance decreases with decreasing concentration.

Figures 6.1.21 to 6.1.25 show the relationship between molar conductance and the square root of concentration. It is found that with increasing concentration, molar conductance decreases for all the Metal-Ciprofloxacin compounds. Therefore it can be concluded that these compounds are weak electrolytes.

Table 6.1.20. Specific conductances of the Cr(III)-Ciprofloxacin compound.

Molar concentration (M)	√(Molarity) x 10^3	Specific Conductance	Molar Conductance
6.10 x 10^{-5}	7.81	24.19	396.56
5.49 x 10^{-5}	7.41	22.59	411.48
4.88 x 10^{-5}	6.99	20.29	415.48
4.27 x 10^{-5}	6.53	18.59	435.36
3.66 x 10^{-5}	6.05	16.89	461.48
3.05 x 10^{-5}	5.52	13.73	450.16
2.44 x 10^{-5}	4.94	11.79	483.20
1.83 x 10^{-5}	4.28	10.05	549.18
1.22 x 10^{-5}	3.49	6.83	559.84
6.10 x 10^{-6}	2.47	4.77	781.97

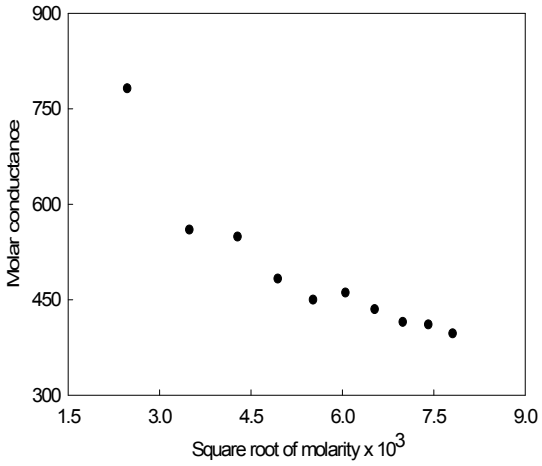

Fig 6.1.21 Variation of molar conductance with square root of molarity in case of Cr(III)-Ciprofloxacin compound.

Table 6.1.21. Specific conductances of the Mn(II)-Ciprofloxacin compound.

Molar concentration (M)	√(Molarity) x 10^3	Specific Conductance	Molar Conductance
4.17 x 10^{-4}	20.42	44.79	107.71
3.75 x 10^{-4}	19.37	43.20	115.20
3.34 x 10^{-4}	18.28	40.49	121.23
2.92 x 10^{-4}	17.09	37.29	127.41
2.50 x 10^{-4}	15.81	35.29	141.16
2.09 x 10^{-4}	14.46	32.59	155.43
1.67 x 10^{-4}	12.92	27.99	167.60
1.25 x 10^{-4}	11.18	22.27	178.16
8.34 x 10^{-5}	9.13	15.74	188.43
4.17 x 10^{-5}	6.46	7.93	190.17

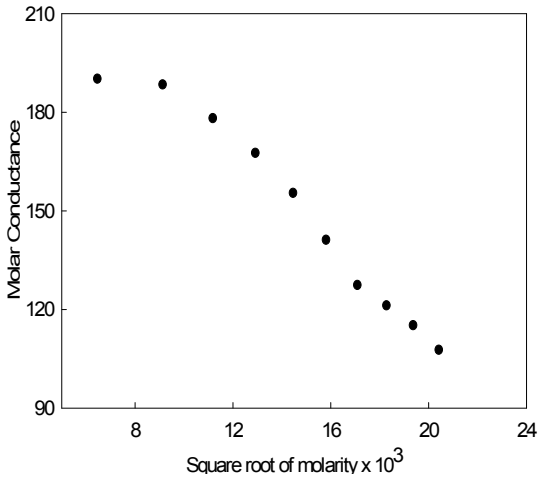

Fig 6.1.22 Variation of molar conductance with square root of molarity in case of Mn(II)-Ciprofloxacin compound.

Table 6.1.22. Specific conductances of the Ni(II)-Ciprofloxacin compound.

Molar concentration (M)	√(Molarity) x 10^3	Specific Conductance	Molar Conductance
3.90 x 10^{-4}	19.75	53.59	137.41
3.51 x 10^{-4}	18.73	50.89	147.99
3.12 x 10^{-4}	17.66	48.19	154.46
2.73 x 10^{-4}	16.52	42.59	156.01
2.34 x 10^{-4}	15.30	37.29	159.36
1.95 x 10^{-4}	13.96	32.60	167.18
1.56 x 10^{-4}	12.49	28.19	180.41
1.17 x 10^{-4}	10.82	22.79	194.79
7.80 x 10^{-5}	8.83	18.56	237.95
3.90 x 10^{-5}	6.24	12.12	310.47

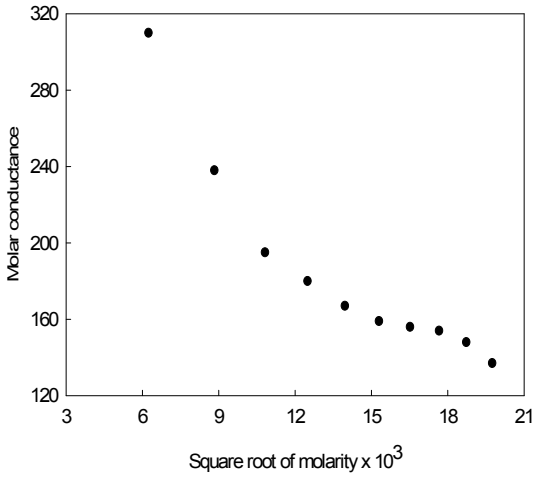

Fig 6.1.23 Variation of molar conductance with square root of molarity in case of Ni(II)-Ciprofloxacin compound.

Table 6.1.23. Specific conductances of the Cu(II)-Ciprofloxacin compound.

Molar concentration (M)	√(Molarity) x 10^3	Specific Conductance	Molar Conductance
1.08 x 10^{-4}	10.39	24.09	230.06
9.72 x 10^{-5}	9.86	23.61	242.90
8.64 x 10^{-5}	9.30	21.10	244.21
7.56 x 10^{-5}	8.69	19.09	252.51
6.48 x 10^{-5}	8.05	17.64	272.22
5.40 x 10^{-5}	7.35	14.87	275.37
4.32 x 10^{-5}	6.57	12.67	293.29
3.24 x 10^{-5}	5.69	9.76	301.23
2.16 x 10^{-5}	4.65	6.60	305.56
1.08 x 10^{-6}	1.04	3.66	338.89

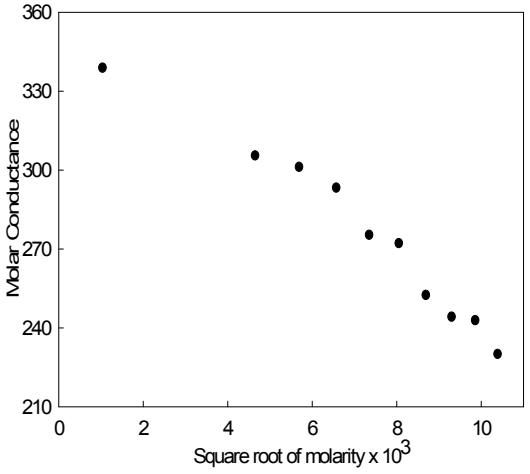

Fig 6.1.24 Variation of molar conductance with square root of molarity in case of Cu(II)-Ciprofloxacin compound.

Table 6.1.24 Specific conductances of the Zn(II)-Ciprofloxacin compound.

Molar concentration (M)	√(Molarity) x 10^3	Specific Conductance	Molar Conductance
4.61 x 10^{-4}	21.47	69.49	150.44
4.15 x 10^{-4}	20.37	67.19	161.90
3.69 x 10^{-4}	19.21	60.69	164.77
3.22 x 10^{-4}	17.94	55.99	173.88
2.77 x 10^{-4}	16.64	48.49	175.05
2.31 x 10^{-4}	15.20	41.09	177.88
1.84 x 10^{-4}	13.56	33.59	182.55
1.38 x 10^{-4}	11.75	25.69	186.16
9.22 x 10^{-5}	9.60	18.06	195.88
4.61 x 10^{-5}	6.79	14.30	210.60

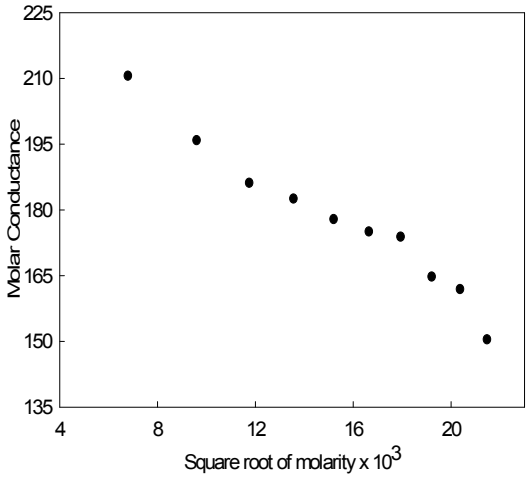

Fig 6.1.25 Variation of molar conductance with square root of molarity in case of Zn(II)-Ciprofloxacin compound.

As is evident from the literature, that when treated with water, all of these compounds are dissociated and the metal ions converted into hydrated ions represented by the general formula $[M(H_2O)_6]^{2+}$. Thus the Metal-Ciprofloxacin compounds are conductors of electricity in aqueous solution because both $[M(H_2O)_6]^{2+}$ and Ciprofloxacin ions have that power[110].

6.1.4 Differential scanning calorimetric (DSC) analysis

Differential scanning calorimetry or DSC is a thermoanalytical technique in which the difference in the amount of heat required to increase the temperature of a sample and reference is measured as a function of temperature. Both the sample and reference are

maintained at nearly the same temperature throughout the experiment. Generally, the temperature program for a DSC analysis is designed such that the sample holder temperature increases linearly as a function of time. The reference sample should have a well-defined heat capacity over the range of temperatures to be scanned.

The technique was developed by E.S. Watson and M.J. O'Neill in 1962, and introduced commercially at the 1963 Pittsburgh Conference on Analytical Chemistry and Applied Spectroscopy. The first adiabatic differential scanning calorimeter that could be used in biochemistry was developed by P.L. Privalov and D.R. Monaselidze in 1964. The term DSC was coined to describe this instrument which measures energy directly and allows precise measurements of heat capacity.

Detection of phase transitions : The basic principle underlying this technique is that

when the sample undergoes a physical transformation such as phase transitions, more or less heat will need to flow to it than the reference to maintain both at the same temperature. Whether less or more heat must flow to the sample depends on whether the process is exothermic or endothermic. For example, as a solid sample melts to a liquid it will require more heat flowing to the sample to increase its temperature at the same rate as the reference. This is due to the absorption of heat by the sample as it undergoes the endothermic phase transition from solid to liquid. Likewise, as the sample undergoes exothermic processes (such as crystallization) less heat is required to raise the sample temperature. By observing the difference in heat flow between the sample and reference, differential scanning calorimeters are able to measure the amount of heat absorbed or released during such transitions. DSC may also be used to observe more subtle physical changes, such as glass transitions. It is widely used in industrial settings as a quality control instrument due to its applicability in evaluating sample purity and for studying polymer curing[111] .

An alternative technique, which shares much in common with DSC, is differential thermal analysis (DTA). In this technique it is the heat flow to the sample and reference that remains the same rather than the temperature. When the sample and reference are heated identically phase changes and other thermal processes cause a difference in temperature between the sample and reference. Both DSC and DTA provide the same information; DSC is the more widely used of the two techniques.

DSC Instrumentation: A typical differential scanning calorimeter consists of two sealed pans: a sample pan and a reference pan (which is generally an empty sample pan). These pans are often covered by or composed of aluminum, which acts as a radiation shield. The two pans are heated, or cooled, uniformly while the heat flow difference between the two is monitored. This can be done at a constant temperature (isothermally), but is more commonly done by changing the temperature at a constant rate, a mode of operation that is also called temperature scanning.

During the experiment, the instrument detects differences in the heat flow between the sample and reference. This information is sent to an output device, most often a computer, and results in a plot of the differential heat flow between the reference and sample cell as a function of temperature. When there are no thermodynamic chemical processes occurring the heat flow difference between the sample and reference varies only slightly with temperature, and shows up as a flat, or very shallow base line on the plot. However, an exothermic or endothermic process within the sample results in a significant deviation in the difference between the two heat flows. The result is a peak in the DSC curve. Generally, the differential heat flow is calculated by subtracting the sample heat flow from the reference heat flow. When following this convention, exothermic processes will show up as positive peaks (above the baseline) while peaks resulting from endothermic processes are negative (below the baseline).

The sample (in a condensed form such as powder, liquid, or crystal) is generally placed in an aluminum sample pan, which is then placed in the sample cell. The reference consists of a matched empty aluminum sample pan that is placed in the reference cell of the instrument. The sample pans are designed to have a very high thermal conductivity. Sample sizes generally range from 0.1 to 100 mg. The instrument cells are often airtight in order to shield the sample and reference from external thermal perturbations. This also allows experiments to be performed under variable pressures and atmospheres.

Types of DSC:There are two main types of differential scanning calorimeters: heat flux DSC and power compensation DSC.

i) Heat Flux DSC: In a heat flux calorimeter, heat is transferred to the sample and reference through a disk made of the alloy constantan. The heat transported to the

sample and reference is controlled while the instrument monitors the temperature difference between the two. In addition to its function in the heat transfer, this disk serves as part of the temperature-sensing unit. The sample and reference reside on raised platforms on the disk. Under each of these platforms there is a chromel (chromel is an alloy containing chromium, nickel and sometimes iron) wafer. The junction between these two alloys forms a chromel-constantan thermocouple. The signal from these sensors is the used to measure the differential heat flow. The temperature is typically monitored by chromel-alumel thermocouples attached beneath the chromel wafers.

ii) Power Compensated DSC: In power compensated calorimeters, separate heaters are used for the sample and reference. This is the classic DSC design. Both the sample and reference are maintained at the same temperature while monitoring the electrical power used by their heaters. The heating elements are kept very small (weighing about 1 gram) in order to ensure that heating, cooling, and thermal equilibration can occur as quickly as possible. The sample and reference are located above their respective heaters, and the temperatures are monitored using electronic temperature sensors located just beneath the samples. Generally platinum resistance thermometers are used due to the high melting point of platinum.

Electronically, the instruments consist of two temperature control circuits. An average temperature control circuit is used to monitor the progress of the temperature control program. This circuit is designed to assure that the temperature scanning program set by the operator is the average temperature of the sample and reference. A differential temperature control circuit is used to determine the relative temperatures of the sample and reference, and adjust the power going to the respective heaters in such a way as to maintain both at the same temperature. The output of the differential temperature control circuit is used to generate the DSC curve.

DSC curves: The result of a DSC experiment is a curve of heat flux versus temperature or versus time. There are two different conventions: exothermic reactions in the sample shown with a positive or negative peak, depending on the kind of technology used in the experiment. This curve can be used to calculate enthalpies of transitions. This is done by integrating the peak corresponding to a given transition. It

can be shown that the enthalpy of transition can be expressed using the following equation:

$$\Delta H = KA$$

where ΔH is the enthalpy of transition, K is the calorimetric constant, and A is the area under the curve. The calorimetric constant will vary from instrument to instrument, and can be determined by analyzing a well-characterized sample with known enthalpies of transition.

Applications : Differential scanning calorimetry can be used to measure a number of characteristic parameters of a sample. Using this technique it is possible to observe fusion and crystallization events as well as glass transition temperatures (T_g). In addition to these applications DSC can be used to study oxidation as well as other chemical reactions. [111]

Glass transitions occur as the temperature of an amorphous solid is increased. A glass transition is characterized by a decrease in viscosity. These transitions appear as a step in the baseline of the recorded DSC signal. This is due to the sample undergoing a change in heat capacity, but no formal phase change occurs. [111]

As the temperature increases, an amorphous solid will become less viscous. At some point the molecules will obtain enough freedom of motion to spontaneously arrange themselves into a crystalline form. This is known as the crystallization temperature (T_c). This transition from amorphous solid to crystalline solid is an exothermic process, and results in a peak in the DSC signal. As the temperature increases the sample eventually reaches its melting temperature (T_m). The melting process results in an endothermic peak in the DSC curve. The ability to ascertain transition temperatures and enthalpies makes DSC an invaluable tool in producing phase diagrams for various chemical systems.

DSC may also be used in the study of liquid crystals. As matter transitions between solid and liquid it often goes through a third state, which displays properties of both phases. This anisotropic liquid is known as a liquid crystalline or mesomorphous state. Using DSC, it is possible to observe the small energy changes that occur as

matter transitions from a solid to a liquid crystal and from a liquid crystal to an isotropic liquid.

Using differential scanning calorimetry to study the oxidative stability of samples generally requires an airtight sample chamber. Usually, such tests are done isothermally (at constant temperature) by changing the atmosphere of the sample. First, the sample is brought to the desired test temperature under an inert atmosphere, usually nitrogen. Then, oxygen is added to the system. Any oxidation that occurs is observed as a deviation in the baseline. Such analyses can be used to determine the stability and optimum storage conditions for a compound.

DSC is widely used in the pharmaceutical and polymer industries. For the polymer chemist, DSC is a handy tool for studying curing processes, which allows the fine tuning of polymer properties. The cross-linking of polymer molecules that occurs in the curing process is exothermic, resulting in a positive peak in the DSC curve that usually appears soon after the glass transition[111].

In the pharmaceutical industry it is necessary to have well-characterized drug compounds in order to define processing parameters. For instance, if it is necessary to deliver a drug in the amorphous form, it is desirable to process the drug at temperatures below those at which crystallization can occur.

DSC curves may also be used to evaluate drug and polymer purities. This is possible because the temperature range over which a mixture of compounds melts is dependent on their relative amounts. This is effect is due to a phenomenon known as freezing point depression, which occurs when a foreign solute is added to a solution. (Freezing point depression is what allows salt to de-ice sidewalks and antifreeze to keep your car running in the winter.) Consequently, less pure compounds will exhibit a broadened melting peak that begins at lower temperature than a pure compound.

6.1.5 DSC curves of Ciprofloxacin and its compounds

In the present study, melting curve for the Metal-Ciprofloxacin compounds were obtained by differential scanning calorimetric study.

Cr(III)-Ciprofloxacin compound: Stresses were built into the compound as a result of thermal history are released when it is heated through its glass transition. The

reason this occurs at Tg is that the molecule goes from a rigid to a flexible structure and thus can move to relieve the stress as well as undergo volatilization of the volatile parts and the minor components. It is found at 162.62 ˚C with an enthalpy change of ΔH = 154.8483J/g. This is also interpreted as softening or decomposition point. Molecular relaxation usually appears as a weak endothermic transition near the end of a glass transition. This behavior can be pronounced enough to either shift the measured glass transition temperature several degrees or lead to misinterpretation of the Tg as an endothermic melting peak. Then relieve the internal stresses in the material by heating it to at least 25˚C above the Tg and then quench cooling it to a temperature below the Tg. After curing at 162.62 ˚C and then quench cooling to 25˚C. Heating the material above the Tg and then cooling it through the Tg at a rate which is equal to, or greater than, the final heating rate during evaluation also reduces the relaxation effect. Again the curve shows a sharper peak at 316.61 ˚C with an enthalpy change of ΔH = 71.8141 J/g and is located at higher temperature, indicating a small melting range. Actually it is the melting point of the compound. In addition to that finally it shows exothermic peaks.

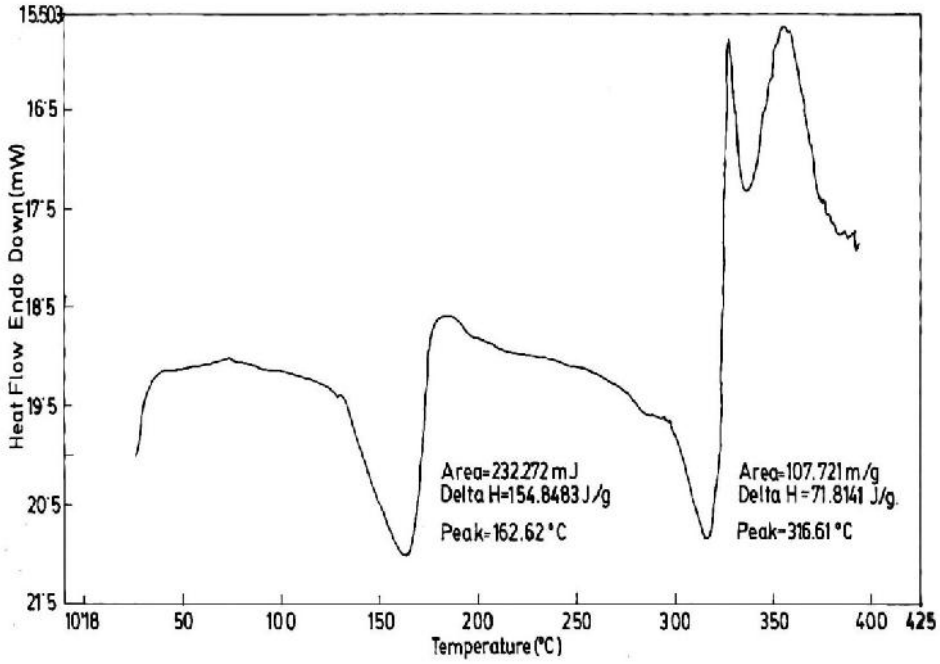

Fig 6.1.26 Differential scanning calorigram for Cr(III)-Ciprofloxacin compound.

Mn(II)-Ciprofloxacin compound: Mn(II)-Ciprofloxacin compound shows a little bit different character. When it is heated through its glass transition, it shows a weak endothermic response at about 75˚C, which may be due to the presence of more minor components . The molecule goes from a rigid to a flexible structure and thus can move to relieve the stress as well as undergo volatilization of the volatile parts components. It is found at 158.21˚C with an enthalpy change of ΔH = 175.9112J/g. This is also interpreted as softening or decomposition point. The relaxation usually appears as a weak endothermic transition near the end of a glass transition. This behavior can be pronounced enough to lead to misinterpretation of the Tg as an endothermic melting peak. Again relieve the internal stresses in the material by heating it to at least 25˚C above the Tg and then quench cooling it to a temperature below the Tg. Heating the material above the Tg and then cooling it through the Tg at a rate which is equal to, or greater than, the final heating rate during evaluation also reduces the relaxation effect. This curve also shows a sharper peak at 316.69 ˚C with an enthalpy change of ΔH = 138.5780 J/g and is located at higher temperature, which indicates a small melting range. Actually it is the melting point of the compound. It also shows exothermic peaks at the end .

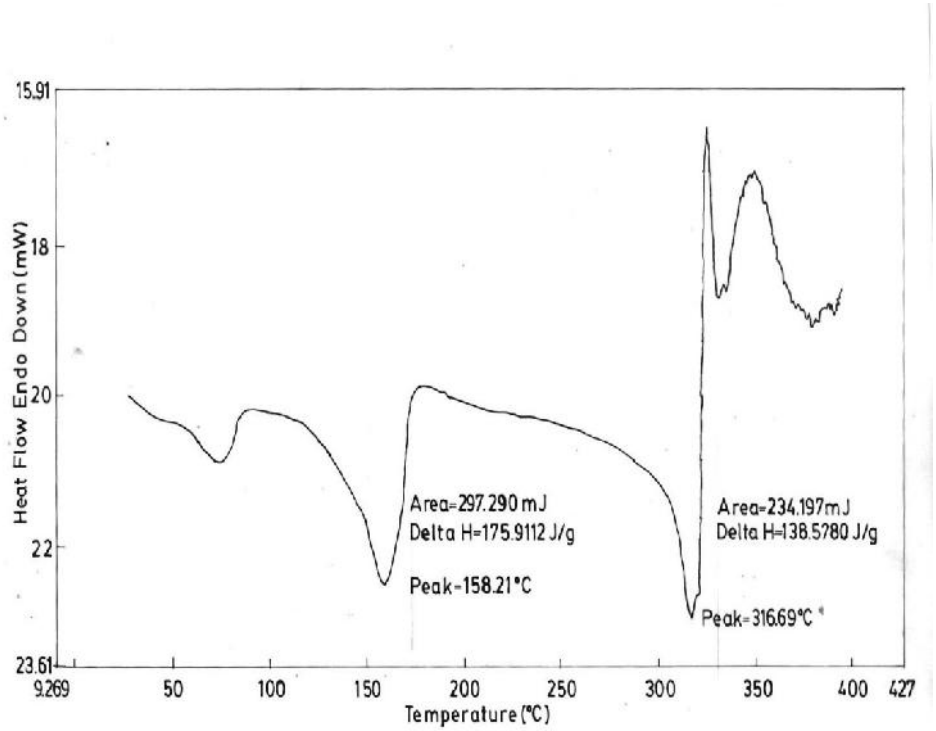

Fig 6.1.27 Differential scanning calorigram for Mn(II)-Ciprofloxacin compound.

Ni(II)-Ciprofloxacin compound: This compond shows a weak endothermic peak at 164.92˚C with an enthalpy change of ΔH = 174.5800 J/g. This indicates that the molecule goes from a rigid to a flexible structure and thus can move to relieve the stress as well as undergo volatilization of the volatile parts and the minor components. This is also interpreted as softening or decomposition point. Molecular relaxation usually appears as a weak endothermic transition near the end of a glass transition. This behavior can be pronounced enough to either shift the measured glass transition temperature several degrees or lead to misinterpretation of the Tg as an endothermic melting peak. After curing at 164.92 ˚C and then quench cooling to 25˚C, the final heating rate during evaluation also reduces the relaxation effect. Again the curve shows a sharper peak at 323.31 ˚C with an enthalpy change of ΔH = 153.4289 J/g and is located at higher temperature, indicating a small melting range, which is actually the melting point of the compound.

Cu(II)-Ciprofloxacin compound: Cu(II)-ciprofloxacin compound shows a very weak endothermic response at 103.19˚C with an enthalpy change of ΔH = 307.8980 J/g. This means that the molecule goes from a rigid to a flexible structure as well as undergo volatilization of

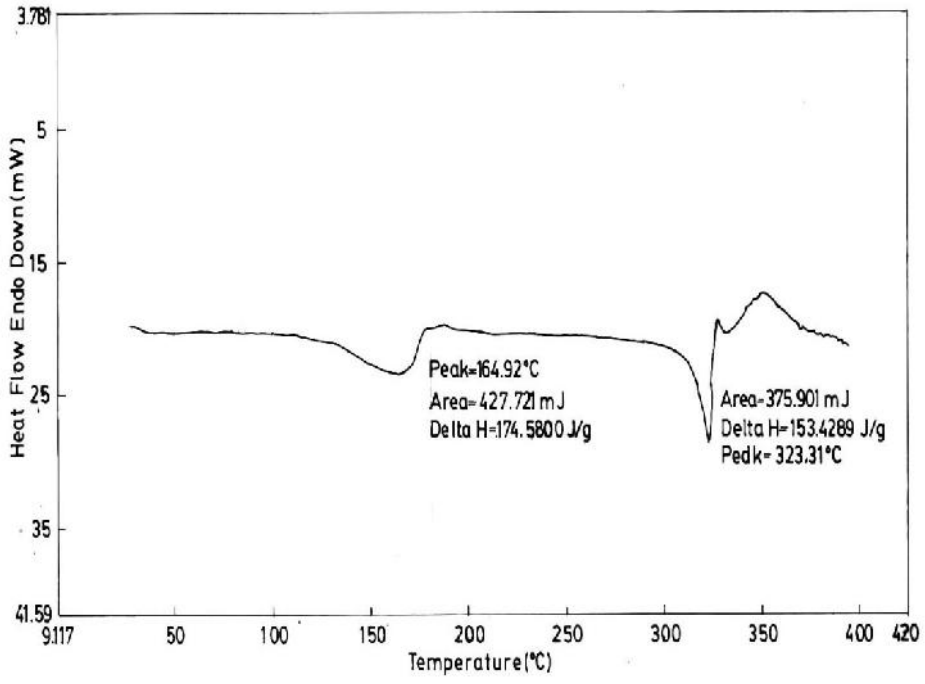

Fig 6.1.28 Differential scanning calorigram for Ni(II)-Ciprofloxacin compound.

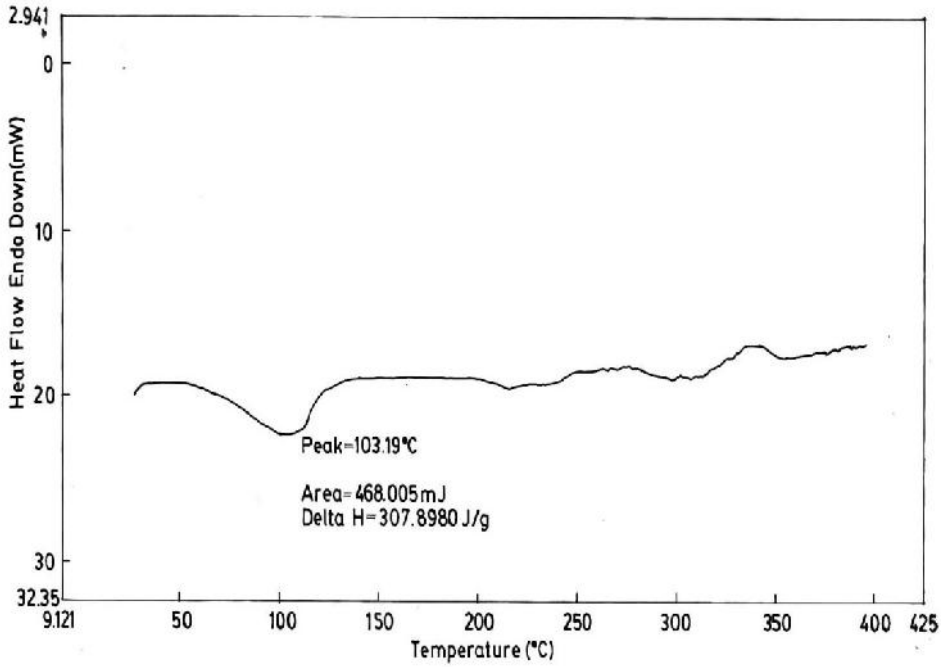

Fig 6.1.29 Differential scanning calorigram for Cu(II)-Ciprofloxacin compound.

the volatile parts and most of the minor components. This is also interpreted as softening or decomposition point. Then after curing it again shows avery weak endothermic response at about 230 ˚C, which is actually the melting point of the compound.

Zn(II)-Ciprofloxacin compound: When a compound is heated through its glass transition, the molecule goes from a rigid to a flexible structure and thus can move to relieve the stress as well as undergo volatilization of the volatile parts and the minor components. For this compound, it is found at 87.70˚C with an enthalpy change of ΔH = 147.8033 J/g. This is also interpreted as softening or decomposition point. Molecular relaxation usually appears as a weak endothermic transition near the end of a glass transition. Then relieve the internal stresses in the material by heating it to at least 25˚C above the Tg and then quench cooling it to a temperature below the Tg. After curing at 87.70˚C and then quench cooling to 25˚C. Heating the material above the Tg and then cooling it through the Tg at a rate which is equal to, or greater than, the final heating rate during evaluation also reduces the relaxation effect. Again the curve shows another weak endothermic response at 305.93˚C with an enthalpy change

of ΔH = 107.8322 J/g and is located at higher temperature, indicating the melting range. In addition to that finally it shows a very weak exothermic response.

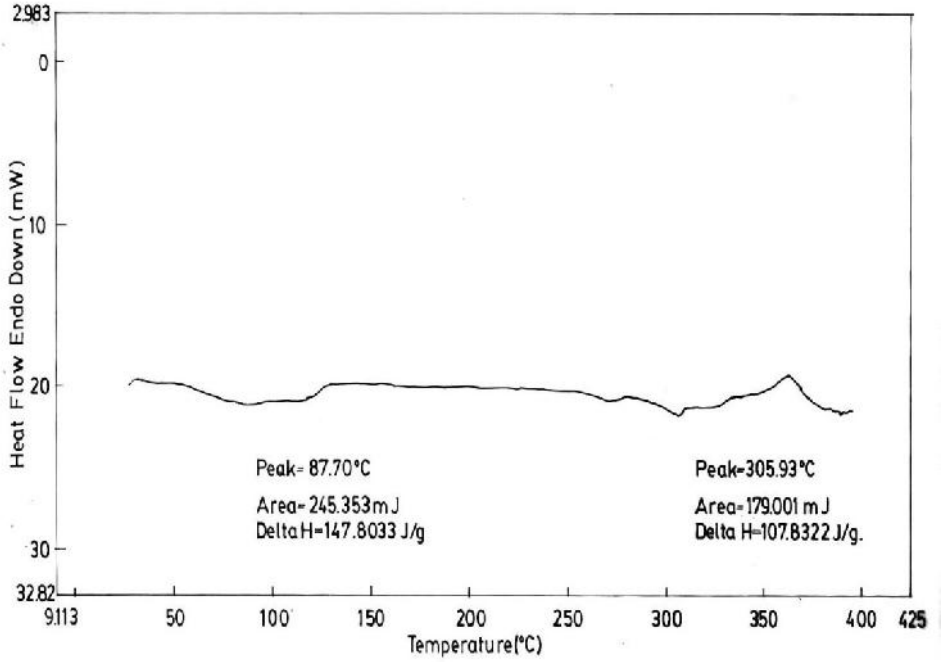

Fig 6.1.30 Differential scanning calorigram for Zn(II)-Ciprofloxacin compound.

`

6.2 Electrochemical Studies of the Metal-Ciprofloxacin Compounds

Cyclic voltammetry : Cyclic voltammetric experiment is performed to study the redox behavior of the metals in the Metal-Ciprofloxacin compounds. In the present study, at first the redox behavior of Cu(II), Mn(II) and Zn(II)-Ciprofloxacin compounds was analyzed using 0.1 N potassium chloride (KCl) as supporting electrolyte. This set of experiment was done using Glassy carbon electrode (GCE) as working electrode. Then another set of analysis was done for Cr(III)-Ciprofloxacin compound using saturated potassium chloride (KCl) as supporting electrolyte. This was accomplished using Platinum (Pt) electrode as supporting electrolyte. In all the cases Ag/AgCl (Saturated KCl) electrode was used as reference electrode and a Pt wire was used as counter electrode.

After the completion of cyclic voltammetric characterization of Metal-Ciprofloxacin compounds, their concentration effects were also studied. These studies were also done using the above environment and set up.

The studies were done using different potential windows, as potential range depends on the electrode material, the solvent, the supporting electrolyte and the acidity of the solution.

The potential windows were from -1.800 V to 2.000 V for Cu(II)-Ciprofloxacin compound, -1.500 V to 2.000 V for Mn(II)-Ciprofloxacin compound and -1.500 V to 2.000 V for Zn(II)-Ciprofloxacin compound in 0.1 M potassium chloride at Glassy carbon electrode (GCE). In addition to this the potential window was found to be from -1.000 V to 1.700 V for Cr(III)-Ciprofloxacin compound in saturated potassium chloride at Platinum electrode. Same potential windows were employed for the observation of concentration effect.

The above mentioned all the observations were found at room temperature. Scan rate variation for all the systems were also examined. Each system was analyzed at six different scan rates, which were 0.050 Vs^{-1}, 0.100 Vs^{-1}, 0.150 Vs^{-1}, 0.200 Vs^{-1}, 0.250 Vs^{-1} and 0.300 Vs^{-1}.

Chronoamperometry and chronocoulometry : In the field of electrochemistry, chronoamperometry as well as chronocoulometry has achieved their importance in characterizing the rate of electrolysis and adsorption criteria of a system. These experiments are a potential step applied suddenly to an electrode. The response of the ensuring electrode reaction is a current decay with time; in chronoamperometry this current-time curve is the measured response. In chronocoulometry one measures the integral of the current time response, as a charge-time curve. Because of the basic similarity of the two methods, they are considered together.

In the present study, at first the redox behavior of Cu(II), Mn(II) and Zn(II)-Ciprofloxacin compounds as well as the concentration effects of the compounds were analyzed using 0.1 N potassium chloride (KCl) as supporting electrolyte by cyclic voltammetric technique. This set of experiment was done using Glassy carbon electrode (GCE) as working electrode. Then another set of analysis was done for Cr(III)-Ciprofloxacin compound as well as the concentration effect using saturated potassium chloride (KCl) as supporting electrolyte. This was accomplished using Platinum (Pt) electrode as supporting electrolyte. In all the cases Ag/AgCl (Saturated KCl) electrode was used as reference electrode and a Pt wire was used as counter electrode. Then with reference to the pair of peaks found, chronoamperometric study was accomplished and the corresponding integrated form, that is the chrococoulometric response is also obtained from it.

6.2.1 Cyclic voltammetric study of Cu(II)-Ciprofloxacin Compound at Glassy Carbon Electrode (GCE).

Redox behavior of Cu(II)-Ciprofloxacin compound

The redox behaviour of Cu(II)-Ciprofloxacin Compound (50.25 ppm solution) in 0.1M potassium chloride and at varying scan rate was studied using cyclic voltammetric technique within the potential window from -1.800 V to 2.000 V at room temperature at glassy carbon electrode (GCE). A CV of the above system at scan rate 0.100 Vs^{-1} is given in Fig 6.2.1.

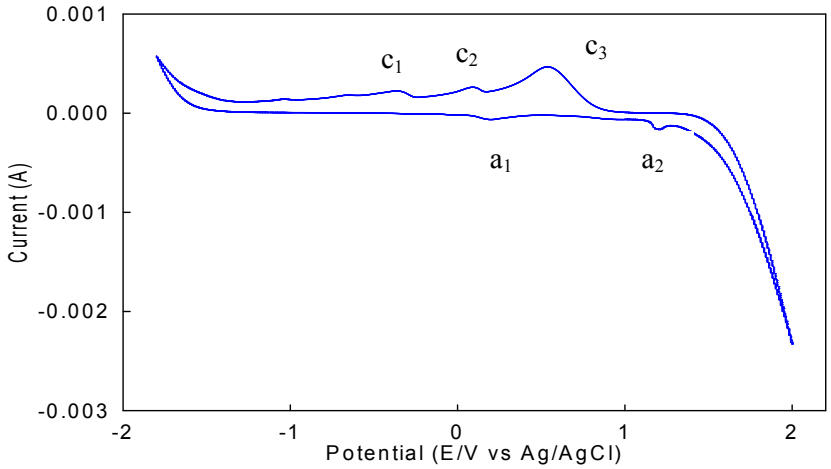

Fig 6.2.1 Cyclic voltammogram of Cu(II)-Ciprofloxacin Compound (50.25 ppm solution) in 0.1 M KCl at scan rate 0.100 Vs^{-1}.

The CV shows three cathodic peaks (c_1, c_2 and c_3) at the potentials of -0.363 V, 0.131 V and 0.731 V and in the anodic region two peaks (a_1 and a_2) at 0.214 V and 1.302 V. The first cathodic may be due to the ligand (Ciprofloxacin) itself and the second as well as the third cathodic peaks may be originated from the parent metal salt (Cu(II)). Compared to the CV of copper together with that of Ciprofloxacin (Figures 6.2.2(a) and (b)), it is found that all the cathodic peaks shift towards more positive potential. Again in the anodic region, the first anodic peak (a_1) represents the first anodic peak of the copper and the second one (a_2) may be a combination of the second anodic peak of copper and the

humplike shape of the ligand in the anodic region. Both the peaks move towards more positive potential compared to the starting materials (Cu(II) and Ciprofloxacin). So, peaks c_2 and a_1 may be considered to be the first pair as well as c_3 and a_2 may be considered to be the second pair reference to the parent metal (Cu(II)). Therefore it may be concluded that after compound formation the number and also the position of the peaks are changed. But in case of Cu(II)-Ciprofloxacin interaction in solution, there are two peaks each in both the cathodic and the anodic regions.

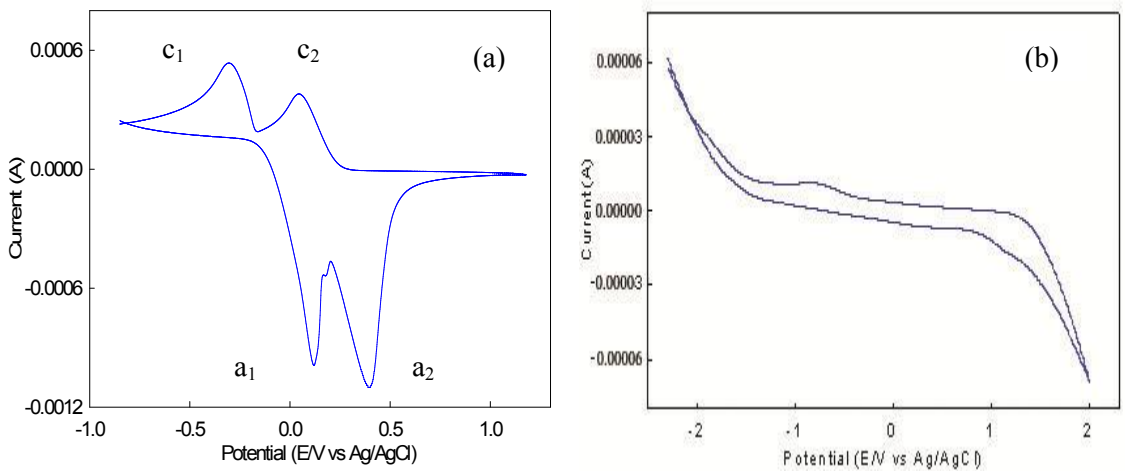

Fig 6.2.2 Cyclic voltammograms of (a) Cu(II) and (b) Ciprofloxacin at scan rate 0.100 Vs^{-1}.

The system was also studied at different scan rates. Scan rate may be defined as the fraction of the potential window analyzed per unit time. The size of the diffusion layer above the electrode surface becomes different depending upon the voltage scan rates used. In a slow voltage scan the diffusion layer grows much further from the electrode in comparison to a fast scan. Therefore, the necessity of scan rate variation is beyond description.

Scan rate variation of Cu(II)-Ciprofloxacin compound is shown in Fig 6.2.3. It shows that with the increase in scan rate the second cathodic peak (c_2) shifts towards less negative potential and the first (c_1) as well as the third (c_3) cathodic peaks moves towards more positive potential. In the anodic region, the first peak (a_1) moves towards more positive

potential upto scan rate 0.200 Vs^{-1} and then the peak disappears. Again the second one (a_2) is absent at scan rate 0.050 Vs^{-1}, appears at scan rate 0.100 Vs^{-1}, then shifts to less positive potential upto scan rate 0.200 Vs^{-1} and then disappears.

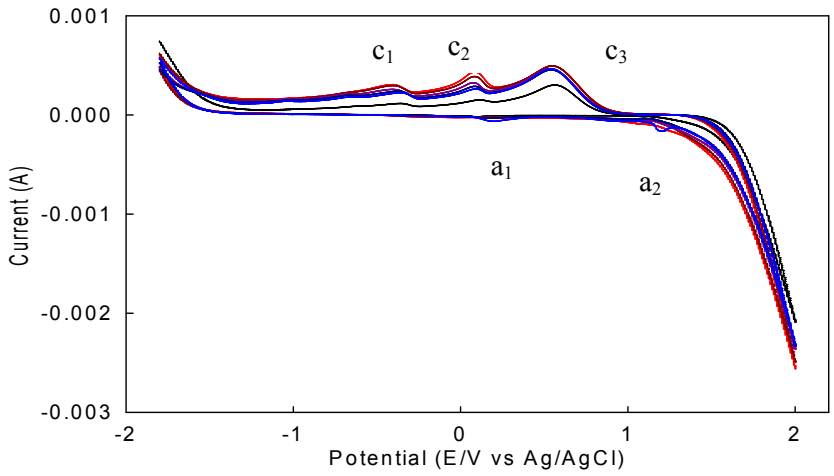

Fig 6.2.3 Cyclic voltammogram of Cu(II)-Ciprofloxacin Complex (50.25 ppm solution) in 0.1 M KCl at different scan rates.

Moreover, with the increase in scan rate, almost all the peaks become broader. Such behavior has been ascribed to slower charge propagation, probably due to difference in salvation and or permeability. Current-potential data for the system under consideration is recorded in Table 6.2.1.

It is evident that after compound formation, the peak separation becomes less for the first pair of peaks but for the second pair the separation becomes more. The peak separation potential for both the first pair of peaks (ΔE_{p1}) increases as well as for the second pair, it (ΔE_{p2}) decreases with the increase in scan rate. The bevaviour is similar to the Cu(II) itself for the first pair but is absolutely opposite behavior in case of second pair. Therefore it may be said that the above system indicate the limitation due to charge transfer kinetics to some extent and simultaneously to some extent does not indicate the limitation due to charge transfer kinetics and are shown in the plot of ΔE_{p1} vs ν and ΔE_{p2} vs ν in Fig 6.2.4(a) and (b).

The peak currents (both in the cathodic and anodic region) increases with increasing scan rate. This can be rationalized by considering the size of the diffusion layer and the time taken to record the scan. The voltammogram takes longer to record as the scan rate is decreased. Therefore, the size of the diffusion layer above the electrode surface becomes

Table 6.2.1 Current-potential data for Cu(II)-Ciprofloxacin compound (50.25 ppm solution) in 0.1 M KCl solution at different scan rates.

Scan rate	SQRT of scan rate	Cathodic peak potential		Anodic peak potential	Cathodic peak current		Anodic peak current	Peak potential separation	Peak current ratio
ν (Vs^1)		E_{pc1} (V) [-]	E_{pc2} (V)	E_{pa1} (V)	i_{pc1} (μA)	i_{pc2} (μA)	i_{pa1} (μA) [-]	ΔE_{p1}= E_{pa1}- E_{pc2} (V)	i_{pa1}/ i_{pc2}
0.050	0.2236	0.341	0.142	0.097	69.22	81.64	60.14	-0.045	0.74
0.100	0.3162	0.363	0.131	0.214	96.11	120.12	105.15	0.083	0.88
0.150	0.3872	0.375	0.125	0.276	103.54	128.53	87.15	0.151	0.68
0.200	0.4472	0.385	0.117	0.292	111.08	152.12	75.25	0.175	0.50
0.250	0.5000	0.389	0.163	-	145.51	175.73	-	-	-
0.300	0.5477	0.399	0.183	-	154.32	181.11	-	-	-
ν (Vs^1)		E_{pc3} (V)		E_{pa2} (V)	i_{pc3} (μA)		i_{pa2} (μA) [-]	ΔE_{p2}= E_{pa2}- E_{pc3} (V)	i_{pa2}/ i_{pc3}
0.050	0.2236	0.744		-	310.84		-	-	-
0.100	0.3162	0.731		1.302	370.25		65.35	0.571	0.18
0.150	0.3872	0.720		1.271	381.41		71.25	0.551	0.19
0.200	0.4472	0.711		1.260	410.33		72.11	0.549	0.18
0.250	0.5000	0.707		-	455.26		-	-	-
0.300	0.5477	0.698		-	466.71		-	-	-

different depending upon the voltage scan rate used. In a slow voltage scan the diffusion layer grows much further from the electrode in comparison to a fast scan. Consequently, the flux to the electrode surface is considerably smaller at slow scan rates than it is at faster rates. As the current is proportional to the flux towards the electrode the magnitude of the current becomes lower at slow scan rates and higher at high scan rates. Again the CV wave shape becomes more irreversible with higher scan rates. This happens because increasing the scan rate is equivalent to increasing the rate of diffusion to the reduced

material from the electrode. As a consequence, the diffusion process competes with the back electron transfer. The general conclusion for this fact is the combination of diffusion and surface control behaviour of the redox system [35, 99].

Again the forward scan peak currents (i_{pc1} and i_{pc2}) are proportional to the square root of the scan rate, which means the system to be diffusion controlled. Diffusion occurs only when a concentration gradient is set up. If the gradient arises from a constant rate of removal of the species across one face of the volume, then this constant flux makes the concentration of the diffusing species vary with distance and time[3]. Moreover with

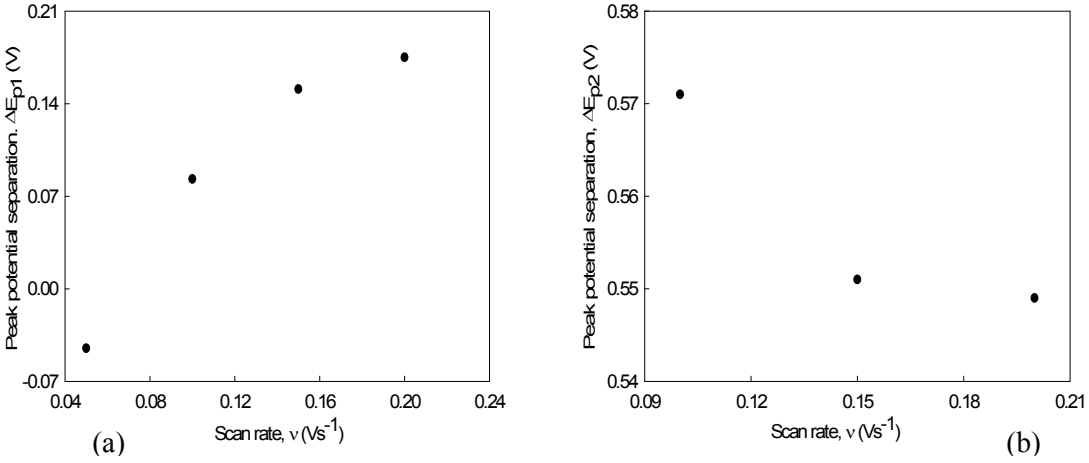

Fig 6.2.4 Variation of peak potential separation with scan rate for Cu(II)-Ciprofloxacin Compound in 0.1M KCl solution (a) first pair (b) second pair of peaks.

increasing $\nu^{1/2}$, the peak currents (Randle-Sevseik plot) for both cathodic and anodic peaks increases linearly (Fig 6.2.5(a) and (b)), giving the conclusion that the processes are adsorptive controlled[35, 99].

The peak current ratio for the first pair of peaks are very much nearest to unity at lower scan rates but at higher scan rates, these are much less. But for the second pair, the peak

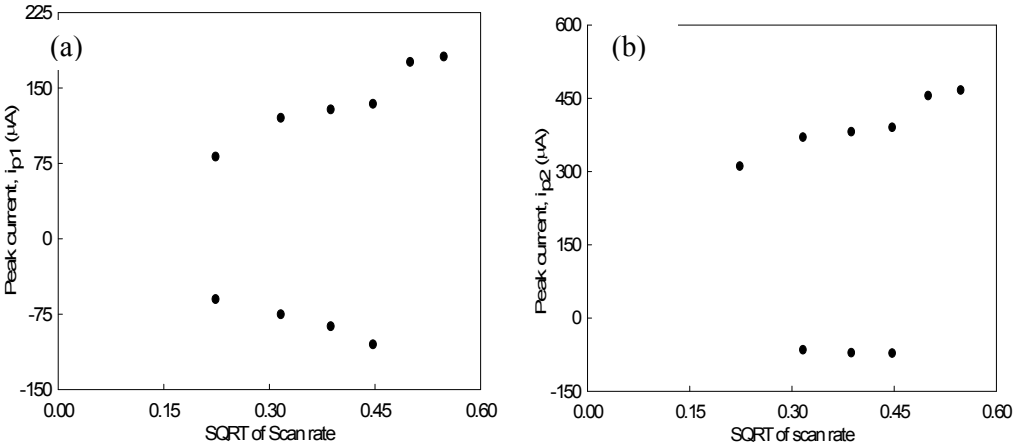

Fig 6.2.5 Variation of peak current withsquare root of scan rate for Cu(II)-Ciprofloxacin Compound in 0.1M KCl solution (a) first pair (b) second pair of peaks.

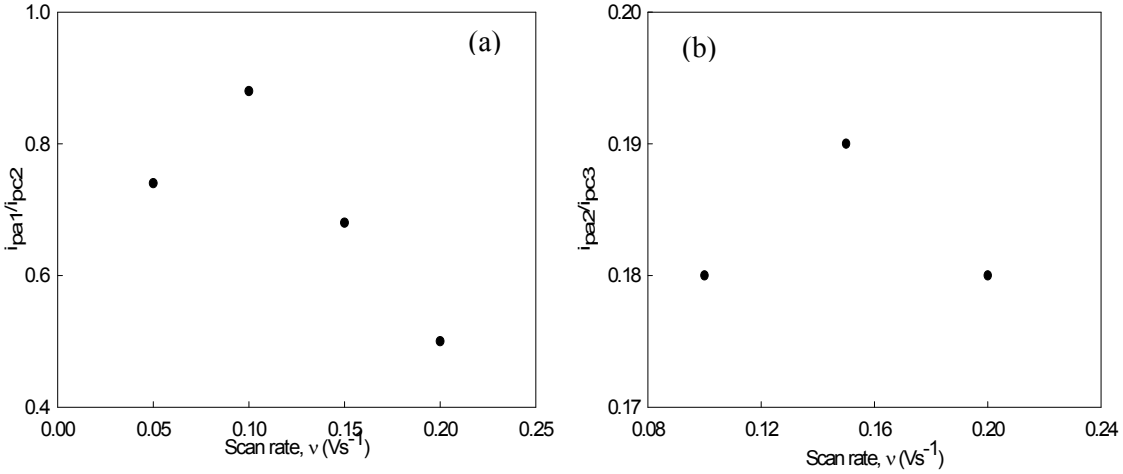

Fig 6.2.6 Variation of peak current ratio with scan rate for Cu(II)-Ciprofloxacin Compound in 0.1M KCl solution (a) first pair (b) second pair of peaks.

current ratio is very much lower than unity. Therefore it may said that system shows almost exceptional character from the reversible behavior[101, 102].

Fig 6.2.6 shows that the peak current ratio decreases with increasing scan rate for the first pair of peaks with an exception at the lowest scan rate. But for the second pair, it shows both increasing and decreasing characteristics. Again peak current function ($i_p/v^{1/2}$) for

the first pair, decreases upto scan rate 0.200 Vs^{-1} (with an exception at 0.100 Vs^{-1}) and then increases with increasing scan rate (Fig 6.2.7). Again for the second pair of peaks it

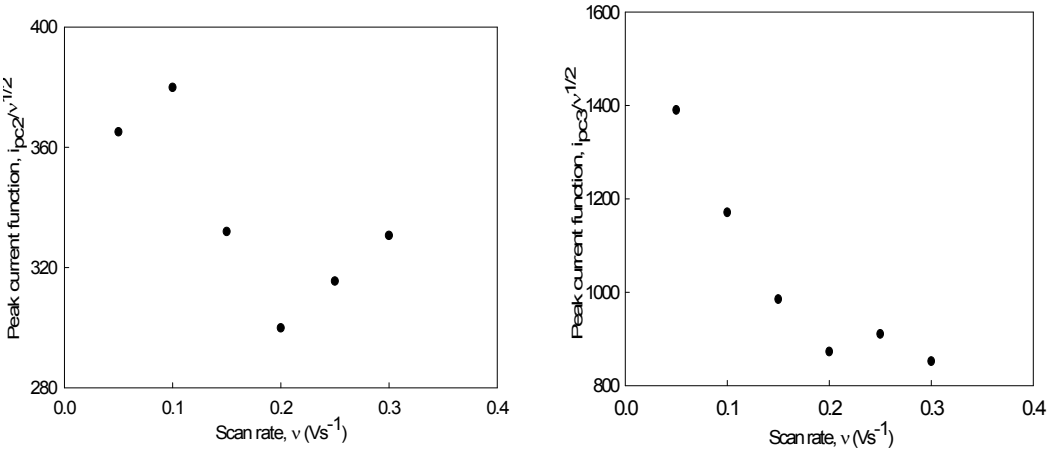

Fig 6.2.7 Variation of peak potential separation with scan rate for Cu(II)-Ciprofloxacin Compound in 0.1M KCl solution (a) first pair (b) second pair of peaks.

decreases with increasing scan rate with a little exception at scan rate 0.250 Vs^{-1}.Therefore, it does not indicate any clear conception about the electrochemical process[101, 102].

Again the plot of log i_p against log ν shows a linear relationship for both pair of peaks. It is found that for both the pair of peaks the slope is more than unity. Therefore it may be said that the process is accompanied by adsorption[3, 112] (Fig 6.2.8).

Tafel plot (peak potential vs log ν) for the first and the second pair of peaks are shown in Fig 6.2.9. The curves express that the slopes of the Tafel plot are not zero. So the electrochemical process will be different from reversibility.

Therefore from the above discussions there are some findings, such as: i) peak potential shifts with scan rate, ii) peak current ratio is not equal to unity, iii) the current function $i_p/v^{1/2}$ is independent of scan rate, iv) peak response broadens as scan rate increases, v) slope of Tafel plot is not equal to zero.

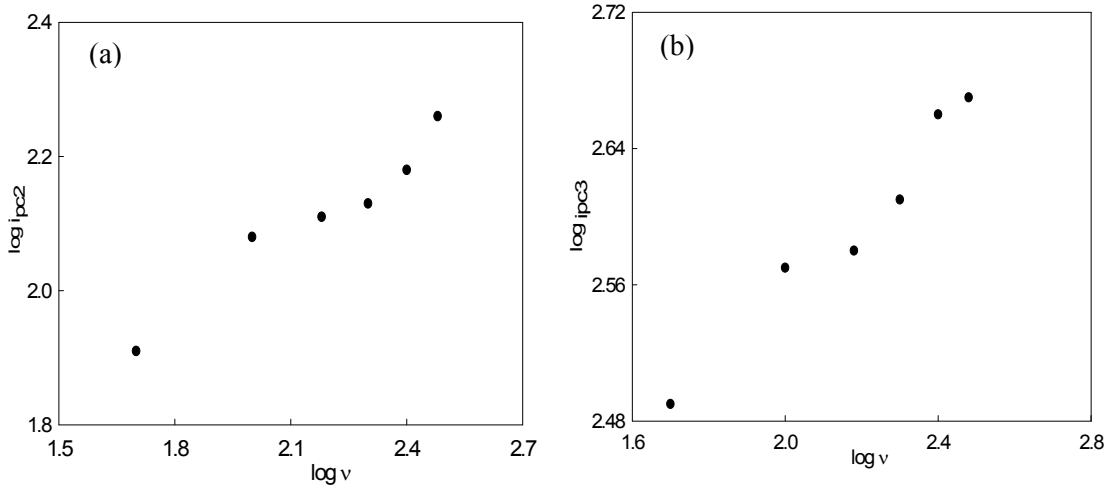

Fig 6.2.8 Plots of log i_p against log ν for Cu(II)-Ciprofloxacin Compound in 0.1M KCl solution (a) first pair (b) second pair of peaks.

Considering all the above points it can be concluded that the electrochemical process involved in Copper is quasi-reversible. The electrochemical reactions of the Cu(II)/Cu(0) system under investigation may be written as:

$$\text{Cu(II)Ciprofloxacin} \underset{-e}{\overset{+e}{\rightleftharpoons}} \text{Cu(I)Ciprofloxacin}$$

$$\text{Cu(I)Ciprofloxacin} \underset{-e}{\overset{+e}{\rightleftharpoons}} \text{Cu(0)Ciprofloxacin}$$

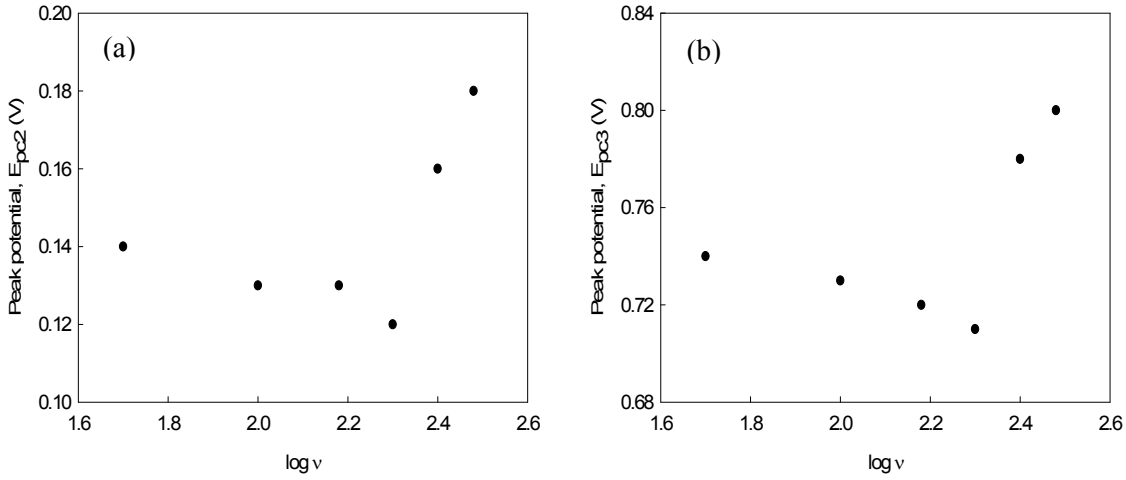

Fig 6.2.9 Plots of peak potential against log ν for Cu(II)-Ciprofloxacin Compound in 0.1M KCl solution (a) first pair (b) second pair of peaks.

Moreover, the system is diffusion controlled as well as adsorptive controlled, which can be declared from the facts that a) in the forward scans, peak currents are proportional to the square root of scan rate, b) peak currents in both the regions (cathodic and anodic) increases linearly with square root of scan rate, c) slope of log i_p against log ν plot is more than unity.

Concentration effect of Cu(II)-Ciprofloxacin Compound

Study on the concentration effect of Cu(II)-Ciprofloxacin compound was also accomplished. This observation was done using three different concentrations (16.75, 33.50 and 50.25 ppm) of Cu(II)-Ciprofloxacin compound and maintaining the same environment as previous. The CVs are overlapped in the Fig 6.2.10 and the parameters are recorded in Table 6.2.2.

The peak current for all the peaks show a gradual increase with increasing concentrations (Table 6.2.2) and a graphical presentation is given in Fig 6.2.11. Again it is also known that the greater the peak current, higher will be the charge acceptance of the electrode.

This linear nature of the peak current with concentrations of the compounds indicate that the processes are diffusion controlled.

Table 6.2.2 Current-potential data for Cu(II)-Ciprofloxacin compound (at scan rate 0.100 Vs^{-1}) in 0.1 M KCl solution at different concentrations.

Concentration (ppm)	Cathodic peak potential			Cathodic peak current		
	E_{pc1} (V)[-]	E_{pc2} (V)	E_{pc3} (V)	i_{pc1} (μA)	i_{pc2} (μA)	i_{pc3} (μA)
16.75	0.402	0.108	0.744	31.51	41.14	171.24
33.50	0.387	0.122	0.738	60.11	80.11	260.89
50.25	0.363	0.131	0.731	96.11	120.12	370.25

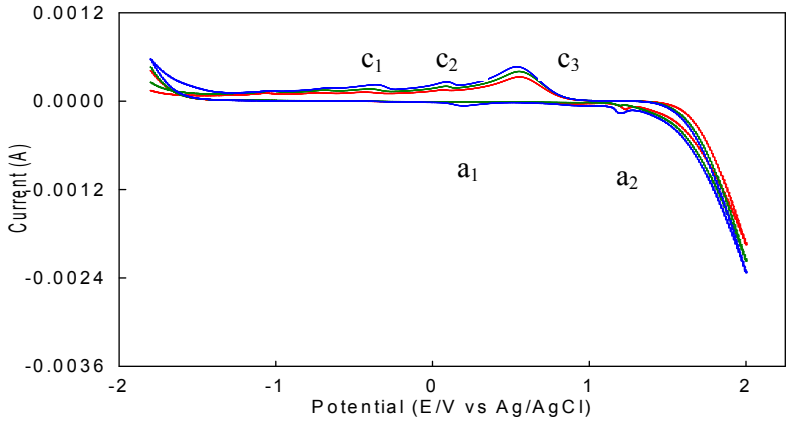

Fig 6.2.10 Cyclic voltammograms of Cu(II)-Ciprofloxacin Compound (at scan rate 0.100 Vs^{-1}) of different concentrations in 0.1 M KCl.

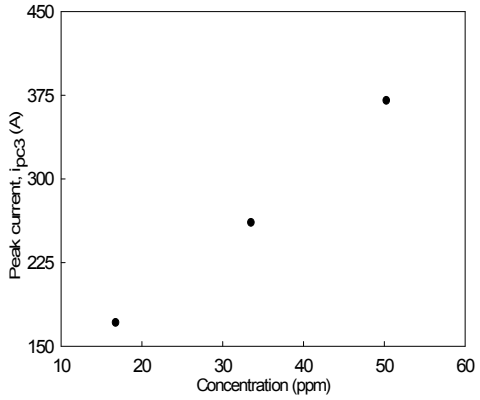

Fig 6.2.11 Variation of peak current with concentration of Cu(II)-Ciprofloxacin Compound in 0.1 M KCl solution.

6.2.2 Chronoamperometric and chronocoulometric study of Cu(II)-Ciprofloxacin Compound

CA and CC Study of Cu(II)-Ciprofloxacin Compound

Chronoamperometric study of Cu(II) system was also done after compound formation with Ciprofloxacin. This study was done using 50.25 ppm solution of Cu(II)-Ciprofloxacin compound. It was observed that there were three peaks after compound formation in the cathodic region but in the anodic region, there are two. Therefore, after compound formation there are two pair of peaks and CA study was also done correspondingly for each of the pair of peaks. The chroamperograms are shown in the Fig 6.2.12.

It shows that the spike height after compound formation with Ciprofloxacin is decreased for each of the pair of peaks (Figures 6.2.13 and 6.2.14) compared to that of Cu(II) before compound formation with Ciprofloxacin. Since the spike height is proportional to the rate of electrolysis, this means that after interaction the rate of electrolysis has been decreased.

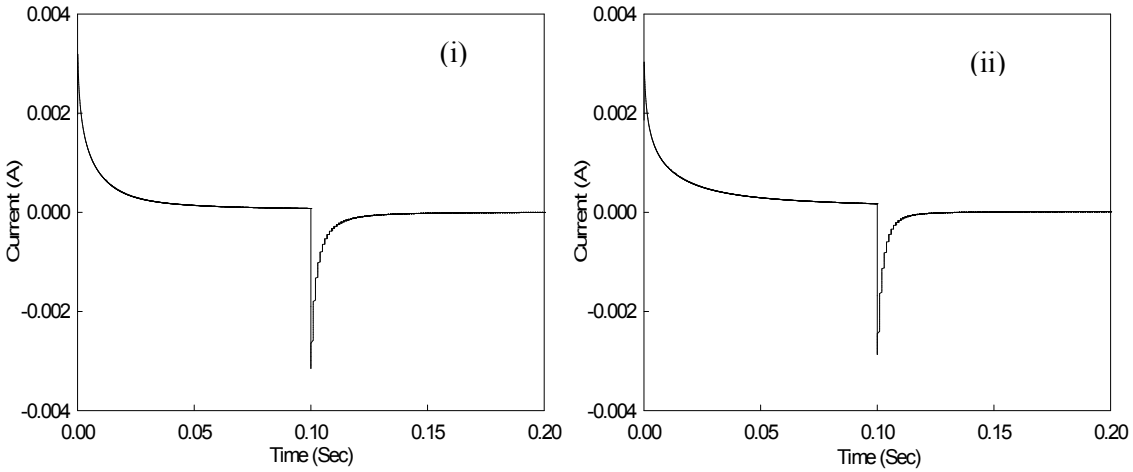

Fig 6.2.12 Current responses for Cu(II)-Ciprofloxacin Compound (50.25 ppm solution) in 0.1 M KCl solution (i) first pair and (ii) second pair of peaks.

Chronocoulometry (CC) is the integrated form of the chronoamperometry. So that in CC the monitored response is charge. It is also known as chronocoulogram. Such charge responses are shown in Fig 6.2.15. Chronocoulometric response (Fig 6.2.15) shows that the charge at τ is decreased after

compound formation with Ciprofloxacin. It was 2.482 μC for the first peak and 2.251 μC

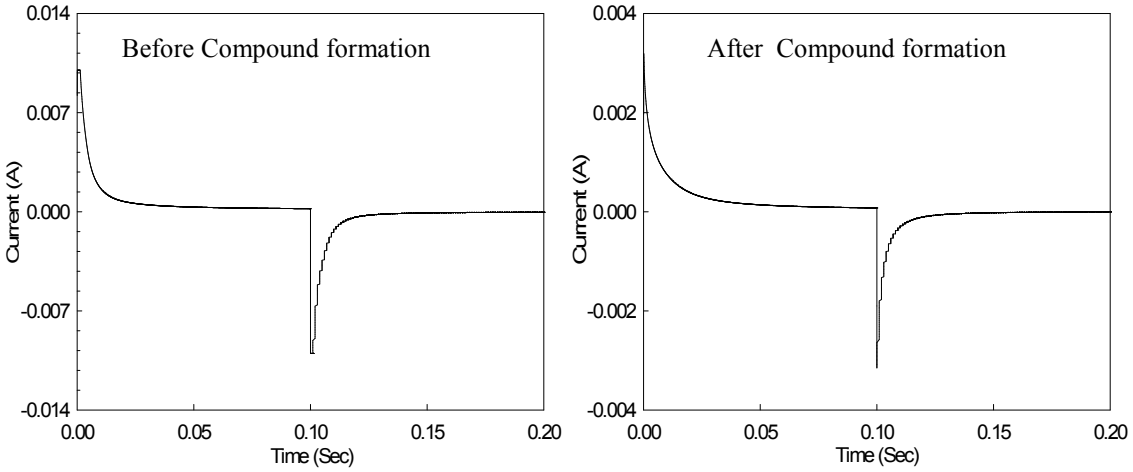

Fig 6.2.13 Current responses for Cu(II) in 0.1 M KCl solution before and after compound formation with Ciprofloxacin for first pair of peaks.

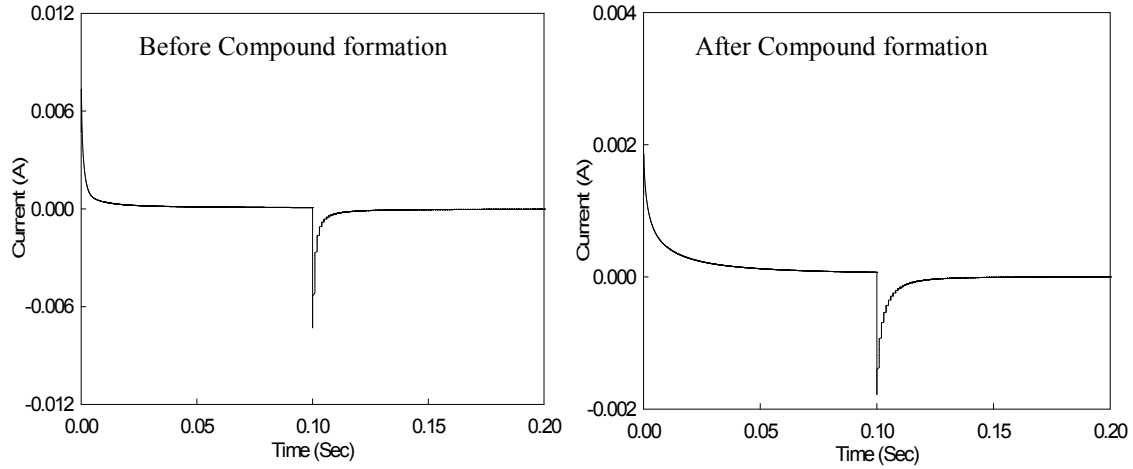

Fig 6.2.14 Current responses for Cu(II) in 0.1 M KCl solution before and after compound formation with Ciprofloxacin for second pair of peaks.

for the second peak in the absence of Ciprofloxacin, whereas it becomes 2.460 μC and 2.240 μC for the first and second pair of peaks respectively after compound formation with Ciprofloxacin.

Now if Q value obtained from time less than τ is plotted versus $t^{1/2}$ and on the same graph $-Q_r$ is plotted versus $\theta = [\tau^{1/2} + (t-\tau)^{1/2} - t^{1/2}]$, there will be two straight lines which

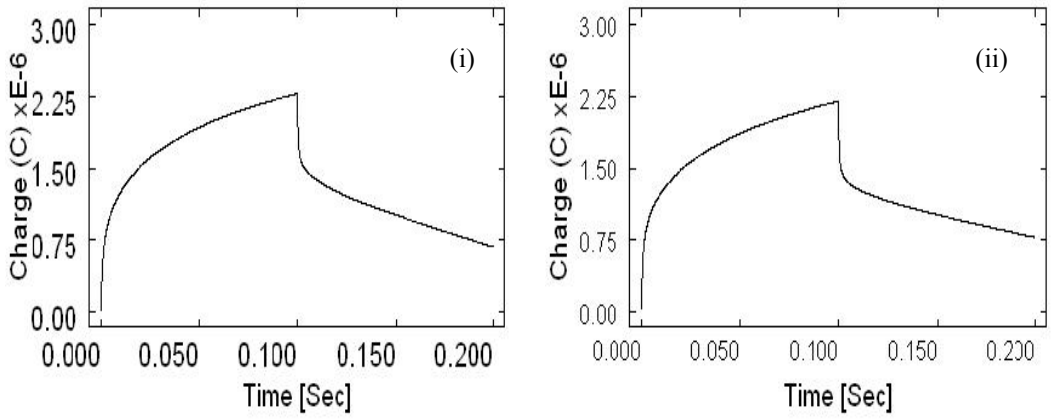

Fig 6.2.15 Charge responses for Cu(II)-Ciprofloxacin Compound (50.25 ppm solution) in 0.1 M KCl solution for (i) first pair and (ii) second pair of peaks.

intersects each other at Q=0 axis with equal slope, if there is no adsorption of reactant or product[31]. Any deviation from such condition means adsorption. Such plots are shown in the Fig 6.2.16.

This shows that the plots Q vs $t^{1/2}$ and $-Q_r$ vs θ do not intersect each other at Q=0 axis. Moreover they do not have equal slopes. Therefore from this plot, it may be said that adsorption of reactant or products occur on the electrode.

Therefore the findings from the Chronoamperometric study is that after compound formation the spike height is decreased, indicating towards a decrease in the rate of electrolysis. And the cases. Both of these facts combinedly indicates towards successful complexation. And the observations from the plots Q vs $t^{1/2}$ and $-Q_r$ vs θ gives conclusion that adsorption of reactant or products occur on the electrode also after compound formation.

Concentration Effect

Chronoamperometric as well as chronocoulometric study on the concentration effect of Cu(II)-Ciprofloxacin compound was also accomplished. This observation was done using three different concentrations (50.25, 33.50 and 16.75 ppm) of Cu(II)-Ciprofloxacin

compound and maintaining the same environment as previous. The CAs are shown in Figures 6.2.17 to 6.2.19.

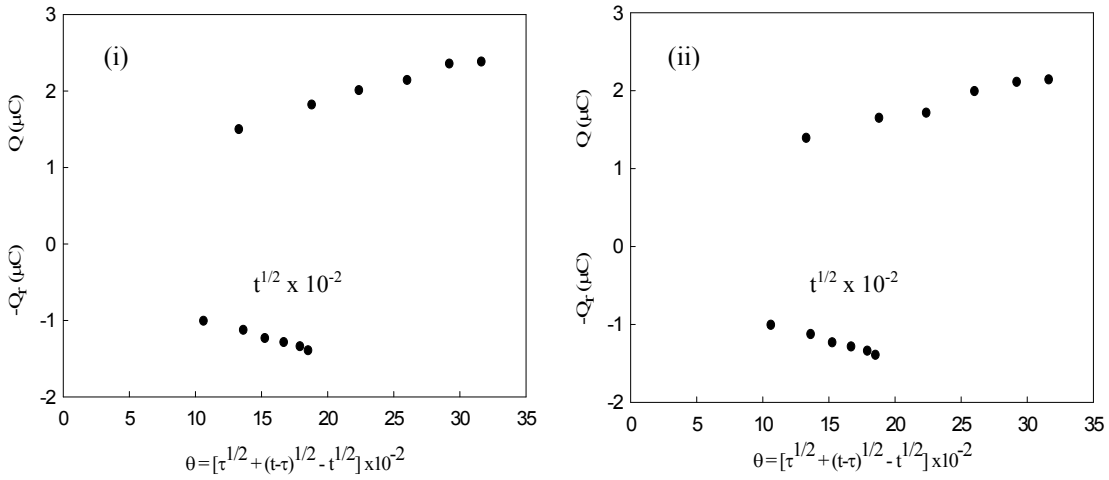

Fig 6.2.16 Plots of Q vs $t^{1/2}$ and $-Q_r$ vs θ for Cu(II)-Ciprofloxacin compound in 0.1 M KCl solution for (i) first and (ii) second pair of peaks.

It is found that with the decrease in concentration of the compound solution the spike height decreases for both the pair of peaks. This fact indicates that as the concentration decreases, the number of electroactive species are decreased. As a result the rate of electrolysis also decreases. Therefore it may be concluded that as the the concentration decreases the rate of electrolysis is decreased. A graphical representation of this fact is shown in Fig 6.2.20.

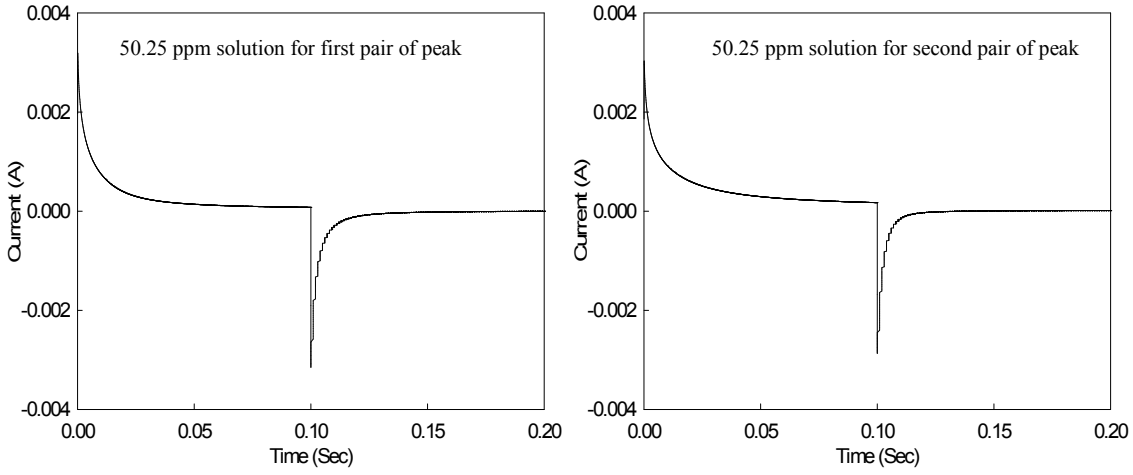

Fig 6.2.17 Current responses for Cu(II)-Ciprofloxacin compound for first pair and second pair of peaks for 50.25 ppm solution.

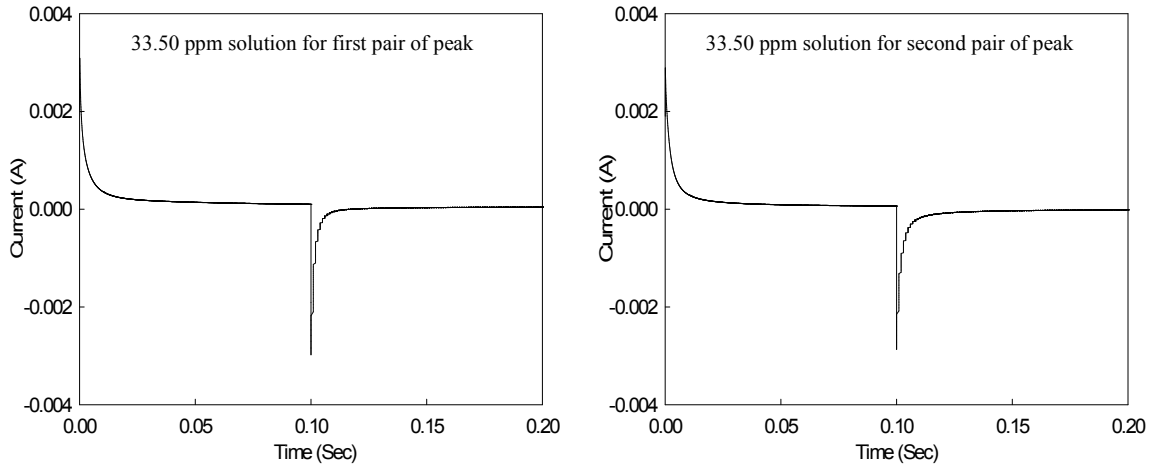

Fig 6.2.18 Current responses for Cu(II)-Ciprofloxacin compound for first pair and second pair of peaks for 33.50 ppm solution.

Chronocoulometry (CC) is the integrated form of the chronoamperometry. Such charge responses corresponding to the chronoamperograms are shown in Figures 6.2.21 to 6.2.23. Here it is also found that with the decrease in compound concentrations, the charge at τ are decreased for both the pair of peaks. The fact behind this is that with the decrease in concentration the number of charged species are also decreased. As a result the charge decreases with decreasing concentration of the compound solution. This can also be represented graphically in Fig 6.2.24.

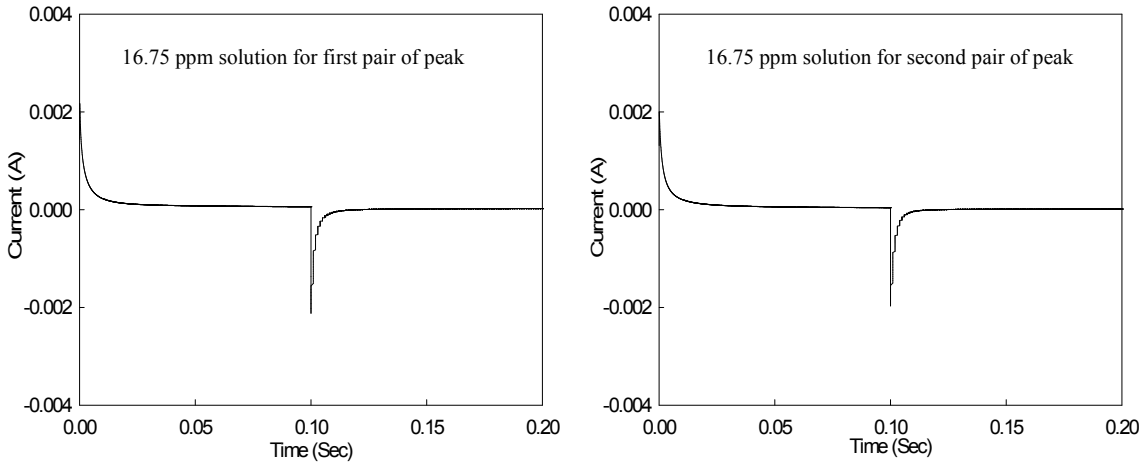

Fig 6.2.19 Current responses for Cu(II)-Ciprofloxacin compound for first pair and second pair of peaks for 16.75 ppm solution.

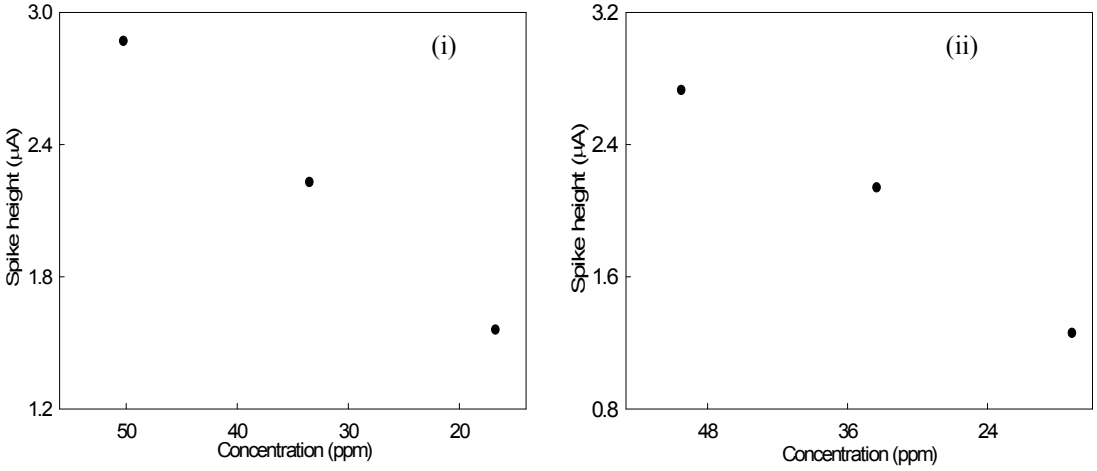

Fig 6.2.20 Concentration effect of Cu(II)-Ciprofloxacin compound on spike height of Chronoamperometry for (i) first pair and (ii) second pair of peaks.

Now if Q value obtained from time less than τ is plotted versus $t^{1/2}$ and on the same graph $-Q_r$ is plotted versus $\theta = [\tau^{1/2} + (t- \tau)^{1/2} - t^{1/2}]$, there will be two straight lines which intersects each other at Q=0 axis with equal slope, if there is no adsorption of reactant or product[31]. Any deviation from such condition means adsorption. Such plots for both the pair of peaks and at all the concentrations are shown in the Figures 6.2.25, 6.2.26 and 6.2.27.

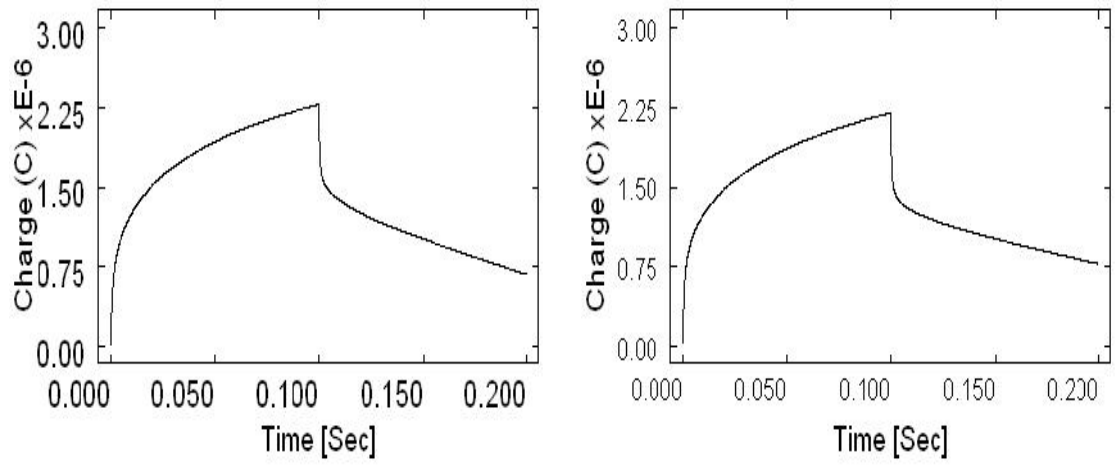

Fig 6.2.21 Charge responses for Cu(II)-Ciprofloxacin compound for first pair and second pair of peaks for 50.25 ppm solution.

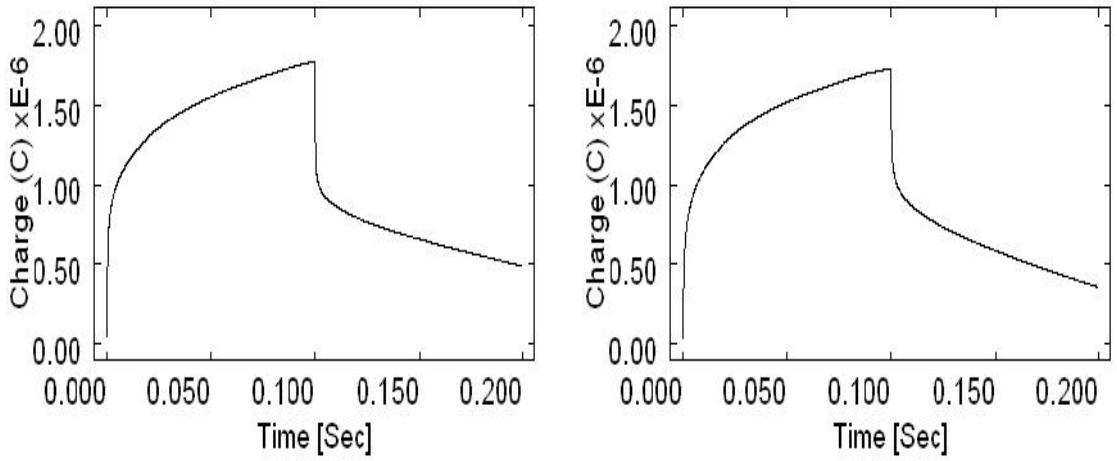

Fig 6.2.22 Charge responses for Cu(II)-Ciprofloxacin compound for first pair and second pair of peaks for 33.50 ppm solution.

This shows that the plots Q vs $t^{1/2}$ and $-Q_r$ vs θ do not intersect each other at Q=0 axis. Moreover they do not have equal slopes. Therefore from this plot, it may be said that adsorption of reactant or products occur on the electrode.

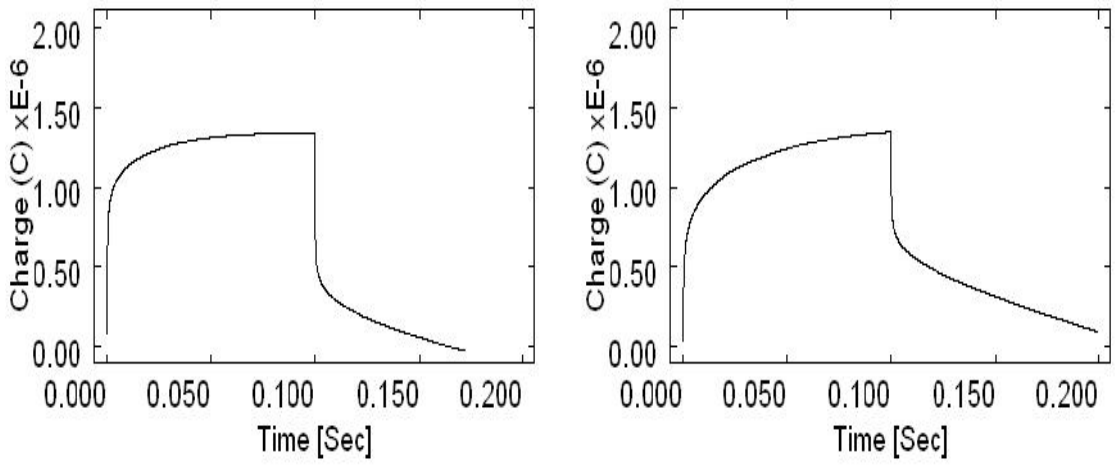

Fig 6.2.23 Charge responses for Cu(II)-Ciprofloxacin compound for first pair and second pair of peaks for 16.75 ppm solution.

Therefore the findings from the Chronoamperometric study is that after compound formation the spike height is decreased, indicating towards a decrease in the rate of electrolysis. And from the Chronocoulometric study, it is observed that the charge at τ are decreased in all the cases. Both of these facts combinedly indicates towards successful compound formation. And the observations from the plots Q vs $t^{1/2}$ and $-Q_r$ vs θ gives

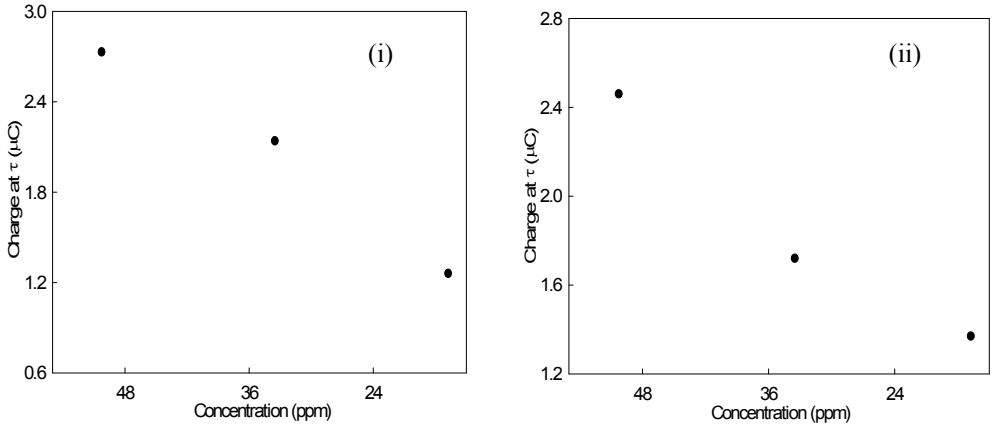

Fig 6.2.24 Concentration effect of Cu(II)-Ciprofloxacin compound on charge at τ of Chronocoulometry for (i) first pair and (b) second pair of peaks.

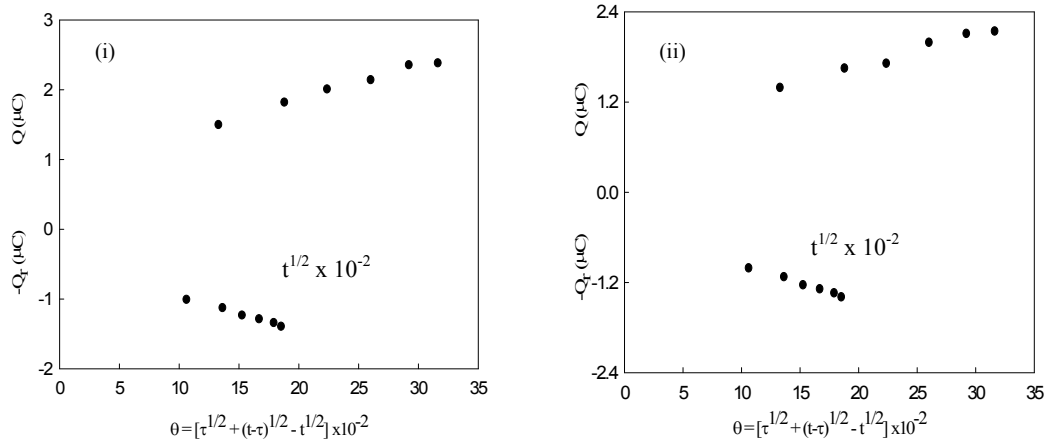

Fig 6.2.25 Plots of Q vs $t^{1/2}$ and $-Q_r$ vs θ for Cu(II)-Ciprofloxacin compound in 0.1 M KCl solution for (i) first pair and (ii) second pair of peaks for 50.25 ppm solution.

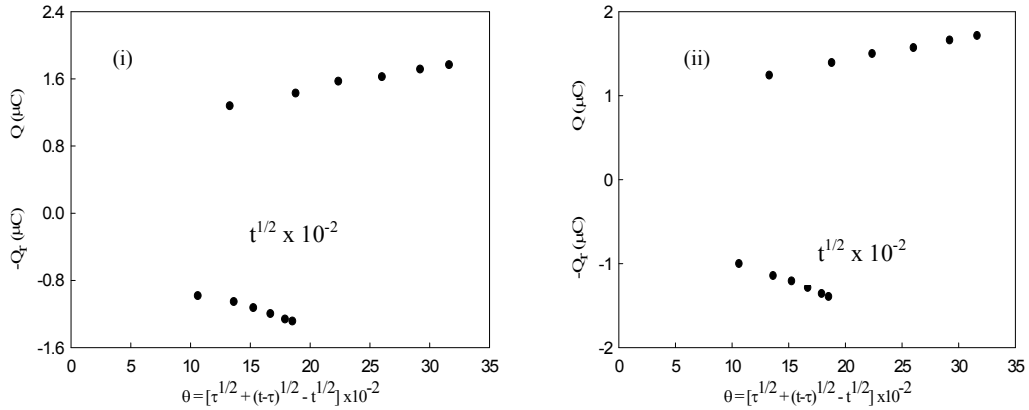

Fig 6.2.26 Plots of Q vs $t^{1/2}$ and $-Q_r$ vs θ for Cu(II)-Ciprofloxacin compound in 0.1 M KCl solution for (i) first pair and (ii) second pair of peaks for 33.50 ppm solution.

conclusion that adsorption of reactant or products occur on the electrode also after compound formation.

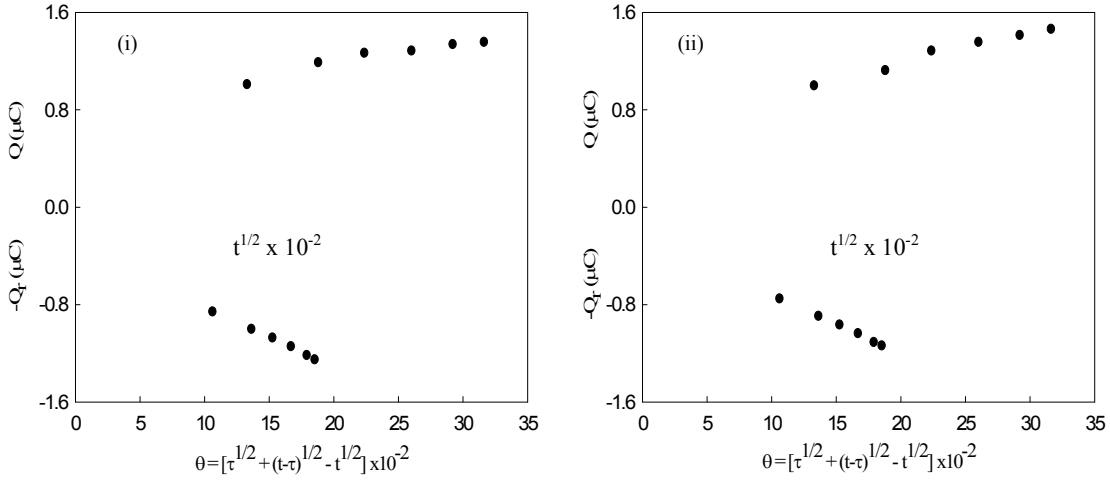

Fig 6.2.27 Plots of Q vs $t^{1/2}$ and $-Q_r$ vs θ for Cu(II)-Ciprofloxacin compound in 0.1 M KCl solution for (i) first pair and (ii) second pair of peaks for 16.75 ppm solution.

6.2.3 Cyclic voltammetric study of Mn(II)-Ciprofloxacin Compound at Glassy Carbon Electrode (GCE).

Redox behavior of Mn(II)-Ciprofloxacin compound

The redox behavior of Mn(II)-Ciprofloxacin compound (330 ppm) in 0.1 M KCl was also analyzed at room temperature using the same technique and same set of electrodes. A CV of the system at scan rate 0.100 Vs^{-1} within the potential window from -1.500 V to 2.000 V, is given in Fig 6.2.28.

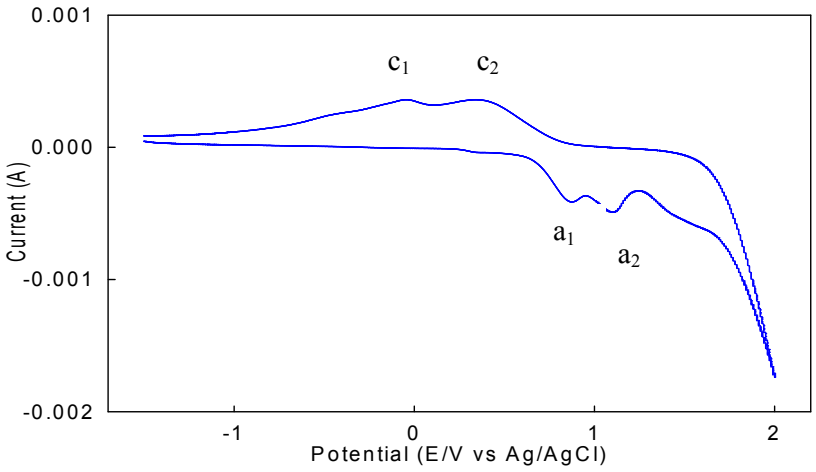

Fig 6.2.28 Cyclic voltammogram of Mn(II)-Ciprofloxacin Compound (330 ppm solution) in 0.1 M KCl at scan rate 0.100 Vs^{-1}.

The CV shows two cathodic peaks (c_1 and c_2) at the potentials of -0.021 V and 0.342 V and in the anodic region two peaks (a_1 and a_2) at 0.776 V and 1.193 V as well as a humplike shape. Compared to the CV of Mn(II), it is found that the first cathodic peak shifts towards less negative as well as the second one towards less positive potential. Again in the anodic region, the first anodic peak moves towards more positive and second one towards less positive potential. In other words, it is evident that after compound formation, both the cathodic and the anodic peaks approach towards each other. Moreover, the humplike shape in the anodic region may be due to the ligand (Ciprofloxacin). But in the Mn(II)-Ciprofloxacin interaction in solution exhibits two peaks in the cathodic and one in the anodic region.

Fig 6.2.29 shows the voltammograms of Mn(II)-Ciprofloxacin compound at different

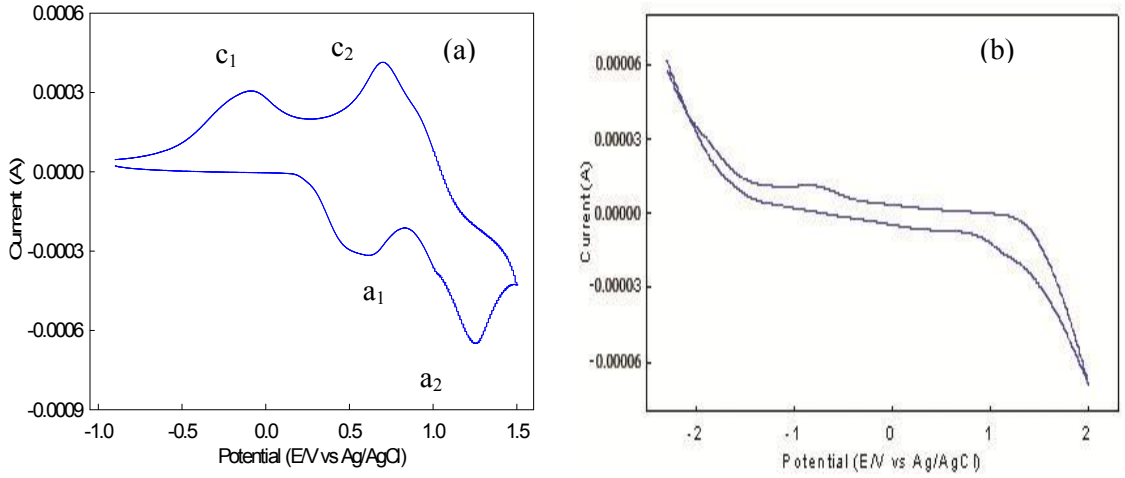

Fig 6.2.28 Cyclic voltammograms of (a) Mn(II) and (b) Ciprofloxacin at scan rate 0.100 Vs^{-1}.

scan rates. It shows that with the increase in scan rate all the peaks both in the anodic andin the cathodic region shifts towards more positive potential. In addition to this, the humplike shape in the anodic region is prominent at the lower scan rate and at the higher scan rates it is almost absent.

And with the increase in scan rate, almost all the peaks become broader. Such behavior has been ascribed to slower charge propagation, probably due to difference in salvation and or permeability. Current-potential data for the system under consideration is recorded in Table 6.2.3.

The peak separation potential for both the pair of peaks (ΔE_{p1} and ΔE_{p2}) decreases with the increase in scan rate, which is absolutely opposite behavior compared to the Mn(II) itself. In the same way it does not indicate the limitation due to charge transfer kinetics and are shown in the plot of ΔE_{p1} vs ν and ΔE_{p2} vs ν in Fig 6.2.30. Again the forward scan peak currents (i_{pc1} and i_{pc2}) are proportional to the square root of the scan rate at all the scan rates, which means the system to be diffusion controlled.

Randle-Sevseik plot shows that with increasing $\nu^{1/2}$, the peak currents for both cathodic and anodic peaks increases linearly (Fig 6.2.31), giving the conclusion that the processes

are adsorptive controlled [101, 102]. The peak current ratio for the first pair of peaks are almost unity at almost all the scan

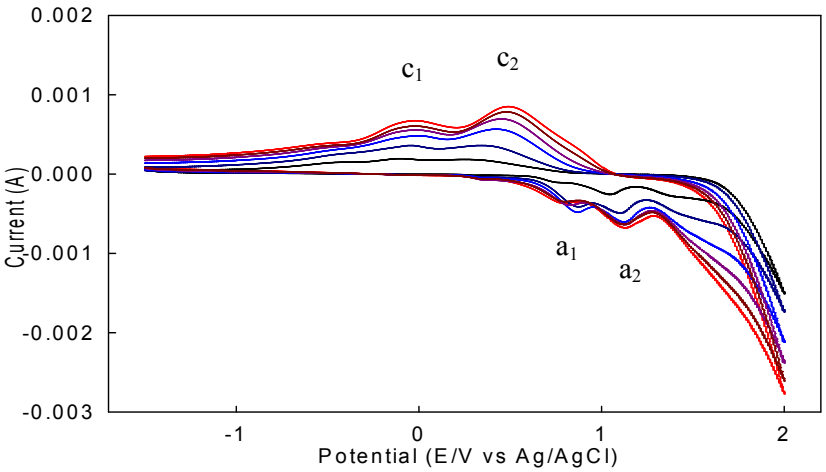

Fig 6.2.29 Cyclic voltammogram of Mn(II)-Ciprofloxacin Compound (330 ppm solution) in 0.1 M KCl at different scan rates.

rates. But for the second pair, the peak current ratio is lower than unity to some extent at the higher scan rates and very much nearest to unity at some scan rates. Therefore it may said that system shows exceptional character from the reversible behavior[101, 102].

Fig 6.2.32 shows that the peak current ratio decreases with increasing scan rate for both the pair of peaks. Again peak current function ($i_p/v^{1/2}$) increases with increasing scan rate for the second pair of peaks. But for the first pair the behavior is anomalous. Therefore, it does not indicate any clear conception about the electrochemical process[101, 102].

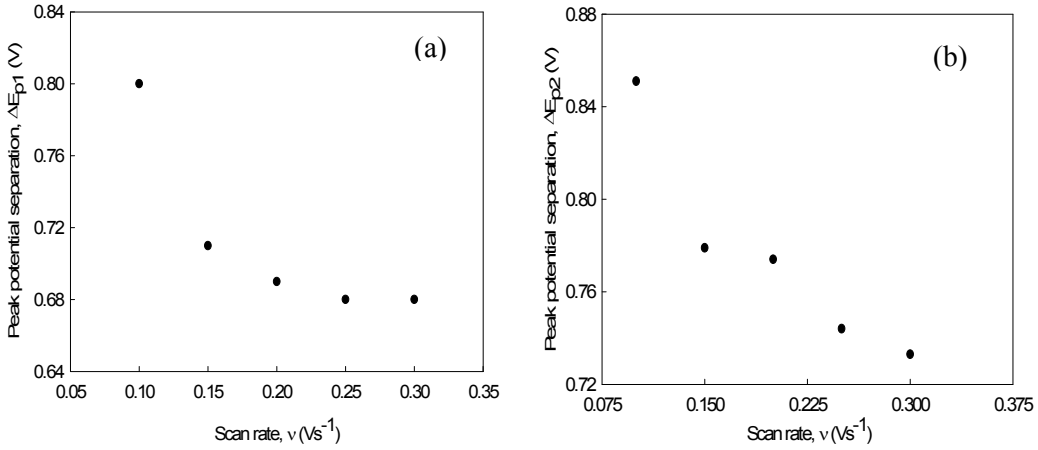

Fig 6.2.30 Variation of peak potential separation with scan rate for Mn(II)-Ciprofloxacin Compound in 0.1M KCl solution (a) first pair (b) second pair of peaks.

Table 6.2.3 Current-potential data for Mn(II)-Ciprofloxacin compound (330 ppm solution) in 0.1 M KCl solution at different scan rates.

Scan rate	SQRT of scan rate	Cathodic peak potential	Anodic peak potential	Cathodic peak current	Anodic peak current	Peak potential separation	Peak current ratio
ν (Vs^{-1})		E_{pc1} (V)	E_{pa1} (V)	i_{pc1} (μA)	i_{pa1} (μA) [-]	$\Delta E_{p1}= E_{pa1}- E_{pc1}$ (V)	i_{pa1}/ i_{pc1}
0.050	0.2236	-0.069	-	51.21	-	-	-
0.100	0.3162	-0.021	0.776	96.22	120.21	0.797	1.25
0.150	0.3872	0.077	0.782	129.51	122.05	0.705	0.94
0.200	0.4472	0.098	0.788	141.66	128.54	0.690	0.91
0.250	0.5000	0.116	0.793	145.71	124.11	0.677	0.85
0.300	0.5477	0.121	0.797	174.08	125.71	0.676	0.72
ν (Vs^{-1})		E_{pc2} (V)	E_{pa2} (V)	i_{pc2} (μA)	i_{pa2} (μA) [-]	$\Delta E_{p2}= E_{pa2}- E_{pc2}$ (V)	i_{pa2}/ i_{pc2}
0.050	0.2236	-	1.110	-	272.01	-	-
0.100	0.3162	0.342	1.193	160.57	298.02	0.851	1.86
0.150	0.3872	0.432	1.211	365.33	346.28	0.779	0.95
0.200	0.4472	0.445	1.219	495.42	349.51	0.774	0.87
0.250	0.5000	0.479	1.223	584.19	354.13	0.744	0.61
0.300	0.5477	0.495	1.228	651.11	357.72	0.733	0.55

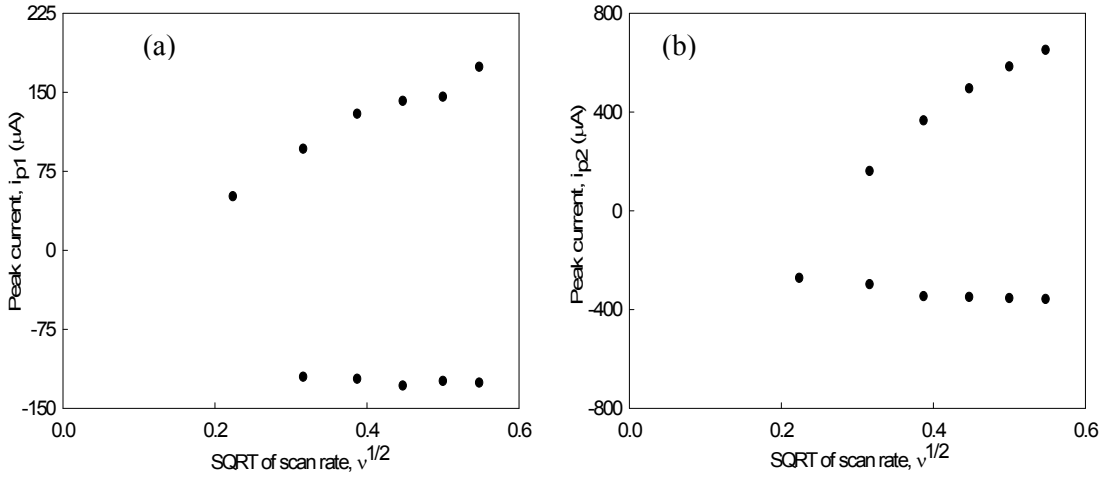

Fig 6.2.31 Variation of peak current with square root of scan rate for Mn(II)-Ciprofloxacin Compound in 0.1M KCl solution (a) first pair (b) second pair of peaks.

Again the plot of log i_p against log ν shows a linear relationship for both pair of peaks. It is found that for the first pair of peaks the slope is less than unity, but for the second pair it is more than unity indicating that the process is accompanied by both diffusion and adsorption[3, 112] (Fig 6.2.34).

Tafel plot (peak potential vs log ν) for the first and the second pair of peaks are shown in Fig 6.2.35. The curves express that the slopes of the Tafel plot are not zero. So the electrochemical process show different character from reversibility.

Therefore from the above discussions there are some findings, such as: i) peak potential shifts with scan rate, ii) peak current ratio is not equal to unity, iii) the current function $i_p/\nu^{1/2}$ is independent of scan rate, iv) peak response broadens as scan rate increases, v) slope of Tafel plot is not equal to zero.

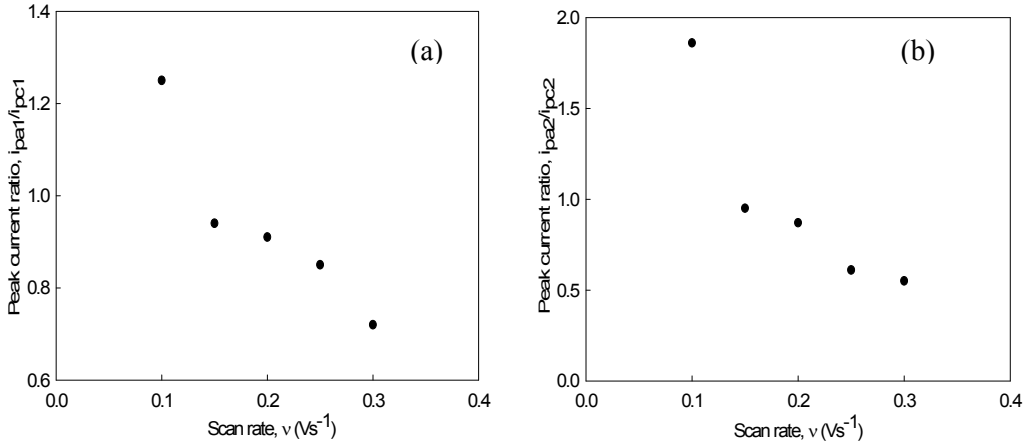

Fig 6.2.32 Variation of peak current ratio with scan rate for Mn(II)-Ciprofloxacin compound in 0.1 M KCl solution (a) first pair (b) second pair of peaks.

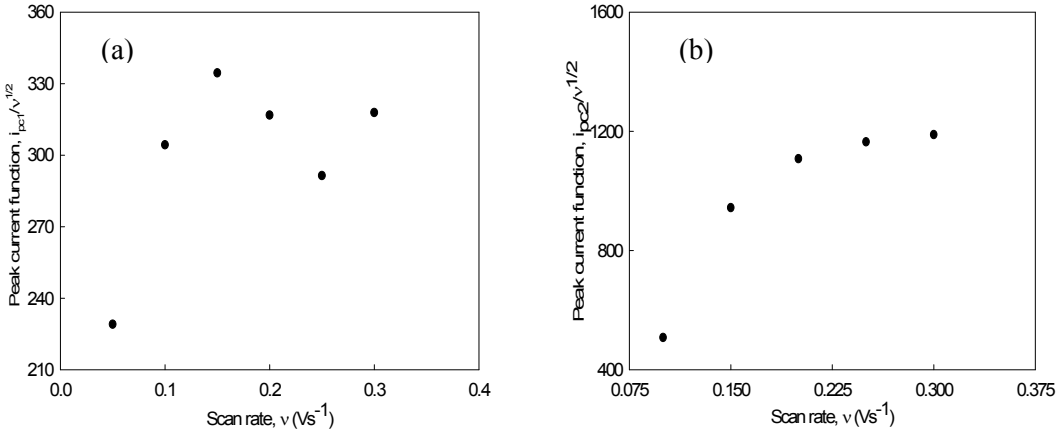

Fig 6.2.33 Variation of peak current function with scan rate for Mn(II)-Ciprofloxacin Compound in 0.1M KCl solution (a) first pair (b) second pair of peaks.

Considering all the above points it can be concluded that the electrochemical process involved in Mn(II) is quasi-reversible. The electrochemical reactions of the Mn(IV)/Mn(II) system under investigation may be written as:

$$\text{Mn(IV)Ciprofloxacin} \underset{-e}{\overset{+e}{\rightleftharpoons}} \text{Mn(III)Ciprofloxacin}$$

$$\text{Mn(III)Ciprofloxacin} \underset{-e}{\overset{+e}{\rightleftharpoons}} \text{Mn(II)Ciprofloxacin}$$

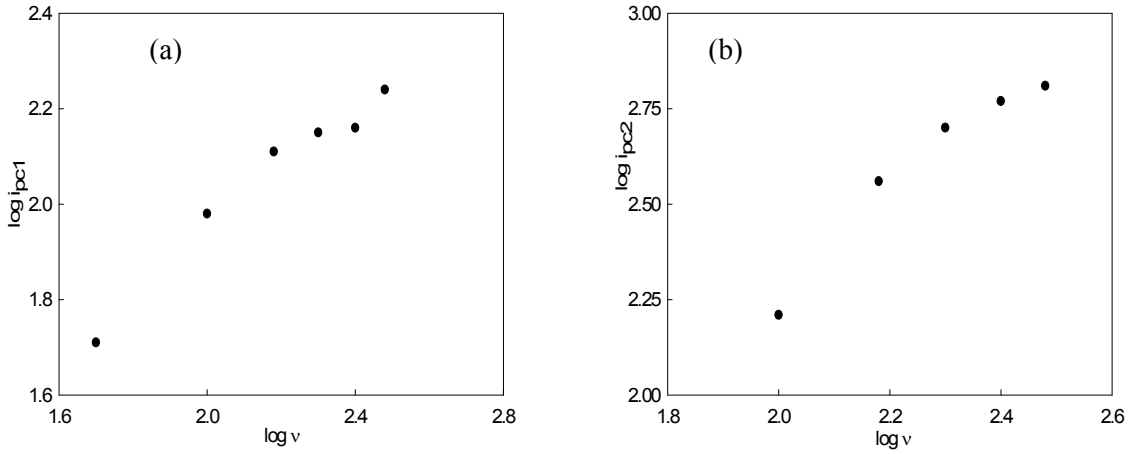

Fig 6.2.34 Plots of log i_p against log ν for Mn(II)-Ciprofloxacin Compound in 0.1M KCl solution (a) first pair (b) second pair of peaks.

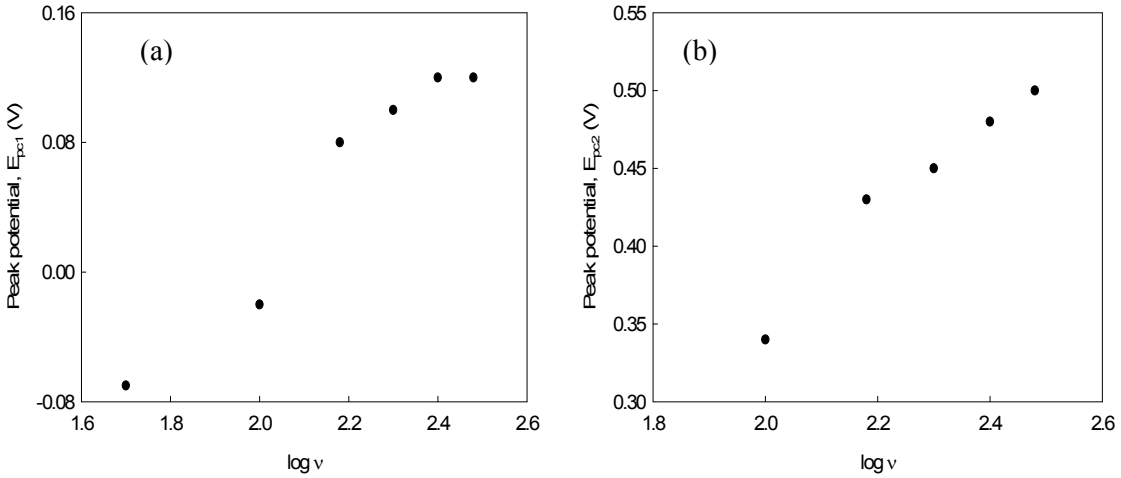

Fig 6.2.35 Plots of peak potential against log ν for Mn(II)-Ciprofloxacin Compound in 0.1M KCl solution (a) first pair (b) second pair of peaks.

Moreover, the system is diffusion controlled as well as adsorptive controlled, which can be declared from the facts that a) in the forward scans, peak currents are proportional to the square root of scan rate, b) peak currents in both the regions (cathodic and anodic) increases linearly with square root of scan rate, c) slope of log i_p against log ν plot is more than unity.

Concentration effect of Mn(II)-Ciprofloxacin Compound

Study on the concentration effect of Mn(II)-Ciprofloxacin compound was also accomplished. This observation was done using three different concentrations (110, 220 and 330 ppm) of Mn(II)-Ciprofloxacin compound and maintaining the same environment as previous. The CVs are overlapped in the Fig 6.2.36 and the parameters are recorded in Table 6.2.4.

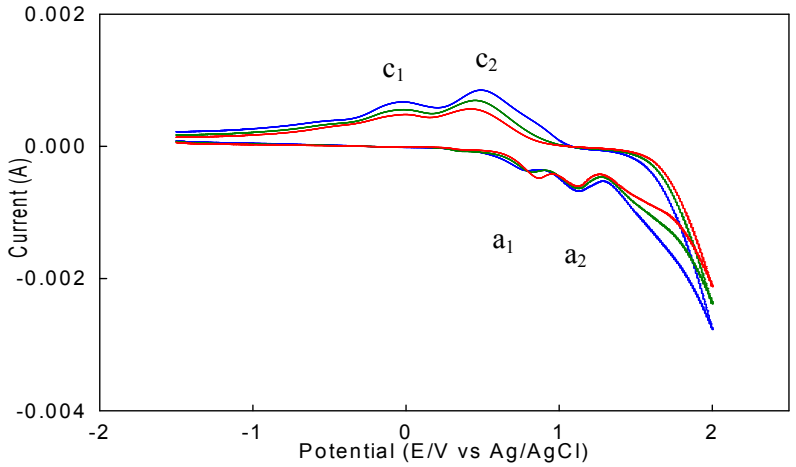

Fig 6.2.36 Cyclic voltammograms of Mn(II)-Ciprofloxacin Compound (at scan rate 0.100 Vs^{-1}) of different concentrations in 0.1 M KCl.

The peak current for all the peaks show a gradual increase with increasing concentrations (Table 6.2.4) and a graphical presentation is given in Fig 6.2.37. Again it is also known that the greater the peak current, higher will be the charge acceptance of the electrode. This linear nature of the peak current with concentrations of the complexes indicate that the processes are diffusion controlled.

Table 6.2.4 Current-potential data for Mn(II)-Ciprofloxacin compound (at scan rate 0.100 Vs^{-1}) in 0.1 M KCl solution at different concentrations.

Concentration (ppm)	Cathodic peak potential		Cathodic peak current	
	E_{pc1} (V) [-]	E_{pc2} (V)	i_{pc1} (μA)	i_{pc2} (μA)
110	0.051	0.426	120.11	200.35

220	0.065	0.501	140.57	245.65
330	0.077	0.586	162.67	287.29

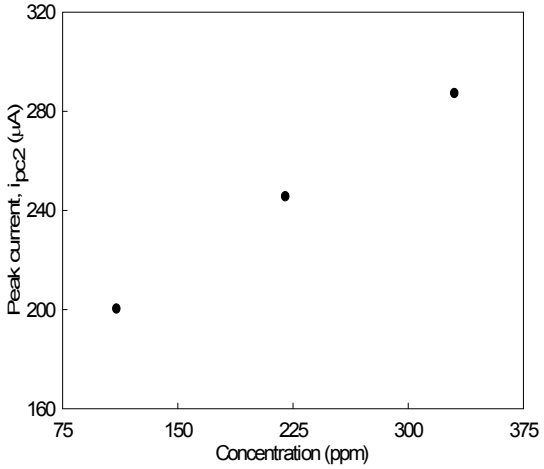

Fig 6.2.37 Variation of peak current with concentration of Mn(II)-Ciprofloxacin Compound in 0.1 M KCl solution.

6.2.4 Chronoamperometric and chronocoulometric study of Mn(II)-Ciprofloxacin Compound

CA and CC study of Mn(II)-Ciprofloxacin Compound

Chronoamperometric study of Mn(II) system was also done after compound formation with Ciprofloxacin. This study was done using 330 ppm solution of Mn(II)-Ciprofloxacin compound. After compound formation, similar to those of Mn(II) before compound formation, it also show two pair of peaks. That is two cathodic and two anodic signals. Therefore, as after compound formation there are two pair of peaks, the CA study was also done correspondingly for each of the pair of peaks. The chroamperograms are shown in the Fig 6.2.38.

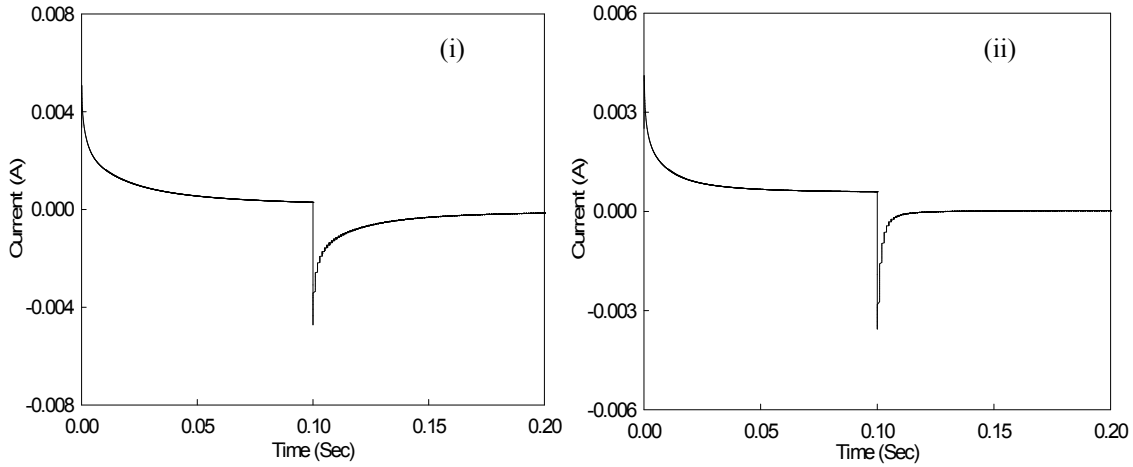

Fig 6.2.38 Current responses for Mn(II)-Ciprofloxacin Compound (330 ppm solution) in 0.1 M KCl solution (i) first pair and (ii) second pair of peaks.

It is found that the spike height after compound formation with Ciprofloxacin is decreased for each of the pair of peaks (Figures 6.2.39 and 6.2.40) compared to that of Mn(II) before compound formation with Ciprofloxacin. Since the spike height is proportional to the rate of electrolysis, this means that after interaction the rate of electrolysis has been decreased.

It is known that chronocoulometry (CC) is the integrated form of the

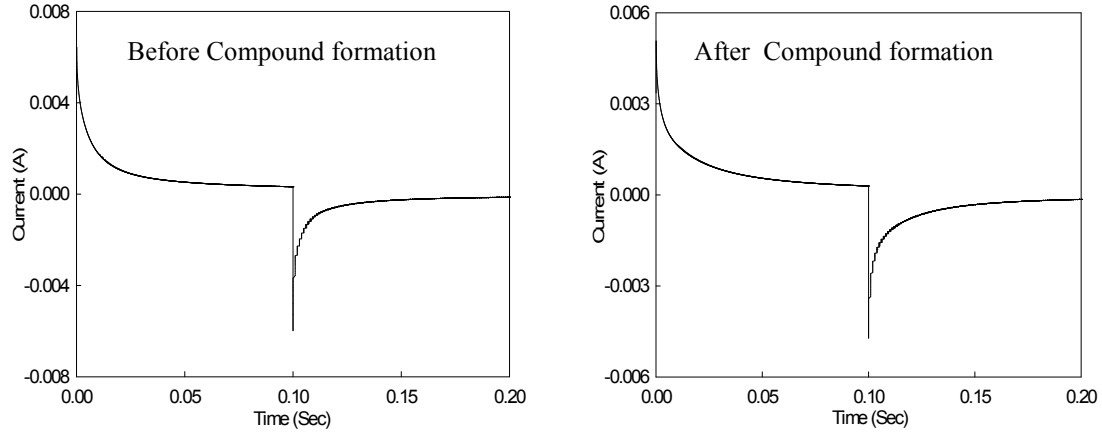

Fig 6.2.39 Current responses for Mn(II) in 0.1 M KCl solution before and after compound formation with Ciprofloxacin for first pair of peaks.

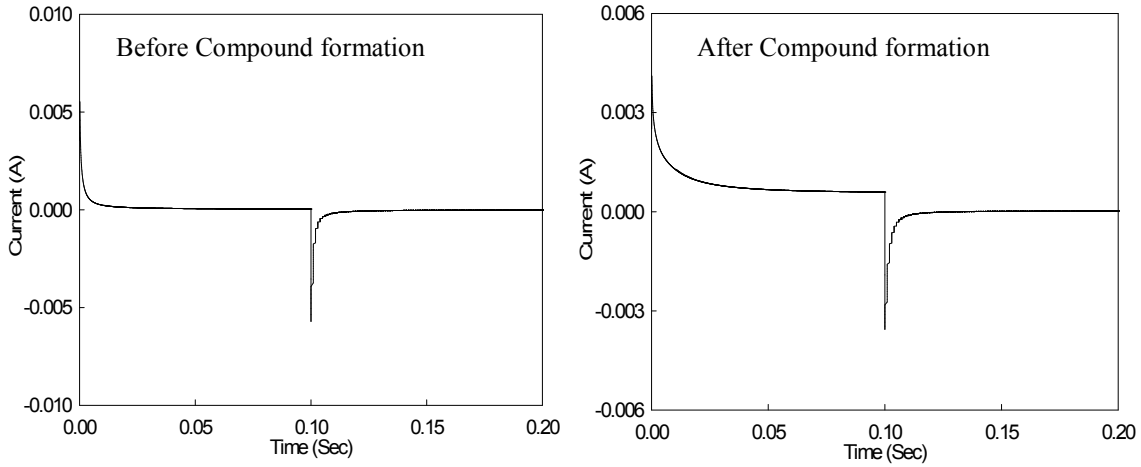

Fig 6.2.40 Current responses for Mn(II) in 0.1 M KCl solution before and after compound formation with Ciprofloxacin for second pair of peaks.

chronoamperometry. So that in CC the monitored response is charge. It is termed as chronocoulogram. Such charge responses for both the pair of peaks in case of Mn(II)-Ciprofloxacin compound are shown in Fig 6.2.41.

Chronocoulometric response shows that the charge at τ is decreased after interaction with Ciprofloxacin. It was 2.211 μC for the first peak and 2.483 μC for the second peak in the absence of Ciprofloxacin, whereas it becomes 2.000 μC and 2.220 μC for the first and second pair of peaks respectively after compound formation with Ciprofloxacin.

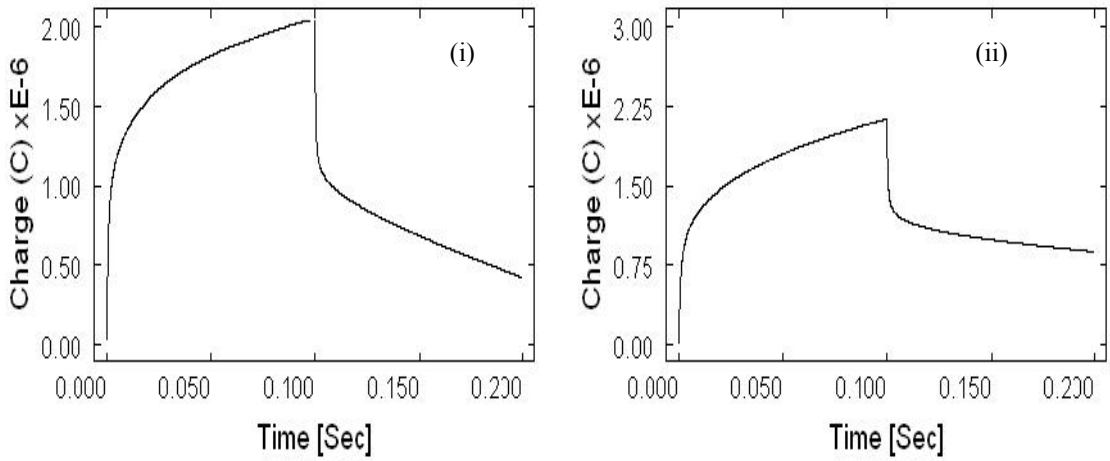

Fig 6.2.41 Charge responses for Mn(II)-Ciprofloxacin Compound (330 ppm solution) in 0.1 M KCl solution (i) first pair and (ii) second pair of peaks.

Now if Q value obtained from time less than τ is plotted versus $t^{1/2}$ and on the same graph $-Q_r$ is plotted versus $\theta = [\tau^{1/2} + (t- \tau)^{1/2} – t^{1/2}]$, there will be two straight lines which intersects each other at Q=0 axis with equal slope, if there is no adsorption of reactant or product. Any deviation from such condition means adsorption. Such plots are shown in the Fig 6.2.42.

This shows that the plots Q vs $t^{1/2}$ and $-Q_r$ vs θ do not intersect each other at Q=0 axis. Moreover they do not have equal slopes. Therefore from this plot, it may be said that adsorption of reactant or products occur on the electrode.

Therefore the findings from the Chronoamperometric study is that after compound formation the spike height is decreased, indicating towards a decrease in the rate of electrolysis. And from the Chronocoulometric study, it is observed that the charge at τ are decreased in all the cases. Both of these facts combinedly indicates towards successful compound formation. And the observations from the plots Q vs $t^{1/2}$ and $-Q_r$ vs θ gives conclusion that adsorption of reactant or products occur on the electrode also after compound formation.

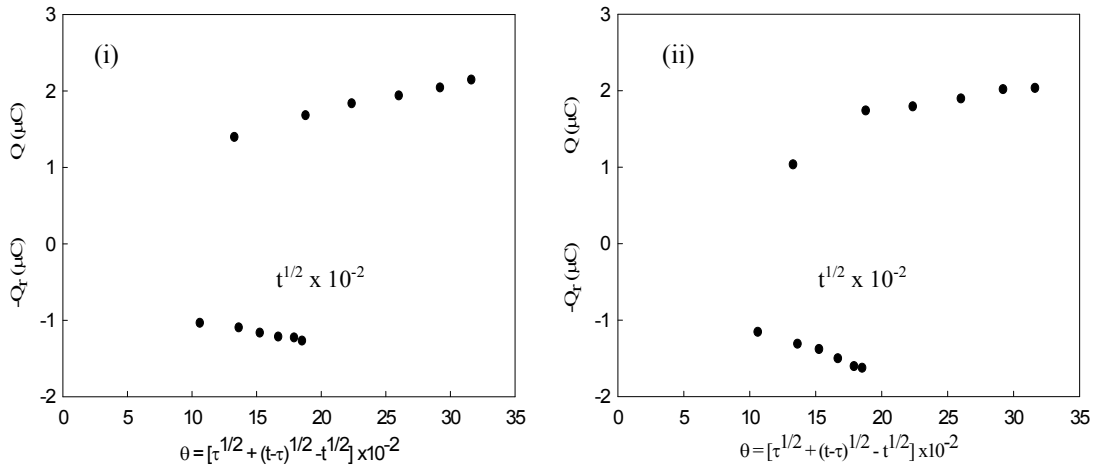

Fig 6.2.42 Plots of Q vs $t^{1/2}$ and $–Q_r$ vs θ for Mn(II)-Ciprofloxacin compound (330 ppm solution) in 0.1 M KCl solution (i) first and (ii) second pair of peaks.

Concentration Effect

The concentration effect of Mn(II)-Ciprofloxacin compound was also studied by Chronoamperometric as well as chronocoulometric method. This observation was done using three different concentrations (330, 220 and 110 ppm) of Mn(II)-Ciprofloxacin compound and maintaining the same environment as previous. The CAs are shown in Figures 6.2.43 to 6.2.45.

It is observed that with the decrease in concentration of the compound solution the spike height decreases for both the pair of peaks. This fact indicates that as the concentration decreases, the number of electroactive species are decreased. As a result the rate of

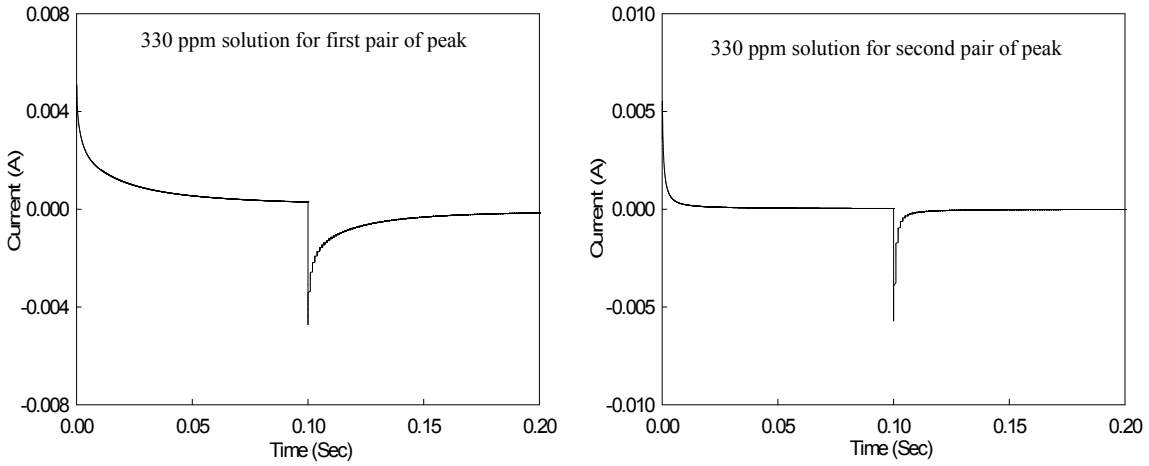

Fig 6.2.43 Current responses for Mn(II)-Ciprofloxacin compound for (i) first and (ii) second pair of peaks in 330 ppm solution.

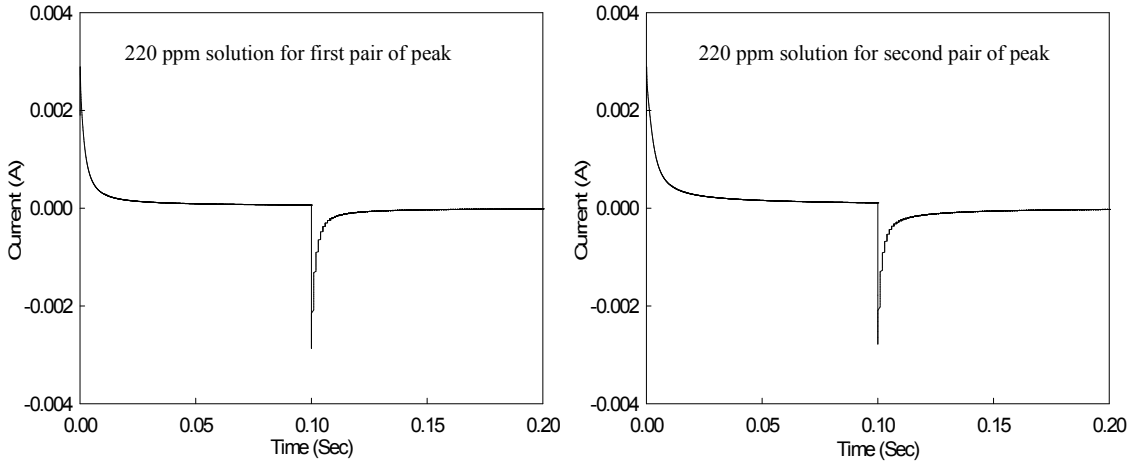

Fig 6.2.44 Current responses for Mn(II)-Ciprofloxacin compound for (i) first and (ii) second pair of peaks in 220 ppm solution.

electrolysis also decreases. Therefore it may be concluded that as the the concentration decreases the rate of electrolysis is decreased. A graphical representation of this fact is shown in Fig 6.2.46.

Again Chronocoulometry (CC), which is the integrated form of the chronoamperometry is also examined. Such charge responses corresponding to the chronoamperograms are shown in Figures 6.2.47 to 6.2.49.

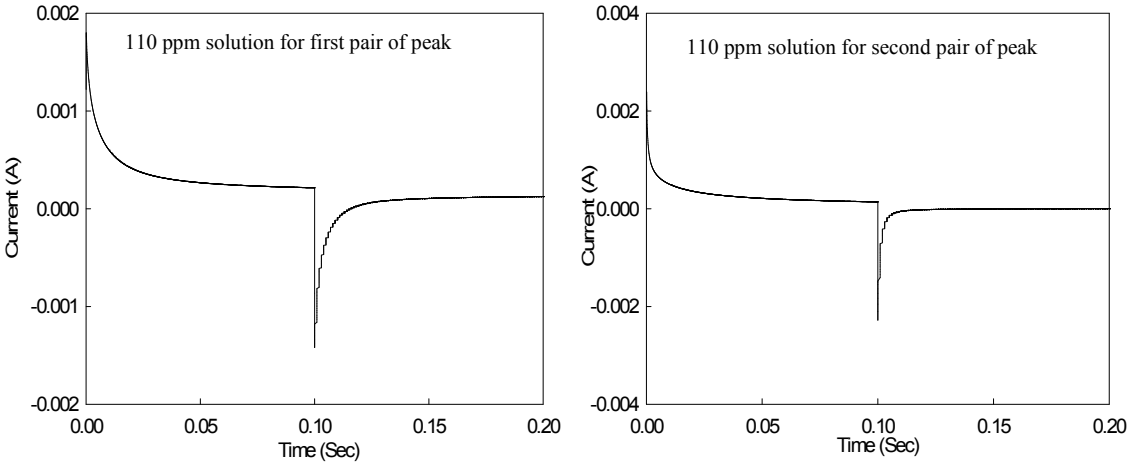

Fig 6.2.45 Current responses for Mn(II)-Ciprofloxacin compound for (i) first and (ii) second pair of peaks in 110 ppm solution.

Here it is also found that with the decrease in compound concentrations, the charge at τ are decreased for both the pair of peaks. The fact behind this is that with the decrease in concentration the number of charged species are also decreased. As a result the charge decreases with decreasing concentration of the compound solution. This can also be represented graphically in Fig 6.2.50.

Now if Q value obtained from time less than τ is plotted versus $t^{1/2}$ and on the same graph $-Q_r$ is plotted versus $\theta = [\tau^{1/2} + (t- \tau)^{1/2} - t^{1/2}]$, there will be two straight lines which intersects each other at Q=0 axis with equal slope, if there is no adsorption of reactant or product. Any deviation from such condition means adsorption. Such plots for both the pair of peaks and at all the concentrations are shown in the Figures 6.2.51 and 6.2.52. This shows that the plots Q vs $t^{1/2}$ and $-Q_r$ vs θ do not intersect each other at Q=0 axis.

Moreover they do not have equal slopes. Therefore from this plot, it may be said that adsorption of reactant or products occur on the electrode.

Therefore the findings from the Chronoamperometric study is that after compound formation the spike height is decreased, indicating towards a decrease in the rate of electrolysis. And from the Chronocoulometric study, it is observed that the charge at τ are decreased in all the cases. Both of these facts combinedly indicates towards successful compound formation.

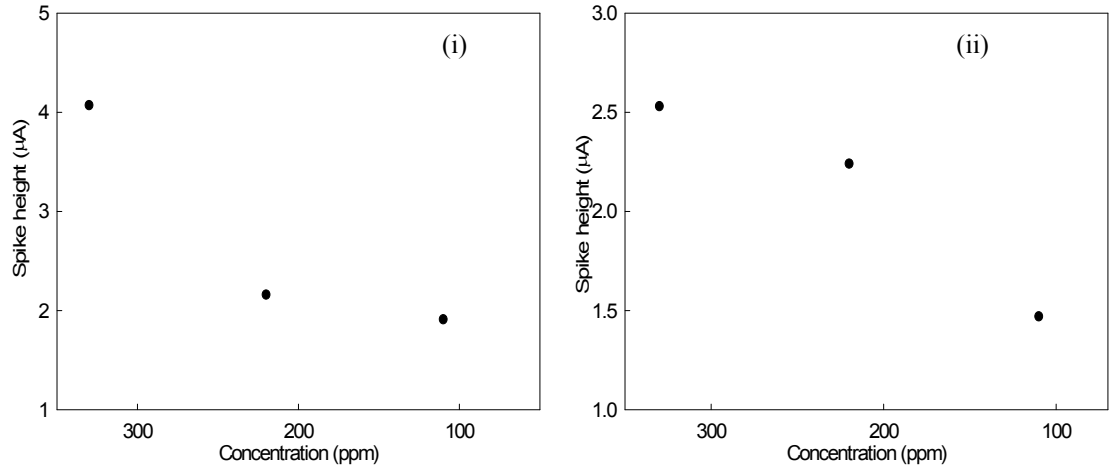

Fig 6.2.46 Concentration effect of Mn(II)-Ciprofloxacin compound on spike height of Chronoamperometry for (i) first pair and (b) second pair of peaks.

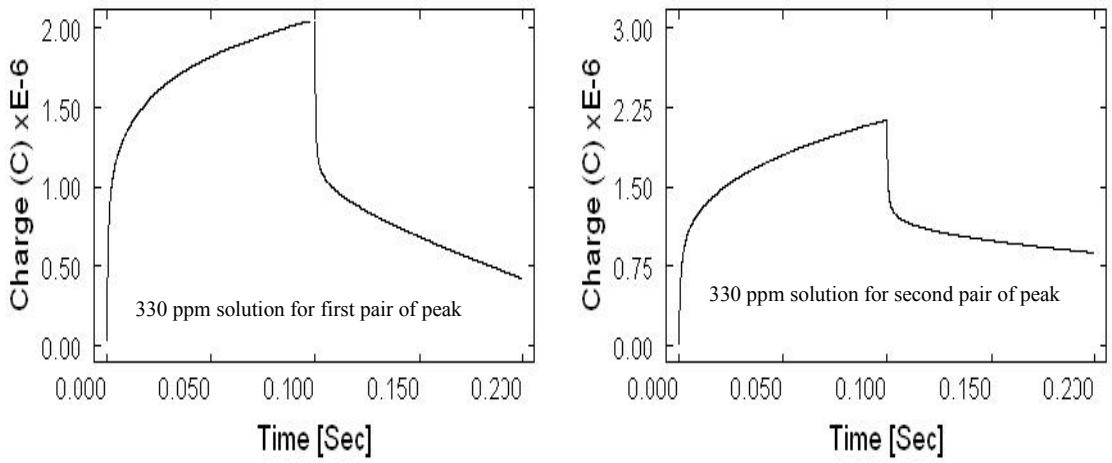

Fig 6.2.47 Charge responses for Mn(II)-Ciprofloxacin compound for first and second pair of peaks in 330 ppm solution.

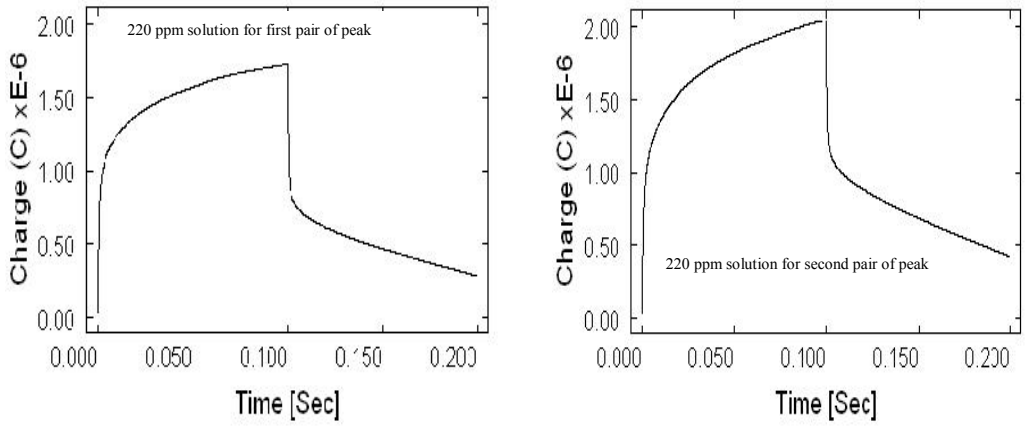

Fig 6.2.48 Charge responses for Mn(II)-Ciprofloxacin compound for first and second pair of peaks in 220 ppm solution.

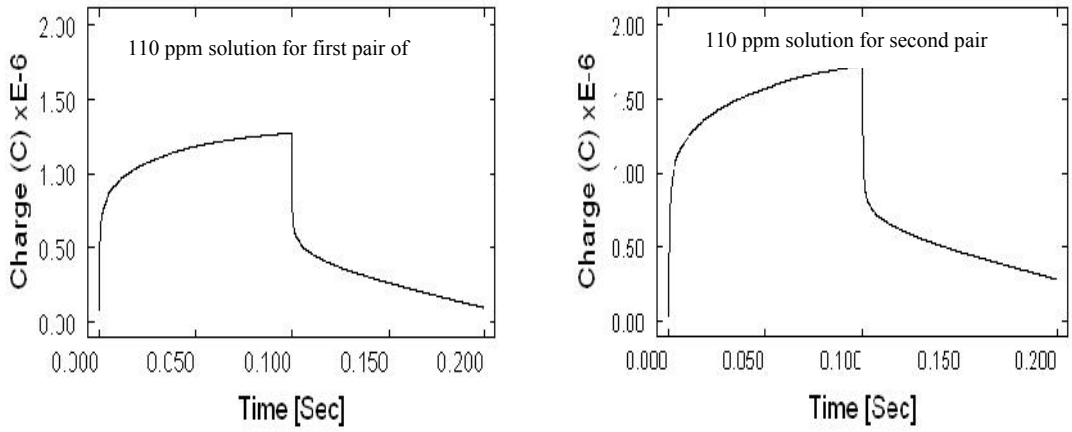

Fig 6.2.49 Charge responses for Mn(II)-Ciprofloxacin compound for first and second pair of peaks in 110 ppm solution.

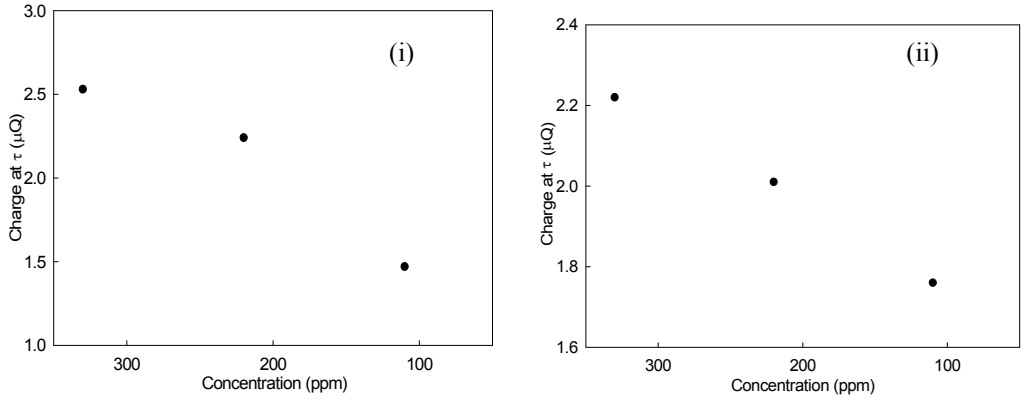

Fig 6.2.50 Concentration effect of Mn(II)-Ciprofloxacin compound on charge at τ of Chronocoulometry for (i) first pair and (ii) second pair of peaks.

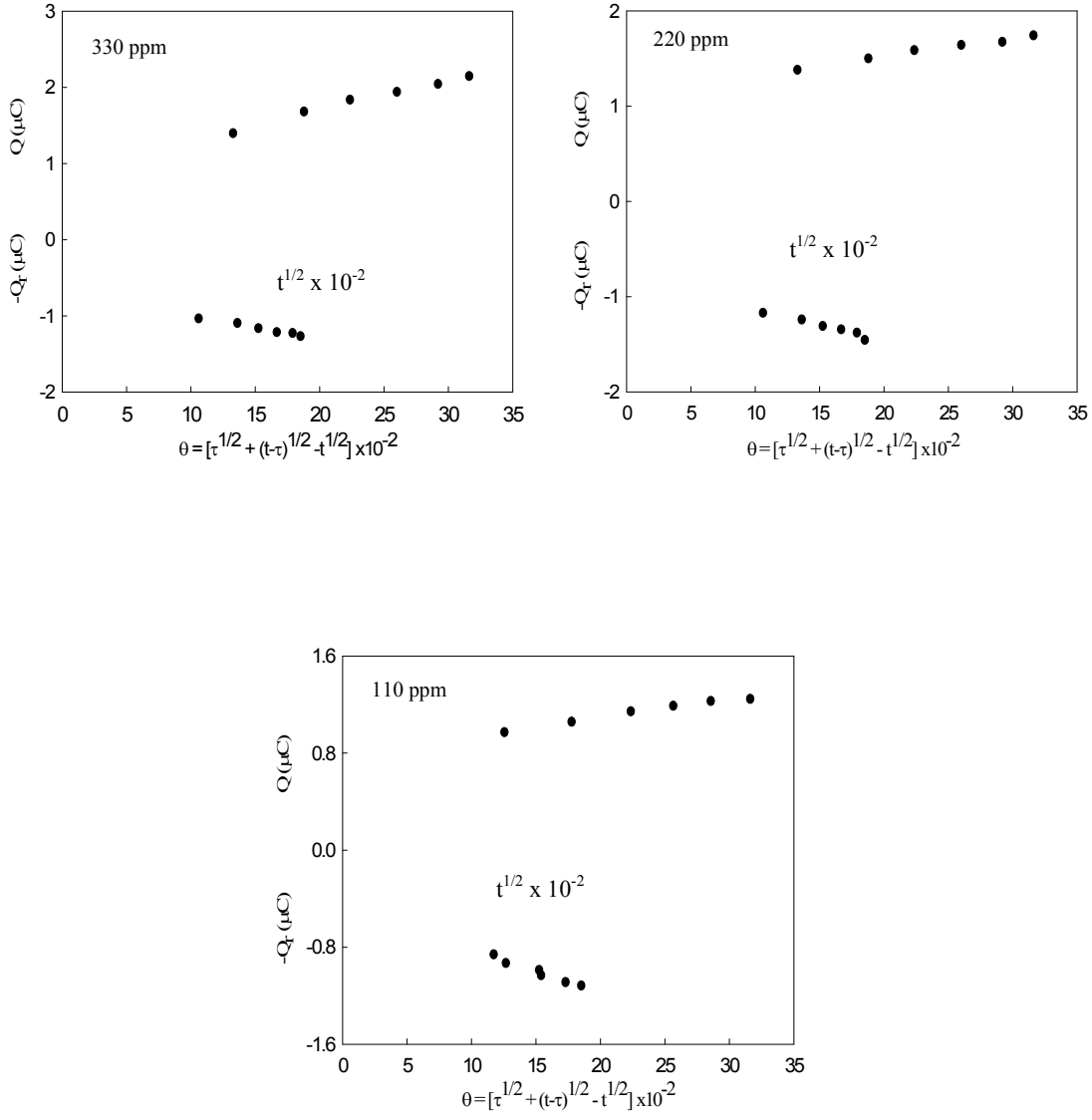

Fig 6.2.51 Plots of Q vs $t^{1/2}$ and $-Q_r$ vs θ for Mn(II)-Ciprofloxacin compound in 0.1 M KCl solution for first pair of peaks at different concentrations.

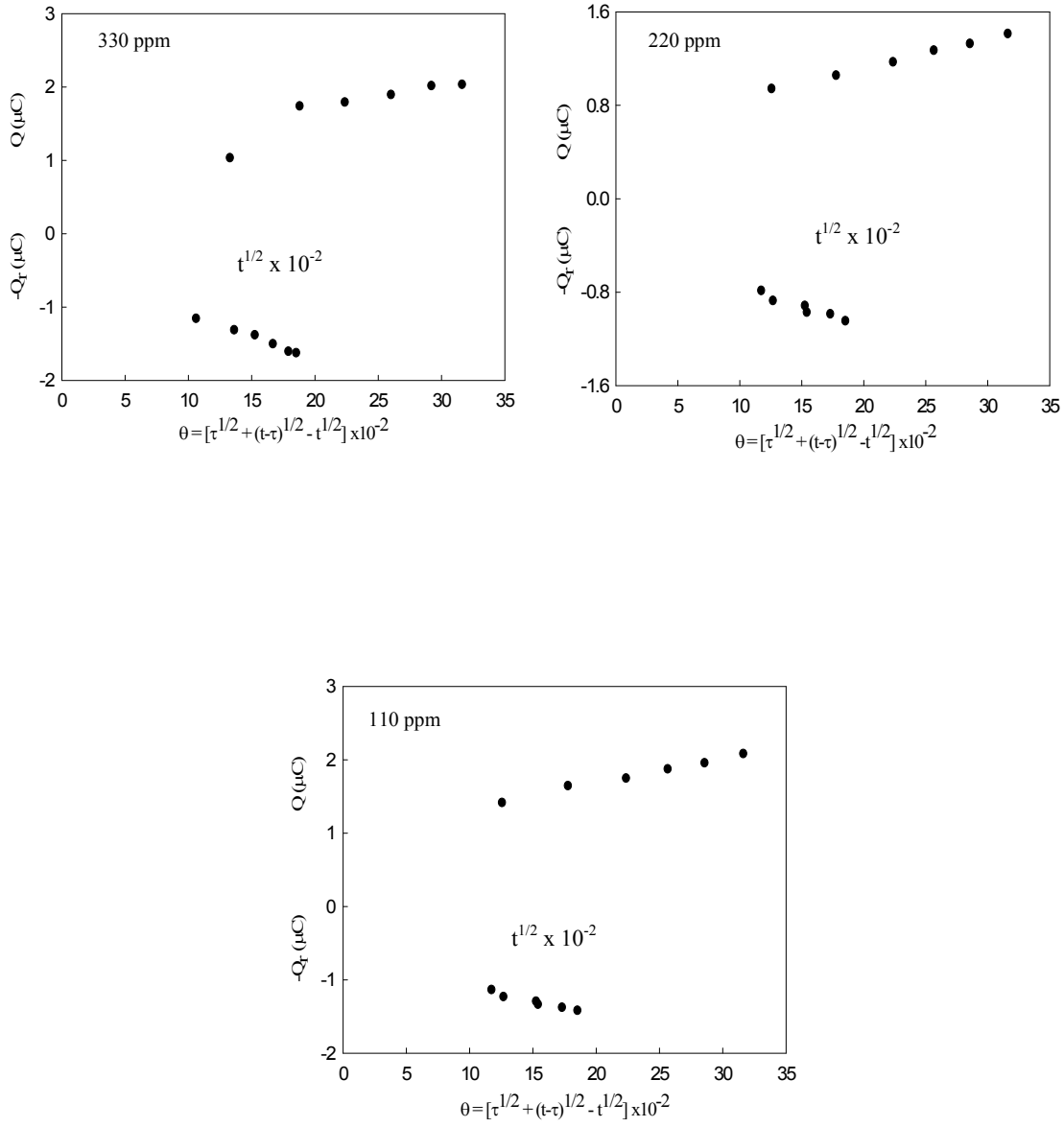

Fig 6.2.52 Plots of Q vs $t^{1/2}$ and $-Q_r$ vs θ for Mn(II)-Ciprofloxacin compound in 0.1 M KCl solution for second pair of peaks at different concentrations.

And the observations from the plots Q vs $t^{1/2}$ and $-Q_r$ vs θ gives conclusion that adsorption of reactant or products occur on the electrode also after compound formation.

6.2.5 Cyclic voltammetric study of Zn(II)-Ciprofloxacin Compound at Glassy Carbon Electrode (GCE).

Redox behavior of Zn(II)-Ciprofloxacin compound

The redox behaviour of Zn(II)-Ciprofloxacin Compound (215.42 ppm solution) in 0.1M potassium chloride and at varying scan rate was studied using cyclic voltammetric technique within the potential window from -1.500 V to 2.000 V at room temperature at glassy carbon electrode (GCE). A CV of the above system at scan rate 0.100 Vs^{-1} is given in Fig 6.2.53.

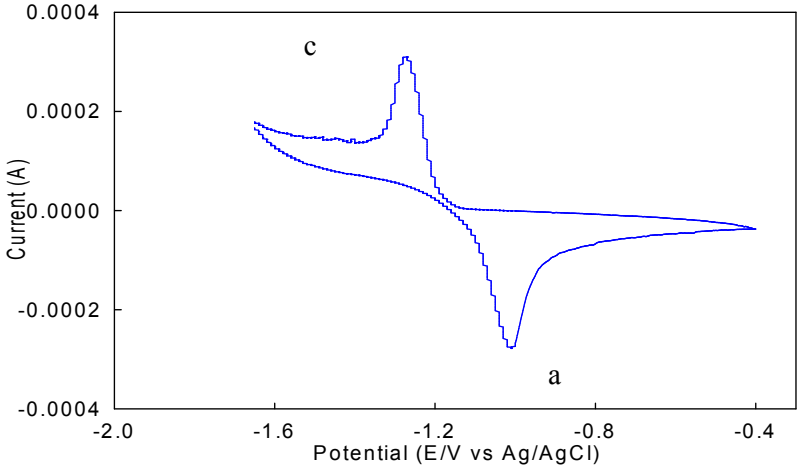

Fig 6.2.53 Cyclic voltammogram of Zn(II)-Ciprofloxacin Compound (215.42 ppm solution) in 0.1 M KCl at scan rate 0.100 Vs^{-1}.

The CV shows one cathodic peaks at the potential of -1.259 V and in the anodic region one peak at -1.029V. Compared to the Zn(II), it is found that the cathodic peak moves towards less negative potential and the anodic one towards more negative potential. The shape of the peaks are also changed (Fig 6.2.54). These have become sharper. Both of these facts indicate towards successful compound formation. In the case of Zn(II)-Ciprofloxacin interaction, also same number of peaks are found.

Fig 6.2.55 shows the voltammograms of Zn(II)-Ciprofloxacin compound at different scan rates. It shows that with the increase in scan rate the first cathodic peak shifts towards

more negative potential. In the anodic region, the peak moves towards less negative potential with increasing scan rate. Moreover, with the increase in scan rate, almost all the peaks become broader. Such behavior has been ascribed to slower charge propagation, probably due to difference in salvation and or permeability. Current-potential data for the system under consideration is recorded in Table 6.2.5.

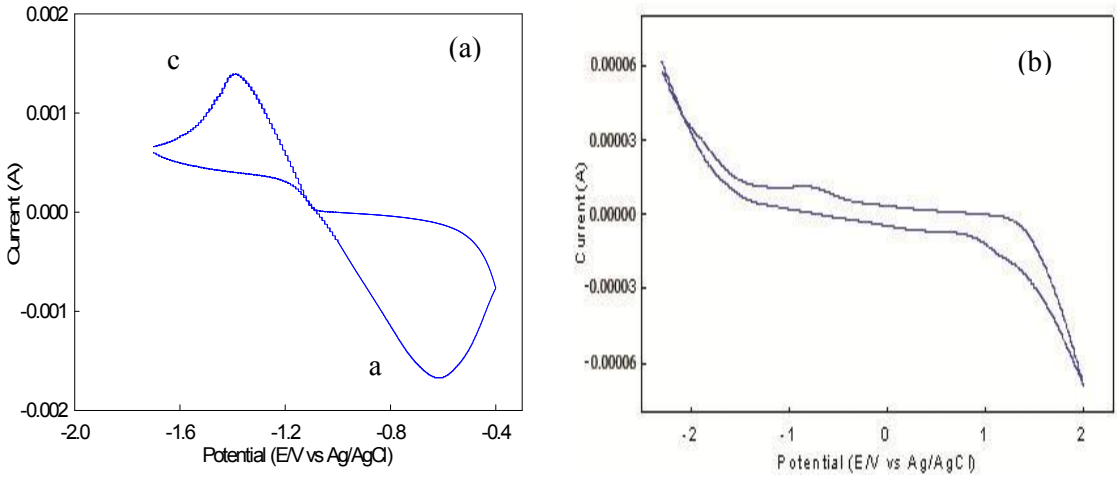

Fig 6.2.54 Cyclic voltammograms of (a) Zn(II) and (b) Ciprofloxacin before Compound formation in 0.1 M KCl at scan rate 0.100 Vs^{-1}

It is evident that after compound formation, the peak separation becomes less. But the trend is similar (with no exception) to the Zn(II) system. The peak separation potential for the pair of peaks (ΔE_p) increases with the increase in scan rate as the cathodic peak

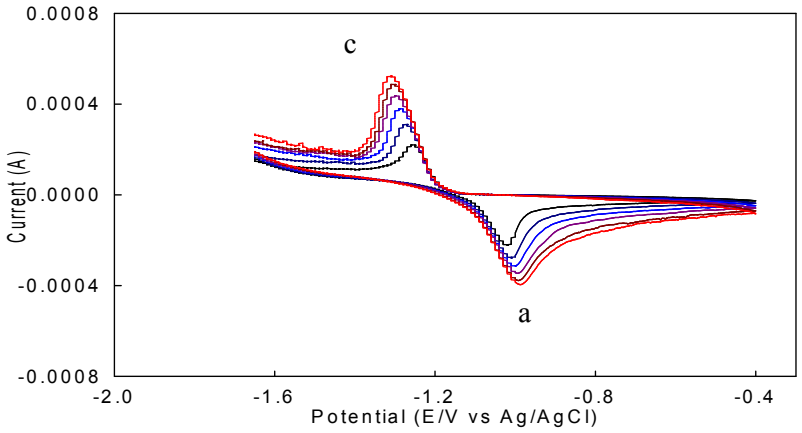

Fig 6.2.55 Cyclic voltammogram of Zn(II)-Ciprofloxacin Compound (215.42 Ppm solution) in 0.1 M KCl at different scan rates.

Table 6.2.5 Current-potential data for Zn(II)-Ciprofloxacin compound (215.42 ppm solution) in 0.1 M KCl solution at different scan rates.

Scan rate ν (Vs^{-1})	SQRT of scan rate	Cathodic peak potential E_{pc} (V) [-]	Anodic peak potential E_{pa} (V) [-]	Cathodic peak current i_{pc} (μA)	Anodic peak current i_{pa} (μA) [-]	Peak potential separation $\Delta E_p = E_{pa} - E_{pc}$ (V)	Peak current ratio i_{pa}/ i_{pc}
0.050	0.2236	1.233	1.071	105.24	130.58	0.162	1.24
0.100	0.3162	1.259	1.059	127.58	157.22	0.200	1.23
0.150	0.3872	1.271	1.043	156.11	170.52	0.228	1.09
0.200	0.4472	1.292	1.026	210.15	184.48	0.266	0.88
0.250	0.5000	1.304	1.018	240.74	191.21	0.286	0.79
0.300	0.5477	1.336	0.967	290.81	214.37	0.369	0.74

shifts towards negative and that of anodic towards less negative potential. Here the cause responsible is the effect of iR drop. Therefore it may be said that the above system indicate the limitation due to charge transfer kinetics and is shown in the plot of ΔE_p vs ν in Fig 6.2.56(a).

Again the forward scan peak current (i_{pc}) is proportional to the square root of the scan rate at all the scan rates, which means the system to be diffusion controlled. Moreover with increasing $\nu^{1/2}$, the peak currents for both cathodic and anodic peaks increases linearly (Fig 6.2.56(b)), giving the conclusion that the process is adsorptive controlled[35, 99] .

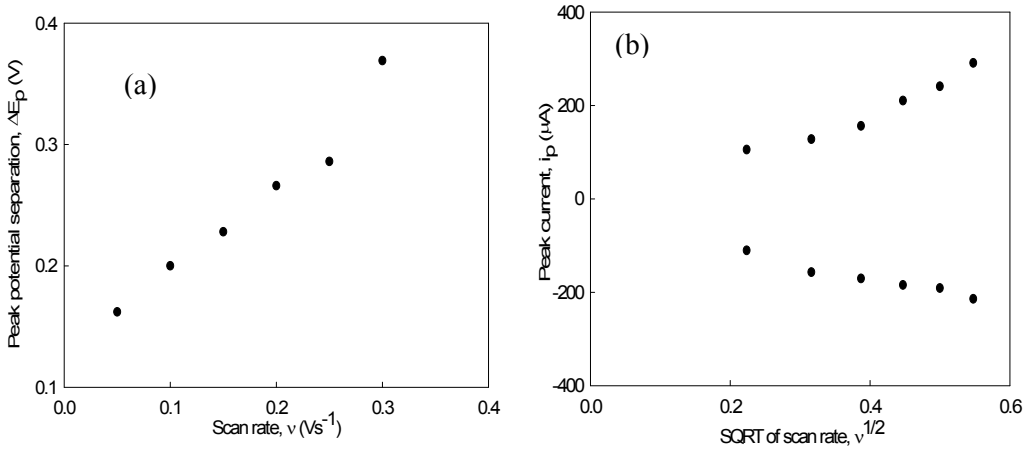

Fig 6.2.56 Variation of (a) peak potential separation with scan rate and (b) peak current with square root of scan rate for Zn(II)-Ciprofloxacin compound in 0.1 M KCl solution.

The peak current ratio for the pair of peaks are less than (or nearest to) unity at higher scan rates and at lower scan rates it is more than (or nearest to) unity. Therefore it may said that system shows exception to some extent from reversible behavior, or it may be quasi-reversible[101, 102].

The peak current ratio decreases with increasing scan rates (Fig 6.2.57(a)). Again peak current function ($i_{pc1}/\nu^{1/2}$) decreases with increasing scan rate upto 0.150 Vs^{-1} and then increases (Fig 6.2.57(b)). Therefore, it does not indicate any clear conception about the electrochemical process.

The plot of log i_p against log ν shows a linear relationship. It is found that in this case the slope is less than unity. Therefore it may be said that the process is accompanied by diffusion[3, 112] (Fig 6.2.58(a)).

Tafel plot (peak potential vs log ν) for the pair of peaks is shown in Fig 6.2.58(b). The curve express that the slope of the Tafel plot is not zero. So the electrochemical process will be different from reversible behaviour

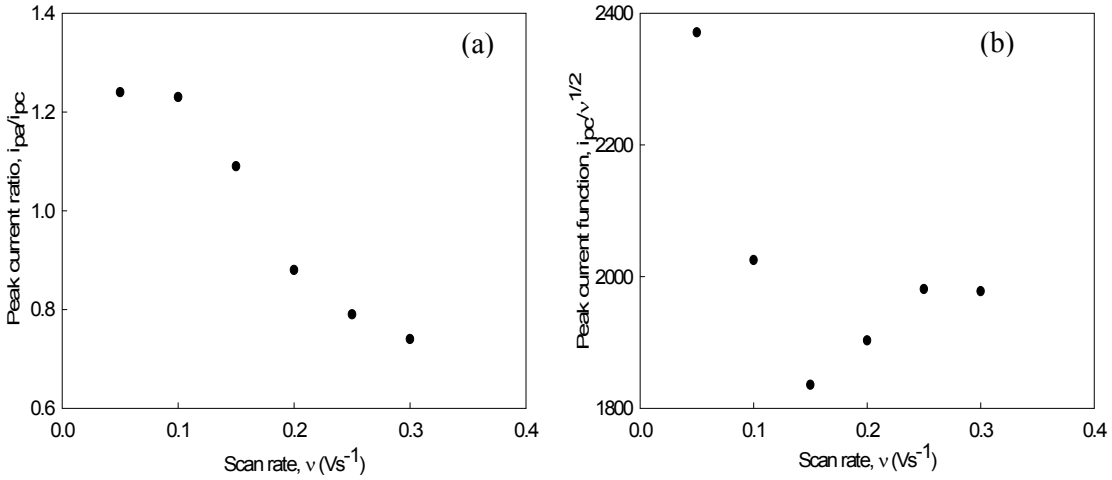

Fig 6.2.57 Variation of (a) peak current ratio (b) peak current function with scan rate for Zn(II)-Ciprofloxacin Compound in 0.1 M KCl solution.

Therefore from the above discussions there are some findings, such as: i) peak potential shifts with scan rate, ii) peak current ratio is not equal to unity, iii) the current function $i_p/\nu^{1/2}$ is independent of scan rate, iv) peak response broadens as scan rate increases, v) slope of Tafel plot is not equal to zero.

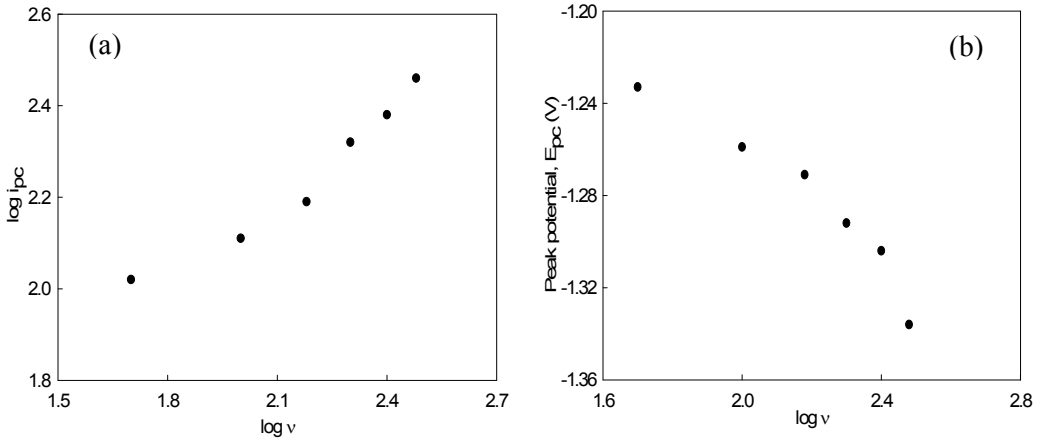

Fig 6.2.58 Plots of (a) log i_{pc1} and (b) peak potential with log ν for Zn(II)-Ciprofloxacin Compound in 0.1 M KCl solution.

Considering all the above points it can be concluded that the electrochemical process involved in Zn(II) is quasi-reversible. The electrochemical reactions of the Zn(II)/Zn(0) system under investigation may be written as:

$$\text{Zn(II)ciprofloxacin} \underset{-2e}{\overset{+2e}{\rightleftharpoons}} \text{Zn(0)ciprofloxacin}$$

Moreover, the system is diffusion controlled as well as adsorptive controlled, which can be declared from the facts that a) in the forward scans, peak currents are proportional to the square root of scan rate, b) peak currents in both the regions (cathodic and anodic) increases linearly with square root of scan rate, c) slope of log i_p against log ν plot is more than unity.

Concentration effect of Zn(II)-Ciprofloxacin Compound

Study on the concentration effect of Zn(II)-Ciprofloxacin compound was also accomplished. This observation was done using three different concentrations (71.81, 143.61 and 215.42 ppm) of Zn(II)-Ciprofloxacin compound and maintaining the same environment as previous. The CVs are overlapped in the Fig 6.2.59 and the parameters are recorded in Table 6.2.6.

The peak current for all the peaks show a gradual increase with increasing concentrations

(Table 6.2.6) and a graphical presentation is given in Fig 6.2.60. Again it is also known that the greater the peak current, higher will be the charge acceptance of the electrode. This linear nature of the peak current with concentrations of the compound indicate that the processes are diffusion controlled.

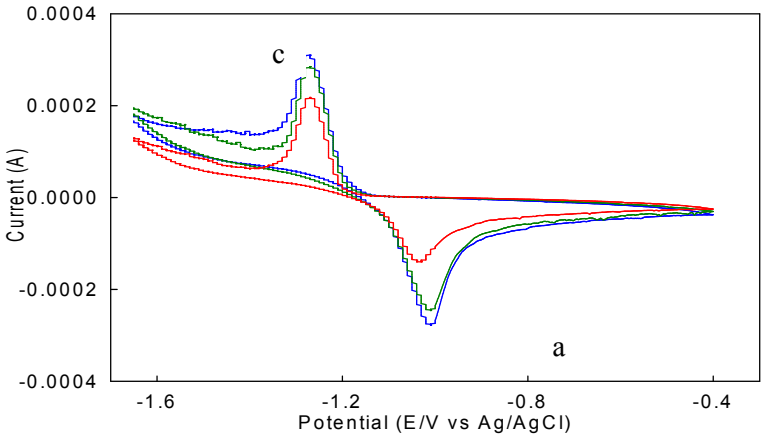

Fig 6.2.59 Cyclic voltammograms of Zn(II)-Ciprofloxacin Compound (at scan rate 0.100 Vs^{-1}) of different concentrations in 0.1 M KCl.

Table 6.2.6 Current-potential data for Zn(II)-Ciprofloxacin compound (at scan rate 0.100 Vs^{-1}) in 0.1 M KCl solution at different concentrations.

Concentration ppm	Anodic peak potential (E_{pa}) V[-]	Cathodic peak potential (E_{pc}) V[-]	Anodic peak current (i_{pa}) μA[-]	Cathodic peak current (i_{pc}) μA
71.81	1.131	1.257	087.27	124.84
143.61	1.099	1.258	123.51	125.67
215.42	1.059	1.259	157.22	127.58

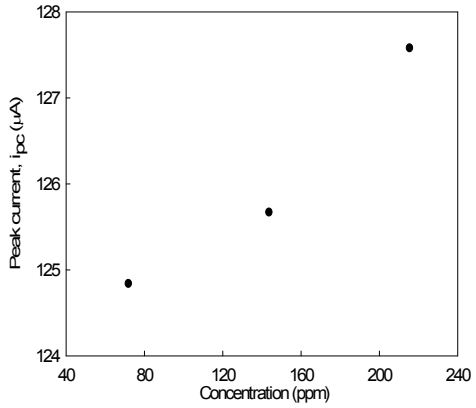

Fig 6.2.60 Variation of peak current with concentration of Zn(II)-Ciprofloxacin Compoud in 0.1 M KCl solution.

6.2.6 Chronoamperometric and chronocoulometric study of Zn(II)-Ciprofloxacin Compound

CA and CC study of Zn(II)-Ciprofloxacin Compound

Zn(II) system was also studied chronoamperometrically after compound formation with Ciprofloxacin. This study was done using 215.42 ppm solution of Zn(II)-Ciprofloxacin compound. After compound formation, there is one signal in the cathodic and also in the anodic region, which is very much similar to those of Zn(II) before compound formation. And the CA study was also done for that pair of peaks. The chroamperogram is shown in the Fig 6.2.61.

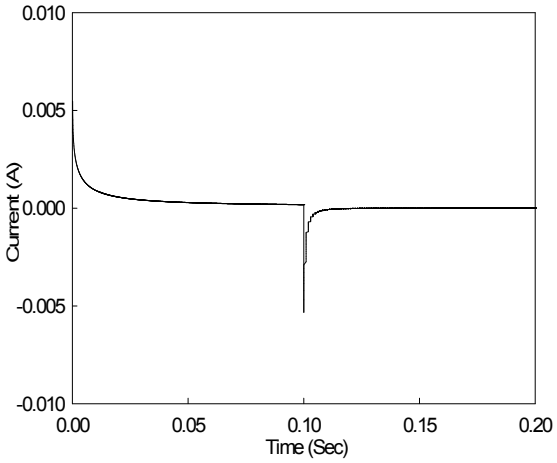

Fig 6.2.61 Current response for Zn(II)-Ciprofloxacin Compound (215.42 ppm solution) in 0.1 M KCl solution.

It is found that the spike height after compound formation with Ciprofloxacin is decreased (Fig 6.2.62) compared to that of Zn(II) before compound formation with Ciprofloxacin. Since the spike height is proportional to the rate of electrolysis, this means that after interaction the rate of electrolysis has been decreased.

It is known that chronocoulometry (CC) is the integrated form of the chronoamperometry. So that in CC the monitored response is charge. It is termed as chronocoulogram. Such charge responses for the pair of peak in case of Zn(II)-Ciprofloxacin compound is shown in Fig 6.2.63.

Chronocoulometric response (Fig 6.2.63) shows that the charge at τ is decreased after compound formation with Ciprofloxacin. It was 4.659 μC in the absence of Ciprofloxacin, whereas it becomes 2.351 μC after compound formation with Ciprofloxacin.

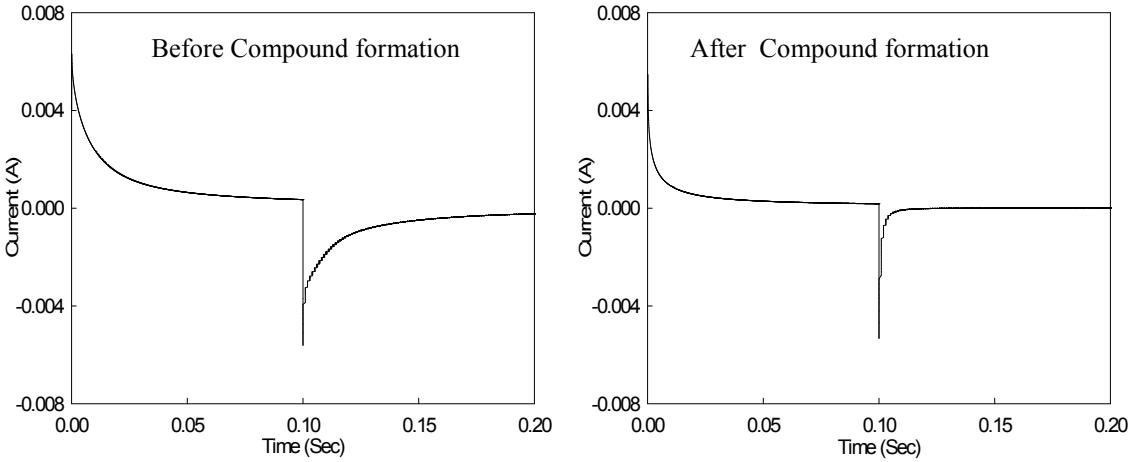

Fig 6.2.62 Current responses for Zn(II) in 0.1 M KCl solution before and after compound formation . with Ciprofloxacin for first pair of peaks.

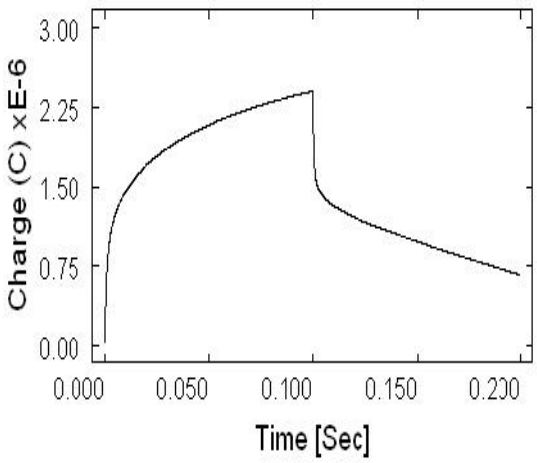

Fig 6.2.63 Charge response for Zn(II)-Ciprofloxacin Compound (215.42 ppm solution) in 0.1 M KCl solution.

Now if Q value obtained from time less than τ is plotted versus $t^{1/2}$ and on the same graph $-Q_r$ is plotted versus $\theta = [\tau^{1/2} + (t- \tau)^{1/2} - t^{1/2}]$, there will be two straight lines which intersects each other at Q=0 axis with equal slope, if there is no adsorption of reactant or product. Any deviation from such condition means adsorption. Such plots are shown in the Fig 6.2.64. This shows that the plots Q vs $t^{1/2}$ and $-Q_r$ vs θ do not intersect each other at Q=0 axis.

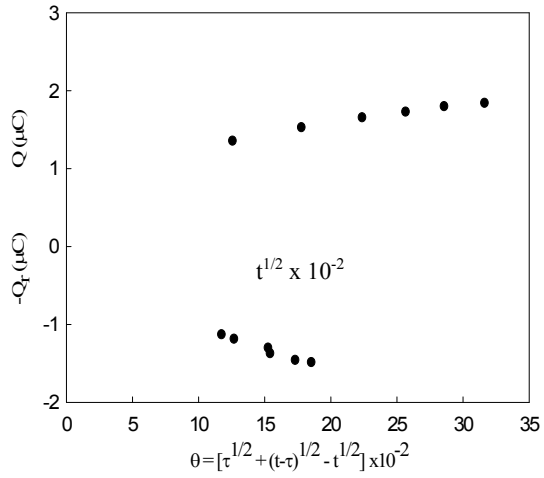

Fig 6.2.64 Plots of Q vs $t^{1/2}$ and $-Q_r$ vs θ for Zn(II)-Ciprofloxacin compound (215.42 ppm solution) in 0.1 M KCl solution.

Moreover they do not have equal slopes. Therefore from this plot, it may be said that adsorption of reactant or products occur on the electrode.

Therefore the findings from the Chronoamperometric study is that after compound formation the spike height is decreased, indicating towards a decrease in the rate of electrolysis. And from the Chronocoulometric study, it is observed that the charge at τ is decreased after compound formation. Both of these facts combinedly indicates towards successful complexation. And the observations from the plots Q vs $t^{1/2}$ and $-Q_r$ vs θ gives conclusion that adsorption of reactant or products occur on the electrode also after compound formation.

Concentration Effect

The concentration effect of Zn(II)-Ciprofloxacin compound was also studied by Chronoamperometric as well as chronocoulometric method. This observation was done using three different concentrations (215.42, 143.61 and 71.81 ppm) of Zn(II)-Ciprofloxacin compound and maintaining the same environment as previous. The CA is shown in Fig 6.2.65. It is observed that with the decrease in concentration of the compound solution the spike height decreases for both the pair of peaks. This fact

indicates that as the concentration decreases, the number of electroactive species are decreased.

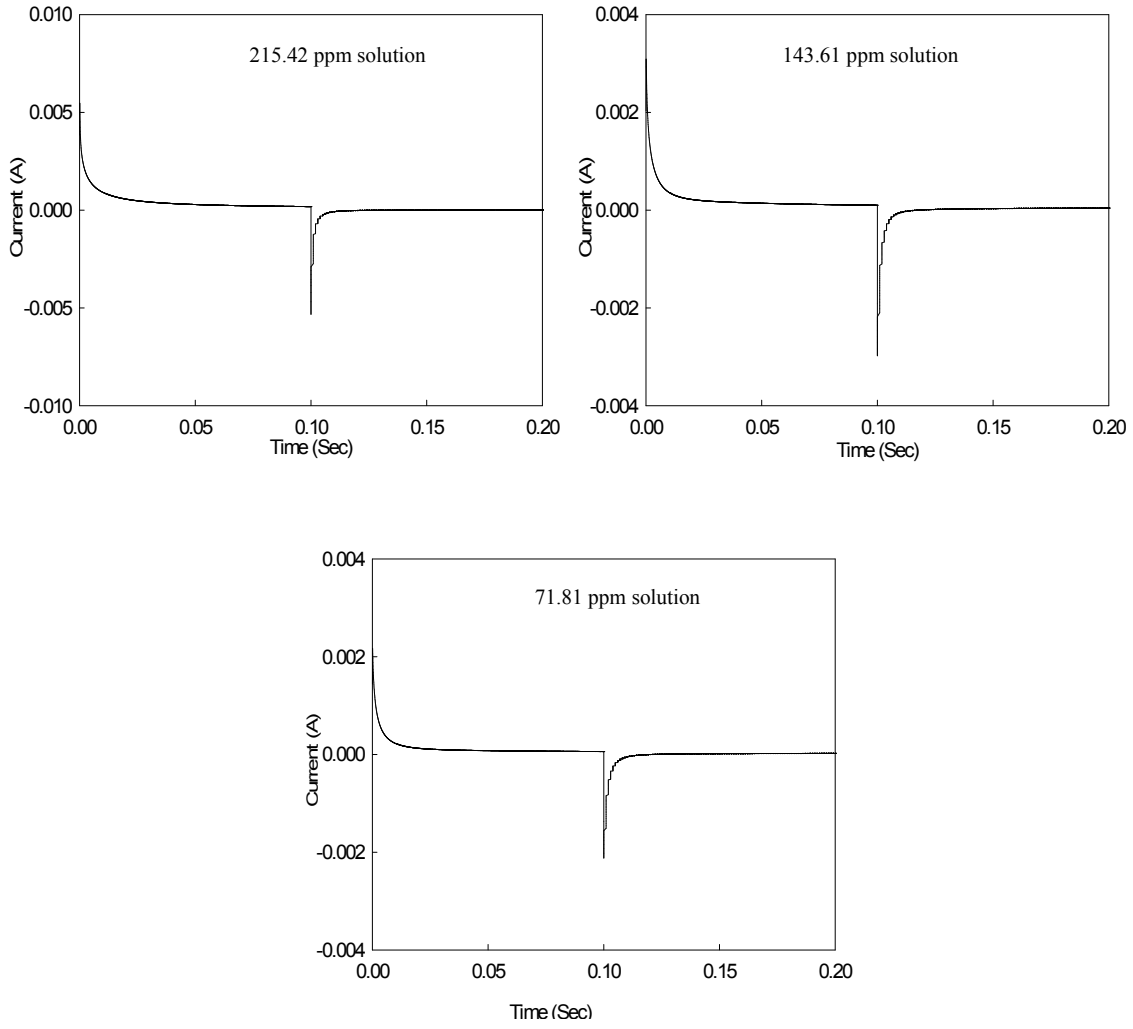

Fig 6.2.65 Current responses for Zn(II)-Ciprofloxacin compound at different concentrations.

As a result the rate of electrolysis also decreases. Therefore it may be concluded that as the the concentration decreases the rate of electrolysis is decreased. A graphical representation of this fact is shown in Fig 6.2.66.

Again Chronocoulometry (CC), which is the integrated form of the chronoamperometry is also examined. Such charge response corresponding to the chronoamperogram is shown in Fig 6.2.67.

Here it is also found that with the decrease in compound concentrations, the charge at τ is decreased. The fact behind this is that with the decrease in concentration the number of charged species are also decreased. As a result the charge decreases with decreasing concentration of the compound solution. This can also be represented graphically in Fig 6.2.68.

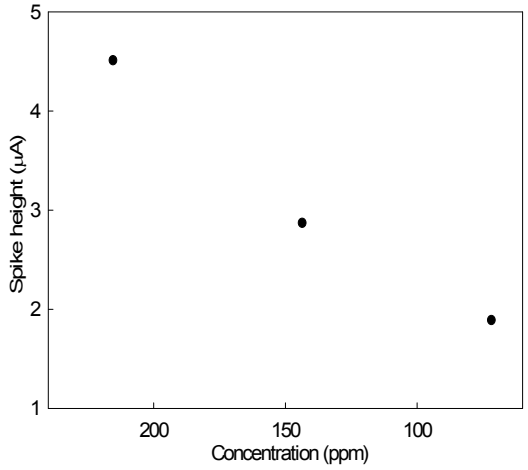

Fig 6.2.66 Concentration effect of Zn(II)-Ciprofloxacin compound on spike height of Chronoamperometry.

Now if Q value obtained from time less than τ is plotted versus $t^{1/2}$ and on the same graph $-Q_r$ is plotted versus $\theta = [\tau^{1/2} + (t- \tau)^{1/2} - t^{1/2}]$, there will be two straight lines which intersects each other at Q=0 axis with equal slope, if there is no adsorption of reactant or product. Any deviation from such condition means adsorption. Such plots for both the pair of peaks and at all the concentrations are shown in the Fig 6.2.69.

This shows that the plots Q vs $t^{1/2}$ and $-Q_r$ vs θ do not intersect each other at Q=0 axis. Moreover they do not have equal slopes. Therefore from this plot, it may be said that adsorption of reactant or products occur on the electrode.

Therefore the findings from the Chronoamperometric study is that after compound formation the spike height is decreased, indicating towards a decrease in the rate of electrolysis. And from the Chronocoulometric study, it is observed that the charge at τ are decreased in all the cases. Both of these facts combinedly indicates towards successful

compound formation. And the observations from the plots Q vs $t^{1/2}$ and $-Q_r$ vs θ gives conclusion that adsorption of reactant or products occur on the electrode also after compound formation.

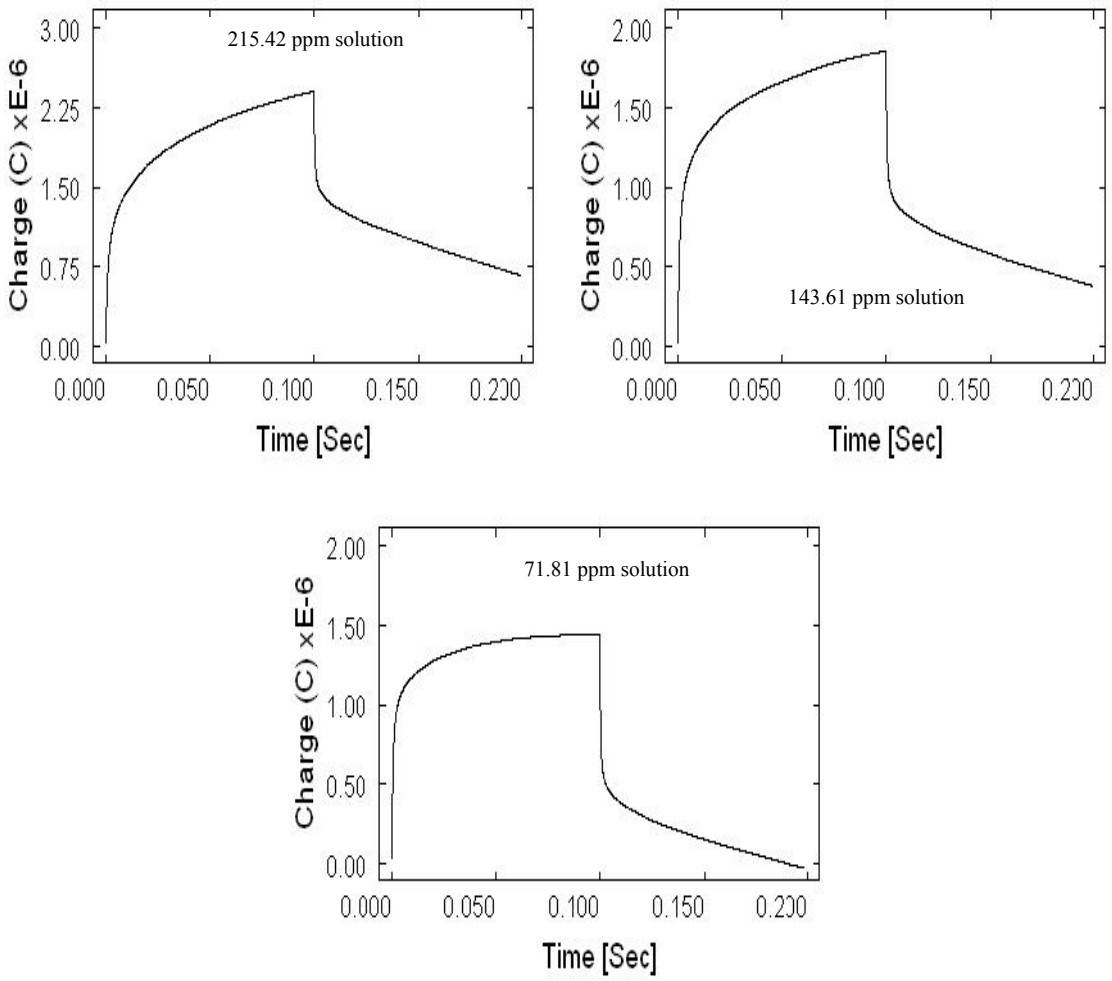

Fig 6.2.67 Charge responses for Zn(II)-Ciprofloxacin compound at different concentrations.

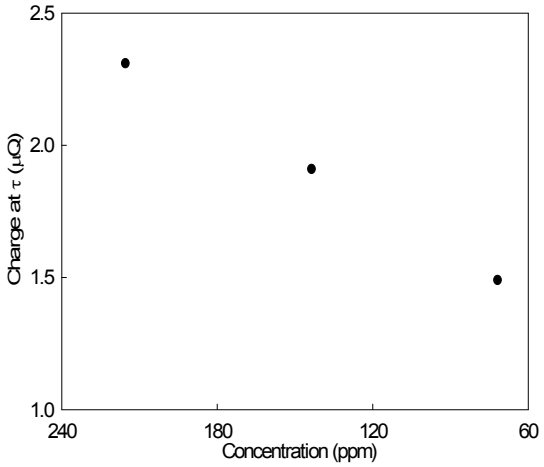

Fig 6.2.68 Concentration effect of Zn(II)-Ciprofloxacin compound on charge at τ of Chronocoulometry.

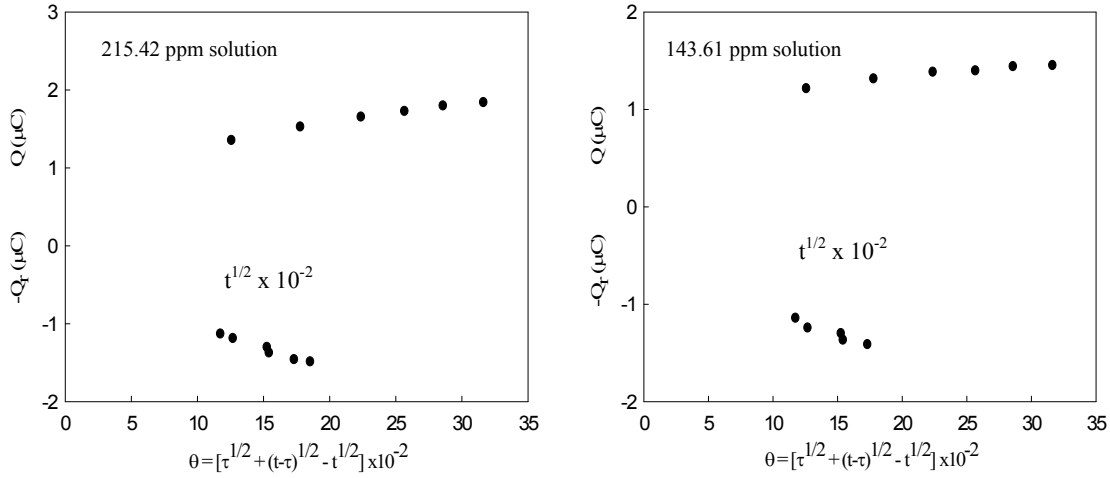

Fig 6.2.69(a) Plots of Q vs $t^{1/2}$ and $-Q_r$ vs θ for Zn(II)-Ciprofloxacin compound in 0.1 M KCl solution at different concentrations(215.42 ppm and 143.61 ppm).

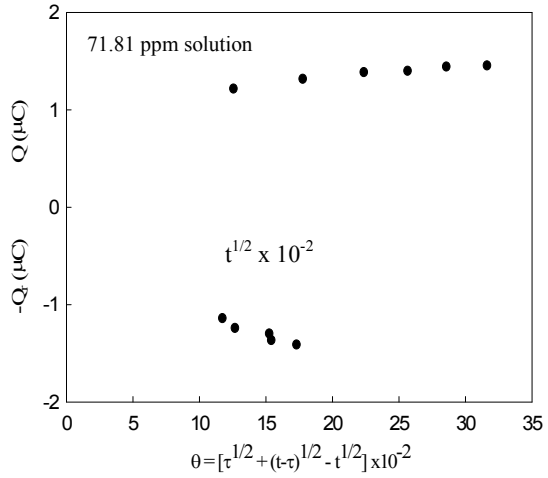

Fig 6.2.69(b) Plots of Q vs $t^{1/2}$ and $-Q_r$ vs θ for Zn(II)-Ciprofloxacin compound in 0.1 M KCl solution at 71.81 ppm.

6.2.7 Cyclic voltammetric study of Cr(III)-Ciprofloxacin Compound at Platinum Electrode

The Cyclic voltammetric study of Cr(III)-Ciprofloxacin compound was observed in some modified environment. This present study was also accomplished in saturated potassium chloride and using Platinum electrode as working electrode.

Redox behavior of Cr(III)-Ciprofloxacin compound

The redox behaviour of Cr(III)-Ciprofloxacin Compound (50 ppm solution) in saturated potassium chloride and at varying scan rate was studied using cyclic voltammetric technique within the potential window from -1.000 V to 1.700 V at room temperature at Platinum electrode. A CV of the above system at scan rate 0.100 Vs^{-1} is given in Fig 6.2.70.

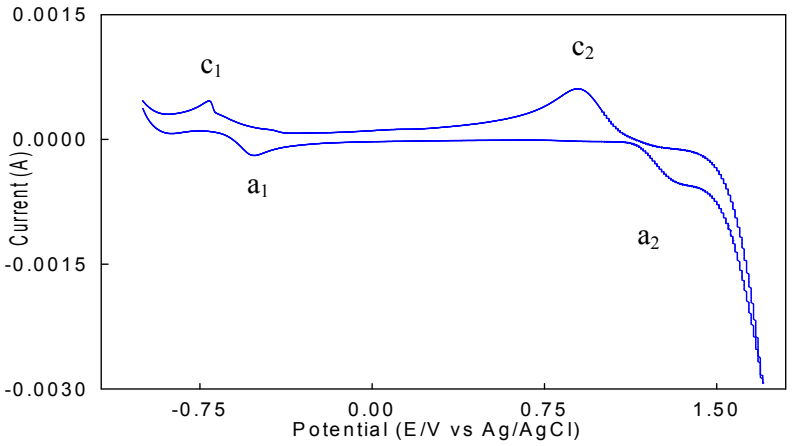

Fig 6.2.70 Cyclic voltammogram of Cr(III)-Ciprofloxacin Compound (50 ppm solution) in saturated KCl at scan rate 0.100 Vs^{-1}.

The CV shows two cathodic peaks (c_1 and c_2) at potentials of -0.698 V and 0.886 V and in the anodic region also two peaks (a_1 and a_2) at -0.515 V and 1.367 V. The first cathodic peak and the anodic one may be due to the ligand (Ciprofloxacin) and the second cathodic as well as anodic peak together represent the metallic part (Cr(III)). Compared to the CV of Cr(III), it is found that after compound formation referred to Cr(III) the cathodic as well as the anodic peak shift towards less positive potential (Fig 6.2.71).

Therefore it is found that after compound formation the number of peaks as well as their position has been changed. These facts indicates towards successful compound formation.

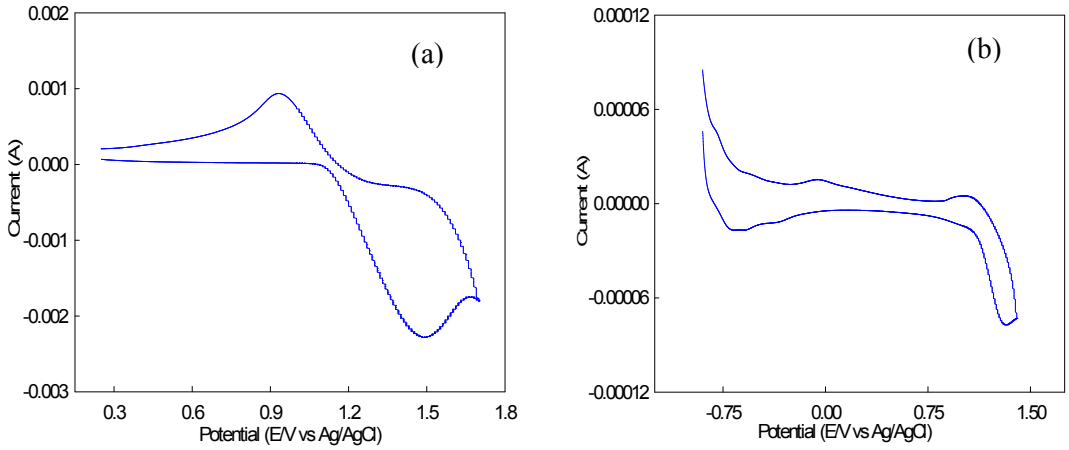

Fig 6.2.71 Cyclic voltammogram of (a) Cr(III) (b) Ciprofloxacin in saturated KCl at scan rate 100 mVs^{-1}

In case of Cr(II)-Ciprofloxacin interaction there were three peaks in the cathodic region and two in the anodic region. Fig 6.2.72 shows the voltammograms of Cr(III)-ciprofloxacin complex at different scan rates. It shows that with the increase in scan rate the first cathodic peak (c_1) shifts towards more negative potential. Similar is the case for the second cathodic peak (c_2). In the anodic region, the peaks (a_1 and a_2) moves towards

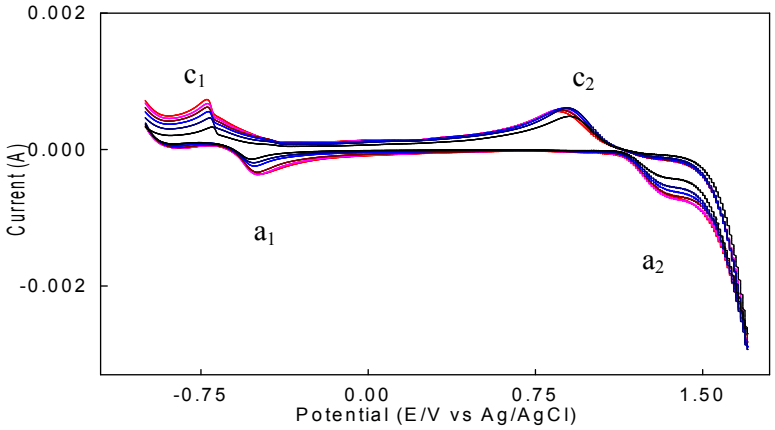

Fig 6.2.72 Cyclic voltammogram of Cr(III)-Ciprofloxacin Compound (50 ppm solution) in saturated KCl at different scan rates.

less negative (or more positive) potential with increasing scan rate. Moreover, with the increase in scan rate, almost all the peaks become broader. Such behavior has been

ascribed to slower charge propagation, probably due to difference in salvation and or permeability.

As the comperative study with the CV of Ciprofloxacin implies that the second pair of peak originates from the metallic (Cr(III)) part. And for that reason all the graphical presentation was done for that pair of peaks. Current-potential data for the system under consideration is recorded in Table 6.2.7.

It is evident that after compound formation, the peak separation becomes less. The peak potential separation (ΔE_{p2}) for both the second pair of peaks increases with the increase in scan rate (with an exception at the highest scan rate). The bevaviour is similar (with no exception) to the uncoordinated chromium itself. Therefore it may be said that the above system indicate the limitation due to charge transfer kinetics and are shown in Fig 6.2.73(a).

Again the forward scan peak currents (i_{pc2}) are proportional to the square root of the scan rate at all scan rates, which means the system to be diffusion controlled. Moreover with increasing $\nu^{1/2}$, the peak currents for both cathodic and anodic peaks as well as for both the pairs increase linearly (Fig 6.2.73(b)), giving the conclusion that the processes are adsorptive controlled .

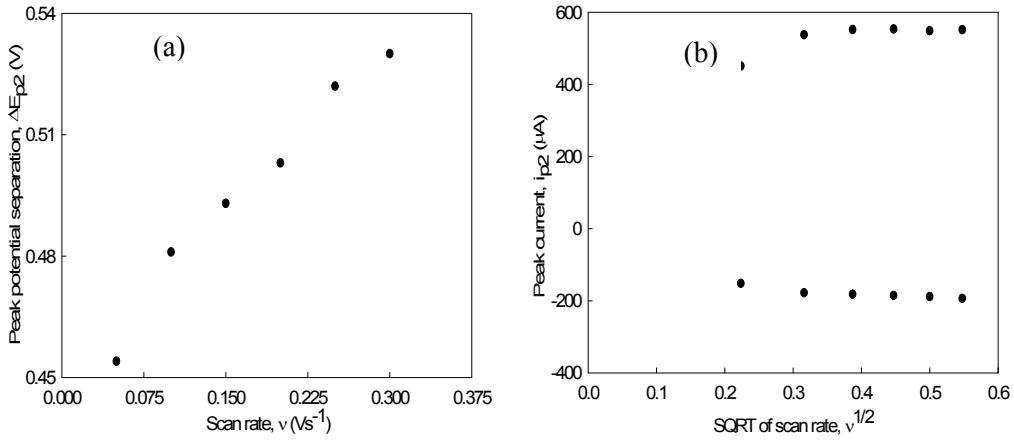

Fig 6.2.73 Variation of (a) peak separation potential with scan rate and (b) peak current with square root of scan rate for Cr(III)-Ciprofloxacin Compound in saturated KCl solution.

Table 6.2.7 Current-potential data for Cr(III)-Ciprofloxacin compound (50 ppm solution) in saturated KCl solution at different scan rates.

Scan rate ν (Vs^{-1})	SQRT of scan rate	Cathodic peak potential E_{pc1} (V) [-]	Anodic peak potential E_{pa1} (V) [-]	Cathodic peak current i_{pc1} (μA)	Anodic peak current i_{pa1} (μA) [-]	Peak potential separation $\Delta E_{p1}= E_{pa1}- E_{pc1}$ (V)	Peak current ratio i_{pa1}/ i_{pc1}
0.050	0.2236	0.687	0.521	155.02	162.51	0.166	1.04
0.100	0.3162	0.698	0.515	192.24	200.18	0.183	1.04
0.150	0.3872	0.710	0.510	215.42	225.64	0.200	1.05
0.200	0.4472	0.712	0.498	240.41	317.54	0.214	1.32
0.250	0.5000	0.724	0.495	265.19	353.09	0.229	1.33
0.300	0.5477	0.739	0.489	285.77	379.36	0.250	1.33
ν (Vs^{-1})		E_{pc2} (V)	E_{pa2} (V)	i_{pc2} (μA)	i_{pa2} (μA) [-]	$\Delta E_{p2}= E_{pa2}- E_{pc2}$ (V)	i_{pa2}/ i_{pc2}
0.050	0.2236	0.907	1.361	450.12	152.01	0.454	0.34
0.100	0.3162	0.886	1.367	537.08	178.02	0.481	0.33
0.150	0.3872	0.879	1.372	551.15	182.28	0.493	0.33
0.200	0.4472	0.875	1.378	553.11	185.51	0.503	0.34
0.250	0.5000	0.861	1.383	548.24	189.13	0.522	0.34
0.300	0.5477	0.858	1.388	550.87	193.72	0.530	0.35

The peak current ratio for the second pair of peaks is much lower than unity. Therefore it may said that system shows almost exceptional character from reversible behavior[101, 102].

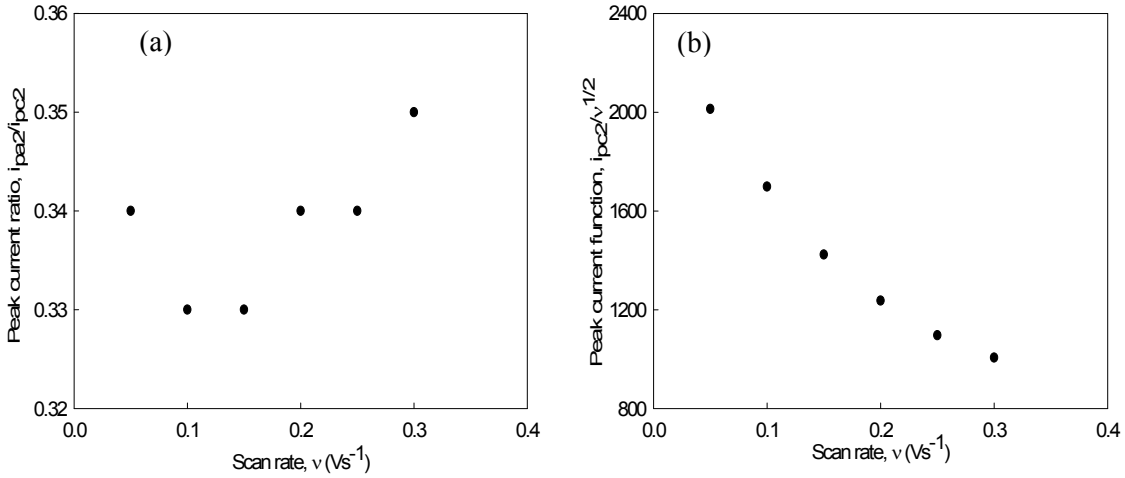

Fig 6.2.74 Variation of (a) peak current ratio and (b) peak current function with scan rate for Cr(III)-Ciprofloxacin Compound in saturated KCl solution.

For the second pair of peaks, the peak current ratio, at first decreases and then increases showing two constant steps. Again peak current function ($i_{pc1}/\nu^{1/2}$) decreases with increasing scan rate for both the second pair of peaks (Fig 6.2.74(b)). Therefore, it does not indicate any clear conception about the electrochemical process[101, 102].

The plot of log i_p against log ν shows a linear relationship for both the second pair of peaks. It is found that the slope is less than unity. Therefore it may be said that the process is accompanied by diffusion[3, 112] (Fig 6.2.75(a)).

Tafel plot (peak potential vs log ν) for the first and the second pair of peaks are shown in Fig 6.2.75(b). The curve express that the slope of the Tafel plot is not zero but nearest to zero. So the electrochemical process may be different from reversible.

Therefore from the above discussions there are some findings, such as: i) peak potential shifts with scan rate, ii) peak current ratio is not equal to unity, iii) the current function $i_p/\nu^{1/2}$ is independent of scan rate, iv) peak response broadens as scan rate increases, v) slope of Tafel plot is not equal to zero.

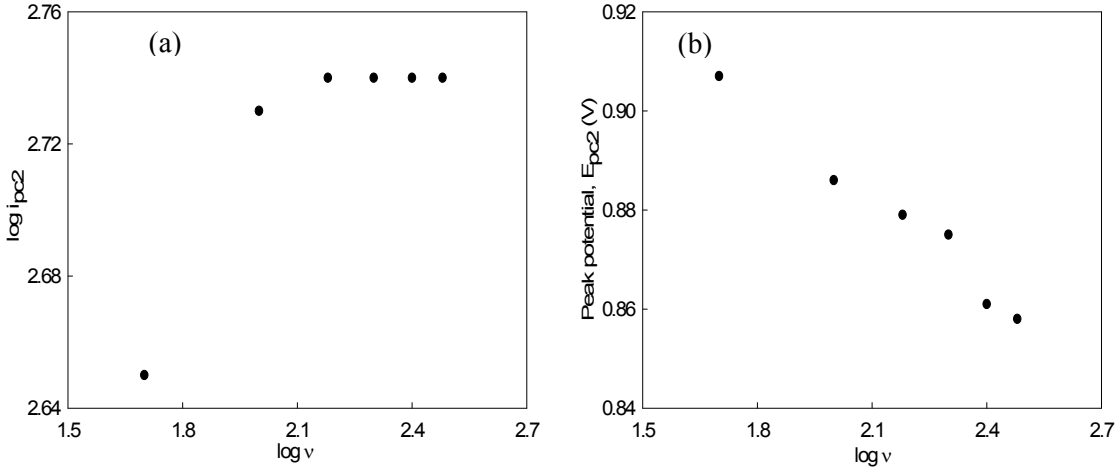

Fig 6.2.75 Plots of (a) log i_{pc2} and (b) peak potential against log ν for Cr(III)-Ciprofloxacin Compound in saturated KCl solution.

Considering all the above points it can be concluded that the electrochemical process involved in Cr(III) is quasi-reversible. The electrochemical reactions of the Cr(III)/Cr(II) system under investigation may be written as:

$$\text{Cr(III)ciprofloxacin} \underset{-e}{\overset{+e}{\rightleftharpoons}} \text{Cr(II)ciprofloxacin}$$

Moreover, the system is diffusion controlled as well as adsorptive controlled, which can be declared from the facts that a) in the forward scans, peak currents are proportional to the square root of scan rate, b) peak currents in both the regions (cathodic and anodic) increases linearly with square root of scan rate, c) slope of log i_p against log ν plot is more than unity.

Concentration effect of Cr(III)-Ciprofloxacin Compound

Study on the concentration effect of Cr(III)-Ciprofloxacin compound was also accomplished. This observation was done using three different concentrations (12.50, 25.00 and 50.00 ppm) of Cr(III)-Ciprofloxacin compound and maintaining the same environment as previous. The CVs are overlapped in the Fig 6.2.76 and the parameters are recorded in Table 6.2.8.

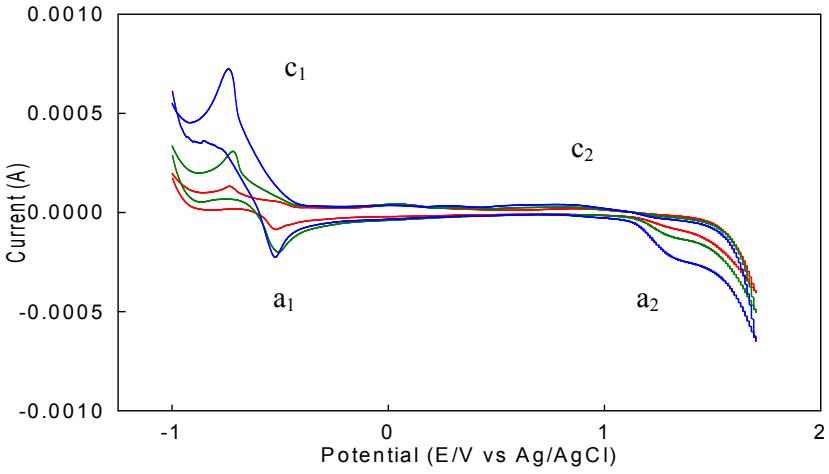

Fig 6.2.76 Cyclic voltammograms of Cr(III)-Ciprofloxacin Compound (at scan rate 0.100 Vs^{-1}) of different concentrations in saturated KCl.

The peak current for all the peaks show a gradual increase with increasing concentrations (Table 6.2.8) and a graphical presentation is given in Fig 6.2.77. Again it is also known that the greater the peak current, higher will be the charge acceptance of the electrode. This linear nature of the peak current with concentrations of the compound solutions

indicate that the processes are diffusion controlled.

Table 6.2.8 Current-potential data for Cr(III)-Ciprofloxacin compound (at scan rate 0.100 Vs^{-1}) in saturated KCl solution at different concentrations.

Concentration ppm	Cathodic peak potential		Cathodic peak current	
	E_{pc1} (V) [-]	E_{pc2} (V)	i_{pc1} (μA)	i_{pc2} (μA)
12.50	0.576	0.778	110.21	9.89
25.00	0.587	0.764	239.47	21.22
50.00	0.632	0.753	358.24	37.08

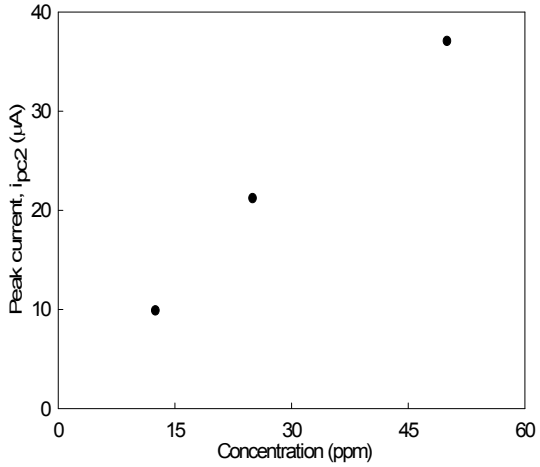

Fig 6.2.77 Variation of peak current with concentration of Cr(III)-Ciprofloxacin Compound in saturated KCl solution.

6.2.8 Chronoamperometric and chronocoulometric study of Cr(III)-Ciprofloxacin Compound

The chronoamperometric as well as chrocoulomeric study of Cr(III)-Ciprofloxacin compound was studied in some modified environment. As like Cyclic voltammetric study of the above system, the present study was also accomplished in saturated potassium chloride and using Platinum electrode as working electrode.

CA and CC study of Cr(III)-Ciprofloxacin Compound

Chromium system was studied in special environment chronoamperometrically after compound formation with Ciprofloxacin. This study was done using 50.00 ppm solution of Cr(III)-Ciprofloxacin compound. After compound formation, there are two signals in the cathodic and also in the anodic region. The comperative study with the CV of Ciprofloxacin implies that the second pair of peak originates from the metallic (Cr(III)) part. And for that reason the CA study was done for that pair of peaks. The chroamperogram is shown in the Fig 6.2.78.

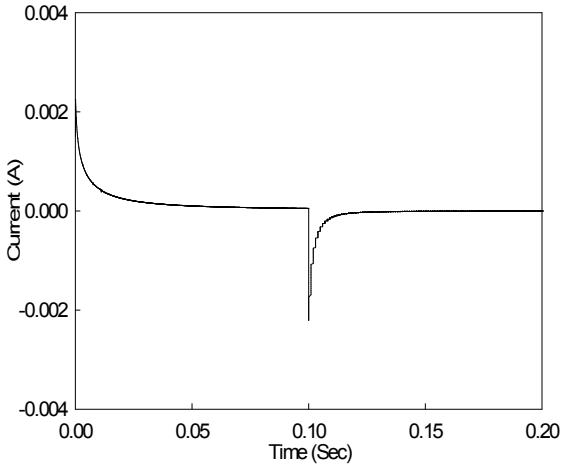

Fig 6.2.78 Current response for Cr(III)-Ciprofloxacin Compound (50.00 ppm solution) in saturated KCl solution.

It is found that the spike height after compound formation with Ciprofloxacin is decreased (Fig 6.2.79) compared to that of Cr(III) before compound formation with Ciprofloxacin. Since the spike height is proportional to the rate of electrolysis, this means that after interaction the rate of electrolysis has been decreased. It is known that

chronocoulometry (CC) is the integrated form of the chronoamperometry. So that in CC the monitored response is charge. It is termed as chronocoulogram. Such charge responses for the pair of peak in case of Cr(III)-Ciprofloxacin compound is shown in Fig 6.2.80. Chronocoulometric response (Fig 6.2.80) shows that the charge at τ is decreased after compound formation with Ciprofloxacin. It was 2.459 μC in the absence of Ciprofloxacin, whereas it becomes 2.249 μC after compound formation with Ciprofloxacin.

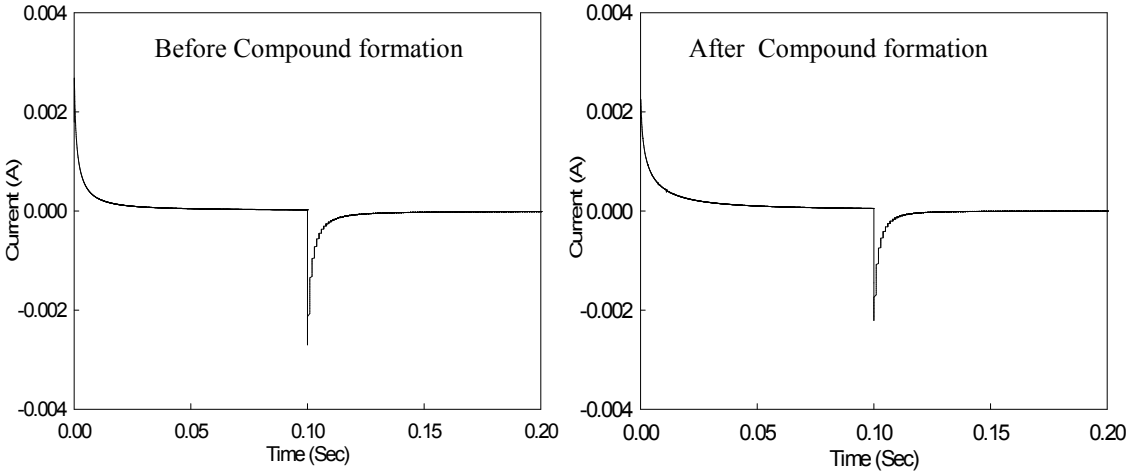

Fig 6.2.79 Current responses for Cr(III) in saturated KCl solution before and after compound formation with Ciprofloxacin.

Now if Q value obtained from time less than τ is plotted versus $t^{1/2}$ and on the same graph $-Q_r$ is plotted versus $\theta = [\tau^{1/2} + (t- \tau)^{1/2} - t^{1/2}]$, there will be two straight lines which intersects each other at Q=0 axis with equal slope, if there is no adsorption of reactant or product. Any deviation from such condition means adsorption. Such plots are shown in the Fig 6.2.81.

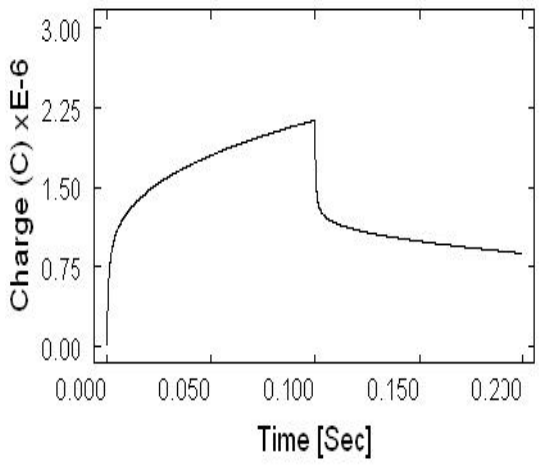

Fig 6.2.80 Charge response for Cr(III)-Ciprofloxacin Compound (50.00 ppm solution) in saturated KCl solution.

This shows that the plots Q vs $t^{1/2}$ and $-Q_r$ vs θ do not intersect each other at Q=0 axis. Moreover they do not have equal slopes. Therefore from this plot, it may be said that adsorption of reactant or products occur on the electrode.

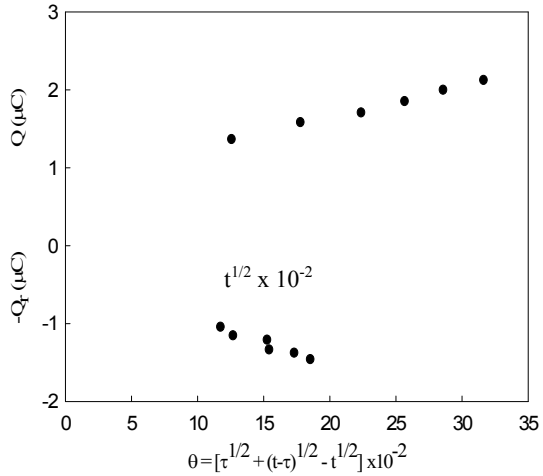

Fig 6.2.81 Plot of Q vs $t^{1/2}$ and $-Q_r$ vs θ for Cr(III)-Ciprofloxacin compound (50.00 ppm solution) in saturated KCl solution.

Therefore the findings from the Chronoamperometric study is that after compound formation the spike height is decreased, indicating towards a decrease in the rate of

electrolysis. And from the Chronocoulometric study, it is observed that the charge at τ is decreased after compound formation. Both of these facts combinedly indicates towards successful compound formation. And the observations from the plots Q vs $t^{1/2}$ and $-Q_r$ vs θ gives conclusion that adsorption of reactant or products occur on the electrode also after compound formation.

Concentration Effect

The concentration effect of Cr(III)-Ciprofloxacin compound was also studied by Chronoamperometric as well as chronocoulometric method. This observation was done using three different concentrations (50.00, 25.00 and 12.50 ppm) of Cr(III)-Ciprofloxacin compound and maintaining the same environment as previous. The CA is shown in Fig 6.2.82. It is observed that with the decrease in concentration of the compound solution the spike height decreases for both the pair of peaks. This fact indicates that as the concentration decreases, the number of electroactive species are decreased. As a result the rate of electrolysis also decreases. Therefore it may be concluded that as the the concentration decreases the rate of electrolysis is decreased. A graphical representation of this fact is shown in Fig 6.2.84(i).

Again Chronocoulometry (CC), which is the integrated form of the chronoamperometry is also examined. Such charge response corresponding to the chronoamperogram is shown in Fig 6.2.83. Here it is also found that with the decrease in compound concentrations, the charge at τ is decreased. The fact behind this is that with the decrease in concentration the number of charged species are also decreased. As a result the charge decreases with decreasing concentration of the compound solution. This can also be represented graphically in Fig 6.2.84(ii).

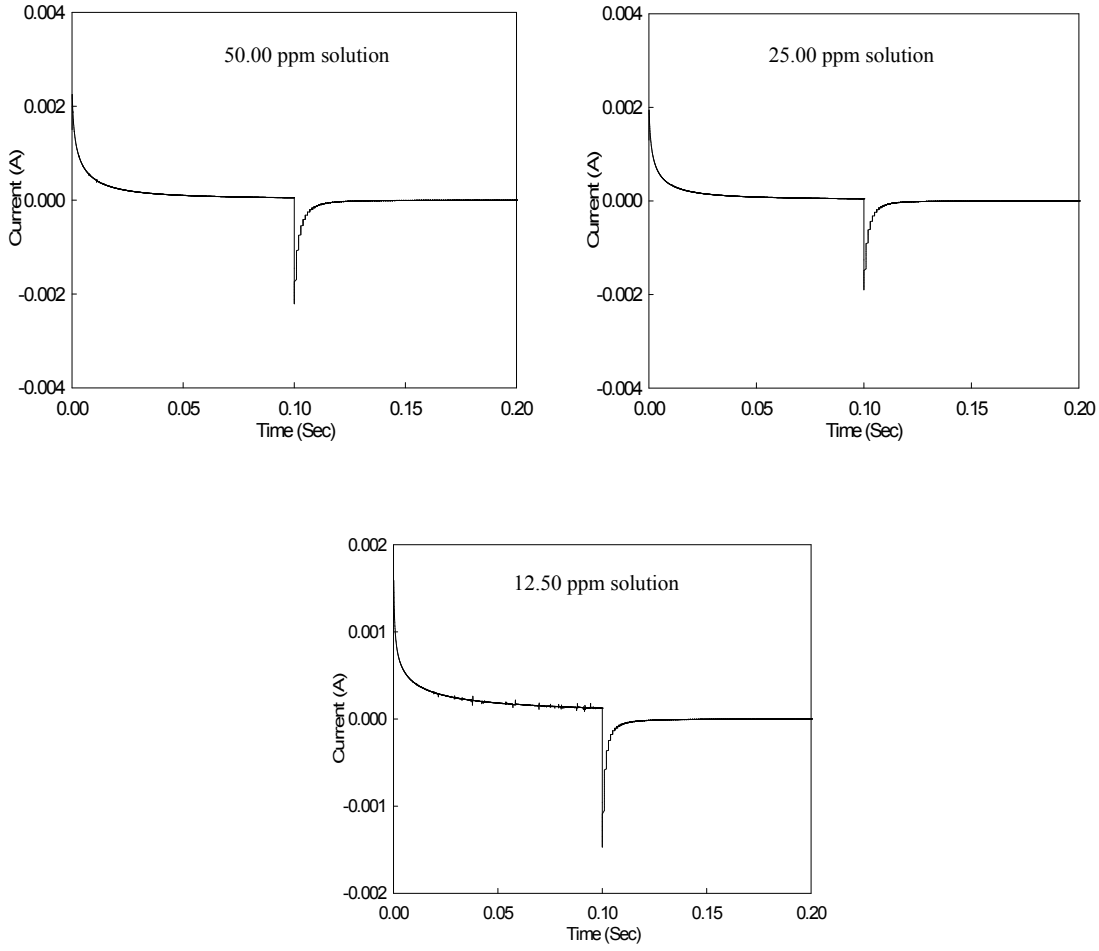

Fig 6.2.82 Current responses for Cr(III)-Ciprofloxacin compound at different concentrations.

Now if Q value obtained from time less than τ is plotted versus $t^{1/2}$ and on the same graph $-Q_r$ is plotted versus $\theta = [\tau^{1/2} + (t- \tau)^{1/2} - t^{1/2}]$, there will be two straight lines which intersects each other at Q=0 axis with equal slope, if there is no adsorption of reactant or product[15]. Any deviation from such condition means adsorption. Such plots for both the pair of peaks and at all the concentrations are shown in the Fig 6.2.85.

This shows that the plots Q vs $t^{1/2}$ and $-Q_r$ vs θ do not intersect each other at Q=0 axis. Moreover they do not have equal slopes. Therefore from this plot, it may be said that adsorption of reactant or products occur on the electrode.

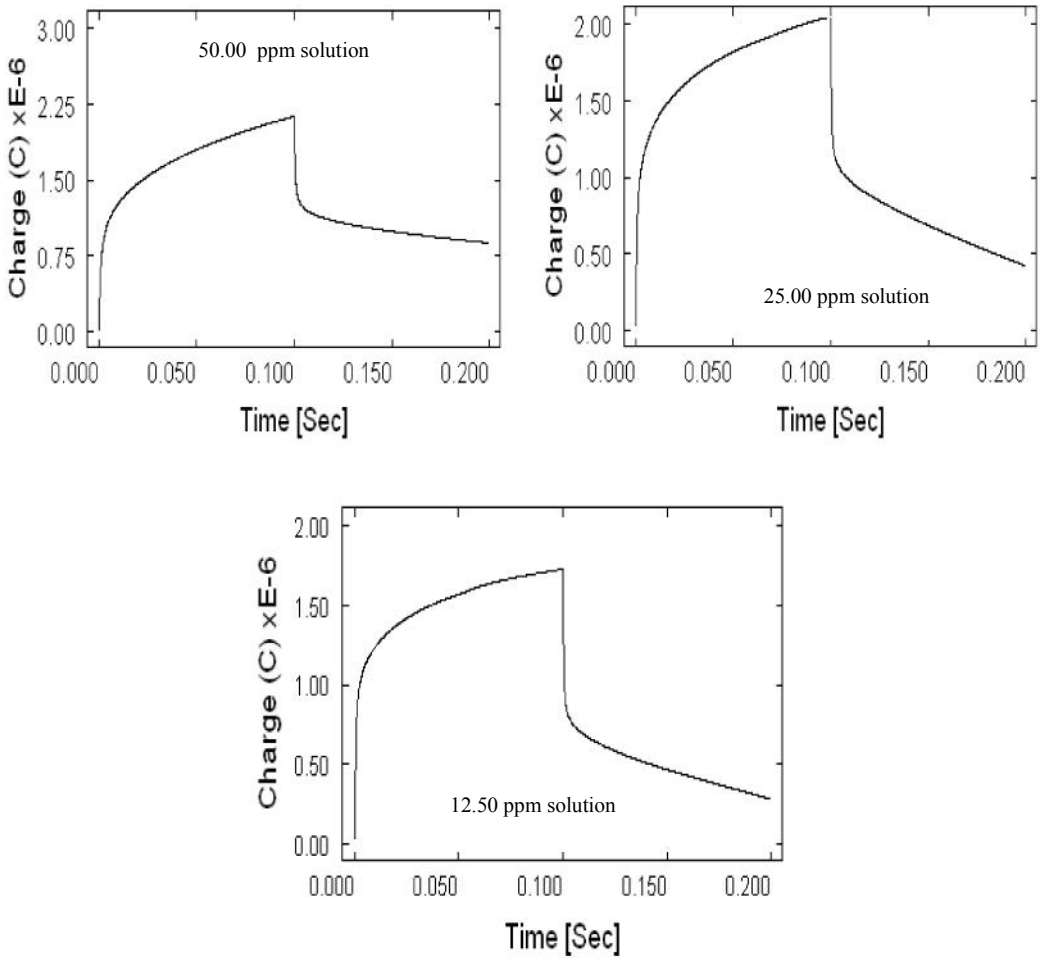

Fig 6.2.83 Charge responses for Cr(III)-Ciprofloxacin compound at different concentrations.

Therefore the findings from the Chronoamperometric study is that after compound formation the spike height is decreased, indicating towards a decrease in the rate of electrolysis. And from the Chronocoulometric study, it is observed that the charge at τ are decreased in all the cases. Both of these facts combinedly indicates towards successful compound formation. And the observations from the plots Q vs $t^{1/2}$ and $-Q_r$ vs θ gives conclusion that adsorption of reactant or products occur on the electrode also after compound formation.

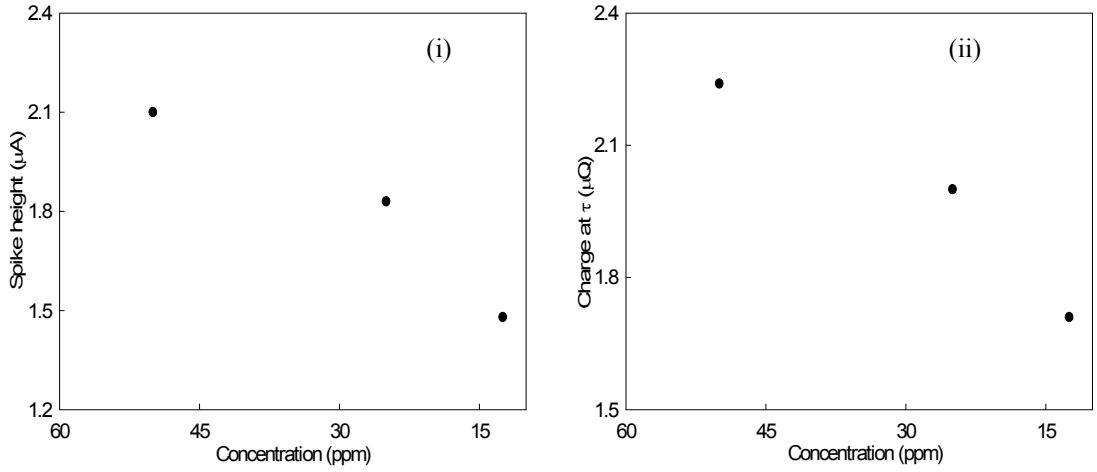

Fig 6.2.84 Concentration effect of Cr(III)-Ciprofloxacin compound on (i) spike height of Chronoamperometry and (ii) charge at τ of Chronocoulometry.

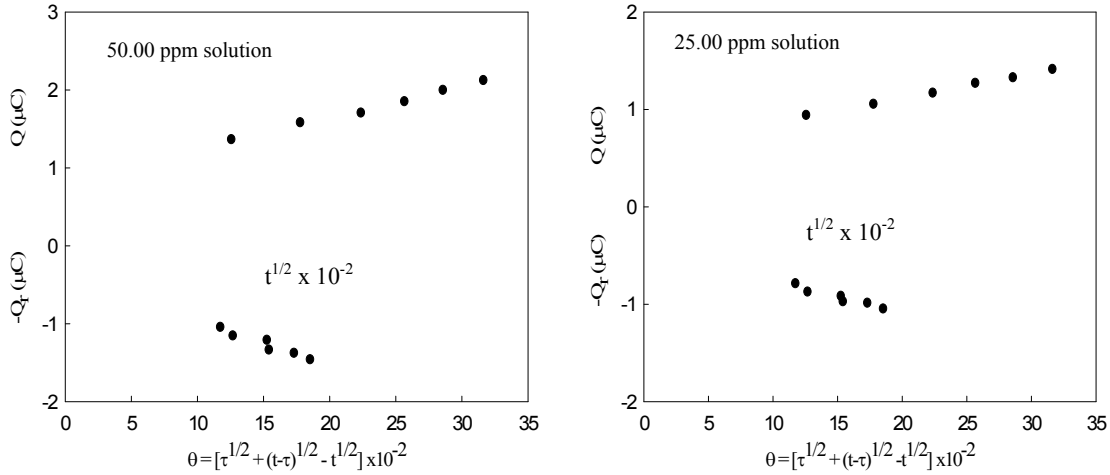

Fig.3.2.85(a) Plots of Q vs $t^{1/2}$ and $-Q_r$ vs θ for Cr(III)-Ciprofloxacin compound in 0.1 M KCl solution at different concentrations (50.00 ppm and 25.00 ppm).

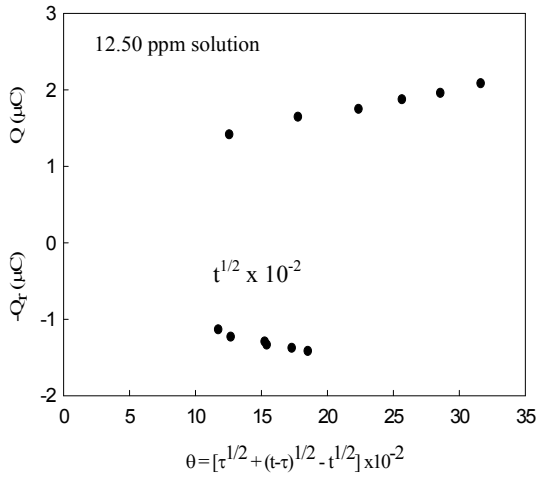

Fig.3.2.85(b) Plots of Q vs $t^{1/2}$ and $-Q_r$ vs θ for Cr(III)-Ciprofloxacin compound in 0.1 M KCl solution at 12.50 ppm concentration.

6.3 Testing Antibacterial Activity of Metal-Ciprofloxacin Compounds

Antibacterial activity of the Metal-Ciprofloxacin compounds was done by Kirby-Bauer antibiotic testing method where the compounds under test is soaked in a filter disc and tested against a bacterium and observed whether the growth of that bacterium is inhibited by that agent.

6.3.1 Preparation of Mueller-Hinton agar

The Mueller-Hinton agar was prepared as per the instructions provided by the manufacturer. After autoclaving the media at 121˚C for 15 minutes, the media was cooled to 50˚C and approximately 12 mL to 15 mL was poured onto the 90 mm Petri dishes. The depth of the agar in the Petri dishes was maintained approximately at 4 mm. The pH of the medium was regularly tested for its consistency.

6.3.2 Turbidity standards (McFarland)

McFarland 0.5 turbidity standards were prepared as per the standard guidelines described by the Clinical and Laboratory Standards Institute (CLSI). A volume of 0.5 mL of a 1.175% (w/v) barium chloride dehydrate ($BaCl_2.2H_2O$) solution was added to 99.5 mL of 0.18 mol/L (1% v/v) sulfuric acid with constant stirring to maintain the suspension. The turbidity standard was then aliquoted into 4 mL test tubes, identical to those used to prepare the inoculums suspension. The McFarland standard tubes were sealed with parafilm to prevent evaporation, and stored in the dark at room temperature (22˚ to 25˚C). Before each use, the standards were shaken well, mixing the fine white precipitate of barium sulfate in the tube. The accuracy of the density of a prepared McFarland standard was checked by a spectrophotometer with a 1 cm light path; for freshly prepared 0.5 McFarland standards, the absorbance at a wavelength of 625 nm is 0.88. The McFarland standards were placed every week with a fresh preparation.

6.3.3 Bacteria inoculum preparation

One isolated colony was selected from the agar plate culture. The top of colony was touched with a loop and transferred into a tube containing 4 mL luria bertani broth and incubated at 37˚C until it achieved or exceeded the turbidity of the 0.5 McFarland standards (usually2-6 hours). Or, a broth culture directly adjusted to the McFarland standards.

6.3.4 Inoculation of test plates

1. Optimally, within 15 minutes after adjusting the turbidity of the inoculums suspension, a sterile cotton swab was dipped into the adjusted suspension. The swab was rotated several times pressed firmly on the inside wall of the tube above the fluid level. This removed excess inoculums from the swab.

2. The dried surface of a Mueller-Hinton agar plate was inoculated by streaking the swab over the entire sterile agar surface. This procedure was repeated by streaking two more times, rotating the plate approximately 60˚ angle each time to ensure an even distribution of inoculums. As a final step the rim of the agar was swabbed. The procedure was done under laminar flow to avoid contamination.

6.3.5 Preparation of solution of antibacterial agent

Metal-Ciprofloxacin compounds were dissolved in water and serially diluted to have the resulting concentration of 1, 2 and 5 mg/mL. Then, presterilized 3 mm diameter Whatmann filter paper was soaked with appropriate amount of the dilutions to maintain the concentrations 30, 50 and 150 µg/disk. The discs were dried in a 37^{o}C incubator.

6.3.6 Application of disks to inoculated plates

1. The predetermined battery of antimicrobial disks was dispensed onto the surface of the inoculated agar plate. Each disk was pressed down individually to ensure complete contact with the agar surface. The disk placed in the agar surface was not closer than 24 mm from center to center. A total of 7 disks were placed on one 90 mm plate.

2. The plates were inverted and placed in an incubator set to 37˚C within 15 minutes after the disks were applied.

6.3.7 Reading of plates and interpreting results

1. After 16-18 hours of incubation, each plate was examined. The resulting zone of inhibition was uniformly circular with a confluent lawn of growth. The diameters of the zones of complete inhibition (judged by the unaided eye) were measured, including the diameter of the disk. Zones were measured to the nearest whole millimeter, using sliding calipers, which were held on the back of the inverted Petri plate. The Petri plate was held a few inches above a black, non reflecting background and illuminated with reflected light. The results were recorded at 16-18 hours post incubation.

2. The zone margin was taken as the area showing no obvious, visible growth that could be detected with the unaided eye. Faint growth of tiny colonies, which could be detected only with a magnifying lens at the edge of the zone of inhibited growth, was ignored.

3. The sizes of zones of inhibition were interpreted by referring to zone diameter interpretive standards from NCCLS 2000, and equivalent minimal inhibitory concentration (MIC) breakpoints are reported as susceptible, intermediate or resistant to the agents that have been tested.

6.3.8 Antibacterial activity of Ciprofloxacin and Metal-Ciprofloxacin compounds

The screening of the Ciprofloxacin and Metal-Ciprofloxacin compounds against different gram negative and gram positive organisms are carried out by disc diffusion method. The bacterial strains viz. *Salmonella sp., Shigella dysenteriae, Escherichia coli, Pseudomonas sp, Bacillus cereus and Staphylococcus aureus* are used for this study. (the full name of an organism is written in the beginning; so, PLEASE WRITE the first letter of the generic name of bacteria followed by a dot)

The zone of inhibition (mm) of Ciprofloxacin and Metal-Ciprofloxacin compounds are given in Tables 6.3.1. The representative photographs for disc diffusion are reproduced in Figures 6.3.1 to 6.3.2.

Table 3.3.1 Antimicrobial activities of Ciprofloxacin and Metal-Ciprofloxacin compounds.

	Ciprofloxacin	Cr(III)-Ciprofloxacin compound	Mn(II)-Ciprofloxacin compound	Ni(II)-Ciprofloxacin compound	Cu(II)-Ciprofloxacin compound	Zn(II)-Ciprofloxacin compound
Organisms	Diameter of zone of inhibition (mm)					
Salmonella sp.	36	32	33	32	30	28
Shigella dysenteriae	30	21	28	25	22	26
Escherichia coli	30	30	33	35	30	30
Pseudomonas sp	10	6	6	6	6	6
Bacillus cereus	30	32	34	30	28	30
Staphylococcus aureus	30	28	35	30	28	31

It is found that Ciprofloxacin is almost equally active against *Salmonella sp., S. dysenteriae, E. coli, Bacillus cereus and S. aureus.* But it is less active against *Pseudomonas sp.* As the concentration of ciprofloxacin is increased (from 30 μg to 150 μg), it also show some proportionally increasing activity.

Cr(III)-Ciprofloxacin compound was found to be active against *Salmonella sp., E.coli., and Bacillus cereus*. These activities are almost similar to those of Ciprofloxacin. But compared to Ciprofloxacin, it shows much less activity against *S. dysenteriae* and *Pseudomonas sp* as well as it also shows almost less activity for *Staphylococcus aureus.*

Mn(II)-Ciprofloxacin compound was found to be active against *Salmonella sp., Escherichia coli., Bacillus cereus and Staphylococcus aureus.* It is found to be more

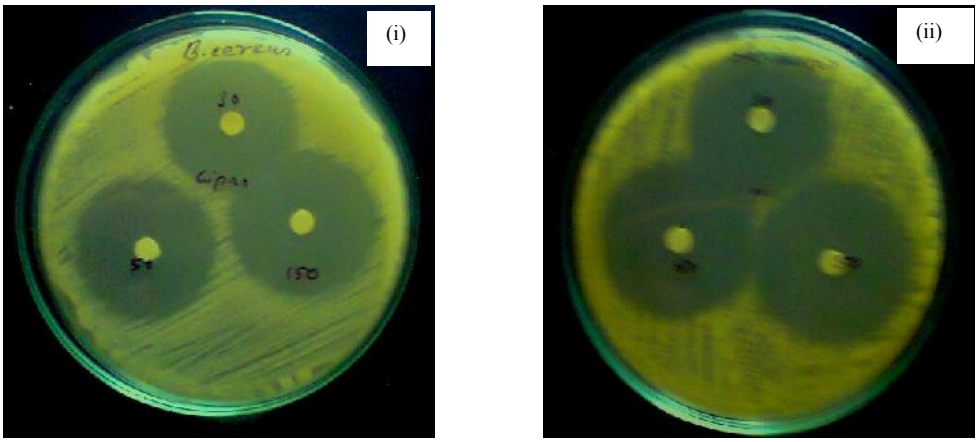

Fig 6.3.1 Zones of inhibition of Ciprofloxacin against (i) *Bacillus cereus* and *(*ii) *Staphylococcus aureus* at different concentrations of Ciprofloxacin.

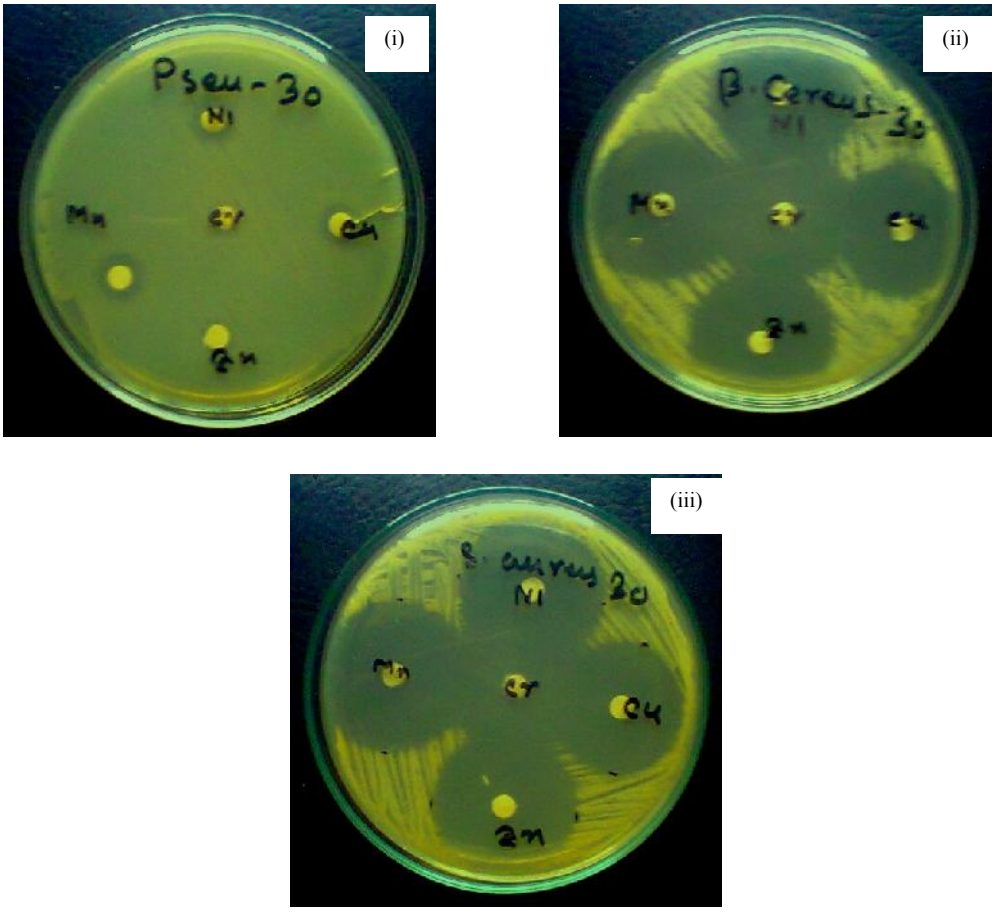

Fig 6.3.4 Zones of inhibition of Metal-Ciprofloxacin compounds against (i) *Pseudomonas sp, (*ii) *Bacillus cereus and* (iii) *Staphylococcus aureus* at 30 µg concentrations of Metal-Ciprofloxacin complexes.

active than Ciprofloxacin against the above organisms. But compared to Ciprofloxacin, it shows much less activity against *S. dysenteriae* and *Pseudomonas sp.* Ni(II)-Ciprofloxacin compound was found to be active against *Salmonella sp.,* and *Escherichia coli.* Its activity against the above two organism is more than that of for ciprofloxacin. But compared to Ciprofloxacin, it shows much less activity against *Shigella dysenteriae* and *Pseudomonas sp.* It shows similar activity against *Bacillus cereus and Staphylococcus aureus* as Ciprofloxacin.

Cu(II)-Ciprofloxacin compound was found to be as active as Ciprofloxacin against *Salmonella sp.,* and *Escherichia coli.* But compared to Ciprofloxacin, it shows much less activity against *Shigella dysenteriae* and *Pseudomonas sp.* It also shows less activity against *Bacillus cereus and S. aureus* than Ciprofloxacin.

Zn(II)-Ciprofloxacin compound was found to be less against *Salmonella sp.,* and *Shigella dysenteriae.* But compared to Ciprofloxacin, it shows much less activity against *Pseudomonas sp.* It also shows similar activities against *Escherichia coli, Bacillus cereus and Staphylococcus aureus* compared to Ciprofloxacin. It is found that in all the cases activity increases with the increase in concentration.

The above findings for the activity of the Metal-Ciprofloxacin compounds with comparison to Ciprofloxacin can be summarized below in a tabular form (Table 3.3.2).

Table 6.3.2 Comparison of activity of Metal-Ciprofloxacin compounds for different organisms.

Metal-Ciprofloxacin compounds	Cr(III)-Ciprofloxacin compound	Mn(II)-Ciprofloxacin compound	Ni(II)-Ciprofloxacin compound	Cu(II)-Ciprofloxacin compound	Zn(II)-Ciprofloxacin compound
Organisms	Activity compared to Ciprofloxacin				
Salmonella sp.	Similar	More	More	Similar	Less
S. dysenteriae	Much less	less	Much less	Much less	Less
E. coli	Similar	More	More	Similar	Similar
Pseudomonas sp	Much less	Much less	Much less	Much less	Much less
Bacillus sp.	Similar	More	Similar	Less	Similar
S. aureus	Less	More	Similar	Less	Similar

7 CONCLUSION

1. Cr(III), Mn(II) and Ni(II) form compounds with Ciprofloxacin with a ratio of 1:2 and on the other hand Cu(II) and Zn(II) form compounds with a ratio of 1:1.
2. Of all the compounds the IR spectrum of Zn(II)-Ciprofloxacin compound is well resolved. Comparing the IR spectrum of Ciprofloxacin and Zn(II)-Ciprofloxacin compounds we see that the peak position of all the functional groups are almost unchanged, which implies that Ciprofloxacin and metal forms adduct type of compounds.
3. The UV-visible spectrum of all the compounds show more or less similar pattern, indicating the similar structure of Ciprofloxacin in all the compounds. This is also important to point out that the spectra of the compounds do not show any significant difference with that of the ligand which indicates towards adduct formation.
4. NIR spectrum of all the compounds also do not show any significant changes compared to Ciprofloxacin. The fact also implies that adduct type of compounds are formed between Ciprofloxacin and metals.
5. The findings from solubility is that all the Metal-Ciprofloxacin compounds are almost soluble in polar solvent but in non-polar solvents these are mostly insoluble. The fact implies that all the compounds have ionic character to some extent.
6. The melting temperature ranges for all the Metal-Ciprofloxacin compounds are at higher temperatures. These compounds are unstable and decomposes at temperatures before melting. This implies the slightly ionic character of the compounds.
7. In all the cases, specific conductance decreases with decreasing concentration. Again it is found that with increasing concentration, molar conductance decreases for all the complexes. Therefore it can be concluded that these compounds are weak electrolytes.
8. The DSC analysis of all the compounds show similar pattern. There is a softening point for the compounds at 87-164˚C range. The endothermic peak at the range 230-323˚C indicate the melting point of the compounds. In addition to that all the

compounds show exothermic peaks of the same pattern due to similar type of change in the compounds during heating.

9. **(i)** The findings from the cyclic voltammetric study of Cu(II)-Ciprofloxacin and Mn(II)-Ciprofloxacin compound implies that the electrochemical processes are quasi-reversible. Similar are the cases for Cu(II), Mn(II) as well as Cu(II)-Ciprofloxacin and Mn(II)-Ciprofloxacin interactions *in solutions*.

   (ii) Again the electrochemical processes involved in Zn(II)-Ciprofloxacin and Cr(III)-Ciprofloxacin compounds are also quasi-reversible. But the Zn(II) and Cr(III) systems are more or less reversible and the Zn(II)-Ciprofloxacin and Cr(III)-Ciprofloxacin interactions in solution are quasi-reversible and irreversible respectively. It was also found that almost all the systems are diffusion controlled as well as adsorptive controlled.

   (iii) The concentration effects of all the compounds show a gradual increase in peak current with the increase in concentrations giving indication towards diffusion controlled situations.

10. **(i)** The findings from the Chronoamperometric study is that after compound formation the spike height is decreased, indicating a decrease in the rate of electrolysis. And from the Chronocoulometric study, it is observed that the charge at τ are decreased in all the cases. Both of these facts combinedly indicates towards successful compound formation. And the observations from the plots Q vs $t^{1/2}$ and $-Q_r$ vs θ gives conclusion that adsorption of reactant or products occur on the electrode also after compound formation.

    (ii) Chronoamperometric as well as chronocoulometric study of the concentration effects of all the metal-Ciprofloxacin compounds show linear relationship between concentration and spike height as well as the charge at τ.

11. The findings from the antibacterial activity of the Metal-Ciprofloxacin compounds show that Mn(II)-Ciprofloxacin and Ni(II)-Ciprofloxacin compound are more active against *Salmonella sp*. compared to Ciprofloxacin. Similar is the case for *E.coli*. Mn(II)-Ciprofloxacin compound is more active than Ciprofloxacin in case of *Bacillus sp.* and *S. aureus*. As a result, it may be concluded that compared to Ciprofloxacin,

Mn(II)-Ciprofloxacin compound shows the best activity against bacteria among the five Metal-Ciprofloxacin compounds used in the present study.

References

[1] Matsumoto and S. Paul, *Journal of Chemical Education,* **82(11),**1660, (2005).

[2] Dwyer and Mellor, *"Chelating Agents and Metal Chelates"*, **5**, 389, (1964).

[3] Jr. D. K. Gosser, "*Cyclic Voltammetry (Simulation and analysis of reaction mechanisms)",* Wiley-VCH, Inc., 30-75, (1993).

[4] W. J. Lindblad, *International Journal of Lower Extremity Wounds,* **7(2)**, 75–81, (2008).

[5] R. D. Forrest, *J R Soc Med,* **75(3), 1**98–205, (1982).

[6] M. Wainwright, *Mycologist,* **3(1),** 21–23, (1989).

[7] W. Kingston, *Irish journal of medical science,* **177(2),** 87–92, (2008).

[8] W. Foster, A. Raoult, *J R Coll Gen Pract,* **24(149),** 889–94, (1974).

[9] R. W. Finberg, R. C. Moellering and F. P. Tally, *Clin. Infect. Dis.,* **39 (9)**, 1314–20, (2004).

[10] M. V. Pirotta and S. M. Garland, *J Clin Microbiol.,* **44(9), 3**213–3217, (2006).

[11] D. V. Ivanov and S. V. Budanov, *Antibiot. Khimioter,* **51(5)**, 29–37, (2006).

[12] M. E. Falagas, P. I. Rafailidis and E. S. Rosmarakis, *Int. J. Antimicrob. Agents,* **29(4)**, 374–9, (2007).

[13] A. J. Mehlhorn and D. A. Brown, *Ann Pharmacother,* **41(11)**, 1859–66, (2007).

[14] R. J. Lewis and J. F. Mohr, *Drug Saf,* **31(4)**, 283–92, (2008).

[15] E. Rubinstein, *Chemotherapy,* **47(3),** 3–8, (2001).

[16] Y. Khaliq and G. G. Zhanel, *Clin Plast Surg,* **32(4)**, 495–502, (2005).

[17] R. Schaumann and A. C. Rodloff, *Anti-Infective Agents in Medicinal Chemistry (Formerly Current Medicinal Chemistry - Anti-Infective Agents),* **6(1)**, 49–56, (2007).

[18] T. Bergan and Bayer, *"Pharmacokinetics of fluorinated quinolones"*, Academic Press, 119–154, (1988).

[19] F. J. Castora, F. F. Vissering and M. V. Simpson, *Biochim Biophys Acta,* **740(4)**, 417–27, (1983).

[20] Kaplowitz and Neil, *Hepatology,* **41 (2)**, 227, (2005).

[21] H. Enzmann, C. Wiemann, H. J. Ahr and G. Schlüter, *Mutat Res,* **425(2)**, 213–24, (1999).

[22] M. J. Suto, J. M. Domagala, G. E. Roland, G. B. Mailloux, and M. A. Cohen, *J Med Chem,* **35(25)**, 4745–50, (1992).

[23] K. Drlica and X. K. Zhao, *Microbiol Mol Biol,* **61(3)**, 377–92, (1997).

[24] S. H. Elsea, N. Osheroff and S. H. Nitiss JL, *J. Biol. Chem.,* **267(19)**, 13150–3, (1992).

[25] S. Z. Haider, "*Introduction to Modern Inorganic Chemistry",* Friends International, Dhaka, Bangladesh, 678-700, (1994).

[26] H. W. Nurnberg, *Pure Appl. Chem.* 54, 853, (1982).

[27] Katz, A. Sidney and H. Salem, *Journal of Applied Toxicology,* **13(3)**, 217–224, (1992).

[28] A. D. Dayan and A. J. Paine, *Human & Experimental Toxicology,* **20(9)**, 439–451, (2001).

[29] K. M. Hambidge and N. F. Krebs, *J. Nutr.,* **137(4)**, 1101–5, (2007).

[30] Muyssen, T. A. Brita, De Schamphelaere, A. C. Karel, Janssen and R. Colin, *Aquatic Toxicology* , **77(4)**, 393–401, (2006).

[31] Instruction manual for BAS Epsilon for electrochemistry. Bioanalytical Systems, Inc. (2000)

[32] F. C. Anson, *Anal. Chem.,* **98,** 55, (1966).

[33] J. H. Christie, R. A. Osteryoung and F. C. Anson, *Anal. Chem*., **13.** 236, (1967).

[34] T. Kambara, *Bull. Chem. Soc. Japan,* **27**, 527, (1954).

[35] A. J. Bard and L. R. Faulkner, "*Electrochemical Methods: Fundamentals and applications"*, John Willey & sons.,228, (1980).

[36] D. J. Barclay and F. C. Anson, *J. Electrochem. Soc.,* **116**, 438, (1969).

[37] A. A. Shaikh, M. Begum, A. H. Khan and M. Q. Ehsan, *Rus. J. of Elec. Chem.,* **42(6)**, 620-625, (2006).

[38] H. M. Naseem Akhtar, A. A. Shaikh and M. Q. Ehsan. *Russian J.of Elec. Chem.* **Vol. 44 no. 12**, 1504-1509, (2008).

[39] S. Pathan, *"Study of interaction of arsenic with sulphur containing amino acids using cyclic voltammetry at platinum electrode"* M.S. Thesis, (2006).

[40] M. M. Jamal. *"Cyclic voltammetric study of the interaction of copper with glutamic acid in solution"* M.S. Thesis (2005).

[41] M. S. Hasan,*"Cyclic voltammetric study of the interaction of ranitidine with copper and iron at glassy carbon, platinum and gold electrodes"* M.S. Thesis (2006).

[42] M. S. Rahman, H. M. Naseem Akhtar, P. K. Bakshi and M. Q. Ehsan. *J. of Saudi Chem. Soc.* **Vol.11 no. 2**, 277-286, (2007).

[43] S. Akter, *"Study of interaction between iron and 2,6-diacetyl pyridine using spectroscopy and cyclic voltammetry",* 4th year project, (2007).

[44] R. J. Mannan and M. M. Alam, *J. of Bang. Aca. of Sci.,***18(2)** 217-227, (1994).

[45] Toshiyuki Abe, Noriaki Kawai, Akio Tajiri and Masao Kaneko. *Bull. Chem. Soc. Jpn.* **76,** 645-650, (2003).

[46] Nurun Nahar, Meher Nigar Chowdhury and A. H. Khan, *J. of Bang. Chem. Soc.,* **12(2)** 173-183, (1999).

[47] Javier Saurina, Santiago Hernandez-Cassou, Esteve Fabregas and Salvador Legret, *Analytica Chimica Acta.,* **405** 153-160, (2000).

[48] Ismat-Ara, A. A. Sheikh, M. Q. Ehsan and A. H. Khan, *J. Saudi Chem. Soc.,* **7(1)**, 129-138 (2003).

[49] Luna N. Rahman, M. Q. Ehsan and A. H. Khan, *Dhaka Univ. J. Sci.,***46(2)**, 223-235, (1998).

[50] F. Nair, M. Sirasnlarain, C. Nataraian, *Talanka,* **40(9)**, 1411-17, (1993).

[51] Mohan, Alam; Yogi, D. S. Kumar, G. NArender; Mohan, M. Srinivas. *Indian J. Chem. Bect. A; Inor. Bio-inorg Phys. Theor. Anal.Chem,* **32 A (9)**, 785-8, (1993).

[52] Peter Gockel, Vahrenkamp, Heirich, Zuber Buehler and Andreas D. Helu. *Chim.*

Acta, **76(1)**, 511-20 (1993).

[53] B. B. Tiwari, R. K. P. Sing, V. Kumar and K. L. Yadava, *Aisan J. Chem.,* **5(1)**, 6-10, (1993).

[54] K. C. Gupta, Frinivasulu and K. Natl. *Acad. Sci. Lett. (Indian),* **13(7)**, 273-4, (1990).

[55] Da, Shilu; Li, Xiaojia, Wanq, Zhonqhue, Fenxi, Huanue, **19(6)**, 700-3, (1991).

[56] A. Rao, Koteswar, M. Mohan and Proc. Srinnivas, *Indian Acad. Sci., Chem.* Sci; **101(1)**, 1-7 (1989).

[57] Masoud, S. Mamdouh, Abd EI-Hamid and H. Omayama, *Transition Met. Chem.*, **14(3)**, 233-41 (1989).

[58] V. Lopez, Gonzalo and P. Afinidad, **45(415)**, 259-62, (1988).

[59] V. Lopez, P. Gomaloo and Afinidad, **45(415)**, 223-8, (1988).

[60] M. Q. Ehsan and M. A. Quyser, *J. Saudi Chem. Soc.*, **6(2)**, 231-236, (2002).

[61] M. Q. Ehsan, Md. Ahidul Islam and M. A. Quyser, *Dhaka Univ. J. Sci.*, **50(2)**, 151-157, (2002).

[62] O. Farook, N. Ahmed and A. U. Malik, *J. Electrochemical Chem. Interfacial Electrochem;*, **24(1)**, 233-6, (1970).

[63] R. G. Denning and T. S. Piper; *Bull Chem. Soc. Japn*, **43(6)**, 1737-43, (1970).

[64] M. Q. Ehsan, *Pak J. Sci. Ind. Res.*, **43(5)**, 271-274, (2000).

[65] M. Q. Ehsan and S. M. Saiful Islam, *Dhaka Univ. J. Sci.*, **48(2)**, 125-128, (2000).

[66] M. Q. Ehsan, *Dhaka Univ. J. Sci.*, **47(2)**, 263-265, (1999).

[67] M. Q. Ehsan, M. Jebin, M. A. Quyser, E. Ahmed, K. M. A. Malik and S. Z. Haider., *Journal of the Bangladesh Chemical Soceity*, **10(1)**, 31-37, (1997).

[68] M. Q. Ehsan, J. M. Arifur Rahman and M. Abul Quyser., *Journal of the Bangladesh Chemical Soceity*, **10(2)**, 187-193, (1997).

[69] M. Q. Ehsan, *Journal of the Bangladesh Academy of Science*, **21(2)**, 207-211 ,(1997).

[70] M. Q. Ehsan, S. Z. Haider, K. M. A. Malik, M. S. Khan and R. J. Quddus, *Dhaka*

University Studies, B, **32(2),** 153-160.

[71] A. Gossmann, *Ann.,*91, 129 (1854); F. Hofmeister, *Ann.,* **6**, 189, (1877).

[72] D. N. Sen, S. L. Mizushima, C. Curran and J. V. Quagliano, *J. Am. Chem. Soc.*, **77,** 211, (1955).

[73] L. Tschugaeff, and E. Serbin, *Compt. Rend.*, **151,** 1361, (1910).

[74] P. Pfeiffer and H. Werner, *Z. physiol. Chem.*, **246,** 212, (1967).

[75] J. P. Greenstein, *J. Biol. Chem.*, **109**, 529, (1935).

[76] P. Pfeiffer, W. Offer/nan, and H. Werner, *J. prakt. Chem.*, **159**, 313, (1942).

[77] P. Pfeiffer, and S. T. Saure, *J. prakt. Chem.*, **157**, 97, (1941).

[78] E. Schulze and E. Steiger, *Z. physiol. Chem.*, **11**, 43**,** (1887).

[79] S. P. L. Sorensen, M. Hoyrup and A. C. Andersen, *Z. physiol. Chem.*, **56**, 44 (1911).

[80] M. Jaffe, *Ber.,* 10, 1926 (1877); **11**, 406, (1878).

[81] M. Jaffe, and R. Cohn, *Ber.,***21**, 3464, (1888).

[82] F. Wrede, *Z. physiol. Client,* **203**, 162, (1931).

[83] A. Taurins, *Can. J. Research, B.* **28**, 762**,** (1950).

[84] P. Pfeiffer, and W. Christelen, *Z. physiol. Chem.*, **245**, 197**,** (1937).

[85] E. Fischer and G. Zemplen, *Ber.,* **42**, 4878 (1909).

[86] L. Tschugaeff, *J. prakt. Chem.*, **75**, 153,(1907).

[87] J. Z. Hearson, D. Burk and A. L. Schade, *Nail. Cancer*, **9**, 337 (1949).

[88] H. Flood and V. Loras, *Tiil/skr. K/emi,* **5**, 83, (1945).

[89] L. E. Maley and D. P. Mellor, *Nature,* **165**, 453, (1950).

[90] M. S. Rahman, H. M. Naseem Akhtar, P. K. Bakshi and M. Q. Ehsan. *J. of Saudi Chem. Soc.* **11(2)**, 277-286, (2007).

[91] R. J. Mannan and M. M. Alam, *J. of Bang. Aca. of Sci.,***18(2),** 217-227, (1994).

[92] R. G. Neville and G. Gorin, *J. Am. Chem. Soc*. **78**, 4893 (1956).

[93] R. J. Neville, *J. Am. Chem. Soc*., **79**, 518, (1957).

[94] J. H. Christie, *J. Electroanal. Chem*., **13,** 79, (1967).

[95] J. H. Christie, G. Lawer, R. A. Osteryoung and F. C. Anson, *Anal. Chem*., **35,** 1979, (1963).

[96] F. C. Anson and R. A. Osteryoung, *J. Chem. Educ.,* **60**, 293, (1983).

[97] J. H. Christie, R. A. Osteryoung and F. C. Anson, *J. Electroanal. Chem.,***13,** 347, (1967).

[98] F. C. Anson, J. H. Christie and R. A. Osteryoung, *J. Electroanal. Chem.,* **13.** 343, (1967).

[99] Zhang, *J. Electroanal. Chem*., **331**, 945, (1972).

[100] P. D. Bear, *Analyst*, **117,**1247, (1992).

[101] R. S. Nicholson and I.Shain, *Anal. Chem,* **37**, 178, (1965).

[102] S. M. Golabi and D. Nimatollahi, *J. Electrocanal. Chem.***481,** 208, (2000).

[103] M. Mascus, F. Pariente, Q. Wu, A. Toffanin, J. P. Shapleigh and H. D. Abruna, *Anal Chem*., **68**, 3128, (1996).

[104] R. H. Wopshall and I. Shain, *Anal. Chem.*, **39**, 1514, (1967).

[105] Gary M. Lampman, Donald L. Pavia, George S. Kriz and James R. Vyvyan, "*Spectroscopy"*, **4th edition**, Cengage Learning India Private Limited, 28-84, (2010).

[106] Gary M. Lampman, Donald L. Pavia, George S. Kriz and James R. Vyvyan, "*Spectroscopy"*, **4th edition**, Cengage Learning India Private Limited, 381-403, (2010).

[107] Jerry Workman Jr. and Lois Weyer. "*Practical Guide to Interpretive Near-Infrared Spectroscopy",* Taylor & Francis Group 6000 Broken Sound Parkway NW, Suite 300 Boca Raton, 12, (2008).

[108] Jerry Workman Jr. and Lois Weyer. "*Practical Guide to Interpretive Near-Infrared Spectroscopy",* Taylor & Francis Group 6000 Broken Sound Parkway NW, Suite 300 Boca Raton, 10, (2008).

[109] K. M. Tichauer, J. A. Hadway, T. Y. Lee and K. St Lawrence, *Journal of Cerebral Blood Flow and Metabolism,* **26**(5), 722–30, (2006).

[110] Samuel Glasstone, *"An introduction to electrochemistry",* East west edition, Affiliated East-West Press Private Limited., 6-11, (2000).

[111] Skoog, A. Douglas, F. James Holler and Timothy Nieman, "*Principles of Instrumental Analysis",* **5th edition**, New York, 805–808, (1998).

[112] F. Mascus, Q. Pariente, A. Wu, J. P. Toffanin, Shapleigh and H. D. Abruna, *Anal Chem*., **68**, 3128, (1996).